

Cochlear implant artifact suppression in EEG measurements

Hanne Deprez

Supervisors:

Prof. dr. ir. M. Moonen

Prof. dr. J. Wouters

Prof. dr. A. van Wieringen

Dissertation presented in partial
fulfillment of the requirements for the
degree of Doctor of Engineering
Science (PhD): Electrical Engineering

March 2018

Cochlear implant artifact suppression in EEG measurements

Hanne DEPREZ

Examination committee:

Prof. dr. ir. P. Van Houtte, chair

Prof. dr. ir. M. Moonen, supervisor

Prof. dr. J. Wouters, supervisor

Prof. dr. A. van Wieringen, supervisor

Prof. dr. ir. A. Bertrand

Prof. dr. ir. T. Francart

Prof. dr. ir. D. Van Compernelle

Prof. dr. M. Mc Laughlin

Prof. dr. sc. techn. Norbert Dillier
(University of Zürich)

Dissertation presented in partial fulfillment of the requirements for the degree of Doctor of Engineering Science (PhD): Electrical Engineering

March 2018

© 2018 KU Leuven – Faculty of Engineering Science
Uitgegeven in eigen beheer, Hanne Deprez, Kasteelpark Arenberg 10 - box 2446, B-3001 Leuven (Belgium)

Alle rechten voorbehouden. Niets uit deze uitgave mag worden vermenigvuldigd en/of openbaar gemaakt worden door middel van druk, fotokopie, microfilm, elektronisch of op welke andere wijze ook zonder voorafgaande schriftelijke toestemming van de uitgever.

All rights reserved. No part of the publication may be reproduced in any form by print, photoprint, microfilm, electronic or any other means without written permission from the publisher.

Preface

Dit doctoraatsonderzoek was een heel interessante, maar bij momenten ook uitdagende ervaring, waar ik veel mensen voor moet bedanken.

Tijdens mijn masteropleiding heb ik een sterke interesse in zowel signaal- als spraakverwerking ontwikkeld. Ik werkte aan automatische spraakherkenning voor cochleaire implantaten tijdens mijn masterproef. Prof. Moonen was lid van de masterproefjury. Hij was de eerste die me vertelde dat hij enkele interessante doctoraatsprojecten had, onder andere in het domein van cochleaire implantaten, en wekte daardoor mijn interesse op om een doctoraat te beginnen. Na een korte meeting met Prof. Wouters, die me het geavanceerde test- en calibratiemateriaal op ExpORL liet zien, was ik overtuigd dat dit doctoraatsproject de ideale mix kon zijn tussen het uitwerken van signaalverwerkingsalgoritmes en -toepassingen enerzijds en het testen bij CI patiënten anderzijds. Die unieke mix van meer theoretisch en meer toegepast onderzoek, dat de sterke punten van beide onderzoeksgroepen zou combineren, was wat me over de streep trok. In de eerste plaats moet ik Marc en Jan dus bedanken omdat zij me überhaupt lieten nadenken over het aanvangen van een doctoraat, maar daarnaast heb ik nog veel andere dingen aan hen te danken.

Marc, bedankt voor de Friday meetings, waarin je veelvuldig je grondige inzicht hebt getoond en me bij momenten troostte om toch door te zetten. Je hebt me enkele keren weer aan het werk gekregen toen ik het niet helemaal meer zag zitten. Jouw gedetailleerde feedback op mijn manuscripten, die een zwarte tekst in een blauw boeltje veranderden, joegen me soms wat angst aan, maar elke opmerking was steeds terecht en maakte de tekst stukken beter. Jan, ik heb ontzettend veel van jou geleerd de laatste jaren. Je leidt een heel diverse onderzoeksgroep, maar je hebt een ongelooflijke visie waar het allemaal naartoe moet leiden. Jouw vermogen om data en onderzoeksresultaten in een oogwenk te beoordelen, en meteen de outliers aan te wijzen “waar we toch nog even verder naar moeten kijken”, heeft me altijd verbaasd. Bedankt om mijn horizon te verbreden en me het ruimere plaatje te laten zien, voor je steun en

voor je waardevolle feedback. Astrid, als mijn derde promotor, ben je altijd beschikbaar geweest voor feedback en voor advies. Ik heb steeds het gevoel gehad dat je achter me stond. Gedurende het laatste anderhalf jaar heb ik dit doctoraatsproject gecombineerd met een lerarenopleiding. Marc, Jan en Astrid, dit was onmogelijk geweest als ik jullie steun niet had gehad. Bedankt daarvoor.

I would also like to thank the jury members, for their feedback on this work. Prof. Francart, Tom, you were a member of my supervisory committee, but much more. You have helped me numerous times with computer or equipment problems, but also gave interesting feedback or new insights during the research meetings we regularly had during the first years of the PhD. Prof. Bertrand, Alexander, we shared an office during the first few months. You made me feel welcome in the group and brought me sandwiches when I fractured my foot. I will never forget your kindness, but also your insight and intelligence have impressed me. Thank you, Tom and Alexander, for being in my supervisory committee. Prof. Van Compernelle, prof. McLaughlin and prof. Dillier, thank you for making the time to read my thesis, for your comments and feedback, and for attending the PhD defense(s). A special thanks goes out to Prof. Dillier for making the trip to Leuven.

This work received funding from Research Project FWO nr. G.066213 'Objective mapping of cochlear implants', IWT O&O Project nr. 110722 'Signal processing and automatic fitting for next generation cochlear implants', and IWT O&O Project nr. 150432 'Advances in Auditory Implants: Signal Processing and Clinical Aspects'. I would also like to thank Cochlear Ltd and Bas van Dijk for their support.

Veel collega's hebben rechtstreeks of onrechtstreeks bijgedragen aan dit doctoraatsproject. Michael, bedankt voor je hulp met inhoudelijke en technische problemen en probleempjes. Jouw hersenen werken ongelooflijk snel, wat het voor mij soms moeilijk maakte om te volgen, maar met eindeloos geduld bleef je volhouden om mij iets bij te brengen. En je hebt me veel bijgebracht: het grootste deel van mijn kennis over CIs, DACIs, EEG, RBA en APEX heb ik aan jou te danken. Ook op persoonlijk vlak heb ik veel troost en steun aan je gehad. Een heel dikke en welgemeende dankjewel daarvoor. Maaïke, in het begin van ons doctoraat werkten we samen op hetzelfde project. Na het behalen van je beurs zijn onze wegen wat gescheiden, maar jij was de eerste die me de weg wees op ExpORL en me de juiste literatuur liet kennen. Robin, jij was mijn project-maatje. We hebben veel en intensief samengewerkt, en ik denk dat ik mag zeggen dat we een goed team vormden. De mannelijke audioloog en de vrouwelijke ingenieur hebben sommige mensen verbaasd, maar jouw kwaliteiten strekken veel verder dan het audiologische. Jouw technisch inzicht heeft me meerdere keren verbaasd. Ik heb dan ook steeds jouw feedback geapprecieerd. Daarnaast was je een echte steun als ik het soms een beetje

moeilijk had. Hartelijk dank daarvoor. Nicolas, bedankt voor de kans om me mee te laten werken op het DACI-project, om telkens snelle en goede feedback te geven mijn verslagen en presentaties, en voor je geduld als het CI-werk even voorrang kreeg. Christiane, bedankt om je inzicht in het CodacsTM systeem met mij te delen en voor je hulp bij de DACI-presentatie op Objective Measures. Tine, mijn Sint-Niklaas-buddy, jouw lieve mailtjes hebben me op vele momenten deugd en plezier gedaan. Onze bezoeken aan Cr  merie Fran  ois zijn steeds een moment geweest om naar uit te kijken, en dat zal zeker zo blijven in de toekomst. Charlotte B., jij bent een ontzettend warm persoon waar ik vanaf het eerste moment een klik mee had. Hopelijk volgen er nog veel musical- en Ikeabezoeken! *Arturo, eres un colega genial y un bailar  n fant  stico. Me encantaron las cenas y las salidas a bares que hicimos juntos, y que nos ense  as “la aut  ntica comida mexicana”.* Team masterproefevaluatie, Anouk, Annelies, Ellen VdW, Sam en Tine, jullie vormden mijn sociale brug naar ExpORL1, maar ook een afleiding en een uitlaatklep als ik even genoeg had van het CI-werk.

Amin, Hasan, Giacomo, Jeroen, Niccol  , Pascalis, and Robbe thank you for co-supervising the DSP project lab sessions.

Sara, jij was mijn eerste mede-ombuds, en samen hebben we het hele systeem mogen en moeten ontdekken. Gelukkig konden we steeds op elkaar rekenen in de uitdagende cases die we als ombuds hebben meegemaakt. Leen, het was heel fijn met jou samen te werken als ombuds; we zaten meteen op dezelfde lijn. Bedankt ook voor de vele andere babbels, over STEM en huizen en verhuizen. Elly, ik apprecieerde onze korte samenwerking en wens je veel succes als mijn ombuds-opvolger! Ook bedankt aan An, Charlotte VC, Inge, Jasper, Kristof, Lore, Lotte, Marjolein en Riet voor de hulp als ik bij jullie kwam binnenvallen met ombuds-vraagjes.

I also want to thank my many other ESAT and ExpORL (ex-)colleagues that have not yet been named here: Bruno, Enzo, Giuliano, Hasan, Joe, Jorge, Pepe, Rodolfo, Rodrigo, Wouter B, Wouter L, Toon, Alejandro, Alexander, Andreas, Ana, Ania, Anneke, Annelies, Annelore, Astrid DV, Ben, Benjamin, Benson, Dimitar, Ehsan, Eline, Ellen R, Ellen VDH, Federico, Frieda, Hamish, Hanne P, Hanneke, Heleen, Ine, Jana, Jonas, Kelly, Lien, Maaike VDM, Neetha, Olivia, Peter, Raphael, Ra  l, Robert, Sanne, Sara, Sofie, Sophie, Stamie, Tinne, Tobias, and Wivine.

Dankzij mijn vrienden kon ik gelukkig ook rekenen op de nodige ontspanning. Tom en Steven, bedankt voor de ontspannende koffie- (voor Tom dan toch) en middagpauzes, en de etentjes met mijn vriendje en jullie vriendinnetjes. Steven, jij hebt gedurende ontelbare wandelingetjes geluisterd naar mijn frustraties en verzuchtingen of naar mijn inhoudelijke monologen, en me bijgestaan met troostende woorden of nuttige adviezen. Daarom ook ontelbaar keer dank

hiervoor. Eline, onze afspraken in Gent, Kortrijk, Leuven of Sint-Niklaas hebben me altijd enorm veel deugd gedaan. Daarnaast dank aan iedereen die interesse toonde in mijn doctoraat, en bleef luisteren als ik een ingewikkelde of lange uitleg afstak.

Tenslotte rest me nog mijn familie en schoonfamilie te bedanken. Dank aan nonkel Johan, die me adviseerde hoe de lerarenopleiding en het doctoraat te combineren. Een dikke merci aan Dries, voor het ontwerpen van de cover. Els en Geert, bedankt om met me mee te leven in de ups en downs van het doctoraat en het publicatieproces, en om Simon aan mij “af te staan” in Leuven. Oma en opa van Belleghem, oma en opa van Geluwe, bedankt voor jullie interesse in mijn doctoraat. Nini, bedankt dat ik, al dan niet met Simon, zo vaak mocht aansluiten voor een aperitiefje of avondeten op Cruysberghs of in het Begijnhof, en voor de ontspannende momenten die we deelden in Leuven. Met jouw vrolijkheid, je soms kinderlijke enthousiasme en je kleine, lieve attenties, slaag je erin een slecht humeur te doen verdwijnen. Mama en papa, zonder jullie was ik nooit geraakt op het punt waar ik nu sta. Jullie kennen me als geen ander, en wisten al dat dit iets was wat ik moest doen, nog voor ik het zelf door had. Jullie hebben me in elke stap van het proces bijgestaan, geduimd voor beurzen en papers, en getroost of gevloekt als iets niet liep zoals ik het wou of verwachtte. Maar jullie lieten me ook zien dat er meer is dan onderzoek of werk in het leven, en trokken me weg uit mijn doctoraatscocon wanneer ik dat nodig had. Bedankt om zo’n warme thuis te creëren, voor alle kansen die jullie Ine en mij hebben geboden en voor jullie geloof in ons. Simon, mijn grootste dankwoord gaat uit naar jou. Bedankt om me tot in Leuven te volgen. Elke dag deelde jij daar met mij elke tegenslag en elk succes, hoe klein of groot ook. Bedankt voor je liefde, je troost en je vertrouwen, en om me te helpen het perspectief te blijven behouden. Nu zijn we klaar om een mooi leven op te bouwen in Sint-Niklaas!

Abstract

Cochlear implants (CIs) aim to restore hearing in severely to profoundly deaf adults, children and infants. Electrically evoked auditory steady-state responses (EASSRs) are neural responses to continuous modulated pulse trains, and can be objectively detected at the modulation frequency in the electro-encephalogram (EEG). EASSRs provide a number of advantages over other objective measures, because frequency-specific stimuli are used, because targeted brain areas can be studied, depending on the chosen stimulation parameters, and because they can objectively be detected using statistical methods. EASSRs can potentially be used to determine appropriate stimulation levels during CI fitting, without behavioral input from the subjects. Furthermore, speech understanding in noise varies greatly between CI subjects. EASSRs lend themselves well to study the underlying causes of this variability, such as the integrity of the electrode-neuron interface or changes in the auditory cortex following deafness and following cochlear implantation.

EASSRs are distorted by electrical artifacts, caused by the CI's radiofrequency link and by the electrical pulses used to stimulate the auditory nerve. CI artifacts may also be present at the modulation frequency, leading to inaccurate EASSR detection and unreliable EASSR amplitude and phase estimations. CI artifacts that are shorter than the interpulse interval (IPI), i.e., the inverse of the pulse rate (in pulses per second (pps)), can be removed with a linear interpolation (LI) over the EEG samples affected by CI artifacts. For clinically used monopolar (MP) mode stimulation, i.e., between an intracochlear and an extracochlear electrode, CI artifacts are longer than for bipolar (BP) mode stimulation, i.e., between two intracochlear electrodes.

In this thesis, CI artifacts are characterized based on the CI artifact duration and based on the CI artifact amplitude growth function (AGF). Furthermore, three methods for CI artifact suppression to enable reliable estimation of EASSR parameters are developed and evaluated.

The CI artifacts are larger and longer in recording channels closer to the implant. Appropriate reference electrode selection may lead to smaller and shorter CI artifacts, that are more easily suppressed. Using LI, CI artifacts may be suppressed in contralateral recording channels for 500 pps stimulation for our recording set-up. More advanced CI artifact suppression methods are needed to measure EASSRs in ipsilateral channels (for source localization or lateralization studies) and in infants and children.

First, a CI artifact suppression method based on independent component analysis (ICA) is developed. Independent components (ICs) associated with CI artifact are automatically identified and rejected based on the component at the pulse rate. In some cases, CI artifacts are successfully removed, although mixed results are obtained in other cases.

Because the ICA method is not fully robust, and since multichannel recordings are needed, a second method, based on template subtraction (TS), is developed. With TS, for each stimulation pulse amplitude, the CI artifact pulse templates are constructed based on a recording containing no significant EASSR. The templates are then put in the correct order and subtracted from the recording of interest. With TS, reliable EASSR amplitudes, phases and latencies are obtained for a high signal-to-noise ratio (SNR) dataset. The template construction recording duration can be reduced to 60 s, while reliable EASSR parameter estimations are still obtained.

Because the previous method requires additional data collection, a third method for EASSR parameter estimation in the presence of CI artifacts is developed. The method is based on a Kalman filter (KF), as proposed in [91]. The CI artifact model presented in [91] consists of constant triangular pulses presented at the stimulation pulse rate, and proved to work well for CI artifacts in contralateral recording channels for BP mode stimulation. In more general cases, i.e., with MP mode stimulation and in ipsilateral channels, CI artifacts are modulated and have an exponentially decaying tail. An extended state-space model is developed that contains additional components modeling these CI artifact features. With the new KF method, reliable EASSR amplitudes, phases and latencies are again obtained for a high signal-to-noise ratio (SNR) dataset, without the need for additional data collection.

The insights provided in this thesis and the developed CI artifact suppression methods may assist researchers and clinicians to record EASSRs in the presence of CI artifacts for clinical stimulation parameters. These responses may then be used to improve CI rehabilitation or CI stimulation strategies, leading to a better quality-of-life for all patients with a CI.

Beknopte samenvatting

Cochleaire implantaten creëren een auditieve perceptie bij ernstig dove patiënten. Elektrisch geëvokeerde auditieve steady-state responsen (EASSRs) zijn neurale responsen opgewekt door continu gemoduleerde pulstreinen, en kunnen objectief gedetecteerd worden in het electro-encephalogram (EEG) op de modulatiefrequentie. EASSRs hebben enkele voordelen tegenover andere objectieve maten, omdat frequentie-specifieke stimuli gebruikt worden, omdat bepaalde hersengebieden doelgericht bestudeerd kunnen worden afhankelijk van de gekozen stimulatieparameters, en omdat ze objectief gedetecteerd kunnen worden d.m.v. statistische methoden. EASSRs kunnen mogelijks gebruikt worden om gepaste stimulatie niveaus te bepalen tijdens CI fitting sessies, zonder gedragsmatige input van de CI subjecten. Spraakverstaan in ruis varieert sterk over CI subjecten. EASSRs zijn de ideale methode om de onderliggende oorzaken van deze variatie te onderzoeken, zoals de integriteit van de elektrode-neuron interface en veranderingen in de auditieve cortex na doofheid en na cochleaire implantatie.

Elektrische artifacten, veroorzaakt door het CI's radiofrequente link en door de elektrische pulsen gebruikt om de gehoorzenuw te stimuleren, beïnvloeden de EASSR. CI artifacten kunnen ook een component op de modulatiefrequentie hebben, wat leidt tot incorrecte EASSR detecties en onbetrouwbare EASSR amplitude en fase schattingen. CI artifacten die korter zijn dan het interpuls interval (IPI), het inverse van de puls frequentie (in pulsen per seconde (pps)), kunnen verwijderd worden door een lineaire interpolatie (LI) over de EEG samples aangetast door CI artifact. Voor klinisch gebruikte monopolaire (MP) stimulatie, tussen een intracochleaire en een extracochleaire elektrode, zijn CI artifacten langer dan voor bipolaire (BP) stimulatie, tussen twee intracochleaire elektrodes.

In deze thesis worden CI artifacten gekarakteriseerd. Verder worden drie methodes ontwikkeld en geëvalueerd voor CI artifact suppressie en betrouwbare EASSR parameter schatting.

CI artifacten zijn groter in amplitude en duren langer voor kanalen dicht bij het implantaat. Geschikte selectie van het referentiekanaal kan resulteren in kleinere en kortere CI artifacten, die gemakkelijker verwijderd kunnen worden. Met LI kunnen CI artifacten verwijderd worden in contralaterale kanalen voor 500 pss stimulatie voor ons opname systeem. Meer geavanceerde CI artifact suppressiemethoden moeten ontwikkeld worden om EASSRs te meten in ipsilaterale kanalen (voor bronlokalisatie en voor lateralizatiestudies) en in kinderen en baby's.

Ten eerste wordt een CI artifact suppressie methode gebaseerd op independent component analysis (ICA) ontwikkeld. Onafhankelijke componenten geassocieerd met CI artifacten worden automatisch geïdentificeerd op basis van de frequentiecomponent op de puls frequentie en vervolgens verwijderd. In sommige gevallen zijn de CI artifacten succesvol verwijderd, hoewel gemengde resultaten bekomen worden in andere gevallen.

Omdat de ICA methode niet volledig robust is, en omdat meerkanaalsmetingen nodig zijn, wordt een tweede methode, gebaseerd op template subtraction (TS), ontwikkeld. Voor elke stimulatiepuls wordt een CI artifact puls template geconstrueerd op basis van een meting die geen significante EASSR bevat. De templates worden dan in de juiste volgorde geplaatst en afgetrokken van de beschouwde meting. Betrouwbare EASSR amplitudes, fases en latenties worden bekomen voor een dataset met EASSRs met grote signaal-ruis verhouding (SNR). De duur van de meting gebruikt voor de template constructie kan beperkt worden tot 60 s met een even betrouwbare EASSR parameterschatting.

Omdat extra metingen nodig zijn bij de vorige methode wordt een derde methode voor EASSR parameterschatting in aanwezigheid van CI artifacten ontwikkeld. De methode is gebaseerd op een Kalman filter (KF), en werd eerst voorgesteld in [91]. Het CI artifact model van [91] bevat constante driehoekspulsen gepresenteerd op de puls frequentie. De methode werkt goed voor CI artifacten in contralaterale kanalen voor BP stimulatie. In meer algemene gevallen, zoals MP stimulatie en metingen in ipsilaterale kanalen, zijn de CI artifacten vaak gemoduleerd en bevatten ze ook een exponentiële staart. Het voorgestelde toestand-ruimtemodel bevat componenten die deze features modelleren. Met de KF methode worden opnieuw betrouwbare EASSR amplitudes, fases en latenties bekomen voor een dataset met EASSRs met grote SNR, zonder dat extra metingen nodig waren.

De besproken inzichten en de ontwikkelde methodes kunnen gebruikt worden door onderzoekers en klinici om EASSRs op te meten voor klinische stimulatieparameters. Deze responsen kunnen dan gebruikt worden om CI rehabilitatie en CI stimulatiestrategieën te verbeteren, wat de levenskwaliteit van alle CI patiënten ten goede zal komen.

List of Abbreviations

ABR auditory brainstem response. 47

AC alternating current. 141

AEP auditory evoked potential. 9, 12, 13, 80

AGF amplitude growth function. 32, 35, 37–40, 42–47, 49, 56, 58, 65, 66, 73, 78, 79, 83, 137

AM amplitude modulated. 15, 116, 121, 143

ASSR auditory steady-state response. 13, 16, 47, 113, 149

BP bipolar. 6, 17, 21, 23, 24, 52–54, 65, 112–115, 118, 138, 141, 143

CAEP cortical auditory evoked potentials. 12, 53, 54

CI cochlear implant. 1–5, 7–18, 21–25, 27–29, 31, 32, 35–37, 39, 40, 42–49, 52–58, 61–67, 69–71, 73, 78–81, 83, 86, 87, 89–95, 97–100, 102, 105, 107–109, 112–119, 121–123, 125, 127, 131–134, 137–149

CPA conditioned play audiometry. 7

CU current level units. 91

DC direct current. 18, 121, 123, 124, 139, 141, 147

DFT discrete Fourier transform. 16, 113–116, 122, 124, 125, 127, 128, 131–134

DR dynamic range. 58

EABR electrically evoked auditory brainstem response. 11–13, 17, 28, 53, 54

EACC electrically evoked auditory change complex. 12

- EAEP** electrically evoked auditory evoked potential. 9, 13
- EALR** electrically evoked late latency response. 12
- EAMLR** electrically evoked auditory middle-latency response. 11, 12
- EASSR** electrically evoked auditory steady-state response. 13–18, 20–25, 27, 29–32, 36, 38, 47, 49, 53–58, 61, 63–67, 69, 71, 73, 78–81, 83, 89, 90, 94, 97, 99, 105, 108, 109, 111–119, 121–125, 127, 128, 131–134, 137–144, 146–149
- ECAP** electrically evoked compound action potential. 10–13, 17, 28, 53, 54
- EEG** electro-encephalography. 2, 3, 13, 15–17, 19–21, 23, 24, 27, 29–31, 35, 37, 48, 53, 54, 57, 62, 64, 65, 78–81, 95, 108, 111–114, 121, 123, 135, 139, 142, 146, 148
- EMMN** electrically evoked mismatch negativity. 12
- ENI** electrode neuron interface. 8, 9, 13, 149
- ESRT** electrically evoked stapedius reflex threshold. 12, 13
- fMRI** functional magnetic resonance imaging. 2, 3
- HI** hearing impairment. 1, 2, 8
- IC** independent component. 23, 55, 62–66, 73, 79–81, 83
- ICA** independent component analysis. 21, 23, 24, 31, 54–58, 62–69, 71, 73, 78–81, 83, 87, 113–115, 133, 138
- ICs** independent components. 23, 138
- IPI** interpulse interval. 21, 54, 113–115, 121, 127, 133, 134, 137, 138, 146
- IQR** interquartile range. 98, 105–107
- KF** Kalman filter. 24, 25, 111–113, 115–117, 122, 123, 125, 127, 131–135, 138, 139, 142, 143, 148
- KF_R** KF based EASSR parameter estimation without CI artifact model. 123, 125, 127, 131, 132, 134
- KF_RA** KF based EASSR parameter estimation with CI artifact model. 123, 125, 127, 128, 131, 132, 134

LI linear interpolation. 21, 23, 24, 54–56, 58, 62, 64, 66–70, 73, 80, 89, 90, 92, 94, 95, 97, 100, 102, 107, 108, 111–116, 121, 122, 124, 125, 127, 128, 131–134, 137, 138, 141–144, 146

MD modulation depth. 58, 63

MDTs modulation detection thresholds. 8

MEG magneto-encephalography. 2, 3

MFTF modulation frequency transfer function. 57, 58, 64, 66, 78, 79, 81, 83, 116, 140

MP monopolar. 6, 17, 20–23, 25, 52–54, 57, 58, 112, 114–116, 138, 139, 141, 143

PCA principal component analysis. 21, 31, 87

PET positron emission tomography. 2, 3

pps pulses per second. 5, 7, 10, 23, 52, 54, 56, 57, 61, 62, 64, 65, 86, 89, 90, 94, 102, 114–116, 121, 133, 134

RC repeatability coefficient. 125, 131

RF radio frequency. 3, 4, 17, 28, 36, 91, 137, 144

SNR signal to noise ratio. 23, 24, 52, 54, 56, 57, 69, 78, 79, 116, 134, 138–140, 142, 148

SPIN speech understanding in noise. 2

TC template construction. 24, 90, 94, 95, 99, 102, 109

TS template subtraction. 24, 89–92, 94, 97–100, 102, 105–109, 111, 113–115, 121, 122, 124, 125, 131, 133, 134, 138, 139, 148

UNHS universal neonatal hearing screening. 1, 7

VRA visual reinforcement audiometry. 7

Contents

Abstract	v
List of Abbreviations	xi
Contents	xiii
List of Figures	xix
List of Tables	xxix
1 Introduction	1
1.1 Motivation	1
1.1.1 Improving rehabilitation options using electrophysiological measures in children	2
1.2 Cochlear implants	3
1.2.1 Influence of stimulation rate	5
1.2.2 Influence of stimulation mode	6
1.3 The need for electrophysiological measures in CI subjects . . .	6
1.3.1 CI fitting	6
1.3.2 Studying the electrode neuron interface	8
1.3.3 Studying auditory plasticity and maturation	8

1.4	Transient electrophysiological responses in CI subjects	9
1.4.1	Electrically evoked compound action potential (ECAPs)	9
1.4.2	Electrically evoked auditory brainstem response (EABRs)	10
1.4.3	Electrically evoked middle-latency response (EAMLR) .	11
1.4.4	Cortical auditory evoked potentials (CAEPs)	11
1.4.5	Electrically evoked stapedius reflex (ESR)	12
1.5	Steady-state responses and CI artifacts	13
1.5.1	Steady-state responses	13
1.5.2	CI artifacts	17
1.6	Outline of the thesis	22
2	Characterization of cochlear implant artifacts in electrically evoked auditory steady-state responses	27
2.1	Introduction	28
2.2	Materials and methods	31
2.2.1	Subjects	32
2.2.2	Stimulation setup	33
2.2.3	Recording setup	35
2.2.4	CI artifact characterization	35
2.3	Results	39
2.3.1	CI artifact AGF slope and intercept	39
2.3.2	STIM artifact duration	41
2.3.3	Influence of reference electrode and hemisphere	42
2.3.4	Influence of pulse rate	46
2.4	Discussion	47
2.5	Conclusion	49

3	Independent component analysis for cochlear implant artifacts attenuation from electrically evoked auditory steady-state response measurements	51
3.1	Introduction	52
3.2	Materials and methods	56
3.2.1	Datasets	56
3.2.2	Signal processing	58
3.2.3	Evaluation	64
3.3	Results	66
3.3.1	40 Hz MFTF dataset	66
3.3.2	90 Hz MFTF dataset	68
3.3.3	40 Hz AGF dataset	70
3.3.4	Noise level reduction and number of rejected ICs	74
3.4	Discussion	74
3.4.1	ICA separation quality	79
3.4.2	Limitations	81
3.4.3	Significance	83
3.5	Conclusion	83
4	Template subtraction to remove CI stimulation artifacts in auditory steady-state responses in CI subjects	85
4.1	Introduction	86
4.2	Materials and methods	90
4.2.1	EASSR dataset	90
4.2.2	Data processing	91
4.2.3	Evaluation of CI stimulation artifact removal methods	97
4.2.4	Influence of TC duration	99
4.2.5	Software and statistical analysis	99

4.3	Results	99
4.3.1	Response properties	99
4.3.2	Influence of TC duration	102
4.4	Discussion	102
4.4.1	Results and interpretation	105
4.4.2	Significance	107
4.4.3	Future work	108
4.5	Conclusion	109
5	A Kalman filter based method for electrically evoked auditory steady state response parameter estimation	111
5.1	Introduction	112
5.2	Materials and methods	115
5.2.1	Dataset	116
5.2.2	Signal model	117
5.2.3	EASSR parameter estimation methods	122
5.2.4	Evaluation	125
5.3	Results	127
5.3.1	EASSR phase	127
5.3.2	EASSR amplitude	127
5.3.3	Response latency	131
5.3.4	Repeatability coefficient	131
5.4	Discussion and conclusion	131
5.4.1	Advantages	132
5.4.2	Limitations and future work	134
6	Discussion	137
6.1	Summary of the work	137

6.2	Interaction between CI artifacts and EASSRs	139
6.3	Recording system specifications	141
6.3.1	Input dynamic range and saturation	141
6.3.2	AC vs DC amplifiers	141
6.3.3	Sample rate and anti-aliasing filter	142
6.4	Future work	142
6.4.1	Improvements of the CI artifact generation model . . .	143
6.4.2	Influence of stimulation reference electrode	143
6.4.3	Reducing CI artifacts by improved stimulus design . . .	145
6.4.4	Improvements to the Kalman filter (KF) based EASSR parameter estimation	147
6.4.5	Clinical applicability of EASSR-based CI fitting	148
6.5	Conclusion	149
Bibliography		151
Curriculum vitae		169

List of Figures

1.1	Cochlear implant system. (1) Sound processor, (2) RF coil, (3) implant system and electrode array, (4) auditory nerve. Figure courtesy of Cochlear Ltd.	4
1.2	Schematic overview of a CI system. Figure obtained from [150].	4
1.3	Schematic overview of how sound is encoded in a cochlear implant system. The incoming sound is passed through a filter bank. For each filter band, envelopes are extracted and used (after compression) to modulate high-rate biphasic pulse trains. The modulated pulse trains are presented to the auditory nerve via the intracochlear electrodes. Figure obtained from [87].	5
1.4	Illustration of ASSR stimuli and measurements, visualized in time or frequency domain or in a polar plot. (a) An acoustic ASSR stimulus, consisting of a modulated sine. (b) Two cycles of an ASSR averaged in time domain. (c) Frequency domain plot of an averaged epoch. The peak in the spectrum is compared to the noise level, that is determined either as based on the adjacent frequency bins (F-test) or based on the variability of the spectral component at the response frequency over time (HT ² test). (d) Polar plot of an ASSR. The ASSR phasor is compared to the noise level, plotted as a black circle around the origin.	14
1.5	Recording electrode locations. The set of recording channels that are often used for analysis are shown in blue (left) and red (right). Often used reference electrodes are indicated in green.	16

1.6	Example of CI artifacts for a subject, with a CI at the right side, measured with 37 Hz AM 900 pps pulse trains at a subthreshold stimulation amplitude. Left: time and frequency domain signals at recording electrodes located near the ear TP ₈ (ipsilateral) and TP ₇ (contralateral), referenced to C _z . The two selected recording electrodes for which the time and frequency domain signals are visualized, were randomly chosen. Right: spatial distribution of spectral power at the modulation frequency, view from the top of the head, referenced to C _z . The units of the topography plot are $dBnV = 20 \log_{10} nV$, where $1 \mu V$ corresponds to $60 dBnV$ and $0.1 \mu V$ corresponds to $40 dBnV$. The colors at the recording electrode locations (black dots) are exact values, the other colors are obtained using interpolation on a fine Cartesian grid. No neural response is expected to be present, as subthreshold stimulation levels were used. Figure (with adjusted caption) taken from [37].	19
1.7	Block diagram showing CI artifact sources, and factors influencing the CI artifact characteristics.	20
2.1	Example of a CI artifact for S8, with a CI at the right side, measured with 37 Hz AM 900 pps pulse trains at a subthreshold stimulation amplitude. Left: time and frequency domain signals at recording electrodes TP ₈ (ipsilateral) and TP ₇ (contralateral), referenced to C _z . Right: spatial distribution of spectral power at the modulation frequency, referenced to C _z . The units of the topography plot are $dBnV = 20 \log_{10} nV$, where $1 \mu V$ corresponds to $60 dBnV$ and $0.1 \mu V$ corresponds to $40 dBnV$. No neural response is expected to be present, as subthreshold stimulation levels were used.	30
2.2	Simulated CI artifact spectrum for unmodulated pulse trains presented at a repetition frequency of 40 pps (left) and for high-rate (900 pps) 40 Hz AM pulse trains (right), in the case of symmetric (top) and asymmetric CI artifacts (bottom).	33
2.3	CI artifact AGFs for S1 and S8, measured with 37 Hz AM 900 pps pulse trains at a subthreshold stimulation amplitude, between an ipsilateral occipital electrode (O ₂) and forehead reference electrode (Fp _z).	36

2.4	CI artifact pulse (top) and $A_m(d)$ AGF with increasing interpolation duration d for subject S2 (bottom). Stimulation below T level at 500 pps, for ipsi- and contralateral recording electrodes. The STIM artifact durations are indicated in dash-dotted lines. Reference electrode C_z	38
2.5	Mean slope θ and intercept I of the CI artifact AGF and mean STIM artifact duration, averaged over all subjects with recordings with stimulation at 500 pps. Average reference (left column) and reference electrode C_z (right column).	40
2.6	CI artifact AGF slope θ and intercept I for ipsi- and contralateral posterior recording electrodes for each subject with recordings with stimulation at 500 pps. Reference electrode C_z . The boxplot shows the median and 25th (q_1) and 75th percentiles (q_3) over the selected recording electrodes for each subject. Outliers (+) are all data points that fall outside the range $[q_1 \pm 1.5(q_3 - q_1)]$	41
2.7	CI artifact AGF slope θ and intercept I for ipsi- and contralateral posterior recording electrodes for each subject with recordings with stimulation at 900 pps. Reference electrode C_z	42
2.8	STIM artifact duration for ipsi- and contralateral posterior recording electrodes for each subject with recordings with stimulation at 500 pps and 900 pps. Reference electrode C_z . Dotted lines indicate the minimum and maximum possible interpolation duration at 500 and 900 pps.	43
2.9	CI artifact AGF slope θ per pulse rate (500 and 900 pps), hemisphere (ipsi- and contralateral) and reference electrode (average reference, C_z and Fp_z). The symbols *, **, and *** indicate that p-values are smaller than 0.05, 0.01, and 0.001, respectively.	44
2.10	CI artifact AGF intercept I per pulse rate (500 and 900 pps), hemisphere (ipsi- and contralateral) and reference electrode (average reference, C_z and Fp_z).	45
2.11	STIM artifact duration per pulse rate (500 and 900 pps), hemisphere (ipsi- and contralateral) and reference electrode (average reference, C_z and Fp_z). Dashed and dotted lines indicate the maximum possible interpolation duration at 500 and 900 pps, respectively. The dash-dotted line indicates the minimum interpolation duration used for the analysis.	46

- 3.1 Example of CI artifacts for a subject, with a CI at the right side, measured with 37 Hz AM 900 pps pulse trains at a subthreshold stimulation amplitude. Left: time and frequency domain signals at recording electrodes TP₈ (ipsilateral) and TP₇ (contralateral), referenced to C_z. Right: spatial distribution of spectral power at the modulation frequency, referenced to C_z. The units of the topography plot are $dBnV = 20 \log_{10} nV$, where 1 μV corresponds to 60 $dBnV$ and 0.1 μV corresponds to 40 $dBnV$. No neural response is expected to be present, as subthreshold stimulation levels were used. Figure (incl. caption) taken from [37]. 55
- 3.2 Recording channel sets c_L (left - blue) and c_R (right - red) with reference electrodes C_z or Fp_z (green). For a subject with a CI on the right side, the channel set c_L is contralateral (c_C) and the channel set c_R is ipsilateral (c_I). 60
- 3.3 First 20 ICs obtained after ICA for subject S07, recording 1 (AGF dataset). For each IC, the amplitude spectrum, and the spatial distribution over recording channels is shown. The amplitude spectrum is colored red for rejected ICs, and blue for the remaining ICs. 67
- 3.4 40 Hz MFTF dataset: $A^{r,C/I}$ (○) and $N^{r,C/I}$ (□) for NO, LI and ICA for the mean contra- and ipsilateral recording channel and for subjects S01-S06. Error bars represent the noise level $N^{r,C/I}$. Only EASSR or CI artifacts dominated data points are included. 69
- 3.5 40 Hz MFTF dataset: $\theta^{r,C/I}$ for NO, LI and ICA for the mean contra- and ipsilateral recording channel and for subjects S01-S06. Only EASSR or CI artifacts dominated data points are included. 70
- 3.6 40 Hz MFTF dataset: response latency for NO, LI and ICA for the mean contra- and ipsilateral recording channel and for subjects S01-S06. The expected range (median: 44.2 ms, interquartile range: 6.8 ms), obtained from [53], is indicated with horizontal lines. 71
- 3.7 40 Hz MFTF dataset: response latencies in individual channels for NO, LI and ICA and for subjects S01-S06. 72
- 3.8 90 Hz MFTF dataset: $A^{r,C/I}$ (gray fill) and $N^{r,C/I}$ (no fill) for NO, LI and ICA. Only EASSR or CI artifacts dominated data points are included. 73

3.9	40 Hz AGF: $A^{r,C/I}$ and $N^{r,C/I}$ for LI and ICA, for subjects S02, S04, S07, S08, S09, S10, S11. The vertical lines correspond to the behavioral threshold.	75
3.10	40 Hz AGF dataset: $\theta^{r,C/I}$ for NO, LI and ICA, for subjects S02, S04, S07, S08, S09, S10 and S11. The vertical lines correspond to the behavioral threshold.	76
3.11	Noise level reduction. Horizontal lines are the 10 and 90 % percentiles of noise reduction levels ΔN_{LI-NO} observed with LI compared to NO. In general, noise levels are reduced after ICA, especially at the ipsilateral side. In many cases, $ \Delta N_{ICA-NO} $ is larger than $ \Delta N_{LI-NO} $. The colored dots represent outliers, i.e., observations that fall outside of the interval $[Q_1 - 1.5IQR, Q_3 + 1.5IQR]$, with the interquartile range IQR, and the first and third quantile Q_1 and Q_3 , respectively.	77
3.12	$\theta_{NO}^{r,C}$ as a function of f_m (40 and 90 Hz MFTF dataset) or stimulation level (40 Hz AGF dataset) without CI artifacts attenuation, in the mean <i>contralateral</i> channel. For the 40 Hz AGF dataset, the red color refers to 37 Hz stimulation, while the blue color corresponds to 42 Hz stimulation, as in Figure 3.10. The dataset is indicated on top. The range and median value of $A_{NO}^{r,C}$ (vector summation of CI artifacts and EASSR) are included as text. No data points are shown for S05 for the 90 Hz MFTF dataset, as only data points with significant synchronous activity are included. Together, amplitude and phase suggest whether the recording is CI artifacts or EASSR dominated. When signals are EASSR dominated in contralateral recording channels, ICA seems to separate the sources good enough to result in adequate CI artifacts attenuation.	82

4.1	Example of an EASSR, measured in subject S4, in contralateral channel PO ₃ and ipsilateral channel PO ₄ , for stimulation with a 45 Hz amplitude modulated 500 pps pulse train (see Section 4.2.1). An average epoch is shown in time and frequency domain (panel C and D), without CI stimulation artifact removal and with LI based CI stimulation artifact removal, denoted as m and $m_{LI_{1900}}$, respectively (panel A and B). CI stimulation artifact peak-to-peak amplitudes are about 50 μV and 300 μV in the contralateral and ipsilateral channel, respectively. The expected EASSR amplitudes are about 20 – 800 nV [64, 53], which is 1000 times smaller than the CI stimulation artifact peak-to-peak amplitude. In the contralateral channel PO ₃ , CI stimulation artifacts are approximately symmetric and therefore have only a small component at the modulation frequency. This component is removed with LI ₁₉₀₀ (panel C). The remaining EASSR has an amplitude of 94 nV . In the ipsilateral channel PO ₄ , CI stimulation artifacts are larger and less symmetric, and have a larger component at the modulation frequency (panel D). Even with LI ₁₉₀₀ , the CI stimulation artifacts cannot completely be removed, because the CI stimulation artifacts are longer in duration than the interpulse interval of 2 ms. After LI, the component at the modulation frequency therefore has a four times larger amplitude in the ipsilateral than the contralateral channel, and consists both of EASSR and residual artifact. More information about the CI stimulation artifact characterization can be found in [37].	88
-----	--	----

- 4.2 Illustration TS method for subject S1 in ipsilateral channel CP₆ for stimulation with an 42 Hz AM 500 pps pulse train. (A) Histogram of stimulation pulse amplitudes used within one stimulation epoch. All stimulation pulse amplitudes p_u between T_u and C_m are used for stimulation. A template $T[p_u, \hat{t}, c]$ is constructed for each of these stimulation pulse amplitudes p_u . (B) Part of a mean epoch without CI stimulation artifact removal $m[t', c]$ (red) and constructed template $T_{epoch}[t', c]$ (blue), in the time domain. The templates are similar to the original signal, although the artifact peaks are not adequately modeled. (C) Mean epoch after TS $m_{TS}[t', c]$ (green), and after TS and LI₁₀₀₀ $m_{TS, LI_{1000}}[t', c]$ (purple), in the time domain. After TS, the mean epoch still contains some residual CI stimulation artifacts, due to inadequate modeling of the artifact initial peak. These are removed with LI₁₀₀₀. (D) Mean epoch in frequency domain, without artifact removal $\bar{m}[f, c]$ (red), CI stimulation artifact template $\bar{T}_{epoch}[f, c]$ (blue), mean epoch after TS $\bar{m}_{TS}[f, c]$ (green), after TS and LI₁₀₀₀ $\bar{m}_{TS, LI_{1000}}[f, c]$ (purple), after LI₁₀₀₀ $\bar{m}_{LI_{1000}}[f, c]$ (orange) and after LI₁₉₀₀ $\bar{m}_{LI_{1900}}[f, c]$ (black). The component at f_m is different for $\bar{m}_{LI_{1000}}$ than for $\bar{m}_{TS, LI_{1000}}$, indicating that the template subtraction does have a beneficial effect. 96
- 4.3 EASSR amplitudes are similar after LI and TS for the channel \hat{c}_{contra} in all subjects. In the ipsilateral channel \hat{c}_{ipsi} , EASSR amplitudes are generally smaller for TS than for LI₁₉₀₀, except for the lowest modulation frequencies. Error bars represent the noise level. 100
- 4.4 EASSR latencies per recording channel for LI and TS. Response latencies are small for some ipsilateral channels in most subjects, but are within the expected range after TS. Response latencies are calculated from a first order fit of the $\theta(f_m)$ curve. Error bars correspond to the 95% confidence intervals of this fit. The horizontal lines indicate the range of expected latencies, and correspond to the median (\pm IQR) values found in [53]. 101
- 4.5 EASSR apparent latencies for LI and TS, for channels \hat{c}_{contra} and \hat{c}_{ipsi} : influence of TC duration. No significant difference is found between TS_{060} , TS_{090} , and TS_{270} in either channel. . . . 104

4.6	Relative amplitude and absolute phase error in function of the difference in response and artifact phase. Generally, larger artifacts result in larger amplitude and phase errors. Amplitude errors are largest when response and artifact are in phase or around 180° out of phase. Phase errors are generally smaller for these phase differences, and are largest when response and artifact are $100 - 150^\circ$ or $200 - 250^\circ$ out of phase.	106
5.1	Comparison of CI artifact shapes, in an averaged epoch, for BP and MP stimulation. Subject S02, reference channel C_z . Left: BP stimulation at C level with $f_m = 40$ Hz, 900 pps. Right: MP stimulation at C level with $f_m = 39$ Hz, 500 pps. Top: contralateral recording channel P_6 . Bottom: ipsilateral recording channel O_2	119
5.2	Illustration of CI artifact template components. First row: observed signal z_k . Second row: CI artifact peak model $p(k)$. Third row: unmodulated CI artifact tail $c(k)$. Fourth row: modulated CI artifacts tail $m(k)$. The second column is a zoomed version of the signals in the first column. The start of each stimulation pulse and the start of each stimulation pulse decay are indicated with a dash-dotted (-.) and a dashed line (:) line, respectively.	122
5.3	EASSR phase estimates for the eight methods, per subject. Left: contralateral recording channel. Right: ipsilateral recording channel.	128
5.4	Blant Altman plot for EASSR phase estimates for the KF based method. Horizontal dashed lines are the mean expected phase errors, based on EASSR and noise amplitudes. Left: contralateral recording channel. Right: ipsilateral recording channel.	129
5.5	Blant Altman plot for EASSR amplitude estimates for the KF based method. Left: contralateral recording channel. Right: ipsilateral recording channel.	130
5.6	Response latency for the KF, LI and TS based method.	132
5.7	Repeatability coefficients (filled dots) for the contralateral channel for the KF and TS based method, compared to the expected variation in amplitude and phase due to the neural background noise (open triangles).	133

6.1	Left: polar plot illustrating the interaction between EASSR and CI artifact components. Right: Relative amplitude and phase errors (in %) depending on the EASSR-to-CI-artifact amplitude ratio and the relative phase difference between EASSR and CI artifact.	140
6.2	Percentage of false detections. Left column: with LI, right column: without LI. Top row: all recording channels, middle row: only contralateral recording channels, bottom row: only ipsilateral recording channels.	145
6.3	CI artifact duration in μs . Top row: reference channel Fp_z , bottom row: reference channel C_z . Left to right: influence of stimulation mode.	146
6.4	The stimulation pulse sequence was adjusted to create EEG samples free of CI artifact. The third CI stimulation pulse was shifted closer to the preceding stimulation pulse, to create a larger gap between the third and fourth pulse.	147

List of Tables

2.1	List of subjects with Cochlear Nucleus® implant details. S: subject identifier; Sex: M: male, F: female; Age: age in years; Exp: CI experience in years; Side of implantation: R: right, L: left; PR: pulse rate tested.	34
3.1	Subject details, including reference channel (Ref) and set of channels (c_C and c_I) used for analysis in the contralateral (C) and ipsilateral (I) hemisphere per subject, for MFTF and AGF datasets.	59
3.2	For three datasets: mean (range) of the number ICs explaining 99% of the signals variance ($\#_{IC_{99}}$), the number of rejected ICs ($\#_{IC_{rej}}$), and the variance explained by the rejected ICs ($var_{IC_{rej}}$), for every subject separately and on average (AVG).	78
4.1	Recording channel selection per subject. As in [53], channels in the parietal-temporal and occipital region were selected. For each subject, channels corresponding to locations on top of the RF coil and channels with excessive noise levels were excluded.	92
4.2	Response properties: response amplitude difference (ΔA) between methods divided by noise amplitude; and response latency difference (ΔRL) between methods. Median(IQR) over modulation frequencies (for amplitude differences), and selected individual contra- and ipsilateral channels (see Table 4.1) for each subject, and over subjects.	103

5.1	Correlation coefficient (p value) between LI-DFT and KF based amplitude and phase estimates for the contralateral and the ipsilateral channel.	126
-----	--	-----

Chapter 1

Introduction

1.1 Motivation

In 1998 Flanders was one of the first regions in the world to implement a universal neonatal hearing screening (UNHS) program. Approximately 98% of newborns are screened with UNHS in order to diagnose hearing impairment (HI) and start rehabilitation as early in life as possible [30]. Early intervention leads to better speech and language development and improved school performance. The prevalence of congenital HI ranges from 1.2 to 2.05 per 1000 infants [138]. About 35% of infants diagnosed with a HI, suffers from severe to profound bilateral HI [137]. A cochlear implant (CI) can partially restore hearing for severely to profoundly hearing impaired infants and adults. For pre-lingually deaf children, it has been shown that implantation before the age of two is associated with better receptive and expressive language skills [11, 109, 132] and enhanced educational and occupational opportunities [72]. In 2010, 95% of profoundly hearing impaired children had received a CI at an early age in Flanders [29]. Also in the Netherlands and other countries, UNHS has reduced the age at implantation [82]. These implanted children may now have access to mainstream education, while they were previously restricted to attend special schools for the deaf. Indeed, due to the early diagnosis and implantation in Flanders, in 2010, three times more children with HI were attending mainstream education than in 1990 [30].

In the adult population, the prevalence of HI ranges between 10 and 20% [108]. Many people acquire a HI during the course of their lives, e.g., due to excessive noise exposure. HI is often associated with reduced quality of life,

with increased chance for depression, distress, loneliness and social isolation [27, 108]. Post-lingually deafened subjects may also receive a CI, which leads to improved speech understanding and localization abilities (in case of bilateral or bimodal CIs). Furthermore, CI subjects generally report improved quality of life after implantation [28, 61, 141].

1.1.1 Improving rehabilitation options using electrophysiological measures in children

Although CIs are the most successful neural prosthesis to date, they do not completely restore normal hearing. Many subjects obtain good speech understanding in quiet, but speech understanding in noise (SPIN) is highly variable. Lazard [83] identified several pre-, per- and postoperative factors that explained 22% of the observed variability. These factors include, but are not limited to, duration of moderate HI, hearing status of the better ear, use of hearing aids, etc [83]. In children, language skills also vary greatly, even when they are implanted early in life. In [11], a model consisting of nine factors, explaining 50% of the variance in language outcomes was presented. It has been suggested that both higher order cognitive factors and peripheral factors may contribute to the residual, unexplained variance. In adult cooperative subjects, these underlying factors may be probed using behavioral techniques. In children and in adults with additional disabilities, however, acquiring these behavioral responses may be challenging. In these cases, electrophysiological measures, based on functional magnetic resonance imaging (fMRI), magneto-encephalography (MEG), electro-encephalography (EEG) or positron emission tomography (PET), may be useful to investigate the status of the periphery and higher order brain regions [88, 90]. Stimulation strategies could then be adjusted accordingly, e.g., by disabling a selection of stimulation electrodes or by increasing the minimum stimulation levels for selected electrodes [45, 46, 153, 121]. In children, electrophysiological measures may be obtained longitudinally to study auditory plasticity and maturation after implantation.

At CI activation and during regular CI fitting sessions, minimum and maximum stimulation levels are set to compensate for inter- and intrasubject differences. CI fitting is usually based on behavioral feedback from the subject. In children and subjects with additional disabilities, it is not easy to obtain such behavioral feedback. Electrophysiological measures could therefore potentially be used for CI fitting.

In summary, electrophysiological measures, obtained in subjects that cannot reliably be tested using behavioral methods, may be useful for three reasons.

First, to assess the status of the periphery and higher brain regions in CI subjects and accordingly adjust stimulation parameters. Second, to study auditory plasticity after implantation in CI adults and children, and to study auditory maturation in CI children. Third and finally, electrophysiological measures could guide objective CI fitting in children and adults with additional disabilities. Acquiring fMRI, MEG and PET images is not recommended for CI subjects due to the magnetic field (fMRI, MEG) and radio-activity (PET). EEG recordings have a high temporal resolution and a spatial resolution that is lower than for fMRI and MEG measures, but still reasonable. Electrophysiological measures based on EEG recordings could therefore be used in CI subjects. However, the CI itself causes electrical artifacts that obscure the neural responses. This thesis focuses on CI artifact suppression methods allowing reliable neural responses to be obtained from the EEG in CI subjects. Chapter 2 focuses on the characterization of the electrical artifacts. In Chapters 3, 4 and 5, three new methods for CI artifact suppression are developed and evaluated.

1.2 Cochlear implants

Cochlear implants (CIs) are used to restore hearing in severely to profoundly hearing impaired infants, children and adults. Currently, there are five CI manufacturers on the market: Cochlear Ltd, Advanced Bionics, Med-El, Oticon Medical and Nurotron, of which Cochlear Ltd owns the largest market share. In this work, Cochlear Nucleus® CIs were used for all experiments, and the hardware components and stimulation parameters used in these implants will be described in further detail. Please note that other CI manufacturers may use different hardware or different stimulation strategies and parameters.

A CI consists of an internal and an external part, as shown in Figure 1.1. The CI's external part consists of a microphone, a sound processor and a radio frequency (RF) coil. The internal parts consist of the actual implant with casing electrode, the ball electrode, and an electrode array inserted in the cochlea.

A schematic overview of a complete CI system is shown in Figure 1.2. The CI processing chain is described shortly, without going into detail. Incoming sounds are picked up by the microphone and converted to electrical stimulation sequences in the sound processor. Envelope encoding is the stimulation strategy most commonly used to convert sounds to electrical pulse sequences [150]. The audio signal is passed through a bandpass filter bank, as shown in Figure 1.3. The envelope of each frequency band is then used to modulate a (high-rate) pulse train, and this modulation pulse train is later applied to one of the stimulation electrodes in the cochlea. Next, the resulting stimulation sequences

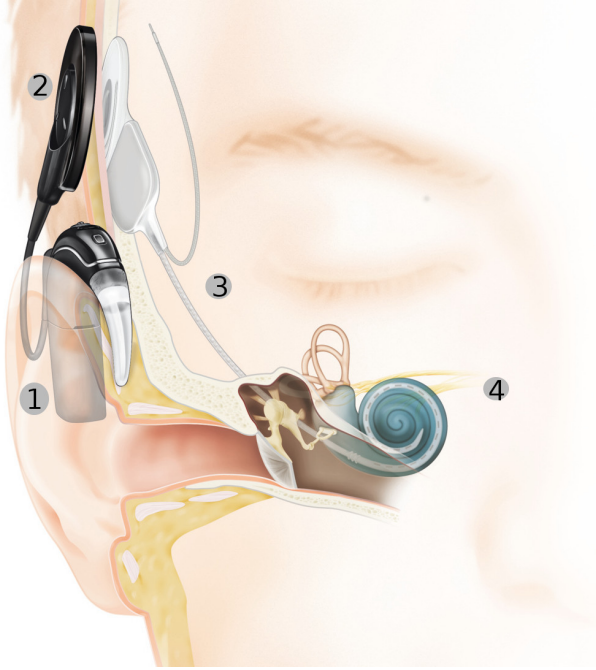


Figure 1.1: Cochlear implant system. (1) Sound processor, (2) RF coil, (3) implant system and electrode array, (4) auditory nerve. Figure courtesy of Cochlear Ltd.

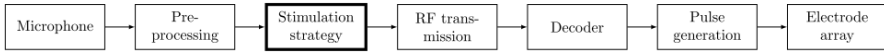


Figure 1.2: Schematic overview of a CI system. Figure obtained from [150].

are encoded and sent to the CI's internal parts via the RF communication link. The RF protocol is described in detail in [152]. The decoded stimulation sequences are then presented to the stimulation electrodes of the electrode array, stimulating the auditory nerve and bypassing the impaired middle and inner ear. Subjects with a functioning auditory nerve will perceive sounds, according to this electrical stimulation.

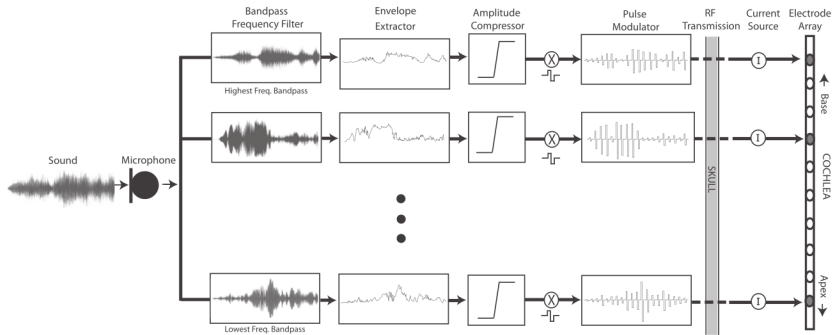


Figure 1.3: Schematic overview of how sound is encoded in a cochlear implant system. The incoming sound is passed through a filter bank. For each filter band, envelopes are extracted and used (after compression) to modulate high-rate biphasic pulse trains. The modulated pulse trains are presented to the auditory nerve via the intracochlear electrodes. Figure obtained from [87].

1.2.1 Influence of stimulation rate

Most modern CIs use modulated high-rate, i.e., > 500 pulses per second (pps) per channel, pulse trains to represent speech envelope information. High-rate stimulation may have several advantages over low-rate stimulation [19, 44, 100, 139]. First, increased temporal detail may be represented in the high-rate stimulation sequences. Second, the neural firing patterns resulting from high-rate stimulation may be more stochastic than for low-rate stimulation, and thus resemble patterns from acoustic stimulation more closely. Third, it has been shown that the pulse rate must be at least a factor four of the modulation frequency for accurate modulation frequency detection [19, 100, 139]. The speech envelope modulations are in the range of 2-40 Hz, while F0 modulation frequencies range from about 80 to 300 Hz. Pulse rates of 320 to 1200 pps are therefore recommended, and are typically used in current CIs. The clinical pulse rate for Cochlear Nucleus® CIs is 900 pps for each stimulation electrode. However, the relevance of pulse rate for speech perception is not well understood, and studies investigating speech perception for high-rate stimulation have produced mixed results [44].

1.2.2 Influence of stimulation mode

The stimulation mode depends on the chosen active and reference stimulation electrode(s) [126]. The monopolar (MP) mode stimulation refers to stimulation between one or more extra-cochlear electrodes and an intra-cochlear electrode, while bipolar (BP) mode stimulation refers to stimulation between two intra-cochlear electrodes. Other stimulation modes, such as tripolar or focused stimulation, are sometimes also used in research. The greater the physical separation between active and reference electrode, the wider the stimulation, and the lower the behavioral threshold values. For wider stimulation modes, there is also less variation in behavioral threshold values across electrodes. The wider MP mode stimulation is the preferred mode in clinical practice. Battery life is prolonged due to the lower stimulation levels needed to elicit auditory percepts [126, 155].

1.3 The need for electrophysiological measures in CI subjects

Clinical and research applications of electrophysiological measures in CI subjects include CI fitting, studying the state of the auditory periphery, and studying auditory maturation and plasticity. These three applications will be described in detail hereafter.

1.3.1 CI fitting

Stimulation parameters, such as stimulation mode, rate, polarity and levels, are set or adjusted at device activation and during regular follow-up visits. The most commonly adjusted parameters are the minimal and maximal stimulation levels for each stimulation electrode, in Cochlear Ltd terminology called threshold (T) and most comfortable (C) levels, respectively [126, 133]. The T level is the stimulation level that elicits a just perceivable auditory perception. The C level is the stimulation level at perceived maximum comfortable loudness. Due to variations in neural survival, electrode placement and cochlear health, T and C levels vary across subjects and across stimulation electrodes within one subject. Maximum and minimum levels are mostly determined based on subjective loudness perceptions for the stimulation electrodes [126, 133]. Levels are then balanced for equal loudness across electrodes [126, 133]. Next, the map, i.e., a selection of stimulation parameters programmed into the speech

processor, is created and the implant is activated for live speech. Additional adjustments can be made based on the subject's reaction [126, 133].

Adults without additional disabilities can usually accurately detect sounds around T level, and judge loudness to determine C levels. Infants and children, and subjects with additional disabilities, may not be able to provide such subjective feedback about perceived sounds. For infants, visual reinforcement audiometry (VRA) is usually employed to estimate threshold levels [131]. The infant learns to associate an audible sound to the appearance of an interesting image on a monitor. The infant is thus visually reinforced to react to sounds he perceives by turning his head. T levels are then set at a fixed level below the level at which the infant turns his head. In older children, conditioned play audiometry (CPA) is used. When an audible sound is perceived, the child is conditioned to indicate a response through a playful activity, such as throwing a ball in a box or putting a piece into a puzzle [7].

For MP mode stimulation, T and C levels vary only slightly across stimulation electrodes [120, 126, 133, 148]. Therefore, audiologists often determine T and C levels at a selection of stimulation electrodes, and interpolate between these measured values to obtain T and C levels for intermediate electrodes. Especially for young children, where CI fitting is already challenging, this results in important fitting time reductions.

Stimulation levels are preferentially determined for the stimulation rates used in daily practice, i.e., 900 pps for Cochlear Nucleus® implants. McKay et al. have recently shown that the largest variability in the threshold-versus-rate curves over subjects occurs for the lower pulse rates (< 500 pps), while the slope is more similar across subjects for rates higher than 500 pps [97]. Therefore, stimulation levels could possibly objectively be determined with 500 pps stimulation, and extrapolated to find appropriate levels for stimulation at 900 pps. However, no research data is available up to this date to corroborate this claim.

The increasing number of implantations due to UNHS and expanding CI candidacy criteria, the emergence of bilateral CIs and electro-acoustic stimulation, and the younger implantation age in infants, place an increasing demand on clinicians and audiologists. Objective measures may be used in the future to assist or automate CI fitting in adults and to obtain (more) reliable responses from infants and children. Objective measures may also be used to “close the loop”, in closed-loop CI systems, where stimulation parameters are dynamically adjusted to the auditory responses obtained [96].

Several electrophysiological measures have been considered to guide objective CI fitting. These are discussed below in Section 1.4 and 1.5.1. Note that many studies focused on correlations between electrophysiological and behavioral

thresholds. This is indeed a necessary first step, although the main aim should be to optimize performance with a CI, rather than exactly predicting behavioral T and C levels.

1.3.2 Studying the electrode neuron interface

Individual variation in electrode placement, neural survival and cochlear health may contribute to variability in speech outcomes. These factors are collectively referred to as the electrode neuron interface (ENI). Variation in the ENI may cause both temporal and spectral cues to be distorted, leading to impaired speech perception. Spectral cues are distorted in CI subjects, due to spread of excitation effects. The larger the electrode-neuron distance and the lower the neural survival, the higher the stimulation levels needed for perception, and the larger the spread of excitation. Due to the reduced spectral cues, CI users rely heavily on temporal modulations for speech understanding. Several studies have assessed the ENI using thresholds to focused stimuli [9], or modulation detection thresholds (MDTs) [112]. It was shown that variation in these measures of ENI state are negatively related to speech understanding. Several studies then used similar behavioral measures of ENI state to adjust stimulation strategies, e.g., by disabling indiscriminable stimulation channels [154] or stimulation channels with high MDTs [45, 46], or alternatively by raising T levels on a selection of stimulation channels with high MDTs [153]. However, behavioral assessment of the ENI may be difficult in infants, children and adults with additional disabilities. In these cases, electrophysiological measures may allow for assessment of the ENI state without behavioral or with limited behavioral input from the subject. It was shown in [90] that electrophysiological measures of modulation detection are significantly correlated with behavioral MDTs. Variability in electrophysiological measures of modulation detection has also been correlated to SPIN [88]. In summary, electrophysiological measures may be used to assess the functional status of the ENI, and to adjust stimulation strategies accordingly.

1.3.3 Studying auditory plasticity and maturation

Speech understanding outcomes vary greatly over CI subjects. In [11], a model of nine clinical and environmental factors was considered to explain receptive and expressive language outcome in CI children. However, only 50 % of the observed variability could be explained using this model. In [83], fifteen factors, including among other factors duration of moderate HI, hearing status of the better ear, use of hearing aids, were considered. However, these factors could only explain

22% of the variability between CI users. It has been suggested that higher order cognitive factors may play an important role [83], next to variability in the ENI as discussed above. Auditory plasticity, and cognitive and cross-modal reorganization may occur due to a lack of auditory input in deaf infants and children, and in post-lingually deafened adults. Animal models have been used to study these structural changes. However, in human subjects, analyses are restricted to behavioral and electrophysiological assessments, because of obvious ethical reasons.

Electrophysiological measures may thus aid our understanding of cortical reorganization following deafness and cochlear implantation, and to derive predictors of CI proficiency. Transient electrophysiological measures and steady-state responses are discussed in more detail in two following sections 1.4 and 1.5.

1.4 Transient electrophysiological responses in CI subjects

An auditory evoked potential (AEP) is an electrical potential generated by acoustic stimulation of the auditory system. Depending on the stimulation parameters, recording electrode placement, filter settings, and the post-stimulus analysis window, AEPs from different sources in the auditory pathway can be analysed. An electrically evoked auditory evoked potential (EAEP) is elicited using electrical stimulation, e.g., through a CI. Stimuli may be delivered via direct stimulation, using dedicated hardware and software, or via sound-field stimulation, e.g., using loudspeakers.

In the following subsections, transient AEPs and EAEPs are discussed. The clinical and research applications of each type of evoked potential are also shortly described. Steady-state responses, that are used in this thesis, are discussed in Section 1.5.1.

1.4.1 Electrically evoked compound action potential (ECAPs)

The electrically evoked compound action potential (ECAP) reflects a synchronous response generated by a group of auditory nerve fibers. A recent review of the possible uses of ECAP measurements can be found in [57]. The ECAP typically consists of an initial negative peak (labeled N1), followed by a positive peak (labeled P2) [57, 68]. In CI users, the ECAP can be measured using reverse telemetry, where an electrical current is applied to an intracochlear

electrode and the neural response is measured from another intracochlear electrode. Reverse telemetry has been built into CIs since 1998. ECAPs may provide three advantages compared to other electrophysiological measures. First, contrary to some other electrophysiological measures in CI users, the ECAP can be measured without additional equipment, since it is measured from the CI electrodes, and with minimal cooperation from the subject as it is not influenced by anesthetics or subject arousal. Second, ECAPs are near field measures, since the CI electrodes are located close to the neural response generation. These near field measures are much larger than far-field measures obtained with scalp electrodes. Third and finally, ECAPs are less influenced by maturational effects than other electrophysiological measures, especially cortical potentials.

In research, different aspects of the ECAP have been studied to assess spatial selectivity, temporal response properties and to estimate neural survival. However, no clear associations between ECAP properties and speech perception with a CI have been shown up to date [57].

ECAPs have also been used clinically to verify CI functioning and for initial programming level estimation. More specifically, ECAP thresholds have been considered for objective CI fitting. ECAP thresholds are mostly higher than behavioral thresholds, and may approximate or exceed upper comfort levels [68]. Correlations between ECAP thresholds and behavioral thresholds to clinical stimuli (>500 pps) are only moderate at best [17, 70]. This is probably because ECAPs are obtained for low repetition rates between 30 and 80 Hz, while higher rates (>500 pps) are typically used in clinical speech processors [98]. At these high rates, peripheral (refractoriness and adaptation) and central factors (temporal integration) may play a different role than at the low rates used to measure ECAPs [98]. Although it is not impossible to measure ECAPs to high-rate stimuli, these measurements are quite time-intensive. Studies have shown that it may be interesting to combine ECAP measures elicited with low-rate stimuli with a selection of behavioral measures to program CI maps [4, 12, 17, 68, 70].

1.4.2 Electrically evoked auditory brainstem response (EABRs)

The electrically evoked auditory brainstem response (EABR) is measured using scalp electrodes, and reflects contributions from the auditory nerve and the brainstem pathways. In normal hearing subjects, the ABR consists of several amplitude peaks with latencies of approximately 1.4 to 6 ms, labeled waves I to V, with earlier peaks associated with more peripheral generators [76]. ABR wave latencies are longer than EABR wave latencies, because of the traveling

wave delay [68]. EABR amplitudes are larger than ABR amplitudes, due to the broader electrical stimulation, and the greater neural synchrony [68].

The EABR may provide two possible advantages compared to the ECAP [68]. First, the EABR is a more central response measure, that can provide information about higher levels in the auditory pathway. Second, the EABR is less influenced by stimulation artifact than the ECAP, because it is a far-field potential and because the EABR occurs at longer latencies than the ECAP.

No strong correlation between EABR measures and speech perception has been demonstrated, probably because speech perception is influenced by central processes, while the EABR merely reflects peripheral neural responsiveness [15].

For objective CI fitting, Brown et al. concluded that there is no one to one correspondence between EABR thresholds and either the T or C levels for older Clarion and Cochlear Nucleus® implants [16, 17, 18]. However, EABR thresholds could potentially be used in conjunction with behavioral T and C level estimates on selected electrodes to guide CI fitting [16, 17, 18]. Again, for these EABR measures, low-rate stimulation was used, which could explain the discrepancy between the low-rate EABR thresholds and the higher-rate clinical thresholds.

1.4.3 Electrically evoked middle-latency response (EAMLR)

The electrically evoked auditory middle-latency response (EAMLR) is a far-field neural response measured with scalp electrodes, originating from the upper brainstem, thalamus and auditory cortex [68]. It consists of a Na-Pa-Nb complex, with latencies between 15 and 55 ms, and is affected by arousal, sleep and anesthetics. EAMLR amplitudes are generally larger than AMLR amplitudes for acoustic stimulation, due to the larger neural synchrony caused by the electrical stimulation. EAMLR latencies seem to be influenced by age and duration of CI use. The clinical use of EAMLR measures for objective CI fitting has not yet been thoroughly evaluated, although EAMLR thresholds correlate well to behavioral measures obtained with the same low-rate stimulus.

1.4.4 Cortical auditory evoked potentials (CAEPs)

Several AEPs are collected under the term cortical auditory evoked potentials (CAEP): the electrically evoked auditory late response (electrically evoked late latency response (EALR)), the electrically evoked auditory change complex (electrically evoked auditory change complex (EACC)), the mismatch negativity (electrically evoked mismatch negativity (EMMN)), and the P300. CAEPs are

typically also measured at the scalp level. Compared to ECAPs, EABRs and EAMLRs, a wider range of stimuli, with varying stimulation durations, can be used. The EALR, EACC, and the EMMN consist of a P1-N1-P2 complex, and are evoked while passively listening to repeated stimuli, a change in an ongoing stimulus, and oddball stimuli, respectively. Similar to the EMMN, the P300 is also elicited using an oddball paradigm, but contrary to the EMMN the listener should actively attend to the oddball stimuli.

CAEPs have mainly been used in research, e.g., to verify that a stimulus difference has been detected. EALR morphology and latency can be used to study auditory maturation in normal hearing children and children with a CI. It has been used to demonstrate the advantages of early (bilateral) implantation [52, 77, 127]. In [144], strong correlations between CAEP and behavioral thresholds were found for clinical stimulation parameters.

1.4.5 Electrically evoked stapedius reflex (ESR)

The stapedius reflex is a stapes contraction occurring in response to loud sounds, presented either acoustically or electrically. For electrical stimulation, the electrically evoked stapedius reflex threshold (ESRT) is then determined as the minimum stimulation level eliciting such a stapes contraction. Intra- or per-operatively, the stapes contraction can directly be observed, while it is detected post-operatively by measuring immittance changes in the non-implanted ear using a clinical tympanometer [3, 68].

While objective fitting methods based on ECAPs and EABRs have focused on both T and C level estimation, ESRTs have been investigated for objective C level estimation. Maximum stimulation levels are set at a loudness that is loud, but comfortable, and thus is usually based on a subjective judgment of the subject. Infants and children often cannot make a reliable judgment of loudness; maximum stimulation levels are therefore often subjectively determined based on children's facial expressions when a sound is presented [3]. An alternative, objective method of determining maximum stimulation levels may be based on the ESRT.

ESRTs can be measured in 37 to 80% of the tested subjects [22, 56, 62, 68, 134]. Some studies have found high correlations between ESRTs and upper comfort levels, while weaker correlations were reported in a number of other studies [68]. Correlations between ESRTs and C levels were not always significant, but ranged between 0.27 and 0.7 when they were [3, 22, 56, 134]. ESRTs were underestimating upper comfort levels in some studies, while ESRTs were higher than the upper comfort level, and even close to the uncomfortable level, in other studies [68]. To summarize, mixed findings have been reported on the relation

between ESRTs and upper comfort levels. The ESRT cannot be measured in all CI subjects, but when present, the ESRT represents a stimulation level that should be audible, but not exceed uncomfortable levels for most CI subjects [68].

1.5 Steady-state responses and CI artifacts

The focus of this thesis is on CI artifact suppression for reliable steady-state response parameter estimation. Steady-state responses are discussed in Section 1.5.1. A discussion of CI artifact causes, morphology and suppression methods is included in Section 1.5.2.

1.5.1 Steady-state responses

In the previous sections, transient AEPs and EAEPs were described and their clinical and research applications were discussed. Transient AEPs are typically evoked using short duration stimuli, and consist of a number of transient peaks with varying latencies. Repetitive presentation of such short duration stimuli, such as clicks in normal hearing subjects and low-rate pulse trains in CI subjects, results in overlapping transient response peaks, leading to a steady-state periodic response at the repetition frequency [64, 115]. Neural phase-locking to modulated sines or noise bands in normal hearing subjects and to modulated high-rate pulse trains in CI subjects also results in a steady-state periodic response at the modulation frequency [65, 115]. While transient responses are typically analyzed by manually labeling response peaks and investigating their amplitude and latency, steady-state responses can objectively and automatically be detected at the response frequency using statistical methods [41, 65, 115]. Furthermore, objective CI fitting based only on ECAPs or EABRs was unsuccessful. Steady-state responses may be a more promising tool for objective CI fitting and for studying the ENI and plasticity in CI subjects. In the remainder of this thesis, the focus will be the auditory steady-state response (ASSR) and the electrically evoked auditory steady-state response (EASSR), that can objectively be detected in the EEG. The ASSR and the EASSR have some advantageous properties compared to the transient AEPs and EAEPs, as discussed below.

The ASSR and the EASSR are neural auditory steady-state responses, present in the EEG, that result from neural phase-locking to a periodic stimulus [115]. EASSRs can be evoked with continuous electrical stimulation [64, 65], either with unmodulated low-rate or modulated high-rate pulse trains. As shown in

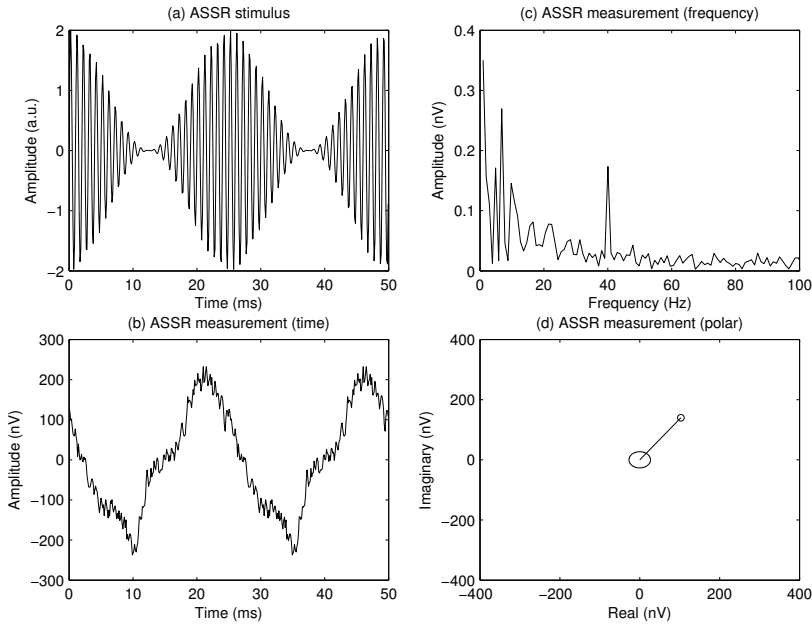


Figure 1.4: Illustration of ASSR stimuli and measurements, visualized in time or frequency domain or in a polar plot. (a) An acoustic ASSR stimulus, consisting of a modulated sine. (b) Two cycles of an ASSR averaged in time domain. (c) Frequency domain plot of an averaged epoch. The peak in the spectrum is compared to the noise level, that is determined either as based on the adjacent frequency bins (F-test) or based on the variability of the spectral component at the response frequency over time (HT^2 test). (d) Polar plot of an ASSR. The ASSR phasor is compared to the noise level, plotted as a black circle around the origin.

Figure 1.4, the ASSR or the EASSR consists of a spectral peak at the repetition frequency (in case of low-rate stimulation) or at the modulation frequency (in case of high-rate stimulation), that is compared to the neural background noise to determine whether a significant response is present.

EASSR stimuli are a good model for CI processing

Most CI stimulation strategies are focused on the coding of the speech envelope, as well as F0 modulations. The speech envelope modulations are in the range of 2-40 Hz, while F0 modulation frequencies range from about 80 to 300 Hz. The

amplitude modulated (AM) pulse trains often used in the EASSR paradigm are a perfect model for these coding strategies.

Recording set-up and signal processing for EASSR detection and parameter estimation

Throughout the thesis, EASSRs were measured using the same set-up. Stimuli were high-rate amplitude modulated (AM) pulse trains, presented directly to the CI, with stimulation amplitudes expressed in μA . The EEG was recorded using a 64 channel Biosemi ActiveTwo system, with a sample rate of 8192 Hz and a 1638 Hz anti-aliasing low pass filter. EEG signals represent the voltage difference between an active and a reference electrode, with amplitudes expressed in μV . Figure 1.5 shows the location of the EEG recording electrodes and electrodes that are often used for (E)ASSR analysis are highlighted [50, 53, 140]. Subjects were lying down or seated in a reclined chair inside a sound isolated Faraday booth, and watching a subtitled movie of their choice. The obtained EEG signals were stored for offline analysis.

Raw EEG signals are usually re-referenced prior to further analysis, by subtracting the reference electrode signal from the other recording electrode signals. Recording electrode C_z is often used as a reference in (E)ASSR measurements. Next, re-referenced EEG signals are filtered with a high-pass filter to remove amplitude drifts and DC bias. Recording channels are then often combined, usually through averaging, over a region of interest, to summarize the multidimensional data. However, single channel EEG signals may also be considered. Recording channels often used for analysis are shown in Figure 1.5.

For synchronization purposes, the start of each stimulation epoch is indicated via a trigger signal that is sent to the recording equipment. In ASSR and EASSR studies, stimulation epochs are often 1.024 s long [50, 53, 54, 89, 90, 91]. The re-referenced and filtered data are split in epochs, based on the trigger signal. A percentage of the available epochs, usually 5%, is rejected, based on the peak-to-peak amplitude, in order to remove movement, muscle, or ocular artifacts. These artifacts are large and broadband signals that may obscure the EASSR parameter estimation and detection. A discrete Fourier transform (DFT) is then applied to each remaining epoch. The mean component at the modulation frequency, averaged over epochs, is calculated. The absolute value and angle of this component are used to estimate the EASSR amplitude and phase, respectively. These values are then compared to the noise level, to decide whether a significant response is present. The noise level is either determined based on frequency bins adjacent to the modulation frequency, i.e., an F-test

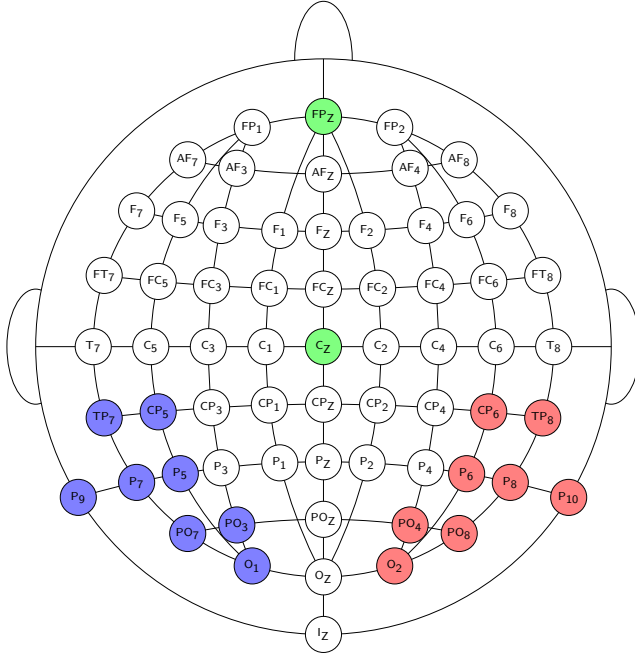


Figure 1.5: Recording electrode locations. The set of recording channels that are often used for analysis are shown in blue (left) and red (right). Often used reference electrodes are indicated in green.

[41], or based on the variance over epochs of the component at the modulation frequency, i.e., a Hotelling T^2 test [64, 66].

Neural generators

Different parts of the auditory pathway are activated during ASSR stimulation, depending on the modulation frequency used [49, 59, 116, 118]. In normal hearing subjects, activity is mostly generated by a brainstem source, for modulation frequencies in the 80–100 Hz range. For 40 Hz range stimulation, thalamic and subcortical sources have been identified. For lower modulation frequencies, activity is mainly generated in the cortical areas. Up to date, only one study has investigated neural EASSR generators in CI users [89]. In this study, results indicated that 40 Hz stimulation resulted in thalamic activity also in CI users.

The choice of modulation frequency thus allows to study several different brain regions.

Advantages compared to transient responses

EASSRs offer a number of advantages compared to transient responses. First, EASSRs are responses elicited by frequency-specific stimuli, activating one stimulation channel, compared to transient responses, which are often evoked with non-frequency specific stimuli, and with free field stimulation, activating multiple stimulation channels. Second, EASSRs can objectively be detected at the modulation frequency [41, 64, 65, 66], while transient responses are typically assessed subjectively by examining the latency and amplitude of visually identified peaks. Although statistical methods could be used for objective detection of transient responses, this is not routinely used in research or in the clinic. Third, depending on the chosen modulation frequency, different brain regions, from brainstem to cortical sources, may be studied. Fourth, as explained before, the stimuli used to elicit the EASSR are a perfect model for the envelope coding in CIs. Fifth, EASSRs may be a more promising tool than ECAPs and EABRs for objective CI fitting, as explained below.

Objective CI fitting

EASSRs can be elicited using high-rate stimulation, while ECAPs and EABRs are traditionally measured with low-rate stimulation. T and C levels vary with stimulation rate [97, 98], and are therefore ideally determined with the clinically used stimulation rate. Although this is not impossible [71], it is not straightforward to record ECAPs and EABRs with clinically used stimulation rates. T levels determined with ECAPs and EABRs, using low-rate stimuli, are only moderately correlated with behavioral T levels. T levels determined with EASSRs, using high-rate stimulation, correlate well with behavioral T levels, at least for stimulation in BP mode [65]. More research is needed to evaluate the usefulness of EASSR based CI fitting for MP mode stimulation.

1.5.2 CI artifacts

EEG measurements in CI subjects in general and EASSRs specifically are corrupted by electrical stimulation artifacts, which can be caused by both the electrical stimulation pulses and the RF communication link between the external speech processor and the implant. The former can have a periodic component at the response frequency which may distort the neural response [65].

Fig. 1.6 shows the EEG signal recorded on two channels in time and frequency domain, for subthreshold stimulation. Both EEG signals have a component at the modulation frequency, which is caused by the electrical stimulation since no neural response is assumed to be present.

The origin of the component at the modulation frequency is now discussed. Symmetric biphasic pulses, with equal phase widths and equal but opposite amplitudes for both phases, are used for stimulation in clinical settings in Cochlear Nucleus® implants, as shown in Figure 1.7. These pulse trains have frequency components at the pulse rate f_c and its harmonics. However, the measured CI artifacts are often asymmetric, as shown in Figure 1.6, resulting in a DC component. The origin of the pulse asymmetry is not well known, but a possible contributor is the constant-current stimulation is used in Cochlear Nucleus® implants. If the impedance of the active CI stimulation electrode (stimulated during the first phase of the pulse) and reference CI stimulation electrode (stimulated during the second phase of the pulse) differ, the voltage of both pulse phases may be different, resulting in pulse asymmetries and a direct current (DC) component in the spectrum. The amplitude modulation used to elicit the EASSR results in CI artifact components at the carrier sidebands and possibly also at the modulation frequency. Amplitude modulation of high-rate pulse trains with modulation frequency f_m results in frequency components at the carrier sidebands $kf_c \pm f_m$, with $k = 0, 1, 2, \dots$. The CI artifact component at f_m is problematic, because it distorts the EASSR and leads to false EASSR detections.

The spatial distribution of the spectral component at the modulation frequency is shown in the topography plot, indicating that the electrical stimulation artifact is present on all recording electrodes. The amount of distortion is highly subject-dependent, and is, at least in theory, affected by (1) the stimulation parameters, (2) the impedances of the electrode-tissue interface, the body tissue and the EEG recording electrode-gel-skin interface, (3) the recording equipment, and (4) post-processing, as shown in Figure 1.7. The exact influence of some of these factors, e.g., the impedances, is difficult to determine, as these factors cannot easily be measured or systematically be varied within or over subjects. The impedance at the CI electrode-tissue interface and at the skin-gel-EEG electrode interface likely has a capacitive component [102]. This capacitance results in distortion of the CI artifact pulse shape, as shown in Figure 1.7. Low pass filters, and possibly also high pass filters, in the EEG acquisition system may further influence the CI artifact pulse shape, as explained in detail in Section 6.3. Further postprocessing may consist of applying digital filters and CI artifact suppression methods, which may both further adjust the CI artifact pulse shape. Suppressing CI artifacts seems more challenging for EASSR recordings than for transient responses because CI artifact and EASSR continuously overlap in

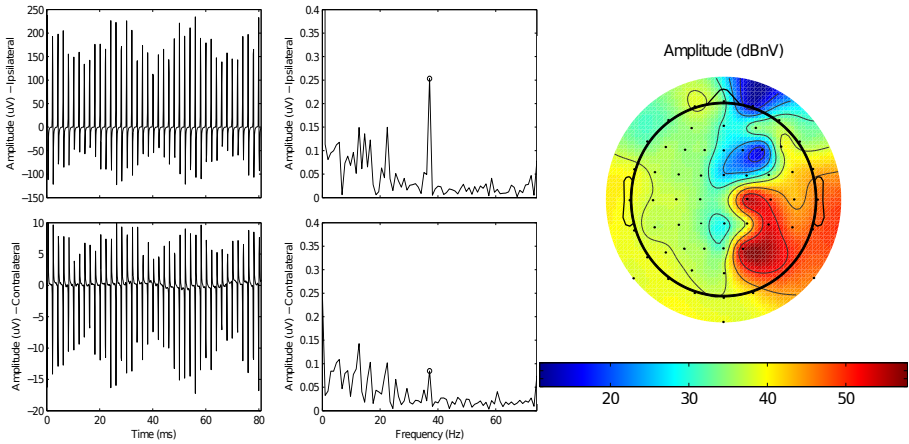


Figure 1.6: Example of CI artifacts for a subject, with a CI at the right side, measured with 37 Hz AM 900 pps pulse trains at a subthreshold stimulation amplitude. Left: time and frequency domain signals at recording electrodes located near the ear TP₈ (ipsilateral) and TP₇ (contralateral), referenced to C_z. The two selected recording electrodes for which the time and frequency domain signals are visualized, were randomly chosen. Right: spatial distribution of spectral power at the modulation frequency, view from the top of the head, referenced to C_z. The units of the topography plot are $dBnV = 20 \log_{10} nV$, where $1 \mu V$ corresponds to $60 dBnV$ and $0.1 \mu V$ corresponds to $40 dBnV$. The colors at the recording electrode locations (black dots) are exact values, the other colors are obtained using interpolation on a fine Cartesian grid. No neural response is expected to be present, as subthreshold stimulation levels were used. Figure (with adjusted caption) taken from [37].

time and frequency.

Existing CI artifact suppression methods

Stimulation artifacts contaminating the EEG are a problem in various domains where electrical or magnetic stimulation is used, including deep brain stimulation, transcranial magnetic and current stimulation, somatosensory and cochlear implant stimulation.

Changes to the measurement set-up, such as maximum separation of stimulation and recording electrode leads, proper grounding of amplifier and subject, and careful skin preparation can help to reduce artifact amplitudes [64, 73].

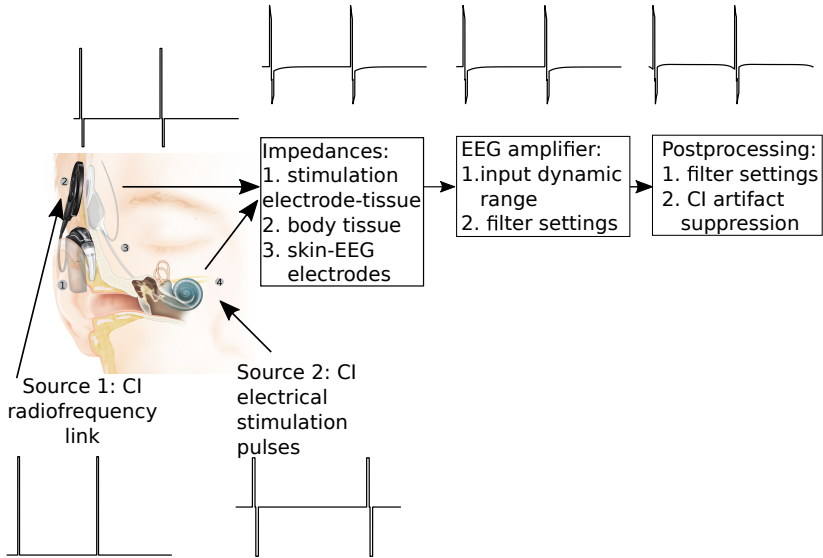


Figure 1.7: Block diagram showing CI artifact sources, and factors influencing the CI artifact characteristics.

However, none of these measures can completely prevent the presence of excessive stimulation artifacts in the EEG. Optimal reference electrode placement has been investigated for transient responses to cochlear implant stimulation [47], but optimal selection of reference electrode is highly subject dependent, and has not yet been assessed for artifact removal in EASSR measurements. Stimulus design can also help to avoid stimulation artifacts: responses to alternating polarity pulses have been averaged in order to reduce the stimulation artifact [75, 93], or short stimuli have been used such that the stimulation artifact has decayed before the response occurs [93]. Adjustments to the stimuli are not desirable, because we want to measure EASSRs to clinically used parameters. Therefore, stimulation is restricted to cathodic-first, biphasic pulses, with fixed pulse width and interphase gap, stimulated at high-rate and in MP mode.

Artifact elimination methods remove EEG channels or epochs that are contaminated with artifacts. This is done for example with ocular artifacts in the EEG. However, all epochs are affected by stimulation artifacts in EASSR measurements because of the continuous stimulation. Furthermore, most recording channels are affected by stimulation artifact. Therefore, artifact elimination methods, removing epochs or channels, are not appropriate for artifact removal in EASSR measurements, since almost all data would be rejected.

Several methods have been proposed for stimulation artifact minimization. Single channel techniques include frequency [2], time-frequency [124, 130, 151], or adaptive filtering [13, 14, 67, 78, 92, 111]. Template subtraction [43, 95, 145, 146] has also been investigated. In the case of EASSR, frequency domain filtering is inappropriate because the stimulation artifact has a component at the response frequency. For adaptive filtering and template subtraction, assumptions concerning the stimulation artifact shape or filtering process need to be made.

Interpolation methods [58, 63, 64, 65] have also been used. For time-restricted stimulation artifacts, a linear interpolation (LI) can be applied between a pre-artifact and post-artifact sample, effectively removing the stimulation artifact. This method is only successful if the interpulse interval (IPI) is longer than the stimulation artifact duration, and it has been validated for EASSR measurements in BP mode stimulation [65].

Multichannel techniques such as beamforming [149], principal component analysis (PCA) [93] and independent component analysis (ICA) [1, 47, 60, 80, 93, 147, 117, 119, 142, 143] were investigated in various domains. CI stimulation artifacts have successfully been removed from the EEG for transient responses using multichannel methods, but these methods have not yet been investigated for steady state responses. Clinically, multichannel EEG systems are expensive and require more subject preparation time.

Challenges for CI artifact suppression in EASSR measurements

The CI artifact duration, in combination with the IPI, determines whether LI can reliably be used for CI artifact suppression. Four main factors influence either the CI artifact duration, or the IPI. First, the pulse rate is inversely proportional to the IPI: LI is less likely to completely suppress CI artifacts at higher pulse rates. Second, the stimulation mode influences CI artifact characteristics: MP mode stimulation results in larger and longer CI artifacts than BP mode stimulation [69, 85]. Third, CI artifacts are usually shorter in recording channels that are placed further away from the CI electrode array and CI coil. Fourth, CI artifacts may be more significant in children than in adults. In children, due to the smaller head size, EEG signals may be CI artifact dominated even in the contralateral hemisphere. As children are the main target audience for objective CI fitting based on EASSR measurements, this is an important issue to consider.

Suppressing CI artifacts seems more challenging for EASSR recordings than for transient responses for three reasons. First, in EASSR recordings, the CI artifacts and EASSR overlap continuously in time. On the contrary, the CI

artifacts typically precede the neural response for transient responses, with only a limited overlap in time. Second, in EASSR recordings, due to the modulated and asymmetric CI artifacts, the CI artifacts and EASSR also have overlapping spectra. The EASSR is in fact not expected to have any frequency components that are not also present in the CI artifacts spectrum. Both signals have a component at the modulation frequency with different amplitude and phase. Third, EASSRs are typically obtained using direct stimulation with one stimulation channel. In studies investigating transient responses in CI subjects, responses are often obtained using free field stimulation with a loudspeaker. In this case, the stimulation pulses delivered to the electrode array are not as exactly controlled as is the case for direct stimulation, and multiple electrodes may be activated, even for narrow band stimuli, due to the maxima selection implemented in many clinical processors and the overlap of the filters of the array filter bank. Furthermore, the clocks of the stimulation and recording systems are not perfectly synchronized, such that in the recording epochs the CI stimulation artifact pulses may be slightly jittered. This leads to CI artifact attenuation when the jittered epochs are averaged. In previous studies, due to free field stimulation [47, 93, 142, 143], stimulation sequences are not identical nor perfectly aligned over recording epochs, resulting in attenuated CI artifacts when epochs are averaged to compute the event-related potential.

1.6 Outline of the thesis

In the previous section, CI artifact suppression methods for transient responses have been summarized and it was discussed that CI artifact suppression may be more challenging for steady state responses than for transients. With the aim of measuring EASSRs to clinically used stimuli, only cathodic-first, biphasic pulses, with fixed pulse width and interphase gap, stimulated at high-rate and in MP mode were used throughout this thesis. Existing methods may not sufficiently suppress CI artifacts in EASSR recording with clinically used stimulation parameters.

The aim of this research is two-fold. First, we aimed to characterize the CI artifacts and to investigate the feasibility of CI artifact suppression with linear interpolation for MP mode stimulation with clinical stimulation parameters. Second, we aimed to develop several methods for CI artifact suppression and for reliable EASSR parameter estimation in the presence of CI artifacts for clinically used stimulation. This thesis consists of four studies. One study considers the nature of CI artifacts. Methods for reliable EASSR parameter estimation in the presence of CI electrical artifacts are developed and evaluated in the remaining three studies.

CI artifacts are characterized in **Chapter 2**, based on the slope of the CI artifact amplitude growth function and on the CI artifact duration. The aim of the first study, presented in Chapter 2, is to characterize the CI artifact for modulated high-rate pulse trains stimulated in MP mode and to investigate the feasibility of CI artifact suppression with linear interpolation. Linear interpolation was chosen as the CI artifact removal method, because its efficiency has been demonstrated for BP mode stimulation, and it can be applied to single channel data which is useful for clinical applications. The CI artifact characterization will help to explore the feasibility of other CI artifact suppression methods. The influence of reference electrode position on the CI artifact characteristics and the operating limits of the interpolation method are investigated. The obtained results indicate that significant CI artifacts are present in most subjects. At contralateral recording electrodes, the artifact is shorter than the interpulse interval across subjects for stimulation at 500 pps, which was not always the case for 900 pps stimulation. Linear interpolation thus allows to suppress the CI artifact at contralateral recording channels for stimulation at 500 pps. This work has been published as Deprez, Hanne, *et al.* "Characterization of cochlear implant artifacts in electrically evoked auditory steady-state responses." *Biomedical Signal Processing and Control* 31 (2017): 127-138. In [53], EASSRs measurements were collected for 500 pps MP stimulation. Measurements were indeed response dominated in contralateral channels after linear interpolation. To measure EASSRs in adults for higher-rate stimulation or in ipsilateral recording channels, new CI artifact suppression methods must be developed. Furthermore, in children, due to their small head sizes, contralateral recording channels may also be severely distorted by CI artifacts.

The first alternative to LI for CI artifact suppression is based on independent component analysis (ICA). ICA has often been used to remove CI artifacts from the EEG to record transient auditory responses, such as cortical evoked auditory potentials. The aim of this study was to investigate how well CI artifacts are suppressed in EASSR measurements using ICA. Multichannel measurement systems are not routinely used in clinical practice. However, if the ICA based CI artifact suppression proves to be a robust method, the minimum number of recording channels needed for reliable CI artifact suppression could be determined, which could possibly be implemented in the clinics. The goal of ICA is to split multichannel signals in statistically independent components (independent component (IC)s), that represent either the neural response, CI artifacts, ocular or muscle artifacts, or neural background noise. In the second study, described in **Chapter 3**, an ICA-based CI artifacts attenuation method is developed and evaluated for EASSR measurements with varying CI artifacts and EASSR characteristics. Artifactual independent components (ICs) are automatically identified based on their spectrum. Three datasets are selected, with overlapping and non-overlapping CI artifacts, and EASSRs of various

signal to noise ratio (SNR). Given the challenges of using ICA for CI artifacts attenuation in EASSR measurements on the one hand, and the reported success of the method on the other hand, the aim of this study is to apply the method on several datasets, with a wide variety of CI artifacts and EASSR characteristics, in order to determine whether and in which conditions the method gives acceptable results. In the contralateral channels of high-SNR recordings, ICA results in the same EASSR amplitude and phase estimates as linear interpolation. For small EASSRs or large CI artifact amplitudes, ICA separation quality is insufficient to ensure complete CI artifacts attenuation without EASSR distortion. As the ICA approach is not very robust, the influence of the number of recording channels on the performance of ICA based CI artifact suppression was not systematically investigated and no recommendations for clinical implementations were made. One conference paper on this work has been published as Deprez, Hanne, *et al.* "Cochlear implant artifact rejection in electrically evoked auditory steady state responses." *Proc. European Signal Processing Conference (EUSIPCO)*, Lisbon, Portugal, Sep. 2014. A journal paper on this work is published as Deprez, Hanne, *et al.* "Independent component analysis for cochlear implant artifacts attenuation from electrically evoked auditory steady-state response measurements." *Journal of Neural Engineering* 15(1) (2018): 16006.

The ICA-based CI artifact suppression lacks robustness, as reliable results are not obtained for all subjects and all stimulation parameters. Furthermore, with ICA, multichannel data are needed, while expensive multichannel set-ups are not routinely used in clinical practice. In **Chapter 4**, a template subtraction (TS) method to remove continuous CI stimulation artifacts is developed. This single-channel method does not require a multichannel recording system, and is possibly more robust than ICA because no independence assumptions must be made. The template construction (TC) is based on an EEG recording containing CI stimulation artifacts but no synchronous neural response. The constructed templates are subtracted from the recording of interest. Response amplitudes and latencies are compared for the TS and LI method, and for different TC durations. TS with a TC duration of only 1 minute allows to suppress CI stimulation artifacts in individual contra- and ipsilateral EEG recording channels and to reliably estimate EASSR amplitudes and phases. This work has been published as Deprez, H. *et al.* "Template Subtraction to Remove CI Stimulation Artifacts in Auditory Steady-State Responses in CI Subjects." *IEEE Transactions on Neural Systems and Rehabilitation Engineering* 25(8) (2017): 1322-1331.

A Kalman filter (KF) has been used in [91] to estimate EASSR amplitudes in the presence of CI artifacts in contralateral recording channels for BP mode stimulation. This approach may pose significant advantages compared to the TS method. First, stationarity of the EASSR or the CI artifact is not assumed.

Second, no extra data is needed for the CI artifact template construction. The proposed state-space model was extended in **Chapter 5** to allow CI artifacts suppression for MP mode stimulation in contralateral and ipsilateral recording channels. The estimated EASSR amplitudes and phases were similar to those obtained with linear interpolation. The KF also results in correct EASSR phase estimates, and KF without inclusion of the CI artifact model is insufficient for correct EASSR parameter estimation. A report on this research has been submitted.

In **Chapter 6**, the results are summarized, additional insights are discussed and some suggestions for future work are given.

Chapter 2

Characterization of cochlear implant artifacts in electrically evoked auditory steady-state responses

Abstract

Objective: Electrically evoked auditory steady-state responses (EASSRs) are neural potentials measured in the EEG in response to periodic pulse trains presented, for example, through a cochlear implant (CI). EASSRs could potentially be used for objective CI fitting. However, EEG signals are contaminated with electrical CI artifacts. In this paper, we characterized the CI artifacts for monopolar mode stimulation and evaluated at which pulse rate, linear interpolation over the signal part contaminated with CI artifact is successful.

Methods: CI artifacts were characterized by means of their amplitude growth functions and duration.

This chapter is an adapted version of the article Deprez, Hanne, et al. “Characterization of cochlear implant artifacts in electrically evoked auditory steady-state responses.” *Biomedical Signal Processing and Control* 31 (2017): 127-138. Changes are limited to layout and representation aspects, and minor editing.

Results: CI artifact durations were between 0.7 and 1.7 ms, at contralateral recording electrodes. At ipsilateral recording electrodes, CI artifact durations are between 0.7 and 2 ms.

Conclusion: At contralateral recording electrodes, the artifact was shorter than the interpulse interval across subjects for 500 pps, which was not always the case for 900 pps.

Significance: CI artifact-free EASSRs are crucial for reliable CI fitting and neuroscience research. The CI artifact has been characterized and linear interpolation allows to remove it at contralateral recording electrodes for stimulation at 500 pps.

2.1 Introduction

A cochlear implant (CI) is an electronic device that can restore hearing in severely hearing impaired subjects. A CI system consists of three main parts: an external speech processor, the implant, and an electrode array inserted in the cochlea. The speech processor converts the incoming sound to an electrical stimulation pattern, which is transmitted to the implant via a radio frequency (RF) link. The electrodes stimulate the auditory nerve with biphasic charge-balanced pulses [86]. Two stimulation modes are often used, depending on the return electrode: bipolar mode for stimulation between intra-cochlear electrodes and monopolar mode for stimulation between intra- and extra-cochlear electrode(s). In clinical settings, pulses are often delivered at high rates in monopolar mode, which requires less battery power than stimulation in bipolar mode. Furthermore, threshold levels vary less over stimulation electrodes with stimulation in monopolar than in bipolar mode, resulting in easier CI fitting.

Since early implantation is proven crucial for speech and language development [11], an increasing number of severely hearing impaired infants receive a CI within the first year of life. Prior to CI activation, the threshold (T) and maximum comfortable (C) stimulation levels are determined based on behavioral (verbal) feedback. This is particularly challenging in infants and subjects who cannot give reliable behavioral feedback. In such cases, objective CI fitting based on electrophysiological measurements could be used.

Objective CI fitting based on electrophysiological measurements is currently under investigation. Transient responses to low-rate stimuli measured at the electrode-nerve interface (ECAPs) and at the brainstem level (EABRs) have been investigated as objective measures for threshold estimation. However, the threshold values obtained with these methods that use low-rate stimuli are

only moderately correlated with behavioral thresholds to high-rate pulse trains [17, 21, 70, 104].

Objective CI fitting based on electrically evoked auditory steady-state responses (EASSRs) is also being researched. EASSRs are neural steady-state responses to electrical stimuli with a periodicity, such as a modulated pulse train. They are the electrical analogue of auditory steady state responses (ASSRs), which are evoked acoustically, and can be recorded with head mounted scalp electrodes. ASSRs are the result of neural phase-locking to an auditory stimulus and the response is believed to result from different brain regions, depending on the repetition or modulation frequency of the stimulus (further called response frequency) [59, 115]). (E)ASSRs can be detected in the frequency domain at the response frequency by means of a statistical test, e.g., an F-test or a Hotelling T^2 test [41, 115].

EASSRs are corrupted by electrical stimulation artifacts, which can be caused by both the electrical stimulation pulses and the RF communication link between the external speech processor and the implant. The former can have a periodic component at the response frequency which may distort the neural response [65]. Figure 2.1 shows the EEG signal recorded on two channels in time and frequency domain, for subthreshold stimulation. Both EEG signals have a component at the modulation frequency, which is caused by the electrical stimulation since no neural response is assumed to be present. The spatial distribution of the spectral component at the modulation frequency is shown in the topography plot, indicating that the electrical stimulation artifact is present on all recording electrodes. The amount of distortion is highly subject-dependent, and is affected by the stimulation parameters and the recording electrode positions. Stimulation in monopolar mode results in larger CI artifacts than in bipolar mode [64, 85].

It was recently demonstrated that EASSRs in response to high-rate stimuli result in electrophysiological thresholds that correlate well with behavioral thresholds for stimulation in bipolar mode [65]. The next step is to evaluate threshold estimation based on EASSRs for clinically used parameters, in particular for stimulation in monopolar mode.

Stimulation artifacts contaminating the EEG are a problem in various domains where electrical or magnetic stimulation is used, including deep brain stimulation, transcranial magnetic and current stimulation, somatosensory and cochlear implant stimulation.

Changes to the measurement set-up, such as maximum separation of stimulation and recording electrode leads, proper grounding of amplifier and subject, and careful skin preparation can help to reduce artifact amplitudes [64, 73]. However, none of these measures can completely prevent the presence of excessive

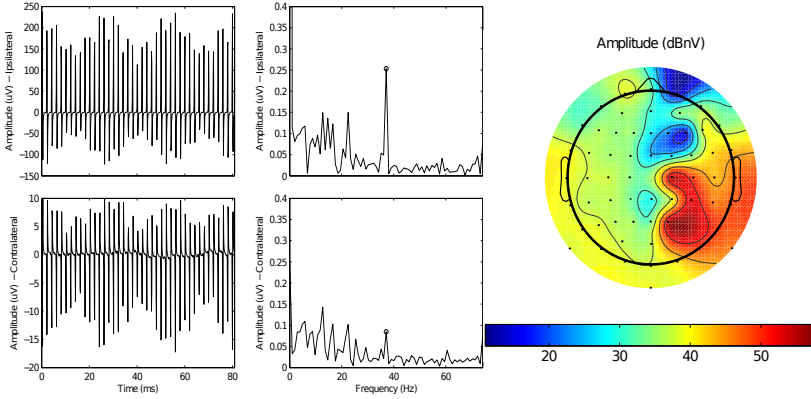


Figure 2.1: Example of a CI artifact for S8, with a CI at the right side, measured with 37 Hz AM 900 pps pulse trains at a subthreshold stimulation amplitude. Left: time and frequency domain signals at recording electrodes TP₈ (ipsilateral) and TP₇ (contralateral), referenced to C_z. Right: spatial distribution of spectral power at the modulation frequency, referenced to C_z. The units of the topography plot are $dBnV = 20 \log_{10} nV$, where $1 \mu V$ corresponds to $60 dBnV$ and $0.1 \mu V$ corresponds to $40 dBnV$. No neural response is expected to be present, as subthreshold stimulation levels were used.

stimulation artifacts in the EEG. Optimal reference electrode placement has been investigated for transient responses to cochlear implant stimulation [47], but optimal selection of reference electrode has not yet been assessed for artifact removal in EASSR measurements. Stimulus design can also help to avoid stimulation artifacts: responses to alternating polarity pulses have been averaged in order to reduce the stimulation artifact [75, 93], or short stimuli have been used such that the stimulation artifact has decayed before the response occurs [93]. Adjustments to the stimuli are not desirable in our case, because we want to measure EASSRs to clinically used stimuli. Therefore, stimulation is restricted to cathodic-first, biphasic pulses, with fixed pulse width and interphase gap, presented at high rates and in monopolar mode.

Artifact elimination methods remove EEG channels or epochs that are contaminated with artifact. This is done for example with ocular artifacts in the EEG. However, all epochs are affected by stimulation artifacts in EASSR measurements because of the continuous stimulation. Furthermore, most recording channels are affected by stimulation artifact. Therefore, artifact elimination methods are not appropriate for artifact removal in EASSR measurements, since almost all data would be rejected.

Several methods have been proposed for stimulation artifact minimization. Single channel techniques include frequency [2], time-frequency [130, 124, 151], or adaptive filtering [111, 67, 13, 14, 92, 78]. Template subtraction [145, 95, 43, 146] has also been investigated. In the case of EASSR, frequency domain filtering is inappropriate because the stimulation artifact has a component at the response frequency. For adaptive filtering and template subtraction, assumptions concerning the stimulation artifact shape or filtering process need to be made.

Interpolation methods [58, 64, 65, 63] have also been used. For time-restricted stimulation artifacts, an interpolation can be applied between a pre-artifact and post-artifact sample, effectively removing the stimulation artifact. This method is only successful if the interpulse interval is larger than the stimulation artifact duration, and it has been validated for EASSR measurements in bipolar stimulation mode.

Multichannel techniques such as beamforming [149], PCA [93] and ICA [47, 93, 143, 142, 1, 117, 147, 60, 80, 119] were investigated in various domains. CI stimulation artifacts have successfully been removed from the EEG for transient responses using multichannel methods, but these methods have not yet been investigated for steady state responses. Clinically, multichannel EEG systems are expensive and require more subject preparation time.

The aim of this study is to characterize the CI artifact for modulated high-rate pulse trains stimulated in monopolar mode and investigate the feasibility of stimulation artifact removal with linear interpolation. Modulated pulse trains are a model for the electrical pulse sequences after processing of speech in the CI processor. Linear interpolation was chosen as the CI artifact removal method, because its efficiency has been demonstrated for bipolar stimulation, and because it can be applied to single channel data. The CI artifact characterization will help to explore the feasibility of other above mentioned CI artifact removal methods. The influence of reference electrode position on the CI artifact characteristics and the operating limits of the interpolation method will be investigated.

2.2 Materials and methods

The CI artifact consists of two main parts from the RF communication link (the RF artifact) and from the electrical stimulation (the STIM artifact). The CI artifact is time-locked to the electrical stimulation pulses and can contain a frequency component at the modulation frequency [64, 65], as can be seen in Figure 2.1 for recorded data and Figure 2.2 for simulated cases. This may

result in distorted EASSR properties such as amplitude and phase and false positive EASSR detections.

In Cochlear Nucleus[®] implants, the stimulation amplitude of the pulses is nonlinearly encoded in the RF transmission and is therefore constant for stimulation pulses with different amplitudes [95, 152], whereas the STIM artifact amplitude is related to the stimulation pulses' amplitude. For stimulation with unmodulated pulse trains, both the RF and the STIM artifact are present at the response frequency (namely the repetition frequency of the stimulation pulses). For stimulation with high-rate modulated pulse trains, only the STIM artifact is present at the response frequency (namely the modulation frequency of the stimulation pulses). Furthermore if the STIM artifact is symmetric, no STIM artifact will be present at the response frequency, as can be seen in Figure 2.2. In the following, we only consider stimulation with high-rate modulated pulse trains. In this case, only the STIM artifact components are problematic for EASSR measurements as they may have a contribution at the modulation frequency.

The scaling of the CI artifacts with increasing stimulation amplitude is quantified by means of the slope of the CI artifact amplitude growth function (AGF). If the slope is zero, the CI artifacts do not scale with changing stimulation amplitude, which indicates that they will not be present at the modulation frequency. If CI artifacts are present at the modulation frequency, they can possibly be removed with a linear interpolation. However, this only works if the CI artifact is shorter than the interpulse interval. Therefore, the STIM artifact duration is also quantified.

EASSRs were measured in 11 subjects with a Cochlear Nucleus[®] CI with stimulation below the subject's behavioral threshold level. Details about subjects, stimulation and recording setup are described in Sec. 2.2.1, 2.2.2 and 2.2.3, respectively. CI artifact AGF intercepts and slopes and STIM artifact durations were determined for all subjects as described below in Sec. 2.2.4. All signal processing and statistical analyses were done in *MATLAB R2013a*.

2.2.1 Subjects

In total, 11 adult subjects participated in the experiments. They all had a Cochlear Nucleus[®] CI. Details can be found in Table 2.1. All subjects took part voluntarily and signed an informed consent form. The experiments were approved by the medical ethics committee of the University Hospitals Leuven (approval number B32220072126).

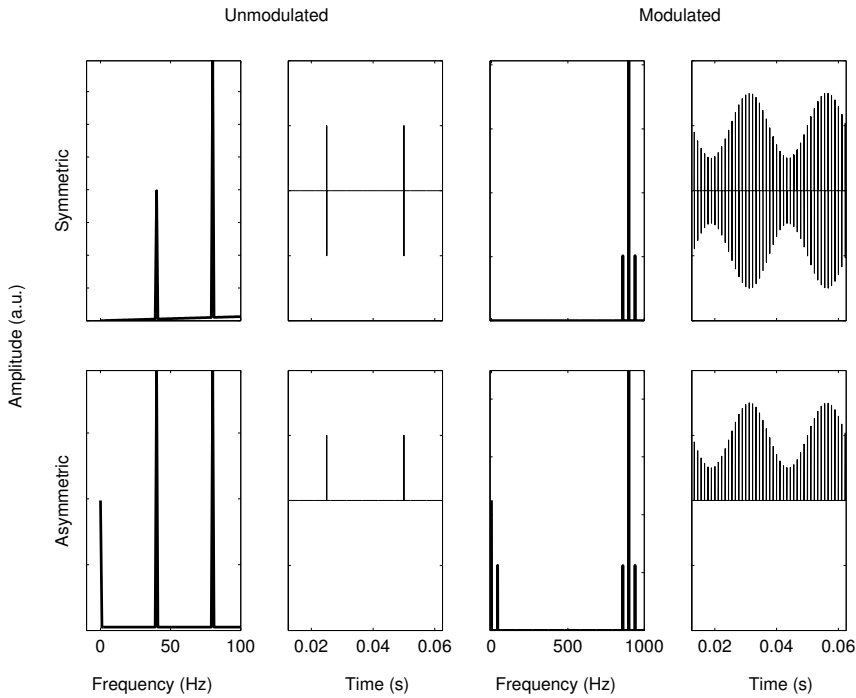


Figure 2.2: Simulated CI artifact spectrum for unmodulated pulse trains presented at a repetition frequency of 40 pps (left) and for high-rate (900 pps) 40 Hz AM pulse trains (right), in the case of symmetric (top) and asymmetric CI artifacts (bottom).

2.2.2 Stimulation setup

An in-house developed stimulation software platform generated the electrical stimulation pulse sequences with specified stimulation parameters, such as pulse rate, modulation frequency, stimulation electrode, etc. [64]. The electrical pulse sequences were sent to a programming device (POD) connected to a L34 research speech processor provided by Cochlear Ltd, thereby bypassing the subject's clinical speech processor.

Cochlear Nucleus[®] implants have two return electrodes outside the cochlea, i.e., the casing and the ball electrode. All subjects were stimulated in monopolar mode MP1+2, i.e., between an intracochlear electrode and the two extracochlear return electrodes which are electrically coupled [148]. An intracochlear electrode in the middle of the array was used: electrode 11 was used for all subjects

Table 2.1: List of subjects with Cochlear Nucleus[®] implant details. S: subject identifier; Sex: M: male, F: female; Age: age in years; Exp: CI experience in years; Side of implantation: R: right, L: left; PR: pulse rate tested.

S	Sex	Age	Exp	Implant type	Side	PR	
						500 pps	900 pps
S1	F	55	16	CI24R	L		x
S2	M	64	11	CI24R	L	x	x
S3	M	19	17	CI24M	L		x
S4	F	85	5.7	CI24R	L	x	x
S5	M	74	1.2	CI24RE	R		x
S6	M	52	1.7	CI24RE	R	x	
S7	M	64	16	CI24R	L	x	x
S8	M	52	1.9	CI24RE	R	x	x
S9	F	44	0.5	CI422	R	x	x
S10	F	77	1.9	CI24Re	L	x	
S11	F	63	2.5	CI24RE	R	x	

except S1, for whom electrode 13 was used. The stimuli consisted of amplitude-modulated (AM) pulse trains with modulation frequencies in the 40 Hz-range, which is often used for testing adults because large responses are expected here. Clinically used symmetric biphasic pulses with a pulse width of 25 μ s and an interphase gap of 8 μ s were used for stimulation.

Threshold and comfort levels were determined for stimulation with unmodulated (T_u and C_u) and AM pulse trains (T_m and C_m). The T level is the stimulation amplitude (in Cochlear clinical current units (cu), a unit of electrical current) that elicits a just perceivable auditory perception. The C level is the stimulation amplitude at perceived maximum comfortable loudness. For AM pulse trains, the determined T_m and C_m refer to the maximum amplitude of the AM pulse trains that result in a just perceivable auditory sensation and a maximally comfortable sound, respectively.

Two stimulation pulse rates were tested: 500 pps which is at the lower end of clinically used stimulation, and 900 pps which is the default pulse rate used in Cochlear Nucleus[®] implants. The stimuli were modulated with frequencies in the 40 Hz range. Subjects were stimulated at subthreshold stimulation pulse train intensities, with modulation depth equal to $\frac{C_m - T_u}{C_m + T_u}$, during 5 minutes.

2.2.3 Recording setup

To study the effect of reference electrode position, a 64-channel active-electrode BioSemi ActiveTwo DC EEG recording system was used. The system has a 24 bit resolution over a dynamic range of 524 mV_{PP} and a sampling rate of 8192 Hz was used. The recording setup has a built-in analog 5th order sinc low-pass filter with a cutoff frequency of 1638 Hz. Recording electrodes were placed on the subject's head according to the positions of the international 10-20 system [74]. A trigger signal was sent to the recording system for synchronization at the beginning of each recording epoch of 1.024 s. After EEG signal recording during 5 minutes, the signals were re-referenced offline to three commonly used reference schemes: average reference, vertex reference C_z, and forehead reference Fp_z.

The recordings were made in a soundproof and electrically shielded room. Subjects were seated in a comfortable chair and were asked to move as little as possible. A silent but subtitled movie of their choice was played, to guarantee the same attentional state across subjects and measurements.

2.2.4 CI artifact characterization

CI artifact amplitude growth

The CI artifact AGF $A(A_s)$ shows how the CI artifact amplitude A changes with increasing stimulation pulse amplitude A_s .

The CI artifact amplitude A_p was determined for every stimulation pulse. Let $x_p(t, c)$ be the EEG signal following pulse p (with stimulation amplitude $A_s(p)$ μA) at time t and channel c . In the following, we will make abstraction of the channel c as the method can be applied to every channel separately. A_p (in μV) was defined as the sum of the pulse's maximal and minimal amplitude.

$$A_p = |\max_t x_p(t) + \min_t x_p(t)| \quad (2.1)$$

For symmetrical artifacts, with equal negative and positive amplitudes, A_p will be zero. For asymmetrical artifacts, A_p will differ from zero.

For each stimulation pulse p stimulated at amplitude $A_s(p)$, the maximal and minimal EEG amplitudes were determined and summed, resulting in A_p . Next, these values were averaged for all pulses presented at the same stimulation amplitude, such that one CI artifact amplitude A is determined for each stimulation pulse amplitude A_s . In a first approximation, the CI artifact AGF $A(A_s)$ can be modeled as a linear function of A_s : $A(A_s) = mA_s + I$ with

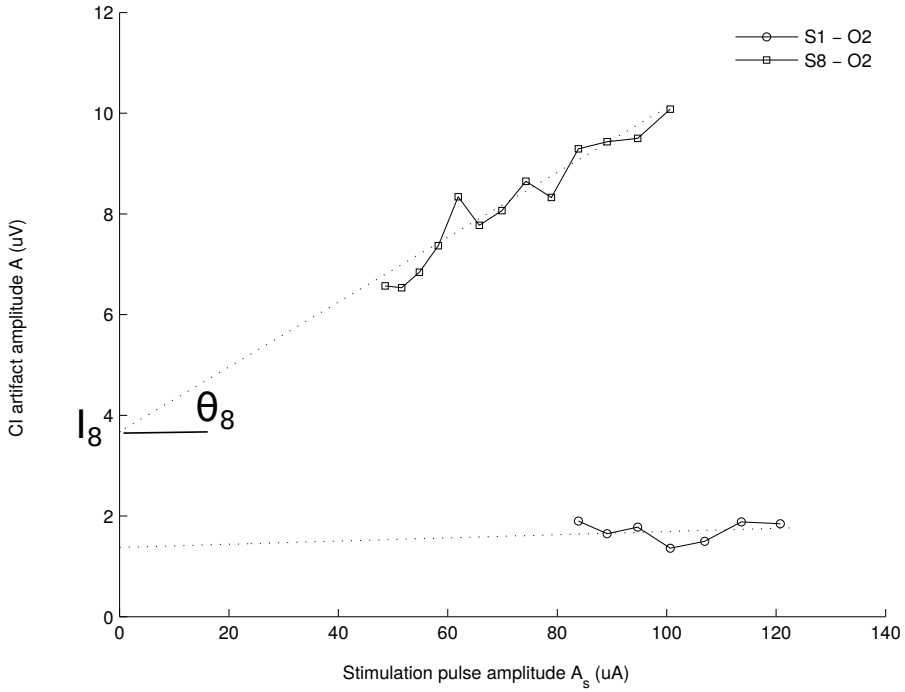


Figure 2.3: CI artifact AGFs for S1 and S8, measured with 37 Hz AM 900 pps pulse trains at a subthreshold stimulation amplitude, between an ipsilateral occipital electrode (O_2) and forehead reference electrode (Fp_z).

intercept I and slope $m = \tan(\theta^\circ)$, as shown in Figure 2.3. The best linear fit was determined for every channel with a least squares procedure, resulting in values for the intercept I and slope θ .

The intercept I represents asymmetric CI artifact components that are constant across stimulation pulse intensities; these artifact components are mainly caused by the RF artifact. The slope θ represents asymmetric CI artifact components that change with increasing stimulation pulse amplitude, namely the STIM artifact. If the CI artifact is symmetric, both θ and I will be zero. If θ is zero and I is non-zero, the CI artifact is mainly caused by RF transmission. If both θ and I are non-zero, the CI artifact consists of RF and STIM artifact. Only the STIM artifact components are problematic for EASSR measurements as these are the only components that have a contribution at the modulation frequency.

A slope of 1° corresponds to an increase of $0.017 \mu V/\mu A$. In this study, the stimulation amplitude range averaged over subjects is about $100 \mu A$. Therefore,

the amplitude difference between the largest and smallest pulse amplitude for $\theta = 1^\circ$ is $1.7 \mu V$ for an average subject. This is a large value, compared to the neural response which has amplitudes between 20 and 500 nV for average subjects in the 40 Hz range [65].

CI artifact AGFs were constructed for all subjects. Examples of such AGFs are shown in Figure 2.3. Pulse rates of 500 and 900 pps were used, although not all subjects were tested with stimulation at both pulse rates, as shown in Table 2.1. The DC bias was removed from the recorded EEG signals with a second-order 2 Hz high-pass filter and the EEG signals were re-referenced to either average reference, C_z , or Fp_z . The values of the intercept I and slope θ of the CI artifact AGF were determined for every recording channel and for different recording electrode configurations.

STIM artifact duration

Artifacts were removed by linear interpolation between a pre-stimulus and post-stimulus sample. The time between the pre- and post-stimulus samples is called the interpolation duration d . The maximum possible interpolation duration is defined as the interpulse interval, which is the inverse of the pulse rate, and equals 2 ms and 1.1 ms for stimulation at 500 and 900 pps, respectively. In this case, one sample per pulse period, the pre-stimulus sample, is retained. A linear interpolation was applied between the pre-stimulus sample at $-100 \mu s$ and post-stimulus samples varying between $+500$ and $+1900 \mu s$, in steps of $100 \mu s$ for 500 pps. For 900 pps, post-stimulus samples varying between $+500$ and $+900 \mu s$, were used, in steps of $100 \mu s$. The sampling rate is not an exact multiple of the pulse rate. Therefore, the start of a stimulation pulse is not exactly aligned to a sample. The start and end samples of the interpolation are calculated for each pulse separately, by rounding the start and end time of the interpolation to the nearest sample. Looking over the whole recording, the average time between the start of the interpolation interval and the start of a stimulation pulse is equal to the pre-stimulus interpolation duration. Equivalently, the average time between the start of a stimulation pulse and the end of the interpolation interval is equal to the post-stimulus interpolation duration. Post-stimulus samples before $+500 \mu s$ were not used, as the CI artifact peak lasts for about 500 μs , as can be seen in Figure 2.4.

After linear interpolation, the signals were filtered with a second-order 2 Hz high-pass filter, re-referenced to either average reference, C_z or Fp_z , and split into 1.024 s epochs. The 300 resulting epochs, corresponding to a 5 min recording length, were then averaged to reduce the noise level n . Then, the

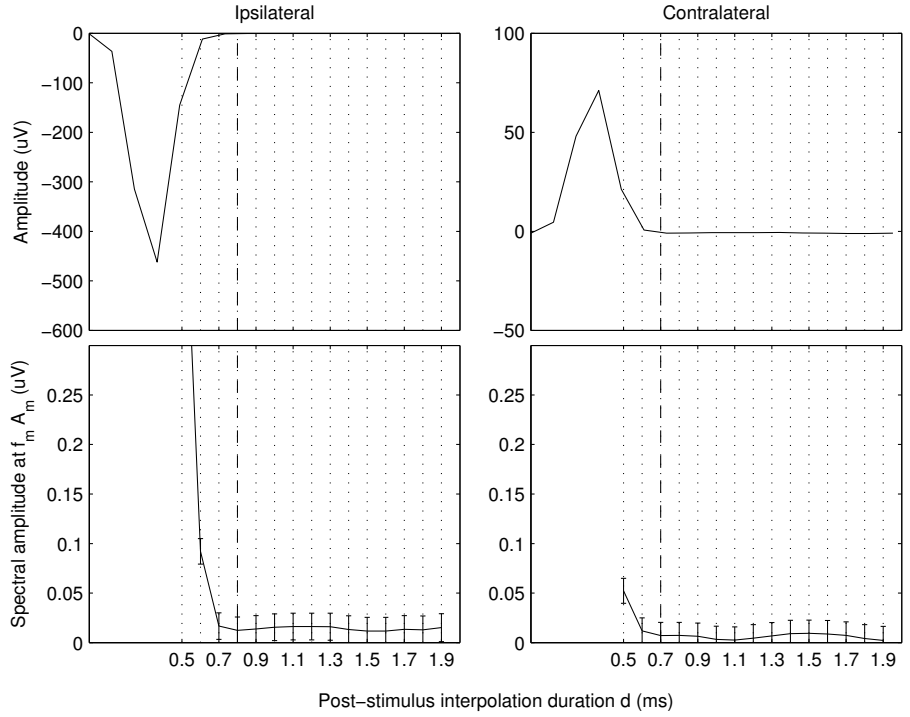


Figure 2.4: CI artifact pulse (top) and $A_m(d)$ AGF with increasing interpolation duration d for subject S2 (bottom). Stimulation below T level at 500 pps, for ipsi- and contralateral recording electrodes. The STIM artifact durations are indicated in dash-dotted lines. Reference electrode C_z .

resulting spectral amplitudes A_m at the modulation frequency in function of the interpolation duration d were determined, as illustrated in Figure 2.4.

When the interpolation duration is shorter than the STIM artifact, $A_m(d)$ may still contain some STIM artifact. However, $A_m(d)$ decreases with increasing interpolation duration, as a larger part of the STIM artifact is then canceled. When the interpolation duration is longer than the STIM artifact duration, $A_m(d)$ stabilizes at the neural response amplitude, namely the real EASSR amplitude. $A_m(d)$ stabilizes to the noise level, in our case, as no neural response is expected to be present for subthreshold stimulation.

An $A_m(d)$ AGF example is shown in Figure 2.4. The differences in A_m for increasing interpolation duration d were compared to the noise level after averaging n . The STIM artifact duration D was defined as the shortest

interpolation duration for which this difference did not exceed the subject dependent noise level n , which is approximately 50 nV.

$$D = d : [A_m(d) - A_m(d - 1)] < n \quad (2.2)$$

If $A_m(d)$ did not saturate, meaning that the difference in $A_m(d)$ was not smaller than the noise level for any interpolation duration d , the STIM artifact duration D was set equal to the maximal interpolation duration.

Statistical analyses

The intercept I and slope θ of the CI artifact AGF and the STIM artifact duration D were determined as described above for all recording electrodes and for three reference electrode configurations in all subjects. Left and right recording electrodes were switched for subjects with a CI at the right hand side, to put the results in the same figure for subjects with a CI at the left and right hand side. The resulting signals were averaged across all subjects to obtain the average CI artifact profile shown in Figure 2.5. This may give a blurred view, as CI artifacts may be localized slightly differently in all subjects.

In the following, only recording electrodes located in the posterior part of the head ($T_x, C(P)_x, P(O)_x, O_x, I_x$) were considered. For each subject, the median value of θ , I and D over the recording electrodes was determined. A statistical analysis investigating the effect of reference electrode, hemisphere, and pulse rate on θ , I and D was carried out. All effects are reported at a significance level of 5 %. The data were not normally distributed according to a Jarque-Bera test, and therefore only nonparametric tests were used. A Friedman analysis was used to investigate the effect of reference electrode on the CI artifact AGF slope and STIM artifact duration for each pulse rate and for each hemisphere. The effect of hemisphere was investigated using Wilcoxon signed rank tests (averaging the results for reference electrodes C_z and Fp_z). The influence of pulse rate on CI artifact AGF slope and STIM artifact duration was checked for each hemisphere (averaging the results for reference electrodes C_z and Fp_z), using Wilcoxon rank sum tests.

2.3 Results

2.3.1 CI artifact AGF slope and intercept

CI artifact AGF slopes and intercepts are shown in Figure 2.6 and 2.7. The CI artifact is symmetric if both θ and I are zero and this is only the case for

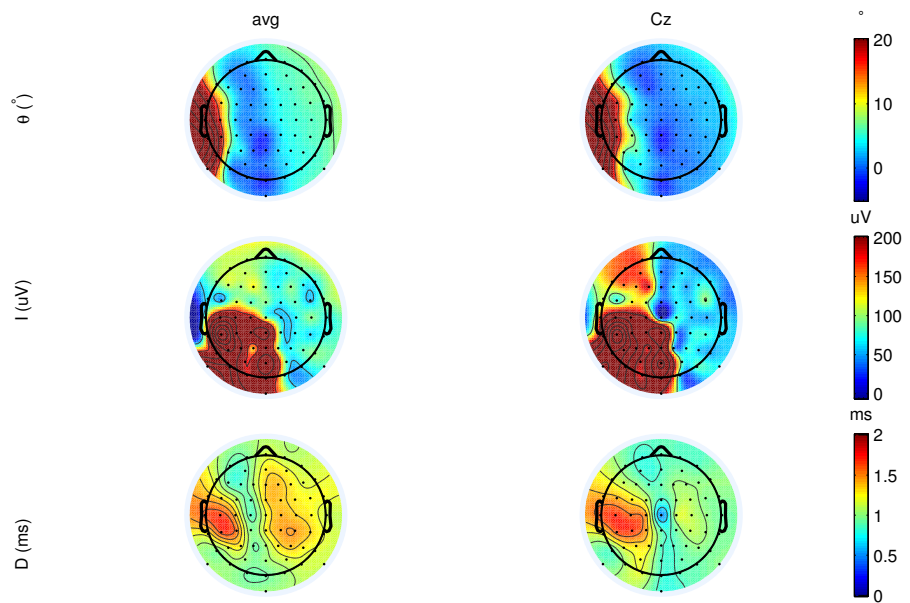


Figure 2.5: Mean slope θ and intercept I of the CI artifact AGF and mean STIM artifact duration, averaged over all subjects with recordings with stimulation at 500 pps. Average reference (left column) and reference electrode C_z (right column).

subject S1 (Figure 2.7).

Most subjects had a CI artifact AGF similar to that of subject S8 in Figure 2.3. The CI artifact slope is different from zero, which means that the STIM artifact contributes to the CI artifact.

The variability of the CI artifact AGF intercepts is smaller in the contralateral hemisphere than in the ipsilateral hemisphere. This is probably because these channels are located further away from the RF coil, and are thus less influenced by the RF artifact. However, in some subjects e.g., S9 and S11 for 500 pps and S8 and S9 for 900 pps, significant RF artifact seems to be present, as large CI artifact AGF intercepts are found in these subjects. However, the variability is small. It is assumed that the cause of the RF artifact on these recording channels is the re-referencing. If the reference contains significant RF artifact, this artifact is present and similar for all recording channels after re-referencing.

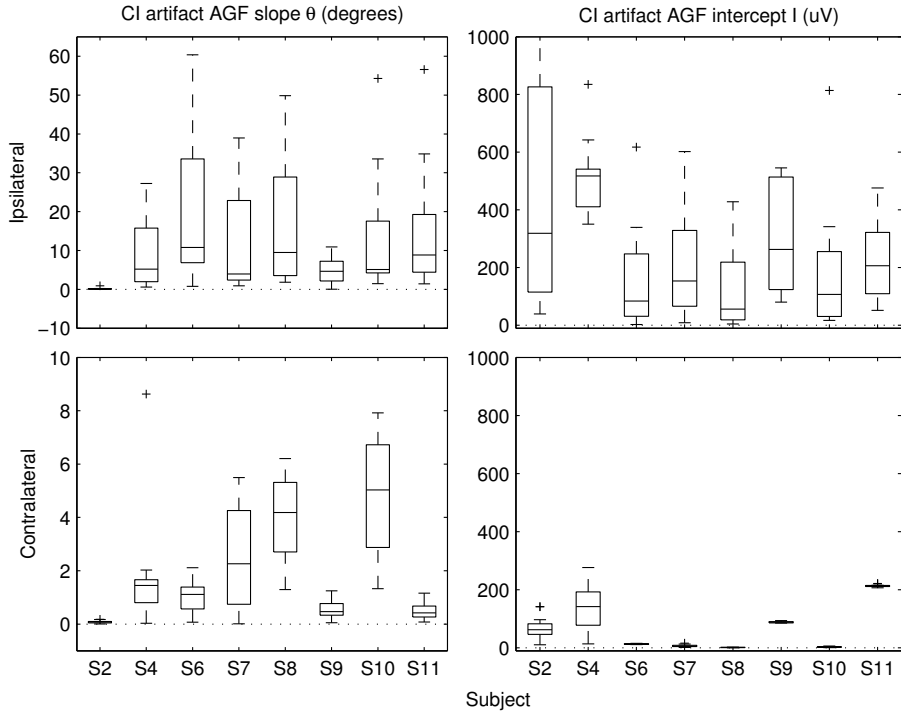


Figure 2.6: CI artifact AGF slope θ and intercept I for ipsi- and contralateral posterior recording electrodes for each subject with recordings with stimulation at 500 pps. Reference electrode C_z . The boxplot shows the median and 25th (q_1) and 75th percentiles (q_3) over the selected recording electrodes for each subject. Outliers (+) are all data points that fall outside the range $[q_1 \pm 1.5(q_3 - q_1)]$.

2.3.2 STIM artifact duration

Figure 2.8 shows STIM artifact durations D for each subject separately, on all ipsilateral and contralateral posterior recording electrodes respectively. For stimulation at 500 pps, the median STIM artifact duration at the ipsilateral posterior electrodes is 1.4 ms, although the STIM artifact duration is close to or longer than 2 ms at some electrodes in some subjects (Figure 2.8). For stimulation at 900 pps, the determined STIM artifact duration is equal to 1.1 ms in almost all subjects at ipsilateral recording electrodes. D is thus larger than the maximum possible interpolation duration.

At contralateral recording electrodes, the median STIM artifact duration is 0.9

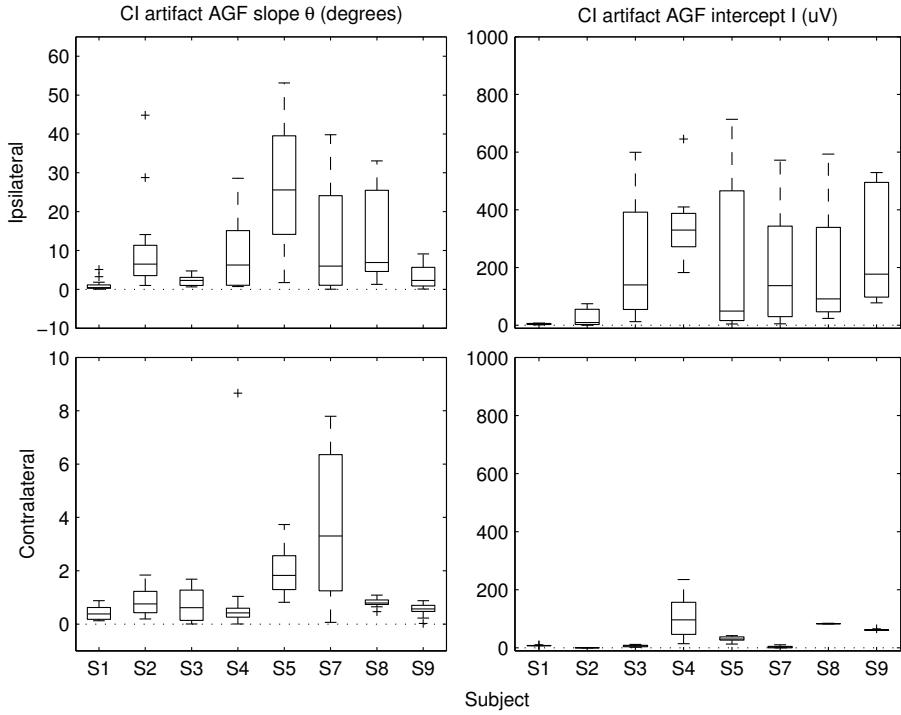


Figure 2.7: CI artifact AGF slope θ and intercept I for ipsi- and contralateral posterior recording electrodes for each subject with recordings with stimulation at 900 pps. Reference electrode C_z .

and 1 ms at 500 and 900 pps, respectively. For stimulation at 900 pps, D is close or equal to 1.1 ms in some subjects (Figure 2.8).

2.3.3 Influence of reference electrode and hemisphere

The slope θ and intercept I of the CI artifact AGF and the STIM artifact duration D are largest in the proximity of the implant (Figure 2.5). θ , I and D are larger in the contralateral hemisphere for average reference than for reference electrode C_z .

For stimulation at 500 pps, a significant influence of reference electrode on CI artifact AGF slopes was found in the ipsilateral ($\chi^2(2) = 7.8, p = 0.021$)

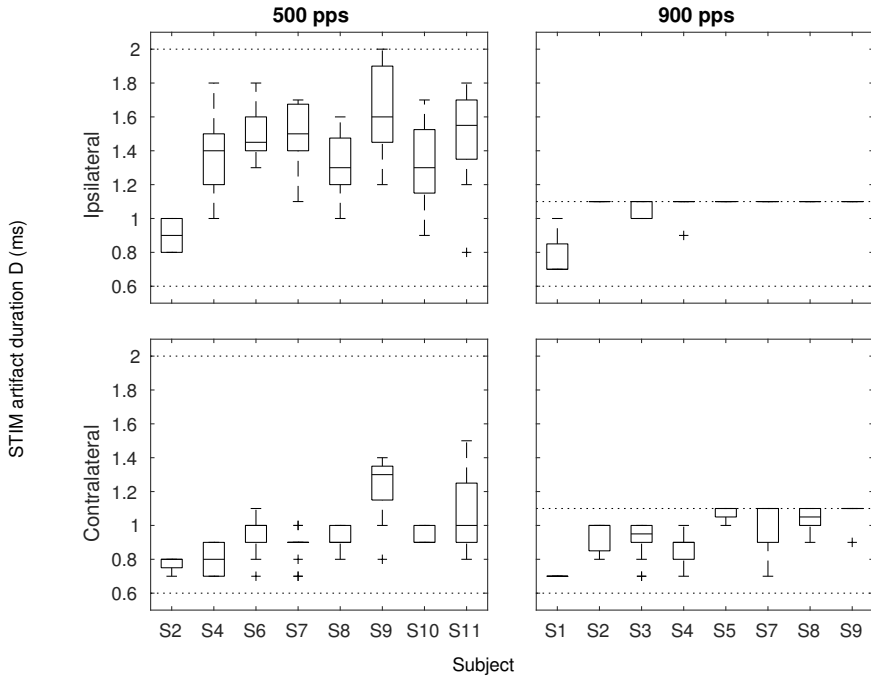


Figure 2.8: STIM artifact duration for ipsi- and contralateral posterior recording electrodes for each subject with recordings with stimulation at 500 pps and 900 pps. Reference electrode C_z . Dotted lines indicate the minimum and maximum possible interpolation duration at 500 and 900 pps.

and the contralateral hemisphere ($\chi^2(2) = 6.8, p = 0.034$), see Figure 2.9. In the ipsilateral hemisphere, larger CI artifact AGF slopes were found for the Fp_z reference electrode montage. In the contralateral hemisphere, more variation in CI artifact AGF slope is observed when reference electrode C_z is used compared to when reference electrode Fp_z is chosen. For stimulation at 900 pps, a significant influence of reference electrode on CI artifact AGF slopes was found in the ipsilateral hemisphere ($\chi^2(2) = 9, p = 0.011$) and in the contralateral hemisphere ($\chi^2(2) = 7, p = 0.030$).

For stimulation at 500 pps, a significant influence of reference electrode on CI artifact AGF intercept was found in the contralateral ($\chi^2(2) = 7, p = 0.030$), but not in the ipsilateral hemisphere ($\chi^2(2) = 1.0, p = 0.607$), see Figure 2.10. In the contralateral hemisphere, smaller CI artifact AGF intercepts

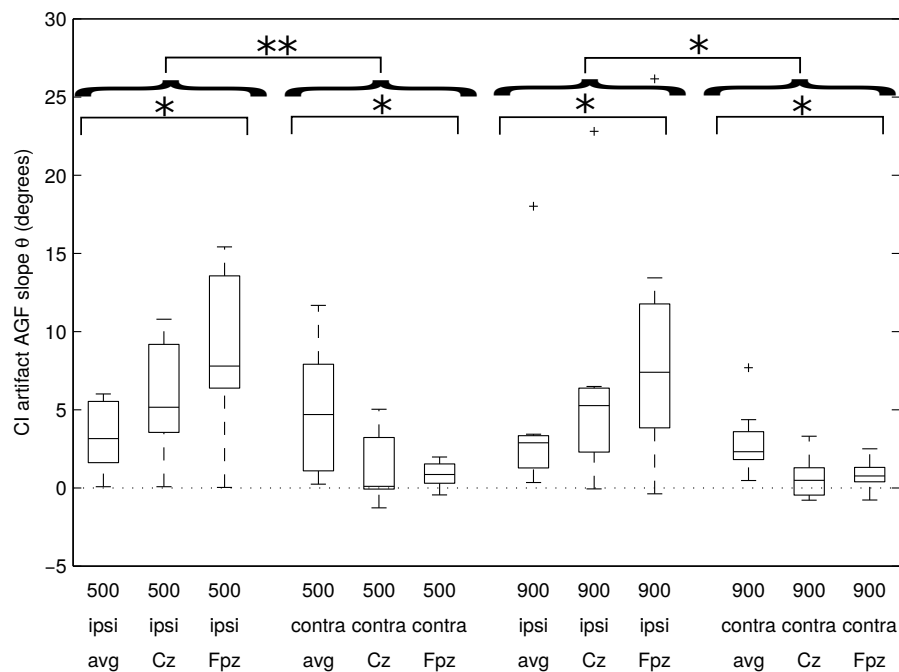


Figure 2.9: CI artifact AGF slope θ per pulse rate (500 and 900 pps), hemisphere (ipsi- and contralateral) and reference electrode (average reference, C_z and F_pz). The symbols *, **, and *** indicate that p-values are smaller than 0.05, 0.01, and 0.001, respectively.

were found for the F_pz reference. For stimulation at 900 pps, no significant influence of reference electrode on CI artifact AGF intercepts was found in the ipsilateral hemisphere ($\chi^2(2) = 1.75, p = 0.417$) or in the contralateral hemisphere ($\chi^2(2) = 0.75, p = 0.687$).

For stimulation at 500 pps, the reference electrode was found to have a significant influence on STIM artifact duration on ipsilateral ($\chi^2(2) = 6.1, p = 0.048$) and contralateral electrodes ($\chi^2(2) = 14.6, p < 0.001$). In the contralateral hemisphere, shorter STIM artifact durations were found for the F_pz reference. In the ipsilateral hemisphere, the STIM artifact duration is larger than the maximum possible interpolation duration for stimulation at 900 pps. Therefore the influence of reference electrode on the STIM artifact duration was only checked in the contralateral hemisphere. The reference electrode was found to have a significant influence on STIM artifact durations in the contralateral hemisphere ($\chi^2(2) = 13.0, p = 0.002$). Shorter STIM artifact durations were

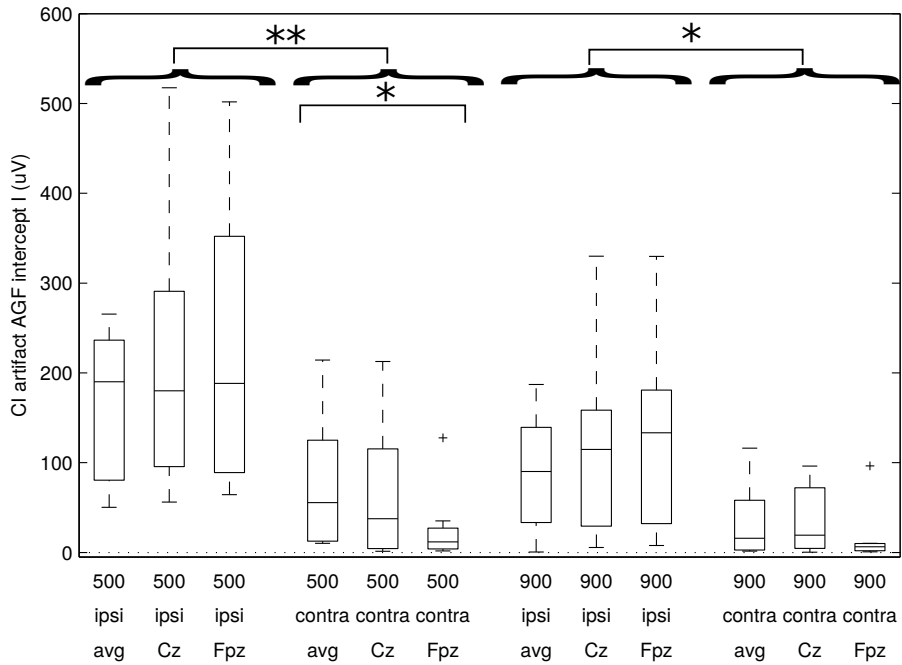


Figure 2.10: CI artifact AGF intercept I per pulse rate (500 and 900 pps), hemisphere (ipsi- and contralateral) and reference electrode (average reference, C_z and F_{pz}).

again found for the F_{pz} reference.

For stimulation at 500 pps there was a significant effect of hemisphere on CI artifact AGF slope, offset and STIM artifact duration ($p = 0.008$, $p = 0.008$, and $p = 0.008$, respectively). Prior to the statistical analysis results for reference electrodes C_z and F_{pz} were averaged. For these reference electrodes, the CI artifact AGF slope is smaller and STIM artifact duration is shorter in the contralateral hemisphere. For stimulation at 900 pps, a significant effect of hemisphere was found on the CI artifact AGF slope and intercept ($p = 0.016$ and $p = 0.016$, respectively), with smaller CI artifact AGF slopes and intercepts in the contralateral hemisphere. The effect of hemisphere on STIM artifact duration could not be investigated, as the STIM artifact duration is longer than the maximal interpolation duration in the ipsilateral hemisphere.

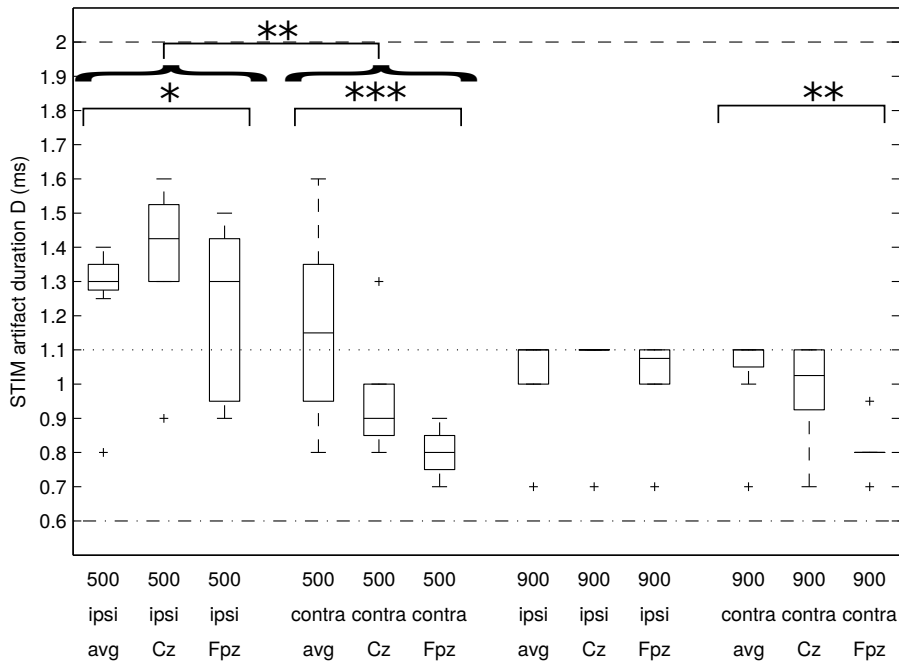


Figure 2.11: STIM artifact duration per pulse rate (500 and 900 pps), hemisphere (ipsi- and contralateral) and reference electrode (average reference, C_z and F_{pz}). Dashed and dotted lines indicate the maximum possible interpolation duration at 500 and 900 pps, respectively. The dash-dotted line indicates the minimum interpolation duration used for the analysis.

2.3.4 Influence of pulse rate

No significant influence of pulse rate on CI artifact AGF slope was found, for neither of the hemispheres ($p = 0.798$ and $p = 0.721$ for ipsi- and contralateral hemisphere, respectively). No significant influence of pulse rate on CI artifact AGF intercept was found, for neither of the hemispheres ($p = 0.235$ and $p = 0.328$ for ipsi- and contralateral hemisphere, respectively). No significant influence of pulse rate on STIM artifact duration was found in the contralateral hemisphere ($p = 0.343$). STIM artifact durations for both pulse rates could not be compared in the ipsilateral hemisphere, as the STIM artifact duration exceeded the maximum possible interpolation duration at 900 pps.

2.4 Discussion

In this study, the CI artifact was characterized based on three properties, namely, the CI artifact AGF slope and intercept and the STIM artifact duration. The CI artifact AGF slope and STIM artifact duration describe how the CI artifact scales with stimulation amplitude and how long it takes the STIM artifact to have decayed completely, respectively. Significantly larger CI artifact AGF slopes and intercepts and STIM artifact durations are found at ipsilateral recording electrodes than at contralateral ones. For electrodes positioned at the contralateral side, the reference electrode location can have an influence on the CI artifact AGF slope and intercept (for stimulation at 500 pps) and STIM artifact duration. No significant influence of pulse rate on any property has been found. Based on the STIM artifact durations (Figure 2.8), it should be possible to remove STIM artifacts at contralateral electrodes with a linear interpolation for stimulation at 500 pps. For stimulation at 900 pps, more advanced methods are needed.

It is not recommended to use average reference subtraction with CI stimulation. When the subtracted reference contains more artifact than the channel from which it is subtracted, the resulting signal in that channel could contain more CI artifact after reference subtraction than before. Large CI artifact signals present at some electrodes will bias the mean signal over channels, resulting in large CI artifacts at all channels after reference subtraction.

The reference electrode has not only an influence on the CI artifact characteristics, but also on the detected EASSR. The source of the EASSRs is oriented along a dipole. In order to record reliable EASSRs with maximal amplitudes, the analysis and reference electrodes should be placed on opposite sides along the axis of this dipole. The location of the EASSR source in the brain varies with varying modulation frequencies. EASSRs to modulation frequencies in the 40 Hz range (20–60 Hz) originate from sub-cortical sources [59]. Whether it is possible to adequately record EASSRs with a specific combination of analysis and reference electrodes thus depends on the selected modulation frequency. EASSRs were also recorded at suprathreshold stimulation levels for the same subjects, and for the modulation frequencies we tested in the 40 Hz range, it was still possible to record reliable EASSRs when reference electrode Fp_z was selected (data not presented). Reference electrode Fp_z is also often used in clinical auditory brainstem response (ABR) and ASSR measurements in infants [55]. It should be noted that referencing the data to Fp_z can lead to increased noise levels, resulting in reduced EASSR detections or requiring longer measurement times.

Only one subject had symmetric CI artifacts, that did not scale with increasing

stimulation amplitude. CI artifacts had a contribution at the modulation frequency for all other subjects.

The amplitude A_m at the modulation frequency, consisting of contributions from the STIM artifact and the neural response, reduces with increasing interpolation duration. The A_m difference for subsequent interpolation durations was compared to the noise level after averaging. The STIM artifact duration is the interpolation duration for which this difference becomes smaller than the noise level. Because we look at the saturation of A_m , and not at its absolute level, this method can also be applied to recordings with stimulation at suprathreshold levels. Furthermore, the time T over which the EEG signals were averaged plays an important role here, since the noise level is dependent on this. The noise level is reduced with a factor $\sqrt{2}$ each time the averaging time is doubled. The STIM artifact duration thus determines whether the STIM artifact can be removed by linear interpolation for recording time T . For longer recording times, the contribution of the STIM artifact may not be below the noise level and the STIM artifact is possibly not completely removed by applying linear interpolation.

For stimulation at 500 pps, the STIM artifact can be removed at contralateral recording electrodes with a linear interpolation. In the contralateral hemisphere, the variability of θ (for stimulation at 500 pps) and D was smaller for more frontal reference electrodes, see Figure 2.9 and Figure 2.11. Therefore, for recording electrodes in the contralateral hemisphere, the chance that the STIM artifact duration is longer than the maximum possible interpolation duration is reduced by choosing a more frontal reference electrode.

Linear interpolation is not sufficient to examine responses at ipsilateral recording electrodes or for stimulation pulse rates higher than 500 pps. Other stimulation artifact removal methods should therefore be examined. Further modeling of CI artifacts could allow template subtraction or adaptive filter design for CI artifact removal. Multichannel methods could possibly be used, with the disadvantage - for CI fitting purposes - that these require a more expensive setup and more subject preparation time.

Only subjects with Cochlear Nucleus® implants participated in this study. However, the stimulation artifacts caused by implants from other manufacturers should be examined, using the methods presented here. Differences can be expected, as other manufacturers use different clinical parameters.

In this study, a 64-channel recording set-up was used, which allowed to investigate the influence of reference electrode position on the CI artifact characteristics. Setups with less channels can usually be operated at higher sample rates and have low pass filters with higher cut-off frequencies, which

could result in shorter STIM artifact durations. The method presented in this study can still be used to determine the STIM artifact duration and the required interpolation duration.

In this study, subjects were only tested at subthreshold stimulation amplitudes. STIM artifact durations may be larger for suprathreshold stimulation amplitudes. Larger stimulation amplitudes may result in larger CI artifact amplitudes. Assuming that the decay constant does not change, it takes longer for larger CI artifact amplitudes to decay below the noise level. However, 11 subjects were tested, where the stimulation amplitudes used were just below the subject's behavioral T levels. The range of T levels observed in these subjects is quite diverse, resulting in maximum stimulation pulse amplitudes used between 108 and 190 cu, and between 86 and 167 cu for stimulation at 500 and 900 pps, respectively. We would argue that the results from this study are representative, since a wide variety of stimulation levels was used.

Here only one stimulation electrode in the middle of the array was used. Future research should focus on the influence of stimulation electrode position on CI artifact characteristics, which can be evaluated with the tools presented in this study.

2.5 Conclusion

In most subjects, the CI artifact was at least partly caused by the STIM artifact. Based on the data presented in Figure 2.5, 2.9, 2.10 and 2.11, it is not recommended to use average reference for EASSR measurements. CI artifact AGF slopes and intercepts and STIM artifact durations are larger in the contralateral hemisphere for the average reference configuration than C_z or Fp_z reference. In the contralateral hemisphere, the reference electrode has a significant influence on the CI artifact AGF slope and intercept for stimulation at 500 pps and on the STIM artifact duration. In the contralateral hemisphere, smaller variabilities in CI artifact AGF slopes (at 500 pps) and STIM artifact durations were observed when more frontal reference electrodes were used. STIM artifact durations were between 0.7 and 1.7 ms and 0.7 and 2 ms, at contralateral and ipsilateral recording electrodes, respectively. This should make it possible to remove the CI artifact at the contralateral recording electrodes with a linear interpolation in most subjects, for stimulation at 500 pps. For stimulation at 900 pps or for stimulation at 500 pps at ipsilateral recording electrodes, more advanced CI artifact attenuation methods are needed.

Chapter 3

Independent component analysis for cochlear implant artifacts attenuation from electrically evoked auditory steady-state response measurements

Abstract

Objective: Electrically evoked auditory steady-state responses (EASSRs) are potentially useful for objective cochlear implant (CI) fitting and follow-up of the auditory maturation in infants and children with a CI. EASSRs are recorded in the electro-encephalogram (EEG) in response to electrical stimulation with continuous pulse trains, and are distorted by significant CI artifacts related to this electrical stimulation. The aim of this study is to evaluate a CI artifacts

This chapter is an adapted version of the article Deprez, Hanne, et al. “Independent component analysis for cochlear implant artifacts attenuation from electrically evoked auditory steady-state response measurements.” *Journal of Neural Engineering* 15(1) (2018): 16006. Changes are limited to layout and representation aspects, and minor editing.

attenuation method based on independent component analysis (ICA) for three EASSR datasets.

Approach: ICA has often been used to remove CI artifacts from the EEG to record transient auditory responses, such as cortical evoked auditory potentials. Independent components (ICs) corresponding to CI artifacts are then often manually identified. In this study, an ICA-based CI artifacts attenuation method was developed and evaluated for EASSR measurements with varying CI artifacts and EASSR characteristics. Artifactual ICs were automatically identified based on their spectrum.

Main results: For 40 Hz amplitude modulation (AM) stimulation at comfort level, in high-SNR recordings, ICA succeeded in removing CI artifacts from all recording channels, without distorting the EASSR. For lower SNR recordings, with 40 Hz AM stimulation at lower levels, or 90 Hz AM stimulation, ICA either distorted the EASSR or could not remove all CI artifacts in most subjects, except for two of the seven subjects tested with low level 40 Hz AM stimulation. Noise levels were reduced after ICA was applied, and up to 29 ICs were rejected, suggesting poor ICA separation quality.

Significance: We hypothesize that ICA is capable of separating CI artifacts and EASSR in case the contralateral hemisphere is EASSR dominated. For small EASSRs or large CI artifact amplitudes, ICA separation quality is insufficient to ensure complete CI artifacts attenuation without EASSR distortion.

3.1 Introduction

Cochlear implants (CIs) can partially restore hearing in severely to profoundly hearing impaired subjects by electrically stimulating the auditory nerve with electrical pulse trains. The internal part consists of an electrode array with 12–22 electrodes inserted in the cochlea, and one or two extra-cochlear electrodes. Stimulation channels are either between two intra-cochlear electrodes (i.e., bipolar mode (BP)), or between an intra-cochlear and an extra-cochlear electrode (i.e., monopolar mode (MP)). Clinically, high-rate stimulation is used, i.e., ≥ 500 pulses per second (pps) [150]. Furthermore, MP stimulation is typically used to save battery life, as it requires less current than BP stimulation to elicit an equal loudness percept [155].

Prior to CI switch-on and during rehabilitation, minimum and maximum electrical stimulation levels (T and C levels), which vary across stimulation channels and CI subjects, must be determined during CI fitting. With MP stimulation, T and C levels vary less across stimulation channels compared

to BP stimulation, which is another reason that MP stimulation is clinically preferred. T and C levels are typically determined based on behavioral feedback, that is not easily obtained from children and subjects with additional disabilities. Objective CI fitting based on electrophysiological measures is therefore under investigation.

Electro-encephalogram (EEG) recordings, which have a high temporal and reasonable spatial resolution, have often been used to study objective CI fitting [17, 65, 64] and auditory plasticity in CI subjects [48, 52, 51, 127, 128, 129]. Transient responses, i.e., electrically evoked compound action potentials (ECAPs), cortical auditory evoked potentials (CAEPs) and electrically evoked auditory brainstem responses (EABRs), as well as electrically evoked auditory steady-state responses (EASSRs) have successfully been measured in CI subjects [47, 53, 64, 65, 103, 142, 143, 149].

EASSRs are potentially useful for objective CI fitting, and for studying temporal processing, auditory maturation and brain plasticity in adults and infants with a CI. (E)ASSRs are neural auditory steady-state responses, present in the EEG, which result from neural phase-locking to a periodic stimulus [115]. EASSRs can be evoked with continuous electrical stimulation [64, 65], either with unmodulated low-rate or modulated high-rate pulse trains. Most speech coding strategies used in modern CIs use envelope coding to convey information of the speech signal to the CI user. The envelopes of a series of band pass filters are used to modulate high-rate pulse trains, and each of these modulated high-rate pulse trains is applied to a CI stimulation channel corresponding to the center frequency of the band pass filter. Modulated pulse trains are therefore a model of the electrical pulse sequences after processing of speech by the CI processor.

EASSRs offer a number of advantages compared to transient responses. First, EASSRs are responses elicited by frequency-specific stimuli, activating one stimulation channel. On the other hand transient responses are often evoked with non-frequency specific stimuli, and with free field stimulation, activating multiple stimulation channels. However, it should be noted that transient responses may also be evoked using narrow-band stimuli and direct stimulation. Second, EASSRs can objectively be detected at f_m , e.g., using an F-test or a Hotelling T^2 test [41, 64, 65, 66], while transient responses are typically assessed subjectively by examining the latency and amplitude of visually identified peaks. Although statistical methods could be used for objective detection of transient responses, this is not routinely used in research or in the clinic. Third, EASSRs can be elicited using high-rate stimulation, while ECAPs and EABRs are traditionally measured with low-rate stimulation. T and C levels vary with stimulation rate [98, 99], and are therefore ideally determined with the clinically used stimulation rate. Although this is not impossible, it is not straightforward

to record ECAPs and EABRs with clinically used stimulation rates. T levels determined with ECAPs and EABRs, using low-rate stimuli, are only moderately correlated with behavioral T levels [17, 70]. T levels determined with EASSRs, using high-rate stimulation, correlate well with behavioral T levels, at least for stimulation in BP mode [65]. The next step is to evaluate T level determination based on EASSRs for clinically used high-rate MP stimulation in MP mode.

However, the electrical stimulation produced by the CI results in electrical artifacts in the EEG (see characterization in [37]) that should be removed before further EEG signal processing. Asymmetric CI artifacts result in components at f_m , distorting the EASSR. The amount of distortion is highly subject, and stimulation parameter dependent [37]. Factors that may influence CI artifacts shape, amplitude and duration include, but are not limited to, (1) the stimulation mode, (2) the stimulation level, (3) the relative placement of stimulation electrode and ball and casing electrodes, (4) the CI electrode-tissue interface impedance, (5) the skin-gel-EEG electrode interface impedance, and (6) the recording reference electrode. A CI artifacts example is given in Figure 3.1.

CI artifacts are larger with stimulation in MP mode compared to BP mode [69, 85]. A linear interpolation (LI) method, interpolating the signal part contaminated with CI artifacts, has been used to remove CI artifacts from EASSRs with stimulation in BP mode [58, 64, 65]. This is only possible when the CI artifacts duration is shorter than the interpulse interval (IPI), i.e., the inverse of the stimulation rate f_c . It has recently been shown [37], for Cochlear Nucleus® implants, that overlapping CI artifacts are present in ipsilateral channels for 500 pps MP stimulation, and in ipsi- and contralateral recording channels for 900 pps MP stimulation. Non-overlapping CI artifacts can be removed from contralateral recording channels with LI for stimulation in MP mode with rates up to 500 pps [37, 53]. In [91] a Kalman filter has been developed that can remove non-overlapping CI artifacts from EASSRs with stimulation in BP mode at 900 pps. Recently, a template subtraction method has been proposed in [38] that has been evaluated for measurements with overlapping CI artifacts and high-SNR EASSRs. In [40] an independent component analysis (ICA) based method has been presented that attenuates CI artifacts in EASSR recordings in one subject for 900 pps MP stimulation. To our knowledge, no other CI artifacts attenuation methods have been developed for EASSR recordings with overlapping CI artifacts.

For transient responses (EABRs and CAEPs), many CI artifacts attenuation methods have been proposed, and a summary is included in [37]. ICA belongs to the most investigated CI artifacts attenuation methods for transient responses, and has successfully been applied in [23, 24, 25, 32, 47, 122, 123, 143, 142], although one case has also been reported where the ICA method does not

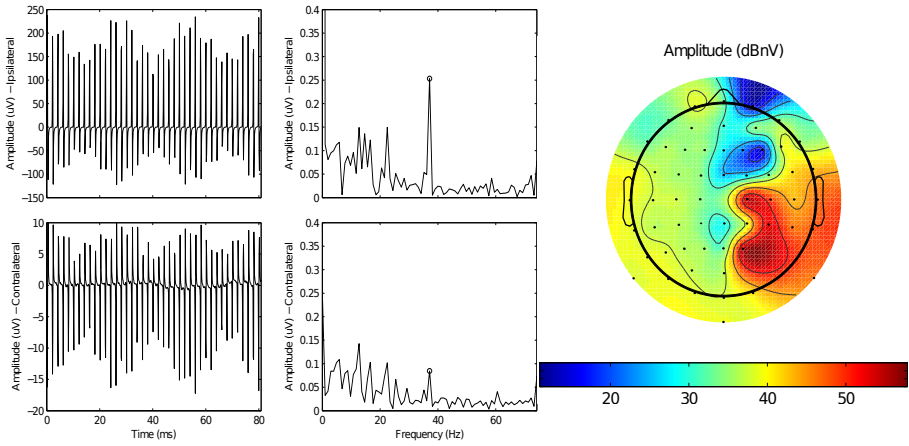


Figure 3.1: Example of CI artifacts for a subject, with a CI at the right side, measured with 37 Hz AM 900 pps pulse trains at a subthreshold stimulation amplitude. Left: time and frequency domain signals at recording electrodes TP₈ (ipsilateral) and TP₇ (contralateral), referenced to C_z. Right: spatial distribution of spectral power at the modulation frequency, referenced to C_z. The units of the topography plot are $\text{dBnV} = 20 \log_{10} \text{nV}$, where $1 \mu\text{V}$ corresponds to 60 dBnV and $0.1 \mu\text{V}$ corresponds to 40 dBnV . No neural response is expected to be present, as subthreshold stimulation levels were used. Figure (incl. caption) taken from [37].

produce satisfactory results [93]. The goal of ICA is to split multichannel signals in statistically independent components (ICs), that represent in this case either the EASSR, CI artifacts, ocular or muscle artifacts, or neural background noise. In most studies, ICs representing CI artifacts are manually identified based on temporal and spatial characteristics, and are then rejected. Although CI artifacts are sufficiently attenuated to study the transient response, it has also been reported that residual CI artifacts are still observable [47, 143, 142]. Furthermore, CI artifacts are usually expressed on multiple ICs, ranging from 2 to 15 ICs [8, 32, 47, 105, 143]. Note, however, that the number of recording channels used in the above mentioned studies also differs.

Motivated by the success of ICA-based CI artifacts attenuation methods for transient responses, an ICA-based CI artifacts attenuation method for EASSRs with automated IC selection has been developed in [40], and compared to the LI method in one subject. This study aims to apply and evaluate this method in a larger pool of subjects, and for different stimulation parameters. Three datasets were selected, with overlapping and non-overlapping CI artifacts, and EASSRs

of various SNRs. The first dataset contains high-SNR EASSRs, elicited by 40 Hz AM 500 pps pulse trains presented at C level, resulting in non-overlapping CI artifacts in contralateral recording channels. The second dataset was acquired in the same subjects, and contains no or low SNR EASSRs, elicited by 90 Hz AM 500 pps pulse trains presented at C level. Again, non-overlapping CI artifacts are present in contralateral recording channels. The last dataset consists of EASSRs with various SNRs, elicited by 40 Hz AM 900 pps pulse trains presented at various stimulation levels. CI artifacts mostly overlap in these measurements. For non-overlapping CI artifacts, the results obtained with the ICA-based CI artifacts attenuation method are compared to the results obtained with LI. Given the challenges of using ICA for CI artifacts attenuation in EASSR measurements on the one hand, and the reported success of the method for cortical responses on the other hand, we do not formulate any hypothesis concerning the performance of the method. The aim of this study was to apply the method on several datasets, with a wide variety of CI artifacts and EASSR characteristics, in order to determine whether the method gives acceptable results.

3.2 Materials and methods

3.2.1 Datasets

Three datasets, with overlapping and non-overlapping CI artifacts, and containing EASSRs with various SNRs, were used to evaluate the ICA-based CI artifacts attenuation method. For all three datasets, all subjects wore Cochlear Nucleus[®] implants, see Table 3.1.

The first two datasets, with non-overlapping CI artifacts, are adopted from [53], where modulation frequency transfer functions (MFTFs) have been acquired for six adult post-lingually deafened CI subjects in two frequency ranges. In the MFTF datasets, stimulation at $f_c = 500$ pps was used, where LI successfully removes CI artifacts in contralateral recording channels [53]. In the contralateral recording channels, the EASSRs obtained with the ICA method can therefore be compared to the baseline measures obtained with LI.

The third dataset, with overlapping CI artifacts, was collected specifically for this study, where amplitude growth functions (AGFs) have been measured in seven adult post-lingually deafened CI subjects. In the AGF dataset, the clinical pulse rate of $f_c = 900$ pps for Cochlear Nucleus[®] implants was used, resulting in mostly overlapping CI artifacts. No baseline EASSR measures are thus available for this dataset.

Five minute recordings were made in a soundproof and electrically shielded room. Subjects were seated in a comfortable chair and were asked to move as little as possible. A subtitled movie of their choice was played, to guarantee the same attentional state across measurements.

MFTF datasets

Two parts of the dataset described in [53] were used to evaluate the ICA-based CI artifacts attenuation method. EASSRs were recorded for a f_m wide range, between 1 and 100 Hz, during multiple recording sessions. Amplitude modulated (AM) high-rate $f_c = 500$ pps pulse trains were presented in MP mode, between intracochlear electrode 11 and the two extra-cochlear electrodes (MP1+2), at maximum comfort level. T and C levels were determined for stimulation with unmodulated pulse trains (T_u and C_u), as well as the C level for stimulation with AM modulated pulse trains (C_m) with minimal level T_u . The stimuli were AM pulse trains, modulated in amperes between T_u and C_m .

The EEG was recorded with a 64-channel ActiveTwo Biosemi system, with a sampling rate of 8192 Hz and a built-in low pass filter with 1638 Hz cutoff. At the start of each 1.024 s epoch, triggers were sent to the recording system. Modulation frequencies were rounded such that each epoch contained an integer number of modulation cycles, and such that the modulation phase was the same at the start of each epoch. In the following, modulation frequencies are rounded to the nearest integer for easier representation.

EASSRs were prominently present in all subjects, for f_m between 30 and 50 Hz [53]. Significant 80–100 Hz f_m EASSRs could only be detected in a limited number of measurements: this could possibly be related to the limited recording duration, the age of the subjects, or the long period of auditory deprivation in these subjects [53]. More details can be found in [53].

Here, per subject, seven recordings with f_m between 30 and 51 Hz with high-SNR EASSRs (further called 40 Hz modulation frequency transfer function (MFTF) dataset), and eight recordings with f_m between 80 and 100 Hz with absent or low SNR EASSRs (further called 90 Hz MFTF dataset), were used for the evaluation of the ICA-based CI artifacts attenuation method. In subject S06, only four recordings with f_m between 80 and 100 Hz were acquired due to time constraints during the first recording session.

AGF dataset

With objective CI fitting in mind, EASSR amplitude growth functions (AGFs) were measured with $f_c = 900$ pps MP stimulation. If the CI artifacts can be attenuated successfully, objective T levels can be determined from these data. Again, T and C levels were determined behaviorally for stimulation with unmodulated pulse trains (T_u and C_u). The C level for AM modulated pulse trains with minimal level T_u was determined (C_m). The modulation depth (MD) was then fixed to $MD = \frac{C_m - T_u}{C_m + T_u}$, and the T level for AM modulated pulse trains was determined (T_m). The stimuli were 37 Hz and 42 Hz AM pulse trains with fixed modulation depth MD at different stimulation levels, ranging from below T_m to C_m . Modulation frequencies were again adjusted such that each epoch contains an integer number of modulation cycles, but in the report integer values for f_m will be used. Stimulation levels were selected per subject, according to the testing time. In the following, stimulation levels SL are expressed in %dynamic range (DR), defined as $100 \frac{SL - T_m}{C_m - T_m}$. Hence, 0%DR corresponds to stimulation at T_m . Recordings were obtained with the same recording system as in [53], described in Section 3.2.1.

3.2.2 Signal processing

The raw signals $x[t, c]$, with t the time index and c the recording channel index, were stored in a matrix $\in \mathbb{R}^{N_t \times N_c}$, with N_t and N_c the number of time samples and channels, respectively.

Two recording channel sets were defined for analysis: (1) $c_L = \{\text{CP}_5, \text{P}_5, \text{P}_7, \text{P}_9, \text{PO}_4, \text{PO}_7, \text{TP}_7, \text{and O}_1\}$ in the left hemisphere, and (2) $c_R = \{\text{CP}_6, \text{P}_6, \text{P}_8, \text{P}_{10}, \text{PO}_4, \text{PO}_8, \text{TP}_8, \text{and O}_2\}$ in the right hemisphere, as shown in Figure 3.2. As in [53, 38], channels located on top of the CI, and channels with excessive noise levels, were excluded from the analysis. The set of channels used is detailed in Table 3.1. Subjects S02 and S04 were included in the MFTF datasets, as well as the AGF dataset. The channel sets used for analysis of the datasets differ, due to different placement of the electrode cap in recording sessions taking place on different dates. Three different signal processing methods were assessed: (1) no CI artifacts attenuation (NO); (2) linear interpolation (LI); (3) ICA-based CI artifacts attenuation (ICA). Note that most recording channels were included for the ICA decomposition, see also Section 3.2.2, and that the channels sets in Table 3.1 are merely used for analysis. The first two processing methods are very similar to the methods described in [38].

Table 3.1: Subject details, including reference channel (Ref) and set of channels (c_C and c_I) used for analysis in the contralateral (C) and ipsilateral (I) hemisphere per subject, for MFTF and AGF datasets.

S (R/L)	Type	Ref	C (c_C)	I (c_I)
MFTF				
S01 (R)	CI24RE	C _z	CP ₅ , P ₅ , P ₇ , P ₉ , PO ₃ , PO ₇ , TP ₇ , O ₁	CP ₆ , PO ₄ , O ₂
S02 (R)	CI24RE	C _z	CP ₅ , P ₅ , P ₇ , P ₉ , PO ₃ , PO ₇ , TP ₇ , O ₁	CP ₆ , PO ₄ , O ₂
S03 (L)	CI24RE	C _z	CP ₆ , P ₆ , P ₈ , P ₁₀ , PO ₄ , PO ₈ , TP ₈ , O ₂	CP ₅ , P ₅ , PO ₇ , O ₁
S04 (R)	CI422	Fp _z	CP ₅ , P ₅ , P ₇ , P ₉ , PO ₃ , PO ₇ , TP ₇ , O ₁	CP ₆ , PO ₄ , O ₂
S05 (R)	CI24RE	Fp _z	CP ₅ , P ₅ , P ₇ , P ₉ , PO ₃ , PO ₇ , TP ₇ , O ₁	PO ₄ , O ₂
S06 (L)	CI24RE	C _z	CP ₆ , P ₆ , P ₈ , P ₁₀ , PO ₄ , PO ₈ , TP ₈ , O ₂	CP ₅ , P ₅ , PO ₃ , PO ₇ , O ₁
AGF				
S02 (R)	CI24RE	C _z	CP ₅ , P ₅ , P ₇ , P ₉ , PO ₄ , PO ₇ , TP ₇ , O ₁	CP ₆ , P ₁₀ , TP ₈ , O ₂
S04 (R)	CI422	C _z	CP ₅ , P ₅ , P ₇ , P ₉ , PO ₄ , PO ₇ , TP ₇ , O ₁	CP ₆ , P ₆ , PO ₄ , PO ₈ , O ₂
S07 (L)	CI24R	C _z	CP ₆ , P ₆ , P ₈ , P ₁₀ , PO ₄ , PO ₈ , TP ₈ , O ₂	CP ₅ , P ₅ , P ₇ , P ₉ , PO ₄ , PO ₇ , TP ₇ , O ₁
S08 (L)	CI24M	C _z	CP ₆ , P ₆ , P ₈ , P ₁₀ , PO ₄ , PO ₈ , TP ₈ , O ₂	CP ₅ , P ₅ , PO ₃ , O ₁
S09 (L)	CI24R	C _z	CP ₆ , P ₆ , P ₈ , P ₁₀ , PO ₄ , PO ₈ , TP ₈ , O ₂	CP ₅ , P ₅ , PO ₃ , TP ₇ , O ₁
S10 (L)	CI24RE	C _z	CP ₆ , P ₆ , P ₈ , P ₁₀ , PO ₄ , PO ₈ , TP ₈ , O ₂	CP ₅ , PO ₃ , O ₁
S11 (L)	CI24R	C _z	CP ₆ , P ₆ , P ₈ , P ₁₀ , PO ₄ , PO ₈ , TP ₈ , O ₂	CP ₅ , PO ₃ , O ₁

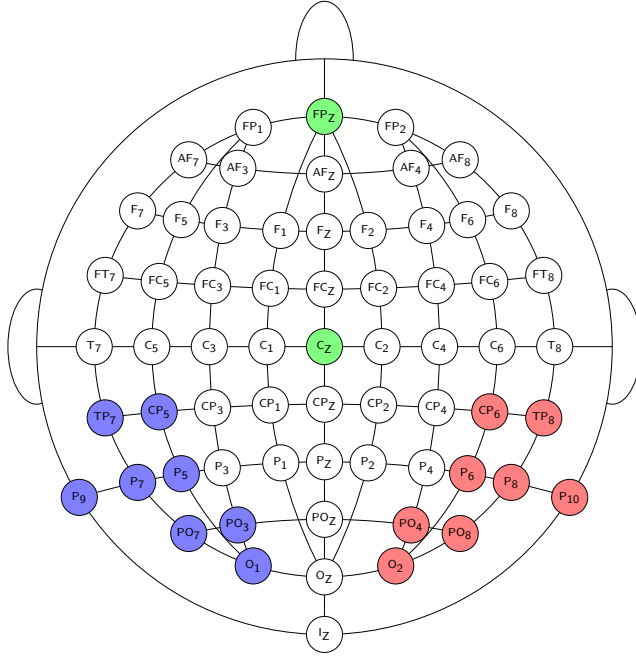


Figure 3.2: Recording channel sets c_L (left - blue) and c_R (right - red) with reference electrodes C_z or Fp_z (green). For a subject with a CI on the right side, the channel set c_L is contralateral (c_C) and the channel set c_R is ipsilateral (c_I).

No CI artifacts attenuation (NO)

To remove DC bias, raw signals $x[t, c]$ were high pass filtered with a zero-phase second order Butterworth filter with 2 Hz cutoff frequency. The filtered signals were then split in 1.024 s epochs based on the trigger signal at the start of each epoch, and 5% of the epochs were rejected based on their peak-to-peak amplitude to eliminate excessive movement, ocular, and muscle artifacts. The epoch signals were stored in a three-dimensional tensor $\mathcal{X}_{NO}[t', e, c] \in \mathbb{R}^{N_{t'} \times N_e \times N_c}$, with $N_{t'}$ the number of time samples in one epoch and N_e the number of epochs. The Fourier transform $\bar{\mathcal{X}}_{NO}[f, e, c]$ of the epoch signals was then determined for each epoch $e = 1 \dots N_e$ and channel $c = 1 \dots N_c$. These signals were re-referenced to either C_z or Fp_z , as indicated in Table 3.1, by subtracting this reference signal, resulting in the tensor $\bar{\mathcal{X}}_{NO}^r[f, e, c]$.

The average signals $\bar{\mathcal{X}}_{NO}^{r,C}[f, e]$ and $\bar{\mathcal{X}}_{NO}^{r,I}[f, e]$ were determined as the mean over the selected channels c_C and c_I in the contralateral and ipsilateral hemisphere.

$$\overline{\mathcal{X}}_{NO}^{r,C}[f, e] = \text{mean}(\overline{\mathcal{X}}_{NO}^r[f, e, c])_{c_C} \quad (3.1)$$

$$\overline{\mathcal{X}}_{NO}^{r,I}[f, e] = \text{mean}(\overline{\mathcal{X}}_{NO}^r[f, e, c])_{c_I} \quad (3.2)$$

The synchronous activity $\overline{m}_{NO}^{r,C/I}$, consisting of EASSR and CI artifacts, was calculated as the component at f_m , averaged over epochs.

$$\overline{m}_{NO}^{r,C/I} = \text{mean}(\overline{\mathcal{X}}_{NO}^{r,C/I}[f_m, e])_e \quad (3.3)$$

The synchronous amplitude and phase were determined as the absolute value and angle of the synchronous activity.

$$\begin{aligned} A_{NO}^{r,C/I} &= |\overline{m}_{NO}^{r,C/I}| \\ \theta_{NO}^{r,C/I} &= \angle \overline{m}_{NO}^{r,C/I} \end{aligned} \quad (3.4)$$

The non-synchronous activity is the standard deviation of the component at f_m over epochs, divided by the square root of the number of epochs N_e .

$$N_{NO}^{r,C/I} = \frac{\text{std}(\overline{\mathcal{X}}_{NO}^{r,C/I}[f_m, e])_e}{\sqrt{N_e}} \quad (3.5)$$

The Hotelling T^2 test [66] compares the real and imaginary components of the synchronous activity to the non-synchronous activity to determine whether significant synchronous activity, relative to the neural background noise, is present. $A_{NO}^{r,C/I}$ and $\theta_{NO}^{r,C/I}$ are used further on to compare the three methods.

Linear interpolation (LI)

A linear interpolation, with duration $d = t_{post} - t_{pre}$, was applied for each stimulation pulse between a pre-stimulus sample t_{pre} and a post-stimulus sample t_{post} that are both assumed to be free from CI artifacts.

The maximum value for d is the interpulse interval, i.e., the inverse of the pulse rate, in this case 2 ms for $f_c = 500$ pps, and 1.1 ms for $f_c = 900$ pps. In

that case, only one sample per stimulation pulse is retained, and the remaining samples are interpolated. In accordance to previous studies [53, 38], the pre-stimulus sample was always chosen at 0.1 ms before the start of the stimulation pulse, the post-stimulus sample was chosen at either 1.9 ms for $f_c = 500$ pps or 1 ms for $f_c = 900$ pps, after the start of the stimulation pulse. Further processing followed the steps outlined above in Section 3.2.2, i.e., high pass filtering, transformation to frequency domain, averaging over channels and epochs with (3.1, 3.2, 3.3), synchronous ($A_{LI}^{r,C/I}$ and $\theta_{LI}^{r,C/I}$, with (3.4)) and non-synchronous activity ($N_{LI}^{r,C/I}$, with (3.5)) calculation, and testing for significant synchronous activity with the Hotelling T^2 test. It has been shown in [53, 37] that LI sufficiently attenuates CI artifacts in contralateral recording channels for $f_c = 500$ pps.

ICA-based CI artifacts attenuation (ICA)

Channels located on top of the CI coil were removed prior to ICA decomposition. All remaining channels were included for the ICA decomposition, and the channel sets described in Table 3.1 were used for analysis. The raw signals $x[t, c]$ were filtered with a second-order 2 Hz high-pass filter to remove any DC bias. Next, the signals were split into epochs of 1.024 s, based on the trigger signal, and 5% of the epochs were rejected to eliminate excessive movement, ocular and muscle artifacts. The resulting epochs were concatenated and transposed into $X = x[c, \hat{t}]$, and then used as the input to the Infomax ICA algorithm as implemented in EEGLAB (v 11.0.5.4b) [34] with default settings. The Infomax ICA implementation was used, because it has widely and successfully been applied to EEG data [36, 32, 33, 143, 142, 35]. The ICA algorithm determines the unmixing matrix W such that the independent components (ICs) S are obtained from X :

$$S = W X \quad (3.6)$$

$$X = P S \quad (3.7)$$

The mixing matrix $P = W^{-1}$ describes how the ICs are mixed together to reconstruct X . ICA aims to separate the EEG signals into statistically maximally independent ICs. Contrary to the methods used in the above mentioned studies, here, no band pass filtering or down-sampling was applied to the data in order to preserve the f_c component, that is used for automated artifactual IC selection. It is possible to use a concatenation of band pass filters, one around f_m and one around f_c , that remove background noise signals but preserve the important frequency components, which could result in a better ICA decomposition.

ICs corresponding to CI artifacts are normally selected manually based on temporal and topographic characteristics. Manual IC selection is a subjective and time-consuming process. Hence, a heuristic approach to automatically select ICs corresponding to CI artifacts was used. It is assumed that ICs contain either EASSR, CI artifacts, ocular, or muscle artifacts, or neural background noise. Only CI artifacts have high frequency components above 200 Hz. Artifactual ICs can therefore be identified based on the spectral amplitude at f_c [40]. It is not possible to directly identify artifactual ICs based on the spectral amplitude at f_m , because ICs with a significant f_m component may represent either CI artifacts, or a genuine EASSR.

Each IC was reconstructed in channel space, by multiplying the time course of the IC (i -th row of S for IC_i) by its spatial distribution (i -th column of P for IC_i). All ICs with a CI artifacts contribution at f_m in any recording channel higher than the noise level were identified as CI artifacts ICs based on the component at f_c , as explained below. Two assumptions are made for the CI artifacts IC spectra; (1) the spectral amplitude at the sidebands $f_c \pm f_m$ is related to the spectral amplitude at f_c through the modulation depth MD: $A_{f_c \pm f_m} = \frac{MD}{2} A_{f_c}$, which is valid for an ideal AM signal, and (2) the spectral amplitude at f_m is equal to the spectral amplitude at the sidebands: $A_{f_m} = A_{f_c \pm f_m}$. The second assumption is based on empirical analysis of the ratio $\frac{A_{f_m}}{A_{f_c \pm f_m}}$, and not on theoretical relations one may expect based on Fourier analysis. With these assumptions, we have $A_{f_c} = \frac{2}{MD} A_{f_m}$. A threshold t_i was defined for each IC_i such that if its spectral amplitude A_{IC_i, f_c} at f_c in source space, was smaller than the threshold, then the spectral amplitude A_{IC_i, c, f_m} at f_m in channel c after reconstruction, was smaller than the noise level, N_{f_m} . Mathematically: if $A_{IC_i, f_c} \leq t_i$, then $A_{IC_i, c, f_m} \leq N_{f_m}$. As the conversion from source space to channel space for IC_i is determined by the i -th column P_i of the mixing matrix P , the largest contribution of IC_i to any channel is thus given by the largest element of P_i (\max_{P_i}). The resulting threshold t_i for IC_i is then equal to $\frac{2}{MD \max_{P_i}} N_{f_m}$. All ICs with $A_{IC_i, f_c} > t_i$ were removed for further analysis.

In reality, the CI artifacts are not ideal AM signals and the spectral amplitude at f_m depends on the non-linearity of the CI artifacts propagation. The noise levels used were 25 nV for the responses in the 40 Hz range, and 5 nV for the responses in the 90 Hz range, which are the expected N_{f_m} values, for 5 minute recordings [65]. Alternatively, noise levels can be determined for each subject separately.

Because the spectral amplitude at f_c is compared to the threshold, and assuming the ICA decomposition is successful such that each IC contains either EASSR or CI artifacts, it is ensured that only the CI artifacts are attenuated and that

the EASSR itself is unchanged. If the ICA decomposition is not successful, ICs may contain both CI artifacts and EASSR, and rejection of these ICs may lead to attenuation of the EASSR.

The CI artifacts ICs were identified as described above, and rejected, and the remaining ICs were projected back to the original recording channels, using the mixing matrix P . Further processing followed the steps outlined above in Section 3.2.2, i.e., transformation to frequency domain, reference channel subtraction, averaging over channels and epochs (with (3.1, 3.2, 3.3)), synchronous ($A_{ICA}^{r,C/I}$ and $\theta_{ICA}^{r,C/I}$, with (3.4)) and non-synchronous activity ($N_{ICA}^{r,C/I}$, with (3.5)) calculation, and testing for significant synchronous activity with the Hotelling T^2 test.

3.2.3 Evaluation

Response properties after ICA-based CI artifacts attenuation

Evaluating the quality of the CI artifacts attenuation is difficult as there generally is no golden standard available. However, it has recently been shown that it is possible to obtain reliable EASSRs in contralateral recording channels with stimulation at 500 pps and LI [37, 53]. Therefore, for the *MFTF* datasets, with $f_c = 500$ pps, EASSR amplitudes $A^{r,C}$ and phases $\theta^{r,C}$ should be similar with LI and ICA-based CI artifacts attenuation.

As in [38, 53], response latencies were determined. The slope of the $\theta(f_m)$ curve, which is related to the neural response latency, indicates whether the measurement is EASSR or CI artifacts dominated. Response latencies increase with decreasing f_m , as neural generators are located higher up in the auditory pathway for lower f_m . For significant EASSRs, the EASSR phase $\theta(f_m)$ should thus decrease linearly with increasing modulation frequency f_m in the 30–50 Hz range and in the 80–100 Hz range [53, 115]. CI artifacts are measured in the EEG almost immediately following stimulation, resulting in very small latencies. Response phases are therefore stable at multiples of 180 degrees, independent of the modulation frequency, when measurements are CI artifacts dominated [53, 64, 65]. The response latency L was calculated as the additive inverse of the slope of the $\theta(f_m)$ curve, for the mean contra- and ipsilateral channel. For the 40 Hz MFTF dataset, response latencies were also determined for the individual channels in the selected sets.

In [53], the response latency was determined for all contralateral recording channels, and the median (44.2 ms) and interquartile range (6.8 ms) over the selected channels are used as a reference value in this study. Note that the

response latency calculation is different in this study: L is determined for the EEG signal averaged over the channel selection, instead of taking the median of L calculated for separate channels.

For the *AGF dataset*, with $f_c = 900$ pps, no ground truth is available. However, from EEG signals recorded in normal-hearing subjects and in CI subjects with BP stimulation, there is some knowledge available about the properties of the EASSR. EASSR amplitudes generally grow nonlinearly with increasing stimulation levels, and range between 0 to 1000 nV [53, 65, 90, 115]. No EASSR should be detected below the subjects' behavioral threshold. The EASSR phase difference, measured between two different modulation frequencies, should be stable when an EASSR is present and depends on the modulation frequency difference [65]. The response latency L can be computed from the two response phases $\theta(f_{m1})$ and $\theta(f_{m2})$ for the two modulation frequencies $f_{m1} = 37$ and $f_{m2} = 42$ Hz.

$$L = \frac{\theta(f_{m2}) - \theta(f_{m1})}{360^\circ(f_{m1} - f_{m2})} \quad (3.8)$$

Noise level reduction and number of rejected ICs

The ICA decomposition aims to separate EASSR, CI artifacts, ocular and muscle artifacts, and neural background noise. In case of perfect separation, the neural background noise level and EASSR amplitude should not be attenuated when the CI artifacts ICs are rejected. For the 40 Hz AGF dataset, there are no baseline values available for the EASSR amplitude, but the change in neural background noise level can be used. Neural background noise levels N_{ICA} that deviate much from the initial values obtained without CI artifacts rejection N_{NO} indicate that the ICA does not completely separate CI artifacts and neural background noise.

The reduction in neural background noise levels was therefore calculated from the non-synchronous activity computed with (4.5) in Section 3.2.2, 3.2.2 and 3.2.2, as follows:

$$\Delta N_{LI-NO} = \frac{N_{LI}^{r,C/I}[f_m] - N_{NO}^{r,C/I}[f_m]}{N_{NO}^{r,C/I}[f_m]} \quad (3.9)$$

$$\Delta N_{ICA-NO} = \frac{N_{ICA}^{r,C/I}[f_m] - N_{NO}^{r,C/I}[f_m]}{N_{NO}^{r,C/I}[f_m]} \quad (3.10)$$

For each recording, the number of rejected ICs was determined. First, the number of ICs explaining 99% of the raw signals' variance ($\#_{IC_{99}}$) was computed. Second, within the set of ICs explaining 99% of the variance, the number of rejected ICs ($\#_{IC_{rej}}$) and the variance explained by these ICs ($var_{IC_{rej}}$) was determined. For each subject, the mean value and range of $\#_{IC_{rej}}$ and $var_{IC_{rej}}$ were determined over all recordings in this subject. For a perfect ICA decomposition, it is expected that the CI artifacts are expressed only on a small number of ICs. Therefore, a large number of rejected ICs indicates that the ICA decomposition is unsuccessful in completely separating CI artifacts and EASSR.

3.3 Results

Figure 3.3 shows the first 20 ICs obtained after ICA decomposition for the first recording in the AGF dataset of subject S07. The amplitude spectrum up to 1000 Hz is plotted, and the scalp plot shows the spatial distribution of the IC over the recording channels. The scalp projections were normalized, for illustration purposes, but scalp projections are usually larger for the first ICs. Rejected ICs have a clear peak at f_c , and show a centroid at the side of the CI (left for subject S07). In some rejected ICs, the sidebands, caused by the modulation of the pulse train, are clearly visible. Neural background noise, with the typical $1/f$ spectrum, is clearly present in some rejected ICs, e.g., IC9.

Two MFTF datasets and one AGF dataset were used: (1) 40 Hz MFTF, (2) 90 Hz MFTF, and (3) 40 Hz AGF. The results are discussed in detail below.

3.3.1 40 Hz MFTF dataset

Figure 3.4 contains $A_{NO}^{r,C/I}$, $A_{LI}^{r,C/I}$, and $A_{ICA}^{r,C/I}$ for the mean contra- and ipsilateral recording channel. In the mean contralateral channel (left panel), amplitudes are similar for all three methods and error bars overlap for LI and ICA, indicating that LI and ICA lead to similar results, and ICA is not distorting the EASSR. In the mean ipsilateral channel (right panel), LI cannot remove all CI artifacts for all subjects [37, 53]: $A_{LI}^{r,I}$ can therefore not be seen as the baseline truth. $A_{ICA}^{r,I}$ is mostly smaller than $A_{LI}^{r,I}$, especially in the higher frequencies (> 40 Hz), suggesting that ICA is better capable than LI of attenuating CI artifacts in the ipsilateral hemisphere.

The same observations can be made based on the synchronous phase $\theta_{NO}^{r,C/I}$, $\theta_{LI}^{r,C/I}$, and $\theta_{ICA}^{r,C/I}$, given in Figure 3.5, and the response latencies $L_{NO}^{r,C/I}$, $L_{LI}^{r,C/I}$,

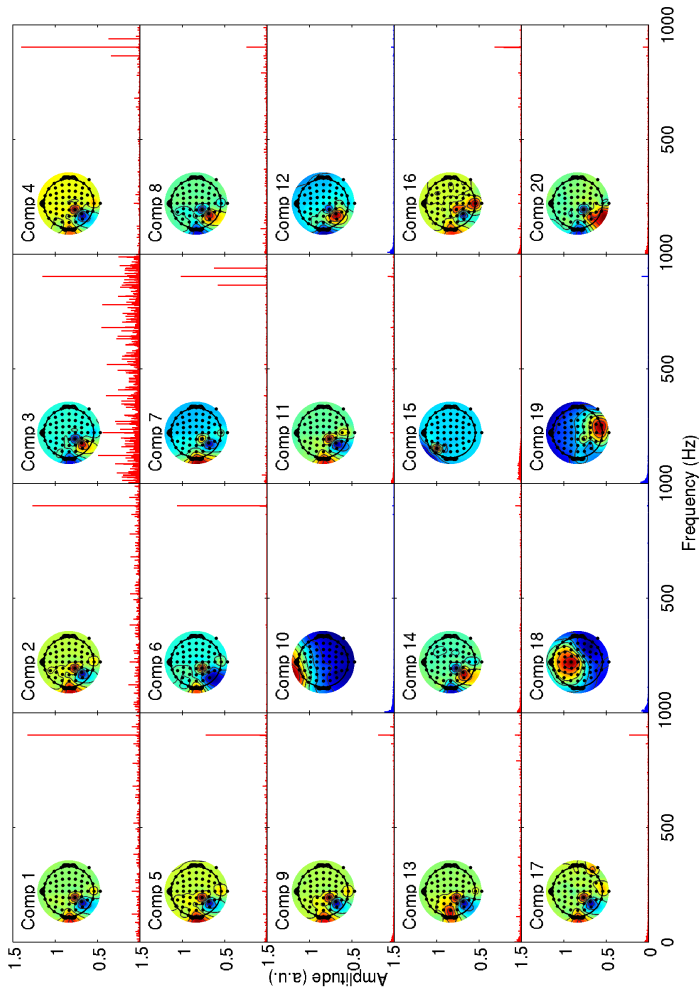


Figure 3.3: First 20 ICs obtained after ICA for subject S07, recording 1 (AGF dataset). For each IC, the amplitude spectrum, and the spatial distribution over recording channels is shown. The amplitude spectrum is colored red for rejected ICs, and blue for the remaining ICs.

and $L_{ICA}^{r,C/I}$, given in Figure 3.6. In the mean contralateral channel (left panels), phases decrease linearly with increasing f_m for all methods, indicating that the measurements are EASSR dominated, even before CI artifacts attenuation, and that all methods lead to similar results. Response latencies $L_{NO}^{r,C}$, $L_{LI}^{r,C}$, and $L_{ICA}^{r,C}$, are also similar and within the expected range obtained in [53]. In the ipsilateral hemisphere (right panels), $\theta_{NO}^{r,I}$ is constant for increasing f_m , resulting in small $L_{NO}^{r,I}$, for subjects S01, S02, S04 and S06. This confirms that the measurements are indeed CI artifacts dominated in the ipsilateral hemisphere. $\theta_{LI}^{r,I}$ is still constant for increasing f_m for subjects S02, and S04, confirming that LI is indeed incapable of removing all CI artifacts in the ipsilateral hemisphere for all subjects. With ICA, $\theta_{ICA}^{r,I}$ linearly decreases with increasing f_m for all subjects, and the obtained response latencies are close to the expected values for all subjects. As noted before, L is calculated differently in this study than in [53]; the obtained values are therefore slightly different from the used reference values.

Good results are thus obtained for mean contra- and ipsilateral channels. Response latencies in individual recording channels are given in Figure 3.7. Overall, response latencies are mostly within the expected range for all three methods. However, some clear improvements of ICA compared to either NO or LI can be seen, i.e., channel CP₆ for S01, channels CP₅, O₂ and PO₄ for S02, channel O₂ and PO₄ for S04, and channel PO₃ for S06. In some cases, ICA performs similarly bad as LI, i.e., channels CP₆ in S02, and channel CP₅ in S06. ICA performs worse than LI, in channel P₅ in S06.

3.3.2 90 Hz MFTF dataset

No consistent 90 Hz EASSRs have been found in the contralateral channels in [53]. In Figure 3.8, it is shown that synchronous amplitudes are largely attenuated by LI and ICA, compared to NO. However, in all subjects but S05, significant synchronous activity was still detected in some data points after ICA. Based on the synchronous phases, it cannot be concluded that these data points are not CI artifacts dominated, and too few data points are available to evaluate the EASSR/CI artifacts properties adequately. No conclusions on how ICA preserves or distorts the EASSR can therefore be drawn based on these low SNR recordings.

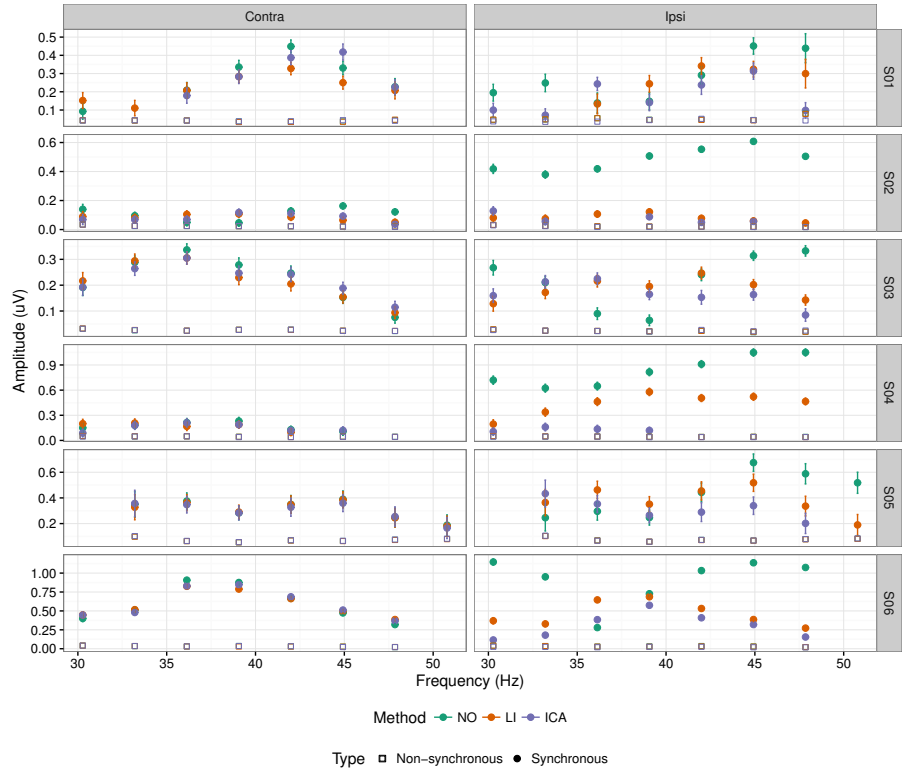


Figure 3.4: 40 Hz MFTF dataset: $A^{r,C/I}$ (\circ) and $N^{r,C/I}$ (\square) for NO, LI and ICA for the mean contra- and ipsilateral recording channel and for subjects S01-S06. Error bars represent the noise level $N^{r,C/I}$. Only EASSR or CI artifacts dominated data points are included.

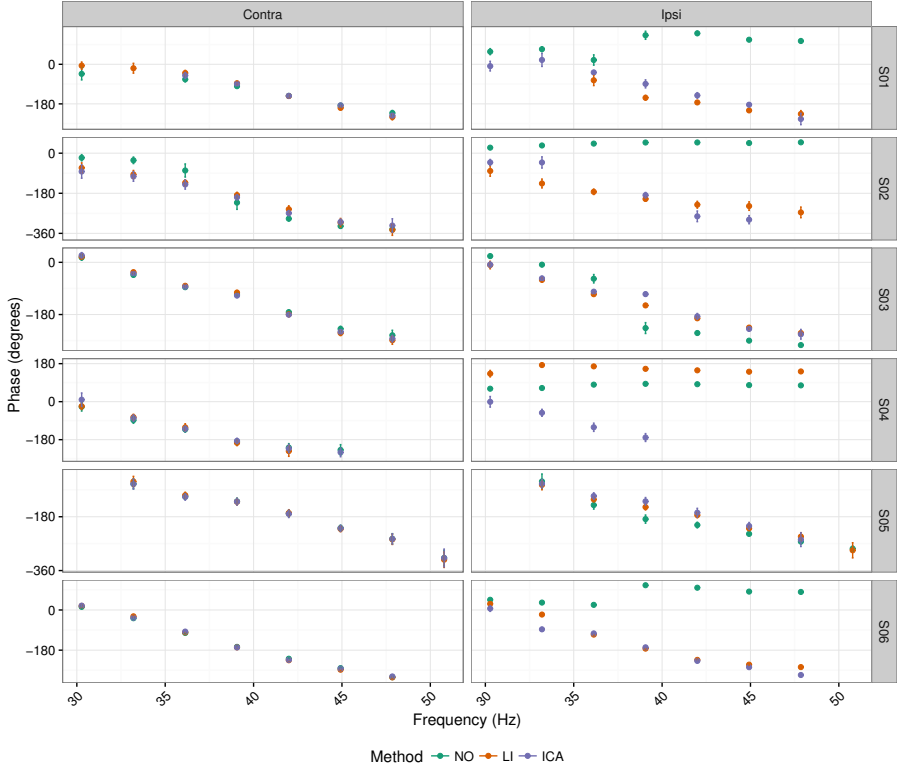


Figure 3.5: 40 Hz MFTF dataset: $\theta^{r,C/I}$ for NO, LI and ICA for the mean contra- and ipsilateral recording channel and for subjects S01-S06. Only EASSR or CI artifacts dominated data points are included.

3.3.3 40 Hz AGF dataset

Figure 3.9a shows $A_{LI}^{r,C/I}$, for varying stimulation levels and $f_m = 37$ and $f_m = 42$ Hz. In general, after LI, $A_{LI}^{r,C/I}$ is large and increasing linearly with increasing stimulation level. With LI, synchronous components are significantly different from the neural background noise in most data points, including subthreshold stimulation levels. This suggests that measurements are CI artifacts dominated in the contralateral and ipsilateral hemisphere, for all subjects, except S07 and S08. Figure 3.9b shows that $A_{ICA}^{r,C}$ and $A_{ICA}^{r,I}$ are similar in order of magnitude. It is clear that $A_{ICA}^{r,C/I}$ is smaller than $A_{LI}^{r,C/I}$. For subjects S02, S04, S09, S10 and S11, $A_{ICA}^{r,C/I}$ changes non-monotonously with increasing stimulation level.

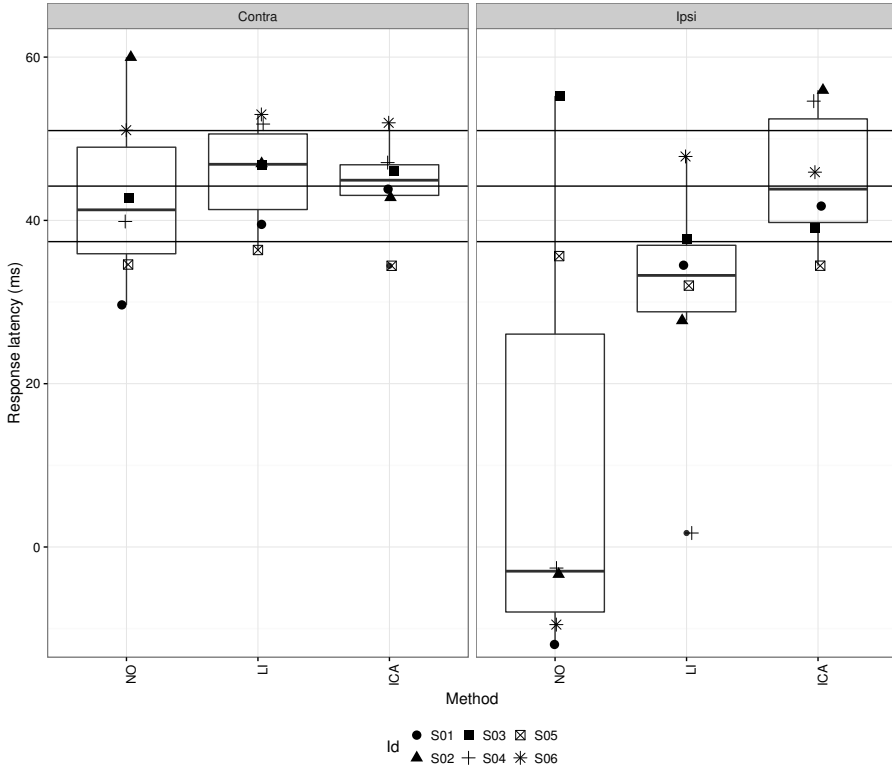


Figure 3.6: 40 Hz MFTF dataset: response latency for NO, LI and ICA for the mean contra- and ipsilateral recording channel and for subjects S01-S06. The expected range (median: 44.2 ms, interquartile range: 6.8 ms), obtained from [53], is indicated with horizontal lines.

In many suprathreshold measurements, no significant synchronous activity is detected, while it is detected in some subthreshold measurements. It seems that ICA attenuates both the CI artifacts, and the EASSR below the noise level in some cases, while in other cases, ICA is incapable of removing all CI artifacts. For subjects S07 and S08, $A_{ICA}^{T,C/I}$ does grow nonlinearly and monotonously with increasing stimulation level. Furthermore, significant synchronous activity is detected in most suprathreshold measurements. No synchronous activity is detected at subthreshold stimulation levels for S08. These results suggest that, for S07 and S08, ICA is capable of removing the CI artifacts from contra- and ipsilateral recording channels without distorting the EASSR.

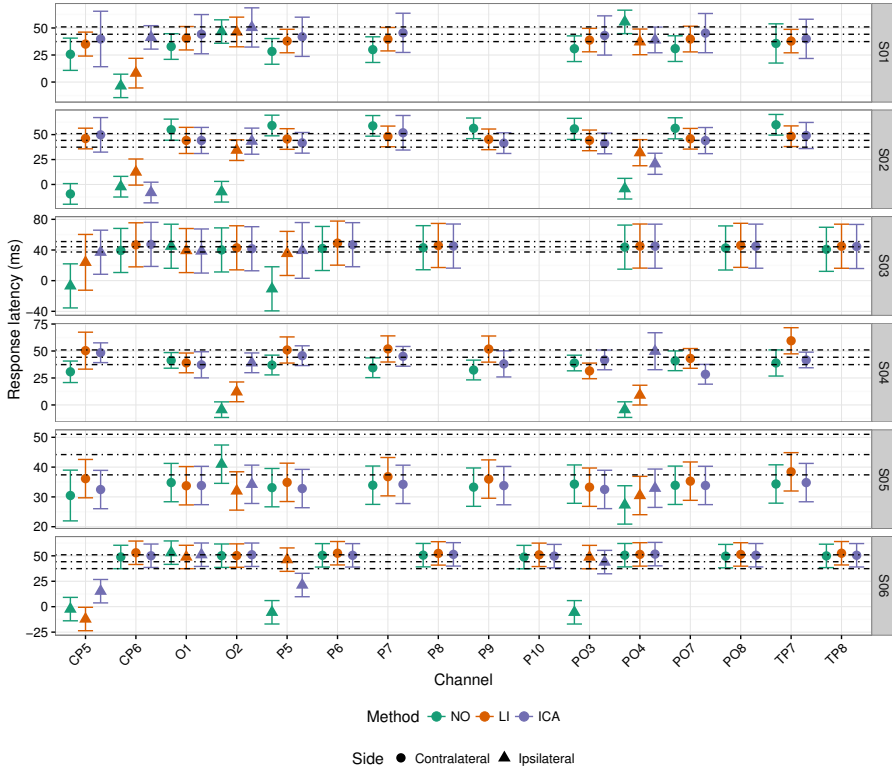


Figure 3.7: 40 Hz MFTF dataset: response latencies in individual channels for NO, LI and ICA and for subjects S01-S06.

Figure 3.10 shows $\theta_{NO}^{r,C/I}$, $\theta_{LI}^{r,C/I}$ and $\theta_{ICA}^{r,C/I}$. It is clear that $\theta_{NO}^{r,C/I}$ and $\theta_{LI}^{r,C/I}$ are equal for $f_m = 37$ Hz and $f_m = 42$ Hz, and constant over stimulation levels, in both hemispheres for all subjects, except S07 and S08. This confirms that measurements are indeed CI artifacts dominated for NO and LI in the contralateral and the ipsilateral hemisphere, for subjects S02, S04, S09, S10, and S11. In the contralateral hemisphere, in subjects S07 and S08, $\theta_{NO}^{r,C}$ and $\theta_{LI}^{r,C}$ are different for $f_m = 37$ Hz and $f_m = 42$ Hz, and constant over stimulation levels. This indicates that measurements are EASSR dominated in the contralateral hemisphere in S07 and S08, for NO and LI.

ICA results in phases $\theta_{ICA}^{r,C/I}$ that are different for $f_m = 37$ Hz and $f_m = 42$ Hz. However, for most subjects, except S07 and S08, $\theta_{ICA}^{r,C/I}$ is not stable over stimulation levels. This indicates that ICA is indeed removing CI artifacts from

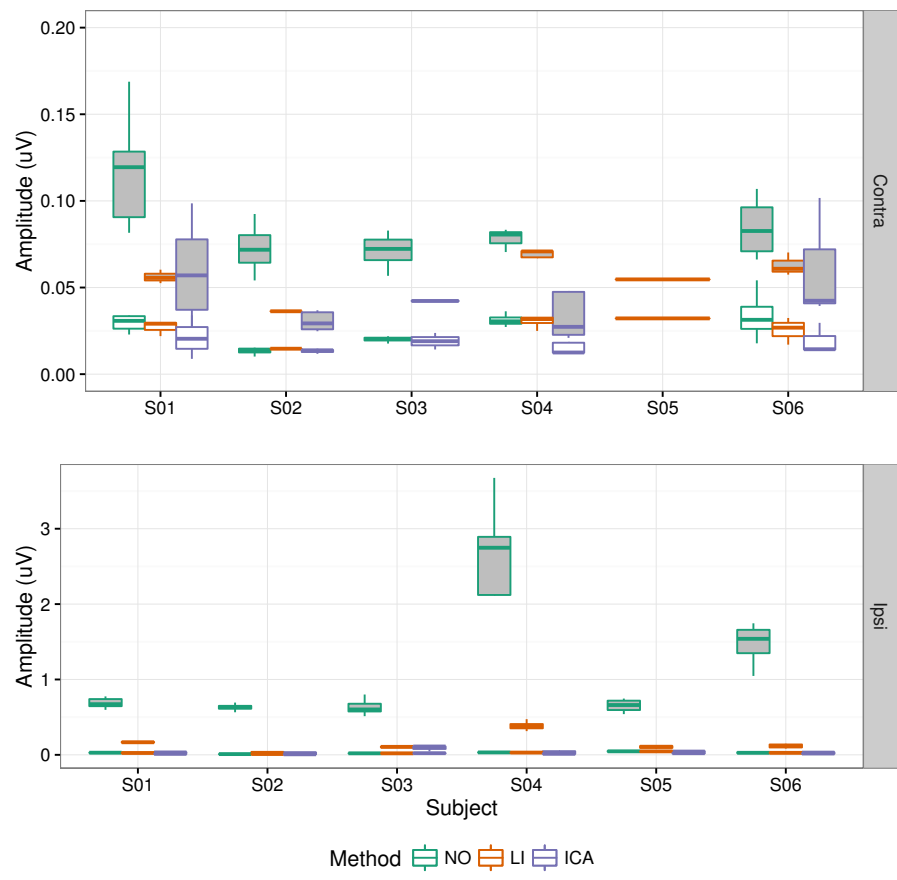


Figure 3.8: 90 Hz MFTF dataset: $A^{r,C/I}$ (gray fill) and $N^{r,C/I}$ (no fill) for NO, LI and ICA. Only EASSR or CI artifacts dominated data points are included.

the measurements, but the EASSR is possibly distorted. For S07 and S08, $\theta_{ICA}^{r,C/I}$ is different for $f_m = 37$ Hz and $f_m = 42$ Hz, and stable over stimulation levels. The phase difference results in a response latency (averaged over hemispheres and stimulation levels resulting in significant EASSRs) of 44 and 49 ms in S07 and S08, respectively. These results confirm that ICA is indeed capable of removing CI artifacts from contralateral and ipsilateral recording channels in S07 and S08.

3.3.4 Noise level reduction and number of rejected ICs

The noise level reduction, calculated with (3.10), is shown in Figure 3.11 for the three datasets. Positive values indicate that the noise level is larger after ICA than for NO; negative values indicate smaller noise levels. In the case of perfect ICA separation, no neural background noise would be rejected with the CI artifacts ICs and hence the noise level would be the same for both methods. Even with LI, a change in the noise levels is observed (ΔN_{LI-NO}). The 10 and 90 % percentiles of ΔN_{LI-NO} were -10 to 10 %, for the three datasets, and are indicated in Figure 3.11 as dashed horizontal lines. With ICA, noise levels change: differences compared to NO of up to 75 % are seen, indicating that the ICA separation is definitely not perfect.

For the three datasets, the number of ICs explaining 99% of the raw signals' variance, the number of rejected artifactual ICs and the variance explained by the artifactual ICs are included for each subject in Table 3.2. The number of rejected ICs varies between 3 and 35, with a large amount of explained variance between 80 and 99%, when the outlier of 11% explained variance is discarded. For the AGF dataset, the number of rejected ICs was not significantly different for subthreshold recordings, compared to suprathreshold recordings.

3.4 Discussion

ICA is often used to remove biological (e.g., ocular, muscle) [36, 35, 34, 101] and CI artifacts [8, 23, 32, 47, 93, 105, 122, 123, 143, 142, 24, 25] from EEG recordings. This study aims to evaluate the performance of ICA-based CI artifacts attenuation on an EEG dataset, containing EASSRs. Three datasets have been used for evaluation, containing either non-overlapping or overlapping CI artifacts in contralateral recording channels, and absent, low SNR, or high-SNR EASSRs.

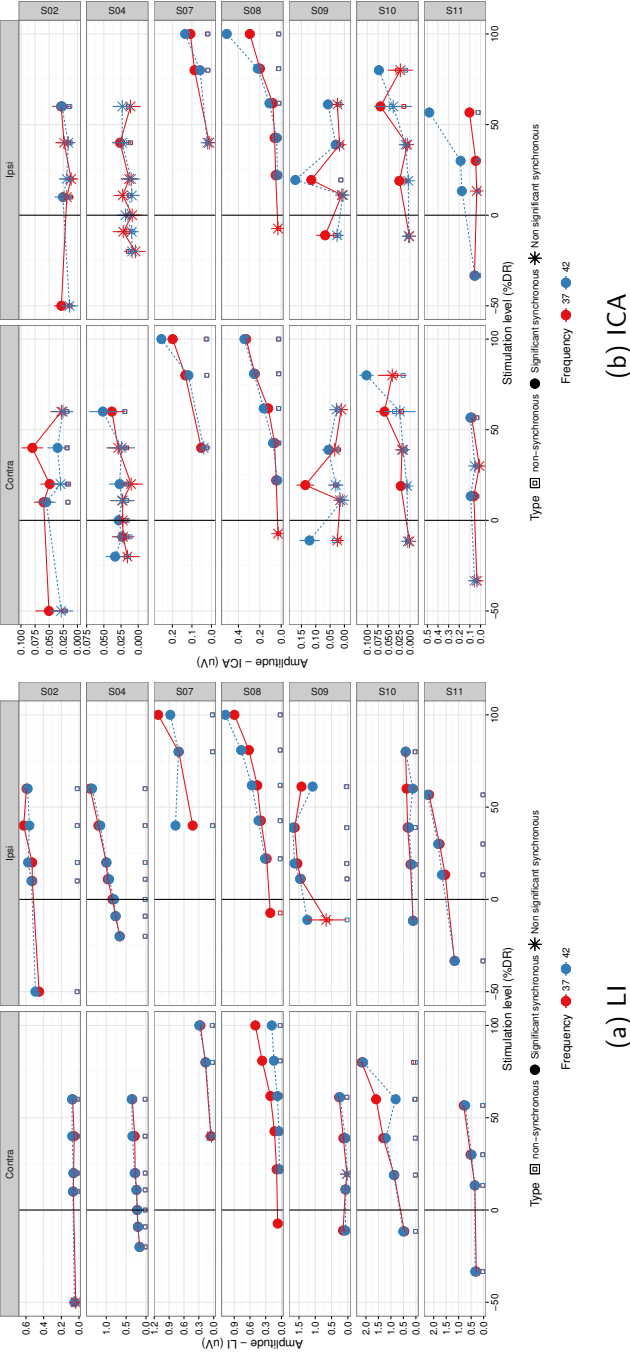


Figure 3.9: 40 Hz AGF: $A^{r,C/I}$ and $N^{r,C/I}$ for LI and ICA, for subjects S02, S04, S07, S08, S09, S10, S11. The vertical lines correspond to the behavioral threshold.

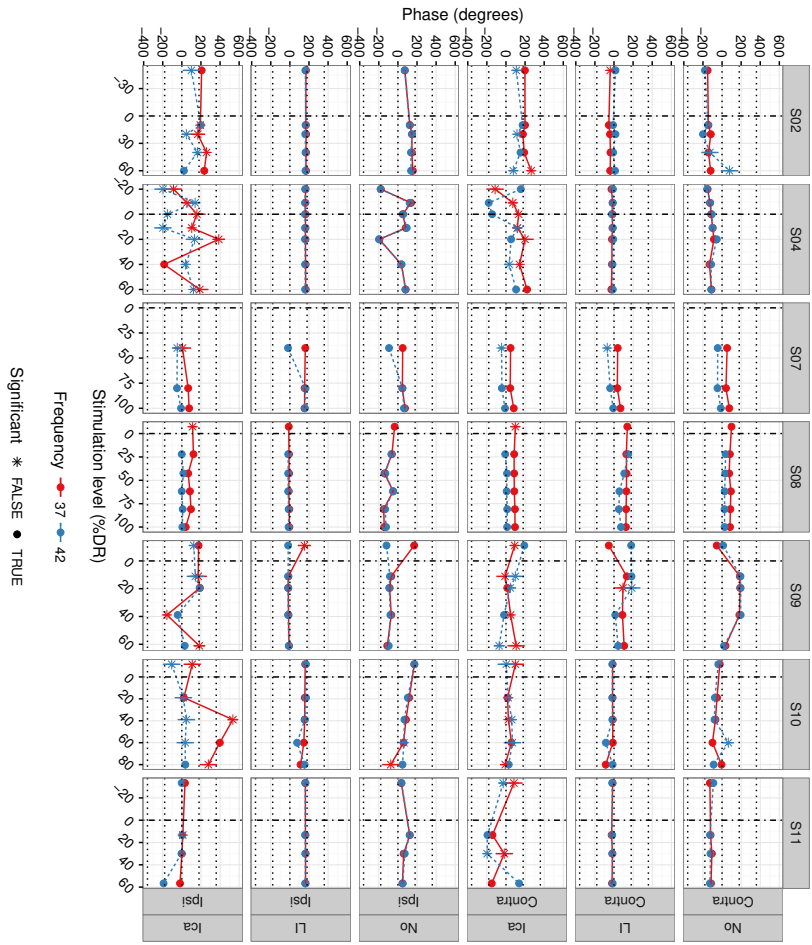


Figure 3.10: 40 Hz AGF dataset: $\theta^{rC/I}$ for NO, LI and ICA, for subjects S02, S04, S07, S08, S09, S10 and S11. The vertical lines correspond to the behavioral threshold.

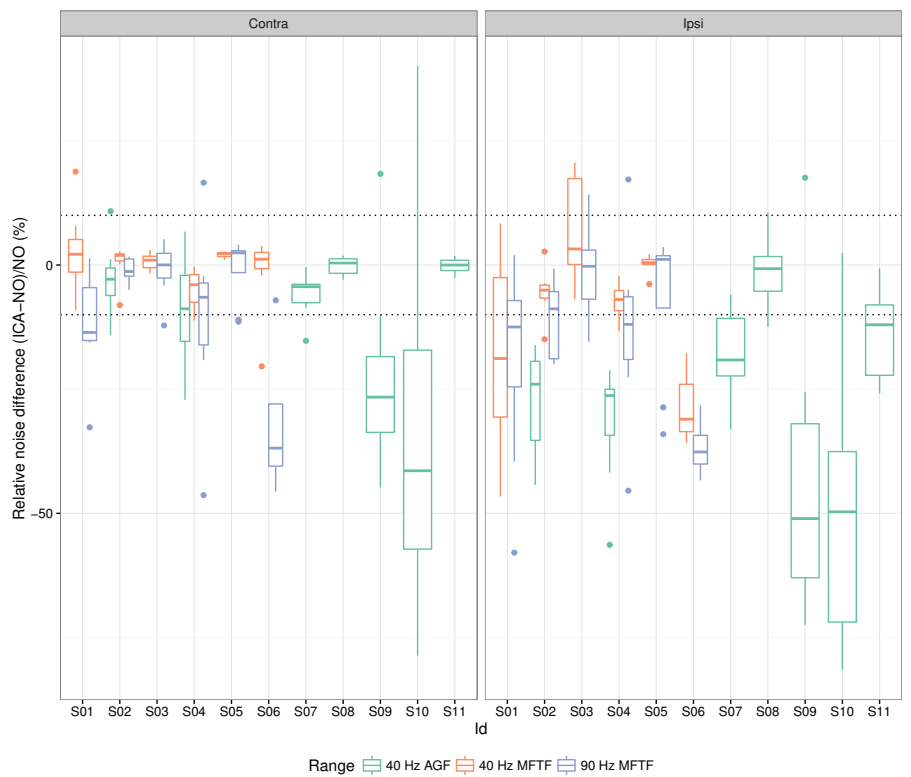


Figure 3.11: Noise level reduction. Horizontal lines are the 10 and 90 % percentiles of noise reduction levels ΔN_{LI-NO} observed with LI compared to NO. In general, noise levels are reduced after ICA, especially at the ipsilateral side. In many cases, $|\Delta N_{ICA-NO}|$ is larger than $|\Delta N_{LI-NO}|$. The colored dots represent outliers, i.e., observations that fall outside of the interval $[Q_1 - 1.5IQR, Q_3 + 1.5IQR]$, with the interquartile range IQR, and the first and third quantile Q_1 and Q_3 , respectively.

Table 3.2: For three datasets: mean (range) of the number ICs explaining 99% of the signals variance ($\#IC_{99}$), the number of rejected ICs ($\#IC_{rej}$), and the variance explained by the rejected ICs ($var_{IC_{rej}}$), for every subject separately and on average (AVG).

S	$\#IC_{99}$	$\#IC_{rej}$	$var_{IC_{rej}}$
40 Hz MFTF			
S01	39 (30-45)	9 (5-12)	87 (80-91)
S02	17 (12-22)	8 (6-10)	97 (97-98)
S03	22 (17-22)	12 (11-15)	97 (96-98)
S04	37 (35-39)	22 (17-29)	93 (91-96)
S05	19 (13-23)	7 (5-8)	95 (94-96)
S06	13 (9-16)	10 (8-11)	99 (98-99)
AVG	25	11	95
90 Hz MFTF			
S01	28 (26-31)	17 (12-22)	97 (95-98)
S02	22 (16-30)	12 (11-14)	97 (96-98)
S03	19 (13-26)	17 (11-21)	99 (98-99)
S04	29 (8-38)	27 (7-35)	98 (97-99)
S05	24 (21-30)	15 (11-21)	97 (96-98)
S06	9 (8-11)	8 (7-10)	98 (98-98)
AVG	23	14	97
40 Hz AGF			
S02	17 (11-29)	14 (10-22)	98 (97-99)
S04	10 (7-12)	8 (6-10)	99 (99-99)
S07	15 (5-35)	7 (3-15)	69 (11-99)
S08	14 (11-19)	12 (10-17)	99 (99-99)
S09	20 (14-24)	18 (12-23)	99 (98-99)
S10	17 (13-19)	14 (9-18)	98 (94-99)
S11	22 (12-28)	12 (9-15)	98 (97-99)
AVG	16	12	96

In summary, ICA performs well for all subjects in the 40 Hz MFTF dataset, with high-SNR EASSRs and non-overlapping CI artifacts in contralateral recording channels. CI artifacts are greatly attenuated in the 90 Hz dataset, with non-overlapping CI artifacts in contralateral recording channels, and absent or low SNR EASSRs. However, it is unclear whether the remaining synchronous activity is CI artifacts, or EASSR dominated. In the 40 Hz AGF dataset, with overlapping CI artifacts, and EASSRs with various SNRs, good performance of ICA is observed in two subjects, while the method fails to produce good results in the remaining five subjects. Contradictory results are thus obtained with the three datasets.

3.4.1 ICA separation quality

The assumption of the ICA algorithm is that the underlying sources (CI artifacts, EASSR, other artifacts and brain background noise) are temporally independent. Although the brain background noise and other artifacts are likely independent from the CI artifacts and the EASSR, the latter two sources are both caused by the electrical stimulation pulses. The assumption of temporal independence may thus not be completely fulfilled, leading to poor ICA separation quality. Note, however, that this is also the case for transient response recordings, where the response and the CI artifact are also both caused by the electrical stimulation pulses. Nevertheless, ICA is one of the most commonly used CI artifact suppression methods for transient response recordings.

Attenuating CI artifacts seems more challenging for EASSR recordings than for transient responses for three reasons. First, in EASSR recordings, the CI artifacts and EASSR overlap continuously in time. On the contrary, the CI artifacts typically precede the neural response for transient responses, with only a limited overlap in time. Second, in EASSR recordings, due to the modulated and asymmetric CI artifacts, the CI artifacts and EASSR also have overlapping spectra. The EASSR is in fact not expected to have any frequency components that are not also present in the CI artifacts spectrum. Both signals have a component at f_m with different amplitude and phase. Third, EASSRs are typically obtained using direct stimulation with one stimulation channel. In the studies that use ICA to measure transient responses [47, 24, 23, 32, 25, 143, 142, 122, 123], responses are often obtained using free field stimulation. In that case, the stimulation pulses delivered to the electrode array are not as exactly controlled as is the case for direct stimulation, and multiple electrodes may be activated, even for narrow band stimuli, due to the maxima selection implemented in many clinical processors. Furthermore, the clocks of the stimulation and recording systems are not perfectly synchronized, such that in the recording epochs stimulation epochs may be slightly jittered. This leads

to CI artifact attenuation when the jittered epochs are averaged. In previous studies, due to free field stimulation [47, 93, 142, 143], stimulation sequences are not identical nor perfectly aligned over recording epochs, resulting in attenuated CI artifacts when epochs are averaged to compute the event-related potential.

Figure 3.12 shows $\theta_{NO}^{r,C}$ as a function of f_m (for the MFTF datasets) or stimulation level (for the AGF dataset). It suggests that the spatial separation of CI artifacts and EASSR could influence the performance. For all subjects in the 40 Hz MFTF dataset, and for subjects S07 and S08 in the 40 Hz AGF dataset, recordings are EASSR dominated in the contralateral hemisphere, evidenced by $\theta_{NO}^{r,C/I}$ that changes with changing f_m . On the contrary, recordings are CI artifacts dominated with constant phases for changing f_m , for all subjects (except S05) in the 90 Hz MFTF dataset and for all subjects (except S07 and S08) in the 40 Hz AGF dataset. Recordings can be CI artifacts dominated due to (1) small or absent EASSRs, or (2) large CI artifacts. EASSRs are small in the 90 Hz range [53], and for subjects S02 and S04 in the 40 Hz range ([53] and Figure 3.4 with synchronous amplitudes of 100–200 nV at comfort level). CI artifacts are large in subjects S09 and S10, see median and range of $A_{NO}^{r,C}$ in Figure 3.12. No reference data are available for subject S11, it is therefore unknown whether EASSRs are small or CI artifacts are large in this subject.

It seems that ICA is capable of separating CI artifacts and EASSR in case EEG signals in the contralateral hemisphere are EASSR dominated, since a reference for the EASSR source is then available. In other cases, it seems not possible to separate CI artifacts and EASSR. It was suggested in [142] that non-overlapping stimuli and responses are beneficial for ICA-based CI artifacts attenuation. Furthermore, lower response SNR may cause more difficulties in separating EASSR and CI artifacts [142].

The change in neural background noise level and the number of rejected ICs again indicate that the ICA separation is not perfect in many cases. In [142], the authors mention that "experts may ignore noise related ICs contaminated with residual CI artifact(s) since these normally explain a small amount of variance in the AEPs". This suggests that improper separation of neural background noise and CI artifacts is also a problem for transient evoked potentials, complementary to our observations for EASSRs.

As an alternative to the ICA decomposition on all recorded channel signals, two additional approaches were developed and evaluated for (a selection of subjects in) the MFTF40 dataset. In the first approach, fewer recording channels, i.e., 32 (ICA32) or 48 (ICA48) channels, are used for the ICA decomposition. ICs containing the same activity may be collapsed into one when fewer recording channels are used. The same results were obtained with ICA32 and ICA48, compared to ICA, for most subjects. The average number of rejected ICs is

10 (31%), 11 (26%) and 12 (21%), for ICA32, ICA48 and ICA, respectively. The minimum (maximum) number of rejected ICs is 4 (20), 5 (27), and 5 (28) for ICA32, ICA48 and ICA, respectively. Furthermore, the percentage of rejected ICs increased when fewer recording channels were used for the ICA decomposition. In the second approach, a LI was applied to the recorded channel signals prior to ICA decomposition (LI+ICA). LI may reduce the CI artifacts amplitude, which could result in a better ICA decomposition. On the other hand, the LI introduces artificial dependencies between the channel signals. ICs representing CI artifacts were then manually identified, because LI distorts the relation between the spectral CI artifacts amplitude at f_m and f_c . While synchronous response phases were mostly similar for ICA and LI+ICA, significant differences in synchronous response amplitude between ICA and LI+ICA were observed for almost all frequencies, in all subjects and in both hemispheres. LI+ICA does not seem to improve the quality of the ICA decomposition, not even for the dataset where ICA seemed successful. It cannot be ruled out that different IC selection criteria would provide better results. However, even if the LI+ICA method would work well, the need for manual IC identification is a serious disadvantage.

3.4.2 Limitations

In this study, only one ICA algorithm, Infomax ICA, has been used. Many reports indicate that Infomax ICA is the most successful ICA algorithm to separate EEG and artifactual sources [36, 32, 33, 143, 142, 35]. This study only aimed to assess the baseline performance of ICA in attenuating CI artifacts, not to find the best ICA algorithm. Furthermore, the algorithm was evaluated using the default settings. Again, since this study aims to evaluate baseline ICA performance for CI artifacts attenuation, optimizing the parameter set was outside the scope of the study.

The selection of ICs associated with CI artifacts was automated using a heuristic measure, by comparing the spectral amplitude at f_c to a predetermined threshold. The value of this threshold was determined by trial and error, and is merely used to create an objective IC selection method. Most probably, better alternatives exist. This study showed that ICA is not capable of completely separating EASSR, CI artifacts, ocular, or muscle artifacts, and neural background noise. Therefore, the optimal setting of the IC selection threshold is not critical for the performance of the method, that is already compromised by the sometimes poor separation quality.

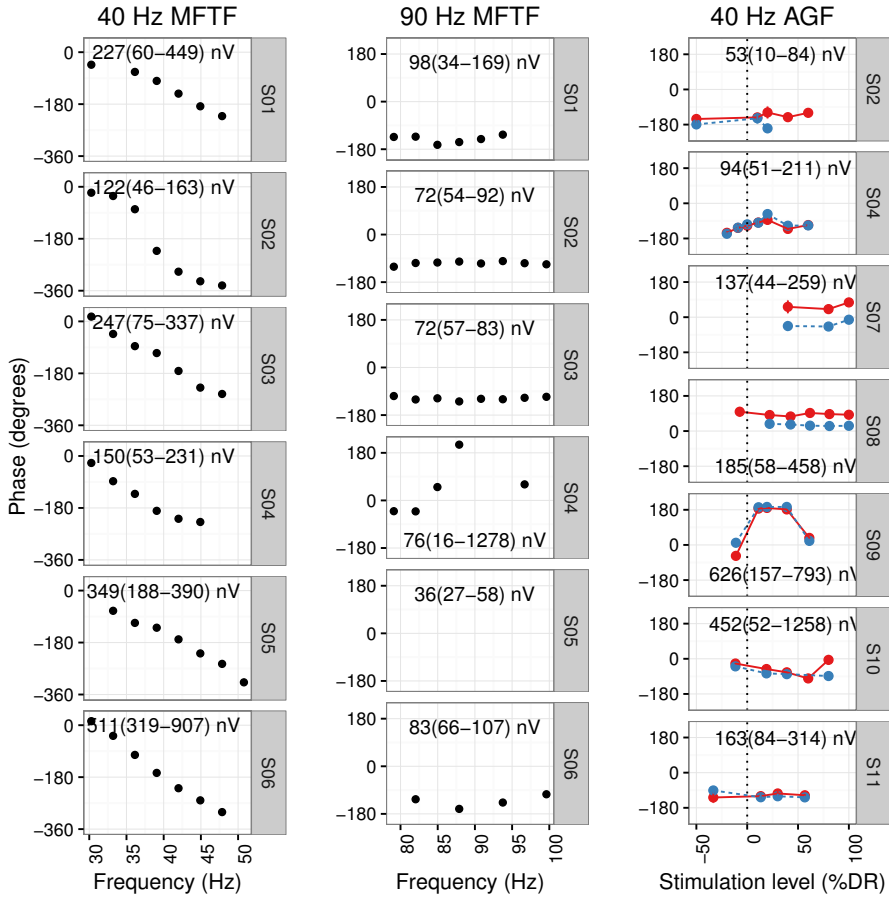


Figure 3.12: $\theta_{NO}^{r,C}$ as a function of f_m (40 and 90 Hz MFTF dataset) or stimulation level (40 Hz AGF dataset) without CI artifacts attenuation, in the mean *contralateral* channel. For the 40 Hz AGF dataset, the red color refers to 37 Hz stimulation, while the blue color corresponds to 42 Hz stimulation, as in Figure 3.10. The dataset is indicated on top. The range and median value of $A_{NO}^{r,C}$ (vector summation of CI artifacts and EASSR) are included as text. No data points are shown for S05 for the 90 Hz MFTF dataset, as only data points with significant synchronous activity are included. Together, amplitude and phase suggest whether the recording is CI artifacts or EASSR dominated. When signals are EASSR dominated in contralateral recording channels, ICA seems to separate the sources good enough to result in adequate CI artifacts attenuation.

3.4.3 Significance

We have shown that the ICA method is only able to sufficiently attenuate CI artifacts for the 40 Hz MFTF dataset. We hypothesize that the ICA separation quality depends on whether the contralateral hemisphere is CI artifacts dominated prior to CI artifacts attenuation. This hypothesis could possibly be verified using simulations, by artificially adding a modeled CI artifacts signal and EASSR. Simulations lack the authenticity of real EEG measurements, and assumptions, e.g., about CI artifacts propagation, and EASSR source location, have to be imposed. Within a subject, for fixed stimulation parameters, it is not possible to manipulate the location or the distribution of the EASSR or the CI artifacts. Therefore, we cannot systematically investigate the influence of EASSR and CI artifacts distribution on the ICA separation quality intra-subject.

Although the ICA does not attenuate CI artifacts below the neural noise level for all tested conditions, we showed that EASSR dominated signals can be obtained in ipsilateral recording channels for the 40 Hz MFTF dataset. Attenuating CI artifacts in ipsilateral channels is crucial for source localization and testing subjects with bilateral CI stimulation.

3.5 Conclusion

This study aimed to evaluate the performance of an ICA-based CI artifacts attenuation method on three datasets containing EASSRs. Results indicate that the separation quality of the ICA depends on the CI artifacts present in the contralateral hemisphere. For the 40 Hz MFTF dataset containing large EASSRs, ICA was capable of removing CI artifacts from all ipsilateral recording channels, without distorting the EASSR in the mean contralateral channel. In the 90 Hz MFTF dataset, EASSR were smaller or absent, and results obtained with ICA were inconsistent. In the 40 Hz AGF dataset, the stimulation level was varied from a subthreshold level to comfort level, covering a whole range of EASSR amplitudes. Good results were obtained for two subjects with large 40 Hz EASSRs and minor CI artifacts in the contralateral hemisphere. For the remaining five subjects, recordings were CI artifacts dominated in the contralateral hemisphere, due to small EASSRs or large CI artifacts. Neural background noise levels were greatly reduced after ICA compared to NO, indicating that ICA did not succeed in perfectly separating neural background noise and CI artifacts (and possibly EASSR). Furthermore, a large number of ICs was rejected in most recordings, whereas it was expected that the CI artifacts would be expressed in a limited number of ICs in case

of perfect separation. In conclusion, the relative contribution of CI artifacts and EASSR in the contralateral recording channels seems to be important for the ICA separation quality. Despite the success of ICA-based CI artifacts attenuation for transient responses, it was found to be only successful in a limited number of cases for steady-state responses.

Chapter 4

Template subtraction to remove CI stimulation artifacts in auditory steady-state responses in CI subjects

Abstract

Objectives: Cochlear implant (CI) stimulation artifacts are currently removed from electrically evoked steady-state response (EASSR) measurements based on a linear interpolation (LI) over the artifact-contaminated signal parts. LI is only successful if CI stimulation artifacts are shorter than the interpulse interval, i.e. for contralateral channels and stimulation pulse rates up to 500 pulses per second (pps). The objective of this paper is to develop and evaluate a template subtraction (TS) method to remove continuous CI stimulation artifacts in order to accurately measure EASSRs.

This chapter is an adapted version of the article Deprez, H. et al. “Template Subtraction to Remove CI Stimulation Artifacts in Auditory Steady-State Responses in CI Subjects.” *IEEE Transactions on Neural Systems and Rehabilitation Engineering* 25(8) (2017): 1322-1331. Changes are limited to layout and representation aspects, and minor editing.

Methods: The template construction (TC) is based on an EEG recording containing CI stimulation artifacts but no synchronous neural response. The constructed templates are subtracted from the recording of interest. Response amplitudes and latencies are compared for the TS and LI method, and for different TC durations.

Results: The response amplitudes and latencies in contralateral channels are the same after TS and LI, as expected. In ipsilateral channels, response amplitudes and latencies are within the expected range only after TS. The TC duration can be reduced from 5 minutes to 1 minute without a significant change in response latency.

Conclusion: TS with a TC duration of only 1 minute allows to remove all CI stimulation artifacts in individual contra- and ipsilateral EEG recording channels.

4.1 Introduction

Cochlear implants (CIs) restore hearing in subjects with severe to profound sensorineural hearing loss. A CI bypasses the impaired cochlea by electrically stimulating the auditory nerve. The CI consists of three main parts: a sound processor which encodes incoming sound to electrical pulse stimulation patterns, a radiofrequency link which communicates between the CI's external and internal parts, and an electrode array consisting of 12–22 electrode contacts which is implanted into the cochlea. A CI also has one or two extra-cochlear electrodes, which are used as a reference in monopolar stimulation mode. This mode consumes less battery power than the bipolar stimulation mode, i.e., between two intra-cochlear stimulation electrodes, and it is therefore the standard mode used in the clinic [155]. Furthermore, in clinical settings, all CIs use high-rate stimulation, with pulse rates that are higher than 500 pulses per second (pps) [150].

Recently, there has been increasing interest in measuring the electroencephalogram (EEG) in CI subjects, both for automating CI fitting [64, 65, 53] and for investigating neural plasticity after cochlear implantation [127, 128, 129, 48, 52]. At CI activation and during audiological rehabilitation, several parameters have to be adjusted in the CI's sound processor, a process called CI fitting. The threshold (T) and maximum comfortable (C) stimulation levels are the main parameters that have to be set for each stimulation electrode. These are typically determined based on behavioral feedback from the CI subject, but could possibly be determined objectively and automatically with electrophysiological measures. For stimulation in monopolar mode, T levels vary less over stimulation electrodes

than in bipolar mode, which is another reason that monopolar mode is generally used in clinical settings.

Objective threshold estimation based on responses at the auditory nerve and brainstem level has been investigated, but the obtained threshold levels are only moderately correlated with behavioral thresholds [17, 70]. These methods use low-rate stimulation, i.e., below 100 Hz, with larger T levels than high-rate stimulation [97]. Electrically evoked auditory steady-state responses (EASSRs) are neural responses elicited with periodic or modulated high-rate pulse trains. These narrow-band responses are obtained at the repetition or modulation frequency and can objectively be detected in the EEG based on frequency domain statistical tests [41]. It has been shown that electrophysiological thresholds obtained with modulated high-rate pulse trains correlate well with behavioral thresholds for stimulation in bipolar mode [65]. The current objective here is to investigate whether EASSRs to clinically used stimulation, e.g., high-rate pulse train stimulation in monopolar mode, could be used for objective threshold estimation.

Electrical stimulation also results in CI stimulation artifacts, which obscure the neural responses. These CI stimulation artifacts may be present at the response frequency [64, 65] and can therefore not easily be removed with frequency domain filtering. The nature of the CI stimulation artifacts varies over subjects and depends on stimulation and recording parameters. CI stimulation artifacts are typically larger and longer in duration for monopolar mode stimulation than for bipolar mode stimulation [69, 85], and are therefore more difficult to remove. CI stimulation artifacts, shown in Figure 4.1 have been characterized in [37], for stimulation and recording parameters that are often used. A CI stimulation artifact typically consists of one or two large initial peak(s) and a slowly decaying tail.

A number of multichannel processing methods, based on principal component analysis (PCA), independent component analysis (ICA) or beamforming, have been investigated for CI stimulation artifact removal in transient EEG responses [47, 93, 149, 25, 142, 1]. An ICA-based method has been developed in [40] for CI stimulation artifact removal in EASSRs. To our knowledge this is the only work evaluating multichannel methods for steady-state responses. Multichannel methods can employ spatial information about the neural response and the CI stimulation artifacts. However, they have the disadvantage that multichannel set-ups are more expensive to purchase than single channel set-ups, and more subject preparation time is required.

Several single channel methods for CI stimulation artifact removal have been investigated for transient [42, 43, 95] and steady-state responses [64, 65]. For EASSRs, the most successful method currently available is a linear interpolation

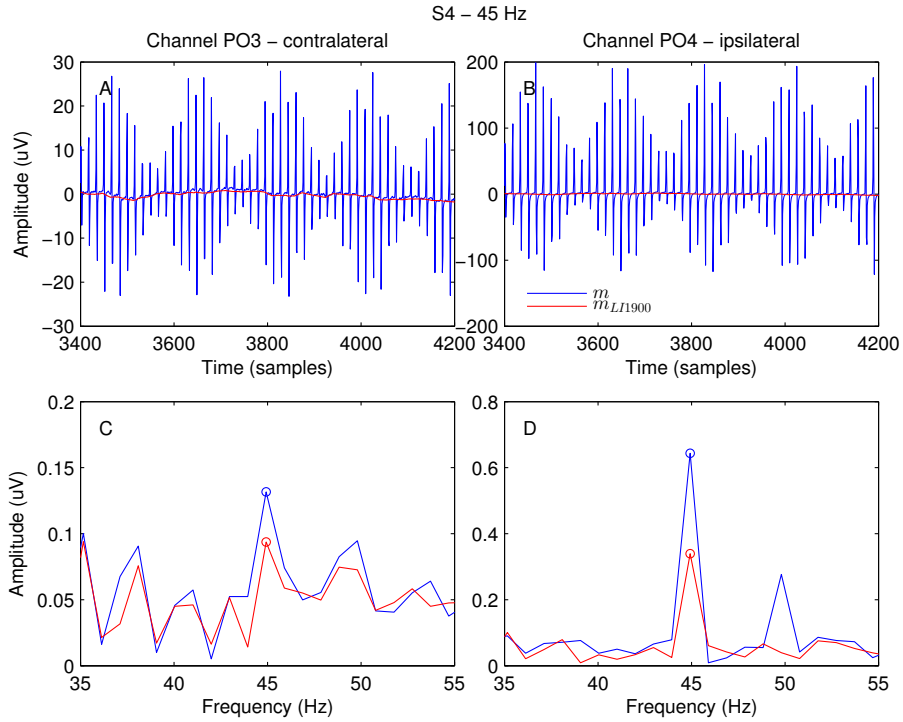


Figure 4.1: Example of an EASSR, measured in subject S4, in contralateral channel PO_3 and ipsilateral channel PO_4 , for stimulation with a 45 Hz amplitude modulated 500 pps pulse train (see Section 4.2.1). An average epoch is shown in time and frequency domain (panel C and D), without CI stimulation artifact removal and with LI based CI stimulation artifact removal, denoted as m and $m_{LI_{1900}}$, respectively (panel A and B). CI stimulation artifact peak-to-peak amplitudes are about $50 \mu V$ and $300 \mu V$ in the contralateral and ipsilateral channel, respectively. The expected EASSR amplitudes are about $20 - 800 nV$ [64, 53], which is 1000 times smaller than the CI stimulation artifact peak-to-peak amplitude. In the contralateral channel PO_3 , CI stimulation artifacts are approximately symmetric and therefore have only a small component at the modulation frequency. This component is removed with LI_{1900} (panel C). The remaining EASSR has an amplitude of $94 nV$. In the ipsilateral channel PO_4 , CI stimulation artifacts are larger and less symmetric, and have a larger component at the modulation frequency (panel D). Even with LI_{1900} , the CI stimulation artifacts cannot completely be removed, because the CI stimulation artifacts are longer in duration than the interpulse interval of 2 ms. After LI, the component at the modulation frequency therefore has a four times larger amplitude in the ipsilateral than the contralateral channel, and consists both of EASSR and residual artifact. More information about the CI stimulation artifact characterization can be found in [37].

(LI) method over each signal part that is contaminated with CI stimulation artifact. This method only works well if the CI stimulation artifacts are shorter than the interpulse interval. It has been shown recently that LI can remove CI stimulation artifacts from contralateral channels electrodes for stimulation in monopolar mode at pulse rates lower than or equal to 500 pps [53, 37]. For higher rates or for channels closer to the CI, the artifact tail has not completely decayed to the baseline level by the time the next pulse is started. Figure 4.1 illustrates that LI cannot completely remove the CI stimulation artifacts at ipsilateral recording channels. The figure shows the component at the modulation frequency for one contralateral and one ipsilateral channel. This component is larger for the ipsilateral channel than for the contralateral channel. Since a suprathreshold measurement is used, this component may consist of both CI artifacts and an EASSR. In this case, the component likely consists at least partly of CI artifacts since the EASSR found in the contralateral channel is a factor four smaller. Although not many studies have investigated lateralization in CI subjects, some studies indicate that responses may be lateralized to the contralateral side in CI subjects [89]. In case the component at the modulation frequency only consists of an EASSR, it would therefore be expected that this component is smaller in the ipsilateral channel. Since the component is larger ipsilateral than contralateral, we conclude that residual CI artifacts are present at the modulation frequency in the ipsilateral channel, similar to the findings in [37, 53].

Template subtraction (TS) methods have been developed in the context of transient EEG responses [95], but have not been considered for steady-state responses. The aim of this work is to develop a TS method for steady-state responses. The TS method can be applied to single channel data, which is an advantage for clinical applications such as objective CI fitting. Furthermore, the method is tailored to individual subjects and therefore copes well with intra- and intersubject variability, as a template is constructed for each channel and each subject separately. Finally, it is not assumed that CI stimulation artifacts are shorter than the interpulse interval (as for LI) or that they are similar in different recording channels (as for multichannel methods). We hypothesize that the TS method, contrary to the LI method, is able to remove CI stimulation artifacts from ipsilateral recording channels for high-rate stimulation in monopolar mode at suprathreshold stimulation levels.

However, it is not straightforward to apply the methods developed for transient responses to steady-state responses. For transient responses, typically the same stimuli are used for all presentations, while modulated pulse trains with varying stimulation pulse amplitudes are used for EASSRs. Therefore, a template should be constructed for each stimulation pulse amplitude, instead of a single template for one recurring stimulus. Furthermore, the steady-state nature

of the stimulation and response imply that both continuously overlap. For transient responses, there is typically some delay between the occurrence of the CI stimulation artifacts and the event-related neural response. Therefore, even if the CI stimulation artifacts are not completely removed from the EEG signals, some information about the neural responses can still be obtained. For steady-state responses, even small residual CI stimulation artifacts can have a component at the modulation frequency, obscuring the event-related neural response. Consequently, the TS method should reduce the CI stimulation artifacts to a level below the brain noise level to reliably measure EASSRs.

The aim of this work is to develop and evaluate a TS method for EASSRs. The template construction (TC) is based on an EEG recording containing CI stimulation artifacts but no synchronous neural response. The constructed templates are subtracted from the recording of interest. Response amplitudes and latencies are compared for the TS and LI method, and for different TC durations.

4.2 Materials and methods

A CI stimulation artifact removal method based on TS was developed, which is described in Section 4.2.2. The TS method was compared to three other methods (no artifact removal and LI with two interpolation durations, see Sections 4.2.2 and 4.2.2) for part of the dataset collected by Gransier *et al* [53] (see Section 4.2.1).

4.2.1 EASSR dataset

A part of the EASSR dataset described in [53] was used to evaluate the TS method. A brief description of the dataset follows.

The EASSRs were recorded for a wide range of modulation frequencies f_m , between 0 and 100 Hz, during either 2 or 3 recording sessions, to determine the most efficient modulation frequency for objective CI fitting. Amplitude modulated (AM) high-rate 500 pps pulse trains were presented at maximum comfort level to 6 post-lingually deafened subjects with a Cochlear Nucleus® implant. Monopolar mode stimulation was used for all measurements, between intracochlear electrode 11 and the two extra-cochlear electrodes (MP1+2). The pulse rate was not an exact multiple of the modulation frequency. The pulse trains were modulated in amperes between the subject's unmodulated threshold level (T_u) and the modulated maximum comfortable level (C_m). Cochlear

Nucleus[®] implants are programmed in discrete current level units (CU) which are logarithmically related to current (in μA). All current levels between T_u and C_m were used for stimulation. The number of different stimulation pulse amplitudes (i.e., current levels) used was constant within subjects and varied between 20 and 89 over subjects. Within one recording, the stimulation pattern used was the same for each epoch. The distribution of stimulation pulse amplitudes used in the stimulation epoch of the $f_m = 42$ Hz recording of subject S1 is shown in panel A of Figure 4.2.

EEG signals were recorded during 5 minutes per condition with a 64-channel ActiveTwo Biosemi system, with a 8192 Hz sampling rate and 1638 Hz built-in low pass filter. Triggers were sent to the recording system at the start of each 1.024 s epoch. In the 30 – 50 Hz range for f_m , EASSRs were prominently present in all subjects. In the 80–100 Hz range for f_m , EASSRs could not effectively be measured in this pool of subjects, contrary to ASSRs in normal hearing subjects. More details can be found in [53].

Here, all recordings with modulation frequency between 30 and 50 Hz, recorded in session 1, were used for the evaluation of the TS method. Prominent responses were present in these recordings. Furthermore, per subject, one recording with a modulation frequency in the 70-100 Hz range (88 Hz for all subjects but S3, and 70 Hz for S3), also recorded in session 1, was selected for the template construction, see Section 4.2.2. This recording did not contain a significant response.

4.2.2 Data processing

The raw data signals $x[t, c]$, with t the time index and c the channel index, were stored in a matrix $\in \mathbb{R}^{N_t \times N_c}$, with N_t and N_c the number of time samples and channels, respectively. The signals were re-referenced offline to either the C_z or Fp_z recording channel (see Table 4.1), depending on the spatial distribution of the subject’s CI stimulation artifact [53], i.e.,

$$x^r[t, c] = x[t, c] - x[t, c_{ref}] \quad (4.1)$$

where c_{ref} refers to either C_z or Fp_z .

A set of specifically interesting recording channels in the parietal-temporal and occipital regions ($CP_{5/6}$, $TP_{7/8}$, $P_{5/6}$, $P_{7/8}$, $P_{9/10}$, $PO_{3/4}$, and $PO_{7/8}$) was selected for analysis. The same set as in [53] was used. For each subject, channels corresponding to locations on top of the RF coil and channels with excessive noise levels were excluded. The set of selected channels for each

Table 4.1: Recording channel selection per subject. As in [53], channels in the parietal-temporal and occipital region were selected. For each subject, channels corresponding to locations on top of the RF coil and channels with excessive noise levels were excluded.

	Ref	Contralateral	Ipsilateral
S1	C_z	CP ₅ , O ₁ , P ₅ , P ₇ , PO ₃ , PO ₇ , TP ₇	CP ₆ , O ₂ , PO ₄
S2	C_z	CP ₅ , O ₁ , P ₅ , P ₇ , P ₉ , PO ₃ , PO ₇ , TP ₇	CP ₆ , O ₂ , PO ₄
S3	C_z	CP ₆ , O ₂ , P ₆ , P ₈ , PO ₄ , PO ₈ , TP ₈	CP ₅ , O ₁ , P ₅
S4	Fp_z	CP ₅ , O ₁ , P ₅ , P ₇ , P ₉ , PO ₃ , PO ₇ , TP ₇	PO ₄ , O ₂
S5	Fp_z	CP ₅ , O ₁ , P ₅ , P ₇ , P ₉ , PO ₃ , PO ₇ , TP ₇	PO ₄ , O ₂
S6	C_z	CP ₆ , O ₂ , P ₆ , P ₈ , P ₁₀ , PO ₄ , PO ₈ , TP ₈	CP ₅ , O ₁ , P ₅ , PO ₃

subject is included in Table 4.1. Raw data signals were also averaged for the set of selected contra- and ipsilateral channels, resulting in two additional fictitious channel signals $\hat{c}_{\text{contra}}(x[t, c_{\text{contra}}])$ and $\hat{c}_{\text{ipsi}}(x[t, c_{\text{ipsi}}])$, and hence N_c became equal to $N_c + 2$.

Four CI stimulation artifact removal methods were used as described below: no artifact removal (NO), LI with interpolation duration $d = 1.1$ ms (LI₁₀₀₀), LI with $d = 2.0$ ms (LI₁₉₀₀) and template subtraction (TS).

No artifact removal (NO)

First, the first-order trend $x^{\text{trend}}[t, c]$ of each channel $x^r[t, c]$, $c = 1 \dots N_c$, was calculated with a non-overlapping 0.5 s sliding window and then subtracted. De-trending was used instead of high pass filtering, in order not to smear the CI artifacts out in time, as in [91].

$$x^d[t, c] = x^r[t, c] - x^{\text{trend}}[t, c] \quad (4.2)$$

The resulting de-trended data signals $x^d[t, c]$ were then split in 1.024 s epochs based on the trigger signal at the start of each epoch, and 5% of the epochs were rejected based on their peak-to-peak amplitude to eliminate excessive movement, ocular, and muscle artifacts. The epoch signals were stored in a three-dimensional tensor $\mathcal{X}[t', e, c] \in \mathbb{R}^{N_{t'} \times N_e \times N_c}$, with $N_{t'}$ the number of time samples in one epoch and N_e the number of epochs. Next, the Fourier transform $\overline{\mathcal{X}}[f, e, c]$ of the epoch signals was calculated for each epoch $e = 1 \dots N_e$ and channel $c = 1 \dots N_c$.

$\overline{\mathcal{X}}[f, e, c]$ was then used to determine the amount of synchronous and non-synchronous activity at the modulation frequency as follows. The synchronous activity (i.e., the neural response and CI stimulation artifacts) and non-synchronous activity (i.e., the brain background noise) were compared to decide whether significant synchronous activity is present. The synchronous activity was calculated for each channel as the average component at the modulation frequency $\overline{m}[f_m, c]$, averaged over epochs.

$$\overline{m}[f_m, c] = \text{mean}(\overline{\mathcal{X}}[f_m, e, c])_e \quad (4.3)$$

The response amplitude and phase were determined as the absolute value and angle of this average component.

$$\begin{aligned} A[f_m, c] &= |\overline{m}[f_m, c]| \\ \theta[f_m, c] &= \angle \overline{m}[f_m, c] \end{aligned} \quad (4.4)$$

This component can consist of both neural response and CI stimulation artifacts, with some residual brain background noise superimposed depending on the number of epochs averaged. For each channel, the brain background noise level was determined as the standard deviation of the component at the modulation frequency over epochs, divided by the square root of the number of epochs N_e .

$$N[f_m, c] = \frac{\text{std}(\overline{\mathcal{X}}[f_m, e, c])_e}{\sqrt{N_e}} \quad (4.5)$$

The Hotelling T^2 test [66] was used to compare the average real and imaginary components at the modulation frequency to the brain background noise level to determine whether significant synchronous activity is present. Response amplitude and phase were used further on to compare the four methods.

Linear interpolation (LI₁₀₀₀ and LI₁₉₀₀)

After re-referencing (4.1), a linear interpolation was applied between each pre-stimulus sample t_{pre} and post-stimulus sample t_{post} that are both assumed to be free from CI stimulation artifact.

$$\begin{aligned}
 x^l[t, c] &= x^r[t_{pre}, c] + \frac{x^r[t_{post}, c] - x^r[t_{pre}, c]}{t_{post} - t_{pre}}(t - t_{pre}) \\
 &\quad t_{pre} < t < t_{post} \\
 &\quad c = 1 \dots N_c
 \end{aligned} \tag{4.6}$$

The time between the pre- and post-stimulus samples is referred to as the interpolation duration $d = t_{post} - t_{pre}$. The maximum possible interpolation duration is the interpulse interval, which is the inverse of the pulse rate, in this case 2 ms. The pre-stimulus samples were always chosen at 0.1 ms before the start of a stimulation pulse, the post-stimulus samples were chosen at either 1 ms (LI₁₀₀₀) or 1.9 ms (LI₁₉₀₀) after the start of a stimulation pulse. Further processing followed the steps outlined above in Section 4.2.2, i.e., de-trending (4.2), averaging (4.3), EASSR (4.4) and brain background noise (4.5) calculation, and testing for significant synchronous activity with the Hotelling T^2 test. It has been shown that this method is indeed capable of removing the CI stimulation artifacts from contralateral recording channels for stimulation rates up to 500 pps [53, 37].

Template subtraction (TS)

The TS method used two recordings: (1) a template construction (TC) recording $x_{TC}[t, c]$ which contained no neural response and was used to construct a template of the CI stimulation artifact for every stimulation pulse amplitude (i.e., current level in CU); and (2) the recording of interest $x[t, c]$ from which the templates were subtracted. A recording without any synchronous neural response was used for the TC, to ensure that the templates only model the CI stimulation artifacts. It is of major importance that the tail of each CI stimulation artifact is modeled accurately; since any inaccuracies due to inadequate modeling of the initial artifact peaks can still be removed by LI. One or multiple artifact-free sample(s) are created, if the CI artifact tail is subtracted from each CI artifact pulse. A LI between two CI artifact-free samples, one before and one after each stimulation pulse, may then be used to remove the remaining CI artifact peak.

After re-referencing (4.1), a 0.5 s sliding window first-order de-trending (4.2) was applied to $x_{TC}[t, c]$ and $x[t, c]$. The resulting signals were split in epochs based on the trigger signal, 5% of the epochs were rejected based on their peak-to-peak amplitude. The remaining epoch signals were stored as $\mathcal{X}_{TC}[t', e, c]$ and

$\mathcal{X}[t', e, c]$. Next, all signals were averaged over epochs, resulting in the mean epochs $m_{TC}[t', c]$ and $m[t', c]$.

$$m_{TC}[t', c] = \text{mean}(\mathcal{X}_{TC}[t', e, c])_e \quad (4.7)$$

$$m[t', c] = \text{mean}(\mathcal{X}[t', e, c])_e \quad (4.8)$$

For the TC recording, a template for each stimulation pulse amplitude was determined based on the mean epoch. First, the mean epoch matrix $m_{TC}[t', c]$ was rearranged into the tensor $\mathcal{M}_{TC}[p, \hat{t}, c] \in \mathbb{R}^{N_p \times N_{\hat{t}} \times N_c}$, with N_p the number of pulses in one epoch and $N_{\hat{t}}$ the number of samples per stimulation pulse (in this case $\lfloor \frac{8192 \text{ samples/s}}{500 \text{ pps}} \rfloor = 16$ samples/pulse). The rows of $\mathcal{M}_{TC}[p, \hat{t}, c]$ contained the CI stimulation artifact following stimulation pulse p . The set of unique stimulation pulse amplitudes was called P_u . Then, all CI stimulation artifacts corresponding to pulses with the same amplitude were averaged, resulting in a template $\mathcal{T}[p_u, \hat{t}, c]$ for each stimulation pulse amplitude p_u and for each channel c . More EEG segments are averaged for the highest and the lowest stimulation levels because these levels occur most according to the histogram in Figure 4.2. This results in lower noise levels for the templates corresponding to the highest and the lowest stimulation levels. Alternatively, to ensure that the noise level is the same for all CI artifact templates, the number of averaged EEG segments for each stimulation level could be limited to the minimum of the histogram.

$$\forall p_u \in P_u : \mathcal{T}[p_u, \hat{t}, c] = \text{mean}(\mathcal{M}_{TC}[p = p_u, \hat{t}, c])_p \quad (4.9)$$

Next, the pulse templates were rearranged based on the stimulation pulse amplitude pattern used in the recording of interest, resulting in an epoch template $T_{epoch}[t', c]$.

Finally, this epoch template was subtracted from the mean epoch of the recording of interest (4.8), resulting in $m_{TS}[t', c]$.

$$m_{TS}[t', c] = m[t', c] - T_{epoch}[t', c] \quad (4.10)$$

A LI was then applied to each channel of $m_{TS}[t', c]$, because the initial peaks of the CI stimulation artifacts are not always adequately sampled with the relatively low sampling rate, which is also shown in panel B and C of Figure 4.2.

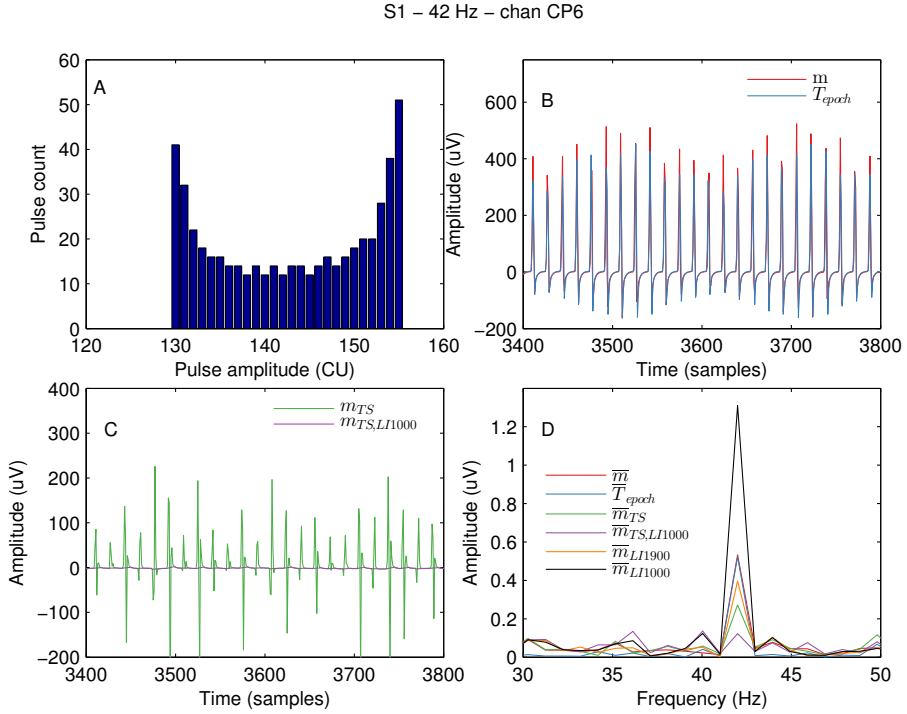


Figure 4.2: Illustration TS method for subject S1 in ipsilateral channel CP₆ for stimulation with an 42 Hz AM 500 pps pulse train. (A) Histogram of stimulation pulse amplitudes used within one stimulation epoch. All stimulation pulse amplitudes p_u between T_u and C_m are used for stimulation. A template $T[p_u, \hat{t}, c]$ is constructed for each of these stimulation pulse amplitudes p_u . (B) Part of a mean epoch without CI stimulation artifact removal $\bar{m}[t', c]$ (red) and constructed template $T_{epoch}[t', c]$ (blue), in the time domain. The templates are similar to the original signal, although the artifact peaks are not adequately modeled. (C) Mean epoch after TS $\bar{m}_{TS}[t', c]$ (green), and after TS and LI₁₀₀₀ $\bar{m}_{TS,LI1000}[t', c]$ (purple), in the time domain. After TS, the mean epoch still contains some residual CI stimulation artifacts, due to inadequate modeling of the artifact initial peak. These are removed with LI₁₀₀₀. (D) Mean epoch in frequency domain, without artifact removal $\bar{m}[f, c]$ (red), CI stimulation artifact template $T_{epoch}[f, c]$ (blue), mean epoch after TS $\bar{m}_{TS}[f, c]$ (green), after TS and LI₁₀₀₀ $\bar{m}_{TS,LI1000}[f, c]$ (purple), after LI₁₀₀₀ $\bar{m}_{LI1000}[f, c]$ (orange) and after LI₁₉₀₀ $\bar{m}_{LI1900}[f, c]$ (black). The component at f_m is different for \bar{m}_{LI1000} than for $\bar{m}_{TS,LI1000}$, indicating that the template subtraction does have a beneficial effect.

We chose $t_{pre} = 0.1$ and $t_{post} = 1$ ms or equivalently $d = 1.1$ ms, as this is a conservative value for the interpolation duration that definitely removes all the initial peaks of the CI stimulation artifacts for the sample rate used in these measurements.

The resulting mean epoch $m_{TS,LI_{1000}}[t', c]$ and its Fourier transform $\bar{m}_{TS,LI_{1000}}[f, c]$ were used to evaluate the response properties. For each channel c , the amplitude and phase of the synchronous activity were calculated as the absolute value and angle of $\bar{m}_{TS,LI_{1000}}[f_m, c]$, as in (4.4). The non-synchronous activity is determined from the original epoch signals $\mathcal{X}[t', e, c]$ as in (4.5). The original epoch signals, without CI stimulation artifact removal, were used to calculate the brain background noise level, as the presence of CI stimulation artifacts should not have any impact on the non-synchronous activity.

An example is shown in Figure 4.2, for the $f_m = 42$ Hz recording of S1 at the ipsilateral channel CP₆.

4.2.3 Evaluation of CI stimulation artifact removal methods

EASSR amplitudes and latencies were determined and used to confirm that the TS method effectively attenuates the CI stimulation artifacts below the noise level of the recordings. The LI₁₀₀₀ results were included because the same interpolation duration was used in the TS method, and were presented in order to rule out that any effects seen may be due to the LI only.

EASSR amplitude

EASSR amplitudes $A[f_m, c]$ were determined after LI and TS and compared for the individual contralateral channels and the channel \hat{c}_{contra} .

The EASSR amplitude difference between any of the first three methods (NO, LI₁₀₀₀ and LI₁₉₀₀) on the one hand and the TS method on the other hand, relative to the noise amplitude $N[f_m, c]$, was determined as follows:

$$\Delta A[f_m, c] = \frac{A[f_m, c]_{No/LI_{1000}/LI_{1900}} - A[f_m, c]_{TS}}{N[f_m, c]} \quad (4.11)$$

Negative values indicate that the response amplitude after TS was larger than for the other method. Amplitude differences were considered small when these were within the noise level, i.e., ΔA between -1 and 1 .

For each subject, the median value (and interquartile range (IQR)) of ΔA over modulation frequencies and channels, was determined. Furthermore, the median value (and IQR) over subjects, modulation frequencies and channels was also calculated.

Response latency

If the neural response is significantly larger than the brain background noise, the response phases $\theta[f_m, c]$ should decrease linearly with increasing modulation frequency f_m in the 30–50 Hz range [79, 53]. The non-zero slope of this linear decrease is related to the response latency. For CI stimulation artifact dominated measurements, response phases are stable at multiples of 180 degrees, regardless of the modulation frequency [64, 65, 53]. The slope of the $\theta(f_m)$ curve thus indicates whether the measurement is either neural response or CI stimulation artifact dominated, as it is related to the response latency.

A straight line was fit to the $\theta(f_m)$ curve, based on a least squares procedure. The response latency was calculated as the additive inverse of the slope, for all individual channel signals and for the channels \hat{c}_{contra} and \hat{c}_{ipsi} . In a causal system, the response latency should be positive. However, the fit is not constrained to negative slopes, i.e., positive response latencies. Therefore, in case of CI stimulation artifact dominated measurements, the response phase does not necessarily decrease with increasing modulation frequency, resulting in positive slopes and a negative response latency. For the channels \hat{c}_{contra} and \hat{c}_{ipsi} , a Wilcoxon signed-rank test was used to determine whether response latencies differed significantly between LI_{1900} and TS. For contralateral channels, response latencies were compared after LI_{1900} and TS as these should be very similar. For ipsilateral channels, response latencies of individual channels were compared to the expected median values of 44.2 (IQR = 6.8) ms. These expected values were taken from [53].

The response latency differences between different methods were calculated as:

$$\Delta RL = RL_{No/LI_{1000}/LI_{1900}} - RL_{TS} \quad (4.12)$$

where RL represents the response latency. Negative values mean that the response latency for TS is larger than for the other method, indicating that the CI stimulation artifacts are better removed with the TS method.

4.2.4 Influence of TC duration

The described method used a full recording $x^{TC}[t, c]$ with $0.95 * 300 = 285$ epochs to construct the CI stimulation artifact templates, which could result in excessive EEG recording times. Therefore, the TC recording duration was varied from 60 to 270 epochs, in steps of 30 epochs, to investigate its influence on the response amplitude and latency values. A Friedman ANOVA was used to test whether the TC duration has a significant influence on the obtained response latency.

4.2.5 Software and statistical analysis

All data processing was done in MATLAB R2013a. R (v3.0.2) was used for statistical analysis, with significance level $\alpha = 0.05$.

4.3 Results

4.3.1 Response properties

EASSR amplitude

EASSR amplitudes observed in the channels \hat{c}_{contra} and \hat{c}_{ipsi} are shown in Figure 4.3 for each individual subject. For the channel \hat{c}_{contra} , EASSR amplitude differences after LI₁₉₀₀ and TS are within the noise level. Therefore amplitudes after LI₁₉₀₀ are not significantly different from amplitudes after TS. For the channel \hat{c}_{ipsi} , EASSR amplitudes are generally smaller for TS than for LI₁₉₀₀, except for the lower modulation frequencies (30 – 33 Hz). The amplitude differences ΔA between the first three methods and TS, as defined in Equation (4.11), are included in Table 4.2.

Response latency

Response latencies for individual channels are included in Figure 4.4. For contralateral recording channels, median response latencies (and IQRs) are 40.4(16.8) ms, 48.2(18.8) ms, 45.3(11.1) ms, and 39.3(12.9) ms without artifact removal, after LI₁₀₀₀, after LI₁₉₀₀ and after TS, respectively. For ipsilateral recording channels, median response latencies (and interquartile ranges) are –3.6(47.9) ms, 5.6(14.6) ms, 32.5(26.7) ms, and 39.4(10.8) ms without artifact

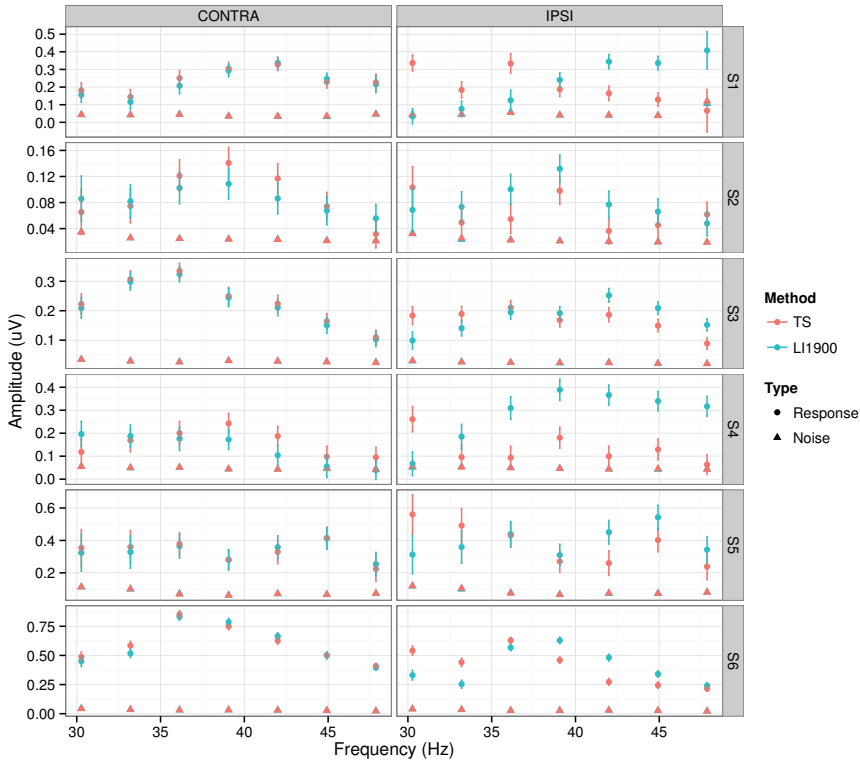


Figure 4.3: EASSR amplitudes are similar after LI and TS for the channel \hat{c}_{contra} in all subjects. In the ipsilateral channel \hat{c}_{ipsi} , EASSR amplitudes are generally smaller for TS than for LI₁₉₀₀, except for the lowest modulation frequencies. Error bars represent the noise level.

removal, after LI₁₀₀₀, after LI₁₉₀₀ and after TS, respectively. The Wilcoxon signed-rank test did not show a significant difference in response latency between LI₁₉₀₀ and TS ($p > 0.05$) for the channel \hat{c}_{contra} . However, for channel \hat{c}_{ipsi} , a significant difference in response latency is found after LI₁₉₀₀ and TS ($p = 0.03$). For most subjects, response latencies are within the expected range [53, 65] for all channels after TS, whereas latencies are smaller than expected for ipsilateral channels after LI₁₉₀₀. For subject S4, response latencies after TS are rather small, although latencies are larger than after LI₁₉₀₀ in ipsilateral channels. TS is thus able to remove more CI stimulation artifact from ipsilateral channels than LI.

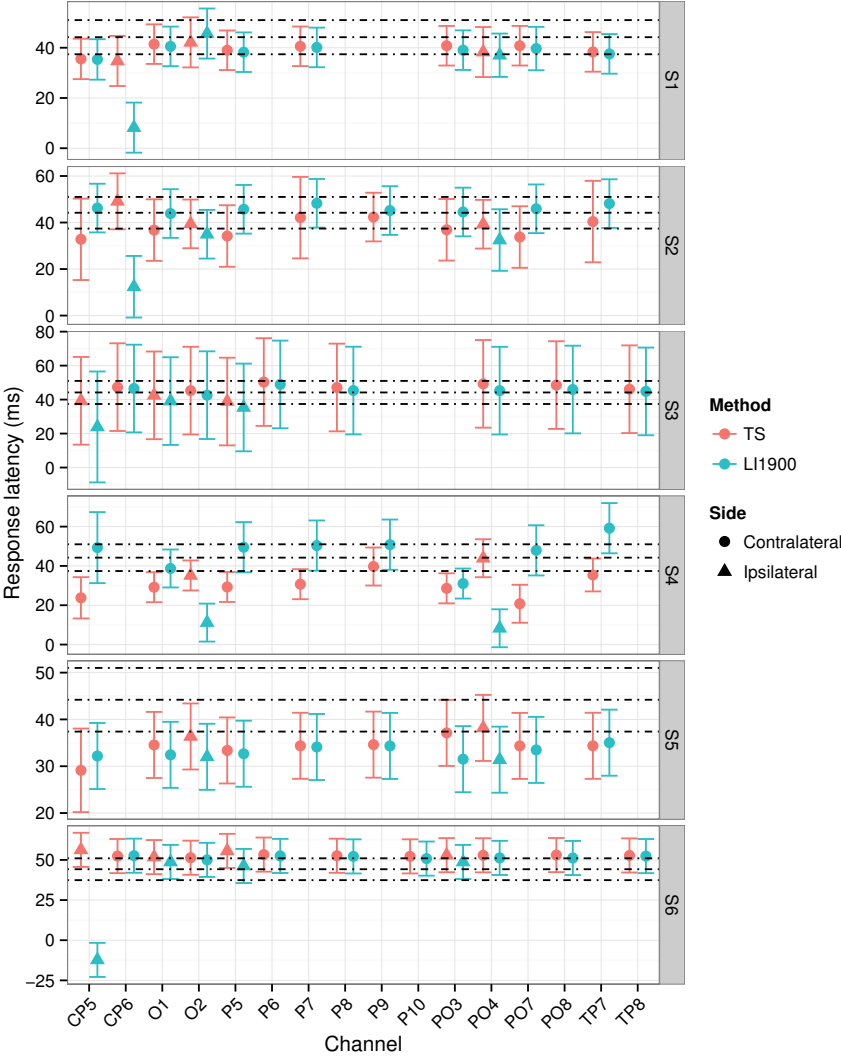


Figure 4.4: EASSR latencies per recording channel for LI and TS. Response latencies are small for some ipsilateral channels in most subjects, but are within the expected range after TS. Response latencies are calculated from a first order fit of the $\theta(f_m)$ curve. Error bars correspond to the 95% confidence intervals of this fit. The horizontal lines indicate the range of expected latencies, and correspond to the median (\pm IQR) values found in [53].

Response latency differences, as defined in Equation (4.12), comparing all available methods to the proposed TS method, are included in Table 4.2.

4.3.2 Influence of TC duration

The influence of the TC duration on the response latency in the channels \hat{c}_{contra} and \hat{c}_{ipsi} is shown in Figure 4.5. Already for short TC durations of 60 (TS_{60}) or 90 (TS_{90}) epochs, the obtained latencies are very close to the ones obtained with 270 (TS_{270}) epochs TC duration, indicating that short TC durations are sufficient for adequate CI stimulation artifact removal. Response latencies are compared for TS_{60} , TS_{90} , and TS_{270} using a Friedman ANOVA. No significant difference in response latency is found in the \hat{c}_{contra} ($\chi^2(2) = 1.33, p = 0.51$) or \hat{c}_{ipsi} channel ($\chi^2(2) = 0.33, p = 0.85$).

4.4 Discussion

EEG signals measured during continuous CI stimulation are distorted by CI stimulation artifacts, which may also be present at the neural response frequency. CI stimulation artifacts have very large amplitudes and their contribution at the response frequency may be several orders of magnitude larger than the neural response itself. Hofmann *et al* showed that CI stimulation artifacts can effectively be attenuated using LI, for low- and high-rate stimulation in bipolar mode [64, 65]. In [53], EASSRs to 500 pps modulation pulse trains were measured for a large range of modulation frequencies with stimulation in monopolar mode, and responses free of CI stimulation artifacts were found and analyzed in contralateral recording channels. In previous work [37], we have shown that CI stimulation artifacts can be characterized based on their duration, which is shorter than the interpulse interval at contralateral channels, for stimulation with 500 pps pulse trains stimulated in monopolar mode. Furthermore, it was shown that the reference channel may have an influence on the artifact characteristics.

It has thus been shown that CI stimulation artifacts can be removed from contralateral recording channels using LI, for stimulation pulse rates up to 500 pps [53, 37]. To our knowledge, none of the available methods are capable of attenuating the CI stimulation artifact below the noise level at ipsilateral recording channels.

In this work, we developed and evaluated an alternative TS based artifact removal method, by constructing artifact templates for each stimulation pulse

Table 4.2: Response properties: response amplitude difference (ΔA) between methods divided by noise amplitude; and response latency difference (ΔRL) between methods. Median(IQR) over modulation frequencies (for amplitude differences), and selected individual contra- and ipsilateral channels (see Table 4.1) for each subject, and over subjects.

		S1	S2	S3	S4	S5	S6	all
ΔA (°) Contralateral	No vs TS	0.3(2.7)	1.0(4.0)	0.0(1.5)	-0.2(1.7)	0.0(0.4)	-0.6(3.7)	0.0 (1.9)
	LI ₁₀₀₀ vs TS	0.0(1.2)	0.6(2.8)	0.5(1.8)	0.3(2.1)	0.0(0.7)	0.1(1.9)	0.1(1.6)
	LI ₁₉₀₀ vs TS	-0.2(0.9)	-0.2(1.0)	-0.3(0.3)	-0.5(1.5)	-0.1(0.5)	-0.2(1.1)	-0.2(0.9)
Ipsilateral	No vs TS	0.4(4.8)	10.2(19.3)	2.0(4.9)	6.5(6.9)	-0.1(5.4)	10.9(19.5)	3.6(11.8)
	LI ₁₀₀₀ vs TS	4.6(9.0)	5.6(16.8)	7.2(12.8)	17.5(5.2)	4.6(4.9)	9.5(20.3)	7.1(15.2)
	LI ₁₉₀₀ vs TS	0.5(3.8)	0.3(0.9)	0.4(3.0)	4.1(2.5)	0.6(2.0)	0.7(6.4)	0.5(3.8)
ΔRL (ms) Contralateral	No vs TS	-9.0(1.7)	17.5(19.1)	-4.9(1.8)	11.2(4.0)	-1.4(0.4)	-2.8(1.1)	-2.1(13.3)
	LI ₁₀₀₀ vs TS	0.4(1.9)	15.7(7.3)	3.3(1.5)	-34.0(40.5)	0.9(2.8)	1.0(2.6)	1.6(5.4)
	LI ₁₉₀₀ vs TS	-0.8(0.4)	7.7(4.8)	-1.8(1.3)	19.9(13.5)	-0.5(1.1)	-1.1(1.0)	-0.4(8.8)
Ipsilateral	No vs TS	4.2(27.7)	-46.4(4.0)	-46.0(26.2)	-43.9(4.3)	-2.5(8.6)	-58.5(15.8)	-43.3(51.0)
	LI ₁₀₀₀ vs TS	-33.0(7.5)	-30.5(12.0)	-33.2(15.1)	-37.3(4.7)	-21.5(4.3)	-49.2(17.7)	-33.0(19.7)
	LI ₁₉₀₀ vs TS	-1.3(15.0)	-6.8(16.1)	-3.5(6.0)	-29.8(5.8)	-5.6(1.2)	-6.8(20.2)	-6.8(20.5)

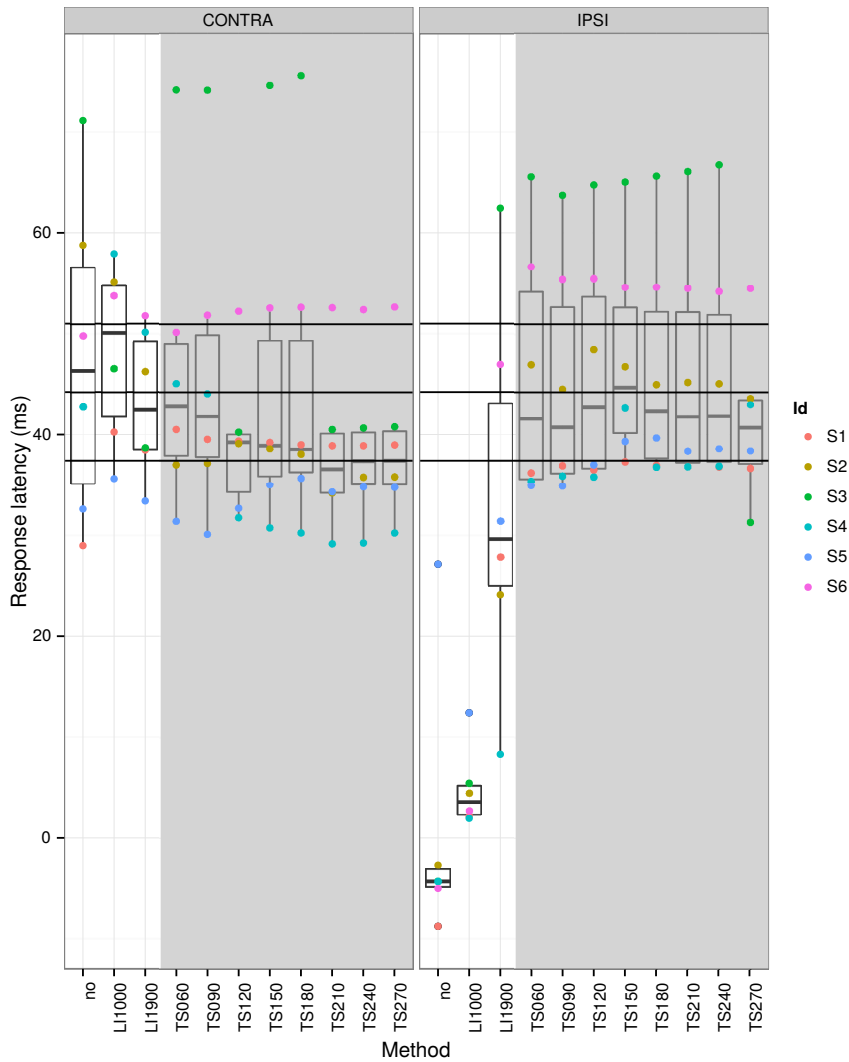


Figure 4.5: EASSR apparent latencies for LI and TS, for channels \hat{c}_{contra} and \hat{c}_{ipsi} : influence of TC duration. No significant difference is found between TS_{060} , TS_{090} , and TS_{270} in either channel.

amplitude and subtracting these from a recording of interest. We hypothesized that such a (single channel) method would be capable of modeling subject- and channel-specific CI stimulation artifacts without imposing an assumption on the artifact duration. The artifact templates are constructed based on a recording that does not contain a significant EASSR, to ensure that the artifact template only models the artifact and does not contain EASSR components. The method was applied to EEG recordings containing significant EASSRs in response to suprathreshold stimulation levels.

4.4.1 Results and interpretation

Contralateral

In the contralateral recording channels, the EASSR is dominant compared to the relatively small contribution of the CI stimulation artifact, as observed in Table 4.2. Median normalized response amplitude errors were between -1 and 1 for all methods. However, the IQR of the error between LI_{1900} and TS seems to be smaller than for the other methods. The obtained amplitudes for LI_{1900} and TS are more similar than for any of the remaining methods (no and LI_{1000} vs TS).

As shown in Section 4.3.1, median response latencies were very similar for all four methods, but IQRs were smaller after LI_{1900} and TS than after NO and LI_{1000} , indicating that LI_{1900} and TS still remove more CI stimulation artifacts.

The same observation can be made based on the response latency differences: median differences were rather small between NO, LI_{1000} , LI_{1900} on the one side and TS on the other side. For most subjects, IQRs of the response latency differences were smaller when LI_{1900} and TS were compared, than for NO and LI_{1000} vs TS.

Ipsilateral

In the ipsilateral channels, EEG signals were clearly dominated by CI stimulation artifacts when no artifact removal or LI_{1000} is applied. In the \hat{c}_{ipsi} channel, EASSR amplitudes are generally smaller for TS than for LI_{1900} , see Figure 4.3, except for the lowest modulation frequencies. We observed that CI stimulation artifact and EASSR are in phase at these modulation frequencies. We modeled the observed amplitude and phase error, for varying artifact-response amplitude ratios and artifact-response phase differences, see Figure 4.6. Amplitude errors are largest when artifact and response are in phase, and increase with higher

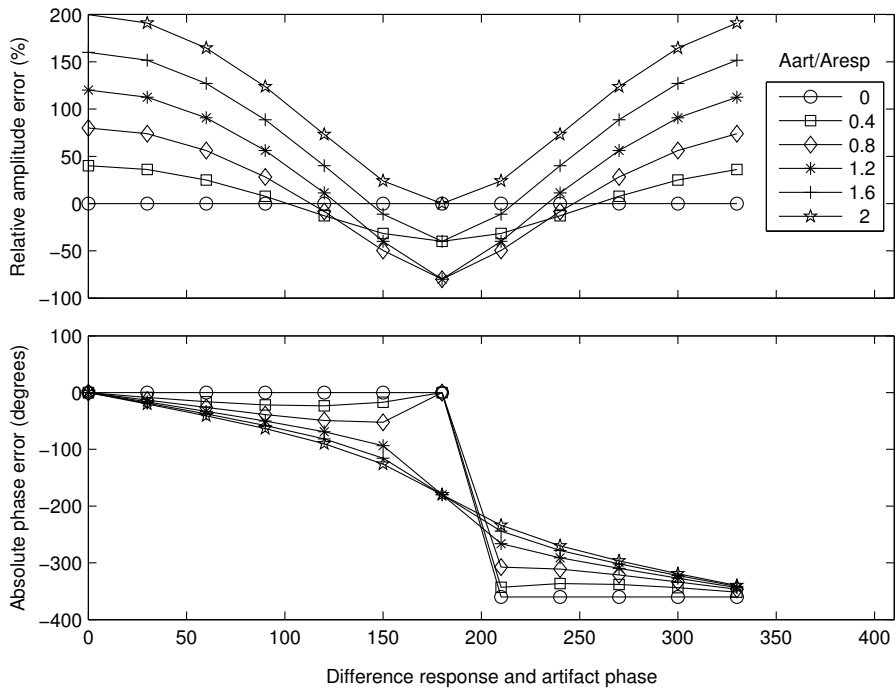


Figure 4.6: Relative amplitude and absolute phase error in function of the difference in response and artifact phase. Generally, larger artifacts result in larger amplitude and phase errors. Amplitude errors are largest when response and artifact are in phase or around 180° out of phase. Phase errors are generally smaller for these phase differences, and are largest when response and artifact are $100 - 150^\circ$ or $200 - 250^\circ$ out of phase.

residual artifact levels. It is thus likely that this result reflects some residual artifact in the 30 and 33 Hz recordings in some subjects.

Response amplitude differences between TS and NO or LI₁₀₀₀ ranged from -0.1 to 17.5 times the noise level (median value). This indicates that response amplitudes were up to 17.5 times the noise level larger for LI₁₀₀₀ and NO than for TS. Furthermore, very large IQRs were observed. The median response amplitude difference between LI₁₉₀₀ and TS was within the noise level for most subjects, but the IQR of this error was variable over subjects, up to 6.4 times the noise level. This indicates that amplitude differences for all methods compared to TS can be quite large for ipsilateral recording channels.

The median response latencies of -3.6 and 5.6 ms obtained with NO and LI₁₀₀₀

methods were rather small, compared to the expected value of 44.2 ms. This indicates that the EEG signals were dominated by the CI stimulation artifacts. Note that a negative apparent latency is not physiologically possible, but is a result of the first-order fit on artifact dominated measurements. The median response latency of 32.5 ms for LI₁₉₀₀ was within the expected range, but the IQR of 26.7 ms was rather large compared to the expected value of 6.8 ms. This indicates that conditions (e.g., subjects, recordings, and recording channels) exist for which the LI₁₉₀₀ does not remove all CI stimulation artifacts. The values obtained after TS (median = 39.4 ms, IQR = 10.8 ms) were in line with the expectations.

The median response latency differences of NO and LI₁₀₀₀ compared to TS were more than 20 ms, for most subjects. After LI₁₉₀₀, appropriate latencies were obtained for some subjects, but not all, while the latencies were within the expected range for all subjects after TS, see Figure 4.4.

The LI₁₀₀₀ method was unable to remove all CI stimulation artifacts from the EEG signals, while reliable response latencies were obtained with the TS method. Importantly, the main contribution of the method is thus in the adequate modeling of the CI stimulation artifact tail, and not in the LI after the template subtraction.

4.4.2 Significance

Good results were obtained in the two fictitious averaged channels \hat{c}_{contra} and \hat{c}_{ipsi} , as shown in Figures 4.3 and 4.5. Furthermore, response properties for individual recording channels are included in Figures 4.4 and Table 4.2. It is interesting to see that reliable response properties were obtained in all individual recording channels as well.

In clinical environments, multichannel systems are often not available or impractical. Because good results were obtained in individual contralateral and ipsilateral recording channels, objective CI fitting methods based on single channel recordings could be developed.

A possible disadvantage of the method is the need of a response-free recording for template construction. We showed that the duration of the recording used for template construction can be reduced to 1 minute, without significant changes in obtained response latencies. The additional recording time could thus be reduced to 1 minute, provided that stimulation is between the same minimum and maximum level in both recordings. In case several stimulation levels are tested, 1 minute extra recording time is needed per tested stimulation level.

Artifact-free EEG signals at ipsilateral channels are of major importance for lateralization studies, that e.g., look into the reorganization or development of the auditory pathway in long-term hearing deprived subjects or infants and children with CIs. In case of bilateral CI stimulation, the LI method is incapable of providing useful information, as ipsilateral channels contain large and long CI stimulation artifacts that cannot be removed. The results presented in the present study indicate the feasibility of removing CI stimulation artifacts at all (including ipsilateral) channels using the TS method. Furthermore, for source localization purposes, it is important that artifact-free EEG signals are obtained over the entire scalp with small spatial resolution. Using the LI method with unilateral CI stimulation, at least a quarter of the channels is excluded, because these are too close to the CI. In case of bilateral CI stimulation, even more channels are unavailable.

4.4.3 Future work

First, future work should focus on improvements of the proposed method. It should be investigated whether additional template construction recordings could be omitted: CI stimulation artifact templates could possibly be constructed based on recordings that have to be acquired during the protocol or based on alternative short template construction recordings. Models describing the scaling behaviour of pulse templates for increasing pulse amplitudes could be used to make generalizations of CI stimulation artifact properties and behaviour. It is expected that CI artifacts would scale linearly with increasing stimulation level. A single subthreshold measurement could therefore be sufficient to construct CI artifact templates that can be applied for all stimulation levels. In this study, templates were constructed based on an existing dataset, and additional assumptions on the CI artifact scaling behavior was avoided by constructing the templates for the same stimulation pulse levels as were used for the recording of interest. The EEG signals may still contain some residual artifact after template subtraction, and methods could be developed to remove this residual CI stimulation artifact.

Furthermore, the performance of the TS method should be investigated for EEG signals with smaller or no neural responses than the ones present in the 40 Hz range dataset used in this study. In this study, only recordings to suprathreshold stimulation at C level were considered. However, the EASSRs amplitudes vary between 40 and 1048 nV in the pool of subjects tested in this study. Therefore, we would argue that a representative range of 40 Hz EASSR amplitudes has already been tested. In infants and children, it may be necessary to use modulation frequencies in the 80 Hz range to measure EASSRs. During neonatal hearing screening, infants are usually tested with

80 Hz range modulated stimuli, as attention effects and sleep do not play a role at these modulation frequencies [5, 84]. To our knowledge, up to date, no study has examined the effect of modulation frequency on EASSRs in infants and children with a CI yet. In NH subjects, it has been shown that EASSR amplitudes are generally smaller in the 80 Hz range, compared to the 40 Hz range, with reduced brain noise levels as well [79]. During CI fitting procedures, EASSRs near and below threshold have to be measured reliably. It is crucial that all CI stimulation artifacts are removed from these recordings to prevent false detections and incorrect threshold estimations. When the CI stimulation artifacts are not attenuated below the noise level, the stimulation artifact is dominant for low EASSR amplitudes, causing large amplitude and phase errors on the observed synchronous component, as shown in Figure 4.6.

4.5 Conclusion

A template subtraction method for CI stimulation artifact removal from EEG signals recorded during continuous CI stimulation has been developed. A template is constructed for every stimulation pulse amplitude based on a template construction recording (TC), containing CI stimulation artifacts but no neural response. This template is then subtracted from the recording of interest.

Response properties are similar for LI_{1900} and TS, at individual contralateral recording channels and for the channel \hat{c}_{contra} . For LI_{1900} , response amplitudes are too large and latencies are too small at individual ipsilateral recording channels and for the channel \hat{c}_{ipsi} . Only the TS method is able to remove the CI stimulation artifacts and results in reliable response amplitudes and latencies. A TC duration of only 1 minute is sufficient to construct adequate templates that result in reliable response properties after subtraction.

Future work will evaluate how well the TS method works on EEG signals with smaller neural responses that are more easily dominated by CI stimulation artifacts. Alternative methods that eliminate any residual CI stimulation artifacts after TS will also be developed and evaluated.

Chapter 5

A Kalman filter based method for electrically evoked auditory steady state response parameter estimation

Abstract

Electrically evoked auditory steady-state responses (EASSRs) can be detected in electroencephalogram (EEG) measurements and used for objective cochlear implant (CI) fitting. Recently, several methods have been developed to estimate EASSR parameters in the presence of CI electrical artifacts. In a previous Kalman filter (KF) based method, the signal model is based on the assumption that CI artifacts are monophasic and of short duration. We propose an extension to the signal model, used by the KF for EASSR amplitude and phase estimation, that accommodates more general CI artifact shapes, including biphasic CI artifacts with an exponentially decaying tail. The KF based method is then compared to a linear interpolation (LI) and a template subtraction (TS) based

This chapter is an adapted version of Deprez, Hanne, et al. “A Kalman filter based method for electrically evoked auditory steady state response parameter estimation.” *Submitted*. Changes are limited to layout and representation aspects, and minor editing.

EASSR parameter estimation method. For a dataset with biphasic, modulated, exponentially decaying CI artifacts, the proposed KF based method results in the same EASSR amplitude and phase estimates as the LI based method. KF based EASSR parameter estimation is a promising tool that can be applied to single-channel measurements without additional data collection to construct the CI artifact template, and could possibly be used for reliable EASSR parameter estimation in the presence of severe CI electrical artifacts in cases where the LI based method fails.

5.1 Introduction

Cochlear implants (CIs) are used to treat severe to profound hearing loss in adults, children and infants. Incoming sounds, picked up by a microphone, are converted to electrical pulse sequences that are delivered to intracochlear electrodes, thereby stimulating the auditory nerve and eliciting an auditory percept. Stimulation parameters, such as minimal and maximal stimulation levels (further called T and C levels, respectively), stimulation mode, pulse rate and pulse width etc., are set at CI activation, and adjusted in subsequent CI fitting sessions. Regularly used stimulation modes are monopolar and bipolar mode stimulation. Monopolar (MP) mode stimulation refers to stimulation between an intracochlear and an extracochlear electrode, while bipolar (BP) mode stimulation refers to stimulation between two intracochlear electrodes. MP mode stimulation is most often used in clinical practice, because stimulation levels vary less over stimulation electrodes compared to BP mode stimulation, and because of the lower battery power consumption [20, 81, 114, 155]. However, determining appropriate stimulation levels is challenging in infants and in subjects with additional disabilities that cannot provide (accurate) feedback on the sounds they perceive.

Objective measures are currently under investigation for objective CI fitting [17, 70], i.e., to determine appropriate stimulation levels, without the need for behavioral feedback from the subject. Electrically-evoked auditory steady-state responses (EASSRs), in particular, are neural responses to periodic low-rate or modulated high-rate pulse trains, that can objectively be detected in the EEG at the repetition or modulation frequency [41]. Similar to acoustic auditory steady-state responses (ASSRs) [79], it has been shown that electrophysiological thresholds based on EASSRs correlate well with behavioral T levels, for high-rate stimulation in BP mode [64, 65]. The possible advantages of EASSRs over other objective measures have been discussed in [37, 38, 39, 53, 65]. Beside CI fitting, EASSRs could possibly be used to study the electron-neuron interface [90] and auditory plasticity and maturation after cochlear implantation. Recently, the

neural processing of modulated signals has been investigated in acoustic and CI listeners, using (E)ASSRs [89]. In this study, a source localization method was developed to study differences in neural generators and hemispheric laterality between both groups of listeners. BP mode stimulation was used for the EASSR recordings in CI subjects.

ASSR parameters, such as ASSR amplitude and phase, can be estimated by means of a discrete Fourier transform (DFT) [115]. The measured EEG signals are then split in epochs, and each epoch is analysed with a DFT. The ASSR amplitude and phase are estimated as the absolute value and angle of the component at the modulation frequency averaged over epochs. Alternatively, a Kalman filter (KF), based on a signal model, may be used for ASSR parameter estimation [91]. The KF based method may have several advantages compared to the DFT based method. First, signal stationarity is not assumed. Second, because EASSR parameter estimations are updated at every sample, changes in response parameters, e.g., due to attention and adaptation effects can be studied.

EASSR measurements, however, suffer from contamination by CI electrical artifacts. Therefore, an additional CI artifact suppression is required in order to obtain a reliable EASSR parameter estimation. Three DFT based methods with CI artifact suppression have been developed and evaluated in [38, 39, 40, 64, 65], and are shortly reviewed here. The first and most commonly adopted method (LI-DFT) uses a linear interpolation (LI) to remove EEG segments affected by a CI artifact. The LI is then applied between two samples that are not affected by a CI artifact [64, 65]. When the CI artifacts are longer than the interpulse interval (IPI), LI is not capable of completely suppressing the CI artifacts, i.e., below the noise level. The second method (TS-DFT) uses a template subtraction (TS) [38]. Based on an EEG recording that contains CI artifacts but no significant EASSR, a CI artifact template is constructed for each stimulation pulse amplitude. CI artifacts typically consist of a peak, followed by a decaying tail. It is mainly the tail that is modeled by the CI artifact template, while the CI artifact peak is attenuated with LI, as this is not accurately represented in the CI artifact template due to the low sampling rate. The third method (ICA-DFT) is based on independent component analysis (ICA) [40, 39]. Multichannel EEG signals are split in statistically independent components, and the components corresponding to the CI artifacts are manually or automatically identified and rejected.

As an alternative to the DFT based method, a Kalman filter (KF) (E)ASSR parameter estimation method has been developed in [91], also including CI artifact suppression. The KF uses a signal model that combines an EASSR model and a CI artifact template. The CI artifact template presented in [91] consists of a train of triangular pulses with a fixed pulse width. While the

template used in TS-DFT is data-driven, i.e., subject- and channel-specific based on an EEG measurement, the template used here is constructed by the researcher and no additional data collection is required.

The CI artifact duration, in combination with the IPI, determines whether LI can reliably be used for CI artifact suppression. Four main factors influence either the CI artifact duration, or the IPI. First, the pulse rate is inversely proportional to the IPI: LI is less likely to completely suppress CI artifacts at higher pulse rates. Second, the stimulation mode influences CI artifact characteristics: MP mode stimulation results in larger and longer CI artifacts than BP mode stimulation [69, 85]. Third, CI artifacts are usually shorter in recording channels that are placed further away from the CI electrode array and CI coil [37]. For our recording set-up, it has been shown in [37, 39, 53] that CI artifacts for MP stimulation are not always completely suppressed in ipsilateral recording channels for stimulation at 500 pulses per second (pps), and in contralateral and ipsilateral recording channels for stimulation at 900 pps. Fourth, CI artifacts may be more significant in children than in adults. In children, due to the smaller head size, EEG signals may be CI artifact dominated even in the contralateral hemisphere. As children are the main target audience for objective CI fitting based on EASSR measurements, this is an important issue to consider.

With LI, reliable EASSR parameter estimation is currently possible in contralateral recording channels in adults for MP mode stimulation at C level at 500 pps, with our recording set-up [37, 53]. In some ipsilateral recording channels, EEG signals are often CI artifact dominated for stimulation at 500 pps, even in adults. This precludes source localization, and studying hemispheric specialization or lateralization in CI subjects.

Although it has been shown in [38, 39] that CI artifacts are reliably suppressed in selected ipsilateral recording channels using TS for 500 pps MP mode stimulation, this method also has its disadvantages. With TS, it is assumed that CI artifacts are stationary over the course of a recording session. Furthermore, there is the extra need for data collection to construct the template. Finally, it is not guaranteed that the template, that is constructed through averaging EEG segments, does not contain any auditory neural response. On the other hand, the method can cope with a variety of CI artifact shapes as no a priori assumptions are made.

ICA-based CI artifact suppression has been applied successfully in some cases, but the separation quality is not always sufficient to ensure a complete and reliable CI artifact suppression, and so the method lacks robustness [39]. Furthermore, an expensive multichannel set-up is needed for ICA-based CI artifact suppression. On the other hand, the method can also cope with a

variety of CI artifact shapes.

The KF based method presented in [91] has successfully been evaluated in a contralateral channel for BP mode stimulation. However, the template is not very flexible and cannot cope with the different CI artifact shapes that are typically observed for MP mode stimulation. On the other hand, depending on the chosen model signal parameters, the KF is able to compensate for slow changes in the CI artifacts amplitude so that stationarity of the CI artifacts amplitude does not have to be assumed.

More advanced methods offering improved performance are thus needed for reliable EASSR parameter estimation in challenging scenarios, e.g., for high-rate MP mode stimulation in children, or for more brain neuroscience related EASSR analyses, such as hemispheric lateralization or source localization. The aim of this paper is to design a more general CI artifact template to be used in the KF based method for reliable EASSR parameter estimation in the presence of CI artifacts of general shapes that are not completely stationary over time. The KF based method may then provide advantages compared to the DFT based method. Unlike LI-DFT, it can be applied in cases where the CI artifact duration is longer than the IPI. Unlike in TS-DFT, stationarity of the CI artifacts is not assumed and no extra data collection is needed for template construction. Unlike for ICA-DFT, no multichannel recordings are needed, and the EASSR parameter estimation is possibly more robust as statistical independence of the EASSR and the CI artifact is not assumed. As a proof of concept, the KF based method is evaluated on an existing EASSR dataset gathered in six post-lingually deafened adults, with 500 pps MP mode stimulation at C level.

The organization of the paper is as follows: the materials and methods are described in Section 5.2, results are presented in Section 5.3, followed by a discussion in Section 5.4.

5.2 Materials and methods

The dataset used for evaluation is described in Section 5.2.1. The signal model used in the KF based method is presented in Section 5.2.2. The EASSR parameter estimation methods are discussed in Section 5.2.3, followed by a description of the evaluation criteria in Section 5.2.4.

5.2.1 Dataset

A modulation frequency transfer function (MFTF) dataset was collected in six adult post-lingually deafened CI subjects in [53]. All subjects had actively used Cochlear Nucleus[®] implants for at least six months at the time of testing. T and C levels were determined for stimulation with unmodulated pulse trains (T_u and C_u), as well as C levels for stimulation with amplitude modulated (AM) pulse trains (C_m) with modulation depth such that the minimal level equals T_u . EASSRs were collected for a large range of modulation frequencies f_m between 1 and 100 Hz for 500 pps pulse trains. All subjects were stimulated in MP mode MP1+2, i.e., between an electrode in the middle of the electrode array and the two reference electrodes outside the cochlea which are electrically coupled [148]. AM pulse trains, modulated between T_u and C_m , were presented to the subjects, and are defined as

$$s(t) = A (1 + M \sin(2\pi f_m t + \phi_m)) p(t) \quad (5.1)$$

$$A = \frac{C_m + T_u}{2} \quad (5.2)$$

$$M = \frac{C_m - T_u}{C_m + T_u} \quad (5.3)$$

$$\phi_m = 90^\circ \quad (5.4)$$

where $p(t)$ denotes a 500 pps pulse train, and C_m and T_u are expressed in amperes. The AM modulation results in (a) constant CI artifacts, which do not scale with changing stimulation pulse amplitudes, as well as (b) modulated CI artifacts, which do scale with changing stimulation pulse amplitudes. More details can be found in [53].

For each subject, seven measurements with f_m between 30 and 48 Hz resulting in high signal-to-noise ratio (SNR) EASSRs were used for evaluation of the proposed KF based method. In the contralateral recording channels, the EASSR parameter estimates obtained with the KF based method can therefore be compared to the baseline estimates obtained with LI-DFT.

Five minute recordings were made per condition, totaling 210 minutes of data gathered over all subjects and conditions. All recordings were made in a soundproof and electrically shielded room.

5.2.2 Signal model

In the following, bold uppercase symbols represent matrices, bold lowercase symbols represent vectors, and regular lowercase symbols represent scalars.

The state-space signal model used in the KF consists of a state transition model (eq. 5.5) and an observation model (eq. 5.6):

$$\mathbf{x}_{k+1} = \mathbf{F}_k \mathbf{x}_k + \mathbf{w}_k \quad (5.5)$$

$$\mathbf{z}_k = \mathbf{H}_k \mathbf{x}_k + \mathbf{v}_k \quad (5.6)$$

with \mathbf{x}_k the state vector, \mathbf{F}_k the state transition matrix, \mathbf{z}_k the observation, and \mathbf{H}_k the observation matrix at discrete time k . \mathbf{w}_k and \mathbf{v}_k are random vectors, representing the process noise and the observation noise, respectively, and are assumed to be zero-mean Gaussian and white with covariance matrix \mathbf{Q}_k and \mathbf{R}_k , respectively.

3-component state-space model

The state-space model as proposed in [91] is briefly presented here for completeness, and is further referred to as the 3-component state-space model.

In [91], a three component state vector $\mathbf{x}_k = [x_{k,1} \ x_{k,2} \ x_{k,3}]^T$ is used to model a single-channel EASSR recording. The EASSR is modeled as a sinusoid with unknown amplitude and phase, while the CI artifacts are modeled by means of a scaled CI artifact template, which is chosen to be a train of triangular pulses, presented at the pulse rate. It is assumed that the states vary slowly, according to a random walk model. The state-space model is then given as follows:

$$\begin{bmatrix} x_{k+1,1} \\ x_{k+1,2} \\ x_{k+1,3} \end{bmatrix} = I_3 \begin{bmatrix} x_{k,1} \\ x_{k,2} \\ x_{k,3} \end{bmatrix} + \mathbf{w}_k \quad (5.7)$$

$$z_k = \begin{bmatrix} \cos(2\pi f_m k T_s) \\ -\sin(2\pi f_m k T_s) \\ a(k T_s, f_c, w) \end{bmatrix}^T \begin{bmatrix} x_{k,1} \\ x_{k,2} \\ x_{k,3} \end{bmatrix} + v_k \quad (5.8)$$

$$a(k T_s, f_c, w) = \begin{cases} 1 - \frac{d(k T_s, f_c)}{w} & \text{for } -w \leq d(k T_s, f_c) \leq w \\ 0 & \text{elsewhere} \end{cases} \quad (5.9)$$

$$\text{with } d(k T_s, f_c) = \min(\text{mod}(-k T_s, \frac{1}{f_c}), \text{mod}(k T_s, \frac{1}{f_c})) \quad (5.10)$$

Here I_3 denotes a 3-by-3 identity matrix, and *mod* denotes the modulo operation. $x_{k,1}$ and $x_{k,2}$ represent the real and imaginary part of the EASSR, respectively, while $x_{k,3}$ models the instantaneous CI artifact amplitude. f_m and f_c denote the modulation frequency and pulse rate, respectively. $T_s = \frac{1}{f_s}$ is the sampling interval. $a(k T_s, f_c, w)$ is the CI artifact template, i.e., a train of triangular pulses of width w , presented at the pulse rate f_c . The process covariance matrix \mathbf{Q}_k is a diagonal matrix with diagonal elements equal to $1E-7$. Finally, z_k is the observed signal with the EASSR, CI artifacts and observation noise v_k . The observation noise covariance R_k is a scalar, equal to the variance of the recorded signal [91]. A realization of the CI artifact template $a(k T_s, f_c, w)$ is provided in [91], Figure 1.

6-component state-space model

In [91], EASSRs have only been considered in response to BP stimulation, and only for contralateral recording channels. Here, the aim is to consider a more general set of stimulation and recording parameters. In the more general case, CI artifacts are not monophasic, but rather biphasic, as shown in Figure 5.1. Furthermore, a CI artifact peak is usually followed by a decaying tail, as can also be seen in Figure 5.1. The CI artifact model proposed in [91] is indeed unable to model and remove biphasic CI artifact peaks and CI artifact tails.

We therefore propose a more general CI artifact template. For a single-channel EASSR recording, the proposed state-space model has a six component state vector $\mathbf{x}_k = [x_{k,1} \ x_{k,2} \ \dots \ x_{k,6}]^T$. The first two components are again used to

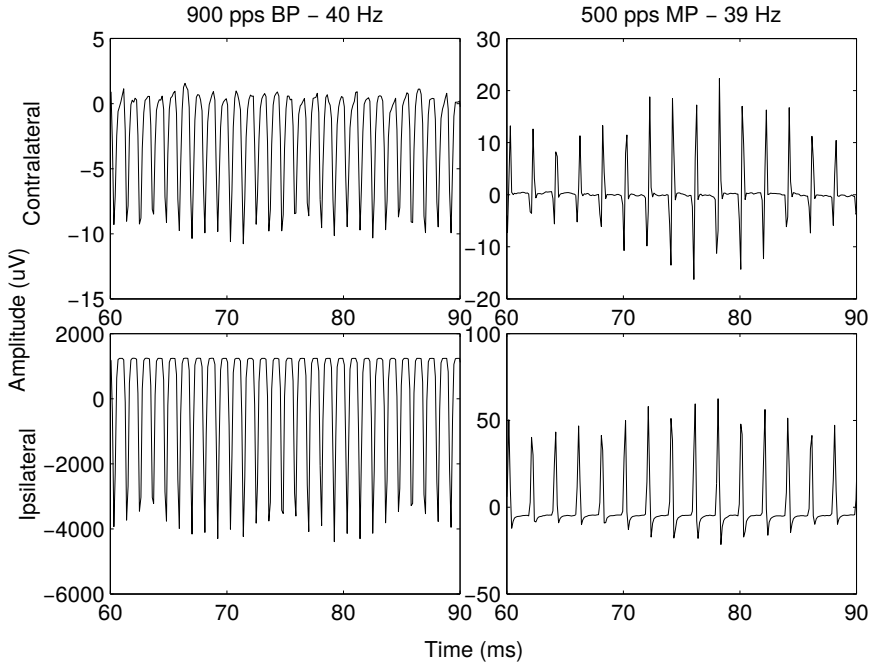


Figure 5.1: Comparison of CI artifact shapes, in an averaged epoch, for BP and MP stimulation. Subject S02, reference channel C_z . Left: BP stimulation at C level with $f_m = 40$ Hz, 900 pps. Right: MP stimulation at C level with $f_m = 39$ Hz, 500 pps. Top: contralateral recording channel P_6 . Bottom: ipsilateral recording channel O_2 .

model the EASSR, as a sinusoid with unknown amplitude and phase. The other four components are used to model the CI artifacts. It is again assumed that the state vector follows a random walk model (eq. (5.11)).

The state-space model is then given as follows:

$$\begin{bmatrix} x_{k+1,1} \\ x_{k+1,2} \\ x_{k+1,3} \\ x_{k+1,4} \\ x_{k+1,5} \\ x_{k+1,6} \end{bmatrix} = I_6 \begin{bmatrix} x_{k,1} \\ x_{k,2} \\ x_{k,3} \\ x_{k,4} \\ x_{k,5} \\ x_{k,6} \end{bmatrix} + \mathbf{w}_k \quad (5.11)$$

$$z_k = \begin{bmatrix} \cos(2\pi f_m k T_s), \\ -\sin(2\pi f_m k T_s), \\ p(k), \\ c(k), \\ m(k), \\ 1 \end{bmatrix}^T \begin{bmatrix} x_{k,1} \\ x_{k,2} \\ x_{k,3} \\ x_{k,4} \\ x_{k,5} \\ x_{k,6} \end{bmatrix} + v_k \quad (5.12)$$

$$p(k) = \begin{cases} 1 & \text{for } T_{p,n} < k T_s < T_{p,n} + w, n = 1 \dots N_t \\ 0 & \text{elsewhere} \end{cases} \quad (5.13)$$

$$c(k) = e^{mod(-\alpha k T_s, \frac{1}{f_c})} * \sum_{n=1}^{Nt} \delta(T_{p,n} + w - k T_s) \quad (5.14)$$

$$m(k) = \sin(2\pi f_m k T_s + \hat{\phi}_m) \quad (5.15)$$

$$e^{mod(-\alpha k T_s, \frac{1}{f_c})} * \sum_{n=1}^{Nt} \delta(T_{p,n} + w - k T_s)$$

$$\mathbf{Q}_k = \begin{bmatrix} 10^{-12} & 0 & 0 & 0 & 0 & 0 \\ 0 & 10^{-12} & 0 & 0 & 0 & 0 \\ 0 & 0 & 10^{12} & 0 & 0 & 0 \\ 0 & 0 & 0 & q_{\text{tail}} & 0 & 0 \\ 0 & 0 & 0 & 0 & q_{\text{tail}} & 0 \\ 0 & 0 & 0 & 0 & 0 & 10^{-12} \end{bmatrix} \quad (5.16)$$

Here, $T_{p,n}$ corresponds to the start sample of the n -th pulse ($n = 1 \dots N_t$, with N_t the total number of CI stimulation pulses in the observed EEG signal).

$T_{p,n}$ can be determined based on the stimulation sequence and the trigger pulses. w is the CI artifact peak width (in samples), and is set to $600 \mu s$. α is the decay constant associated with the CI artifact exponential tail, which is determined as explained below. f_m and $\hat{\phi}_m$ are the modulation frequency and angle, respectively, which are determined from the stimulation parameters.

The CI artifact model thus uses four templates. The first three templates are shown, together with the observed signal z_k , in Figure 5.2. The first template $p(k)$ models the CI artifact peaks. By allowing its amplitude $x_{k,3}$ to vary quickly, cf 10^{12} for the third diagonal element in Q_k , all samples in intervals $T_{p,n} < k T_s < T_{p,n} + w$ are “blanked” for each pulse n , i.e., other state variable estimates are almost not adjusted during this interval. This is similar to the LI operation. However, while the LI interval is usually set approximately equal to the IPI ($2000 \mu s$ for 500 pps), the CI artifact peak width w is chosen here to be only $600 \mu s$ to blank the interval that cannot be properly modeled by the other templates $c(k)$ and $m(k)$. Because of the AM stimulation, we expect to find (a) constant CI artifacts, as well as (b) modulated CI artifacts (cf. supra), the tails of which are modeled by the second and third template respectively. The second template $c(k)$ is an unmodulated exponential decay. The third template $m(k)$ is a modulated (at f_m) exponential decay. The decay constant α was estimated from the recordings as follows: All EEG signal segments corresponding to the stimulation pulses were averaged. From the resulting signal, the first $600 \mu s$, or 5 samples out of the 16 – 17 samples per pulse, containing the CI artifact peaks, were discarded. A decaying exponential $Be^{-\alpha i T_s}$ was fitted to the remaining 11 samples of an averaged pulse $i = 1 : 11$. Finally, the fourth template is a slowly varying DC bias component.

The speed at which the state vector components, i.e., the template amplitudes, are allowed to change is determined by the process noise covariance matrix Q_k . The influence of the process covariance associated with the CI artifact tail components (q_{tail} for the fourth and the fifth diagonal elements in Q_k) will be investigated, in Section 5.3, where five parameter values (0.01, 0.1, 1, 10, 100) will be considered. The observation noise covariance R_k is chosen corresponding to the measurement noise level of $0.05 \mu V$.

The proposed model provides two advantages compared to TS, to ensure reliable EASSR parameter estimation in the presence of CI artifacts. With TS, it is not guaranteed that the template, that is constructed through averaging EEG segments, does not contain any auditory neural response. Here, the CI artifacts are modeled with decaying exponentials. The EASSR itself consists of steady-state components at f_m and its harmonics, and hence never contains such decaying exponentials. Furthermore, the 6-component state vector includes (a) two components uniquely modeling the EASSR, and (b) four components uniquely modeling the CI artifacts, where the specific assumptions provide extra

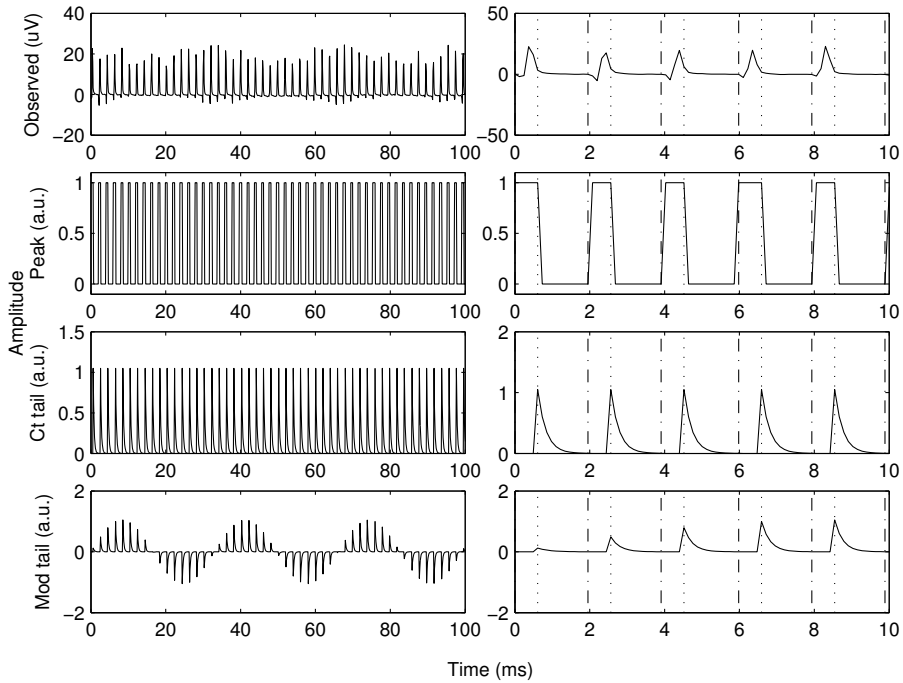


Figure 5.2: Illustration of CI artifact template components. First row: observed signal z_k . Second row: CI artifact peak model $p(k)$. Third row: unmodulated CI artifact tail $c(k)$. Fourth row: modulated CI artifacts tail $m(k)$. The second column is a zoomed version of the signals in the first column. The start of each stimulation pulse and the start of each stimulation pulse decay are indicated with a dash-dotted (.-) and a dashed line (:.) line, respectively.

protection against confusing the EASSR on the one hand and the CI artifacts on the other hand.

In the following, the KF based EASSR parameter estimation method using the 6-component state-space model will be compared to two DFT based methods. The influence of the parameter q_{tail} will be investigated.

5.2.3 EASSR parameter estimation methods

Three methods for EASSR parameter estimation are considered. The first method is based on the KF. The second method (LI-DFT) and third method (TS-DFT) are DFT based.

KF based EASSR parameter estimation

The analysed channel at the contralateral side was either P_5 or P_6 (depending on the side of implantation), in accordance to [91]. At the ipsilateral side, channel P_6 or P_5 was on top of the CI coil for most subjects. Therefore, the analysed channel at the ipsilateral side was either O_1 or O_2 , as these channels were never on top of the CI coil for the six tested subjects.

The raw EEG data signals are denoted by $y_o[k, c]$, with k the time index, and c the channel index. As in [38, 39, 53], the raw data signals were first re-referenced to either C_z or Fp_z , by subtracting the reference signal. The reference electrode was chosen depending on the spatial distribution of the CI artifacts. To remove slow drifts and DC bias, the signals were then de-trended using a second order polynomial over a 0.5 s window, as in [91]. A notch filter ($Q = 35$, $f_{\text{cutoff}} = 50$ Hz) was applied to remove line interference. The resulting signal $y[k, c]$ was then split in 1.024 s epochs based on the trigger signal, resulting in $\mathcal{Z}[k, e, c]$, with e the epoch index. 5% of epochs were rejected based on their peak-to-peak amplitude, in order to remove excessive movement, muscle, or ocular artifacts. Finally, the signals were averaged over epochs, resulting in the mean epoch $z[k, c]$.

The mean epoch $z[k, c]$ was then passed to the standard KF and Rauch-Tung-Striebel (RTS) smoother [91]. It is noted that, similar to [38], the mean epoch was used for EASSR parameter estimation. Contrary to [91], the focus of the present study is not on fast response detection, but rather on adequate CI artifacts suppression. CI artifacts can be more accurately modeled based on a mean epoch, because the brain noise is reduced by the averaging over epochs.

In this evaluation, two different signal state-space models were used. First, as in [91], a 2-component state-space model was used, that includes only the EASSR, i.e., the first two components of the state-space model given in eq. (5.11)–(5.16). The resulting method is referred to as KF based EASSR parameter estimation without CI artifact model (KF_R), because it includes only the response (R) model. Second, the 6-component state-space model given in eq. (5.11)–(5.16) was used with different values for q_{tail} . The resulting method is referred to as KF based EASSR parameter estimation with CI artifact model (KF_RA), because it includes both a response (R) model and a template for the CI electrical artifacts (A).

The EASSR amplitude A_k and phase θ_k were calculated from the Kalman smoother output for each sample k as

$$A_k = \sqrt{x_{k,1}^2 + x_{k,2}^2} \quad (5.17)$$

$$\theta_k = \arctan\left(\frac{x_{k,2}}{x_{k,1}}\right) \frac{180^\circ}{\pi} \quad (5.18)$$

The mean amplitude averaged over all samples was used for comparison with LI-DFT and TS-DFT, as in [91].

Similar to [91], the initial estimates were set to:

$$\begin{bmatrix} x_{0,1} \\ x_{0,2} \\ x_{0,3} \\ x_{0,4} \\ x_{0,5} \\ x_{0,6} \end{bmatrix} = \begin{bmatrix} 0 \\ 0 \\ \max_k(z[k, c]) \\ \frac{\max_k(z[k, c])}{4} \\ \frac{\max_k(z[k, c])}{4} \\ 0 \end{bmatrix} \quad (5.19)$$

DFT based EASSR parameter estimation

The details of LI-DFT and TS-DFT are summarized here, and are described in more detail in [38].

- LI-DFT

The same analysis and reference channels as detailed above were used here. After re-referencing, a LI was applied between a sample 100 μs before and a sample 1900 μs after each stimulation pulse. The resulting signals were then filtered with a second-order 2 Hz high-pass filter to remove DC bias. The signals were then split in epochs, and 5% of epochs were rejected. The EASSR amplitude and phase were then calculated based on the f_m component of the mean epoch.

- TS-DFT

The same analysis and reference channels as detailed above were used here. The resulting signals were then de-trended with a second-order polynomial over 0.5 s non-overlapping windows to remove DC bias. The signals were then split in epochs, and 5% of epochs were rejected. The mean of the resulting epochs was calculated. As described in [38], stimulation pulse templates were calculated based on a recording containing no significant

EASSR. The templates were then arranged in the correct order and subtracted from the mean epoch. The EASSR amplitude and phase were then calculated based on the f_m component of the resulting mean epoch.

5.2.4 Evaluation

Eight methods were compared for EASSR data obtained in six subjects (as explained in Section 5.2.1): LI-DFT, TS-DFT, KF_R, KF_RA_ q_{tail} with five values for q_{tail} (0.01, 0.1, 1, 10 and 100).

The EASSR amplitude, phase and response latency estimated with the KF based methods were compared to the estimates obtained with LI-DFT and TS-DFT.

The LI-DFT EASSR parameter estimates were used as a baseline for the contralateral channel, as CI artifacts can indeed reliably be suppressed by LI-DFT in the contralateral channel. The correlation between LI-DFT and KF based EASSR amplitude estimates and between LI-DFT and KF based EASSR phase estimates was determined. A Blant Altman analysis was used to compare the LI-DFT and the KF based EASSR parameter estimates [94]. The repeatability coefficient (RC) was determined for the contralateral recording channel. The absolute difference between the LI-DFT and the KF based EASSR parameter estimates is expected to lie below the RC with a probability of 95%. The RC was compared to the noise level to determine whether the difference between the LI-DFT and the KF based EASSR parameter estimates could be related to the noise level.

Phases θ are stable at a multiple of 180° for all f_m , for CI artifact dominated measurements. On the other hand, phases decrease linearly for increasing f_m , for EASSR dominated measurements. The response latency L was calculated as the additive inverse of the slope of the $\theta(f_m)$ curve, for the contra- and ipsilateral channel. Response latency values close to 0 ms indicate that the measurements are CI artifact dominated, while values around 40 ms (for f_m around 40 Hz [54]) indicate that the measurements are EASSR dominated. Response latencies can therefore be used to determine whether CI artifacts have sufficiently been suppressed.

Table 5.1: Correlation coefficient (p value) between LI-DFT and KF based amplitude and phase estimates for the contralateral and the ipsilateral channel.

Method	Contralateral		Ipsilateral	
	Amplitude	Phase	Amplitude	Phase
KF_R	0.960 (<0.001)	0.479 (0.002)	0.780 (<0.001)	0.307 (0.058)
KF_RA_0.01	0.980 (<0.001)	0.995 (<0.001)	0.916 (<0.001)	0.332 (0.004)
KF_RA_0.1	0.994 (<0.001)	0.996 (<0.001)	0.985 (<0.001)	0.991 (<0.001)
KF_RA_1	0.995 (<0.001)	0.996 (<0.001)	0.981 (<0.001)	0.992 (<0.001)
KF_RA_10	0.996 (<0.001)	0.996 (<0.001)	0.975 (<0.001)	0.990 (<0.001)
KF_RA_100	0.994 (<0.001)	0.997 (<0.001)	0.952 (<0.001)	0.960 (<0.001)

5.3 Results

5.3.1 EASSR phase

The EASSR phase estimates for the eight methods are shown in Figure 5.3. In the contralateral channel, EASSR phases seem to decrease with increasing f_m for most subjects and methods. With KF_R, EASSR phase estimates seem CI artifact dominated for subject S02, suggesting that the acoustic model does not result in correct EASSR parameter estimates. In the ipsilateral channel, EASSR phases seem to decrease with increasing f_m , even with LI-DFT. This suggests that CI artifacts are shorter than the IPI for the chosen recording channel, although we know that this is not the case for all ipsilateral recording channels. For subjects S02 and S04, KF_R and KF_RA_0.01 result in inaccurate EASSR phase estimates. EASSR phase estimates are significantly correlated between LI-DFT and all KF_RA methods, while no significant correlation was found between LI-DFT and KF_R, see Table 5.1. Correlations seem to be the largest for the intermediate q_{tail} value of 1, although the differences are probably not very relevant.

A Blant Altman plot comparing the KF based EASSR phase estimates to the LI-DFT estimates is included in Figure 5.4. The difference between the phase estimates obtained with LI-DFT and each KF based method is plotted against the phase estimates averaged for LI-DFT and each KF based method. It is clear that KF_R results in large EASSR phase differences for subjects S02 and S04. Furthermore, the EASSR phase difference seem the smallest for larger values of q_{tail} . The phase difference between LI and KF_RA_100 is larger than for lower q_{tail} values between 0.1 and 10.

5.3.2 EASSR amplitude

A Blant Altman plot comparing the KF based EASSR amplitude estimates to the LI-DFT estimates is shown in Figure 5.5. Again, the EASSR amplitudes estimates averaged for LI-DFT and each KF based method are plotted on the x-axis, while the EASSR amplitude estimate difference between LI-DFT and each KF based method is shown on the y-axis. For the contralateral channel, the largest amplitude differences are seen for KF_R. Most KF_RA methods result in EASSR amplitude estimates similar to the LI-DFT estimates, in the contralateral channel. EASSR amplitude estimates are significantly correlated between LI-DFT and KF based methods, see Table 5.1.

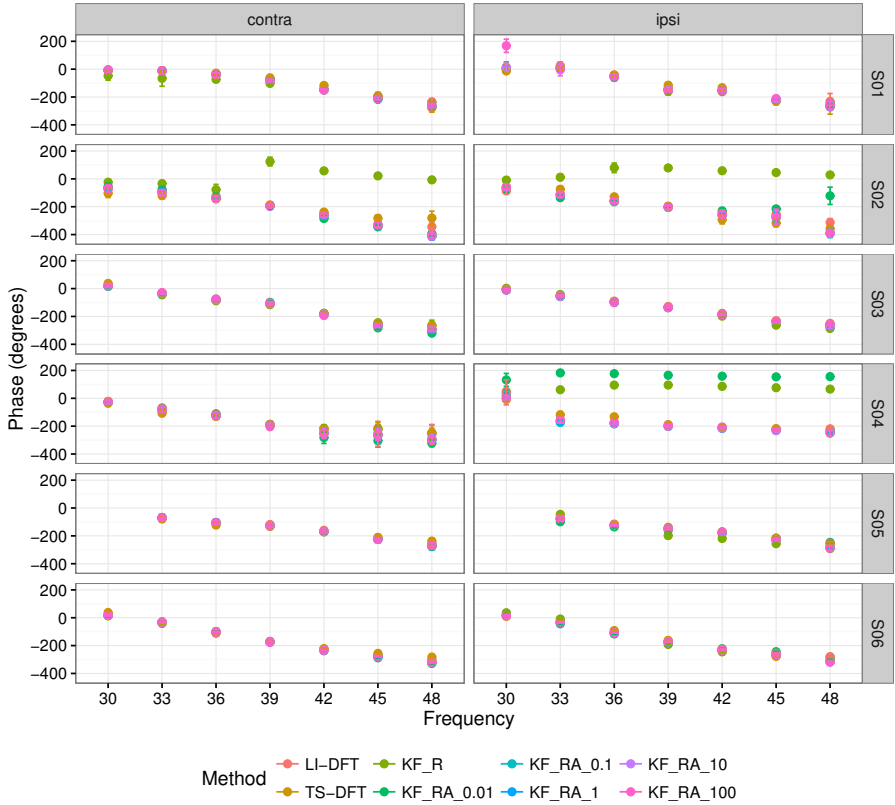


Figure 5.3: EASSR phase estimates for the eight methods, per subject. Left: contralateral recording channel. Right: ipsilateral recording channel.

For the ipsilateral channel, it is unclear whether the LI-DFT amplitude estimates are a good reference value. Based on the EASSR phase result, it would seem safe to conclude that the measurements are EASSR dominated in the ipsilateral channel after LI-DFT. In case the LI-DFT estimates are trustworthy, it seems that larger values for q_{tail} again result in more accurate EASSR amplitude estimates. Again, large and significant correlations are found between estimates for LI-DFT and KF_RA methods. Correlations seem to be the largest for intermediate q_{tail} values between 0.1 and 10, although the differences are probably not very relevant.

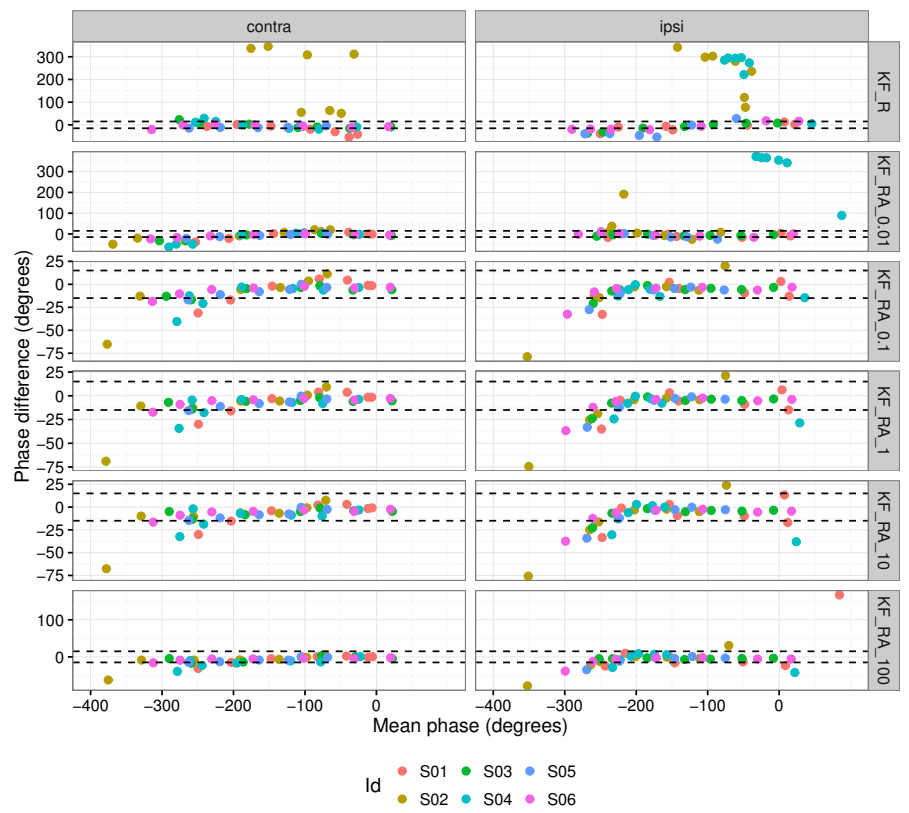


Figure 5.4: Blant Altman plot for EASSR phase estimates for the KF based method. Horizontal dashed lines are the mean expected phase errors, based on EASSR and noise amplitudes. Left: contralateral recording channel. Right: ipsilateral recording channel.

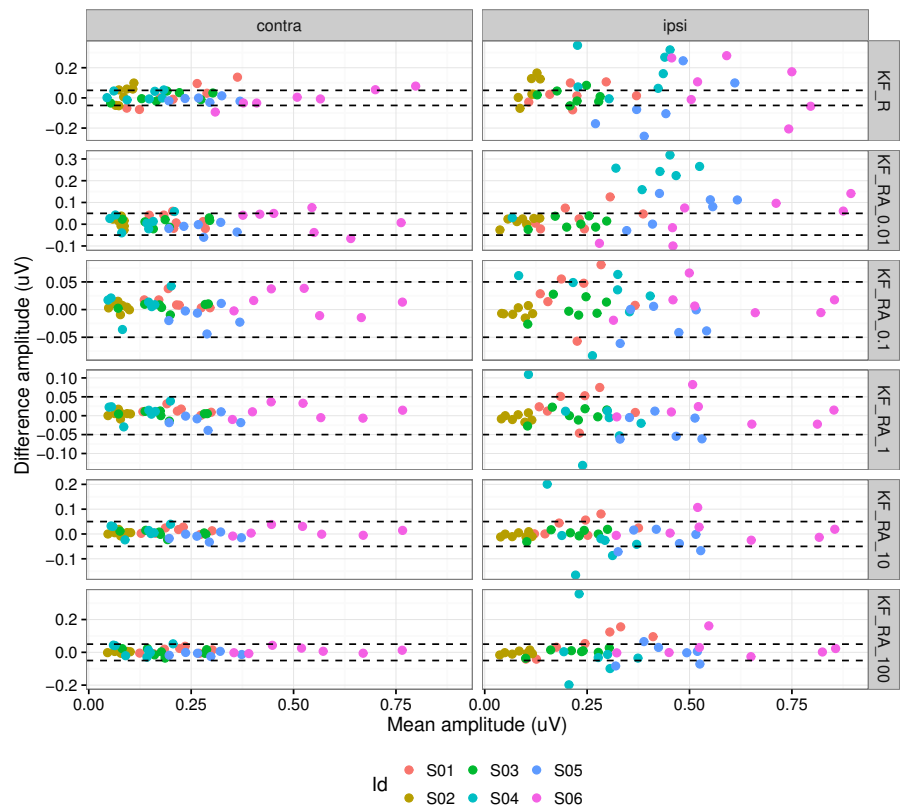


Figure 5.5: Blant Altman plot for EASSR amplitude estimates for the KF based method. Left: contralateral recording channel. Right: ipsilateral recording channel.

5.3.3 Response latency

A comparison of the response latencies obtained with the eight methods is shown in Figure 5.6. For the contralateral channel, the response latency seems too small for some subjects (S01, S04 and mainly S02) with KF_R. All other methods seem to result in good latency estimates. Response latencies obtained with TS-DFT seem somewhat smaller than those obtained with KF_RA and LI-DFT, indicating that TS-DFT may not sufficiently suppress CI artifacts for the chosen recording channel.

For the ipsilateral channel, response latencies obtained with LI-DFT seem acceptable. While KF_R and KF_RA_0.01 result in small latency values (of less than 10 ms) in some subjects, latencies obtained with the other methods are in the expected range.

5.3.4 Repeatability coefficient

For the contralateral recording channel, the RC of EASSR phase and amplitude estimates for the TS-DFT and the KF based methods compared to LI-DFT are included in Figure 5.7. The mean phase error and noise amplitude are included for comparison with the EASSR phase and amplitude estimate RCs, respectively. Obtained EASSR phase and amplitude estimates look reliable when the RC is below or close to the expected phase or amplitude error. q_{tail} values above 0.01 ($q_{\text{tail}} = 0.1/1/10$) again seem to result in the most accurate EASSR amplitude and phase estimates. The minimum EASSR phase estimate RC is obtained for $q_{\text{tail}} = 1$, while the best q_{tail} is 10 for EASSR amplitude estimation.

5.4 Discussion and conclusion

CI artifacts may result in false EASSR detections and inaccurate estimates for the EASSR amplitude and phase. Several methods have been developed for reliable EASSR parameter estimation in the presence of CI artifacts. In this study, a KF based method has been proposed that results in accurate EASSR amplitude and phase estimates. The CI artifact peaks are effectively blanked by including a fast changing state vector component scaling a CI artifact peak template, while CI artifact tails are modeled with an unmodulated and modulated decaying exponential template. EASSR phase and amplitude estimates obtained with KF_RA are similar to LI-DFT, while the KF_R fails to produce accurate estimates. Note that no LI was used in the KF_RA methods,

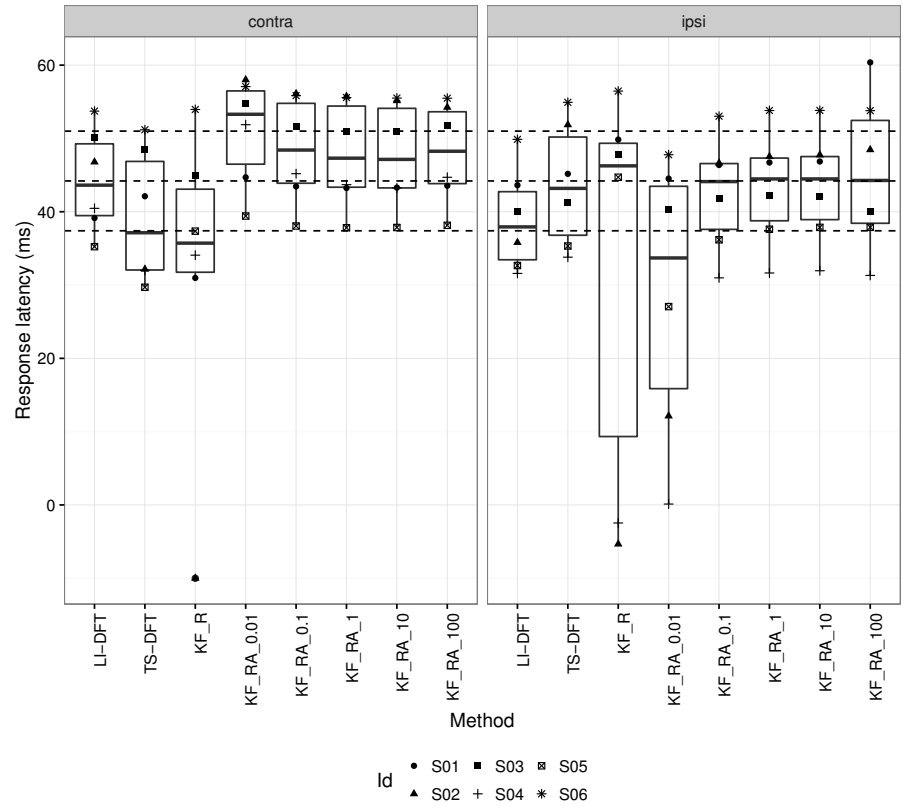


Figure 5.6: Response latency for the KF, LI and TS based method.

so that improvements obtained with KF_RA compared to KF_R can entirely be attributed to the CI artifact template. Although LI-DFT resulted in reliable EASSR parameter estimates for this dataset, KF_RA could possibly be used in more general cases where LI-DFT based EASSR parameter estimation is unreliable.

5.4.1 Advantages

The KF based method using a 6-component state-space model provides several advantages compared to existing EASSR parameter estimation methods, i.e.,

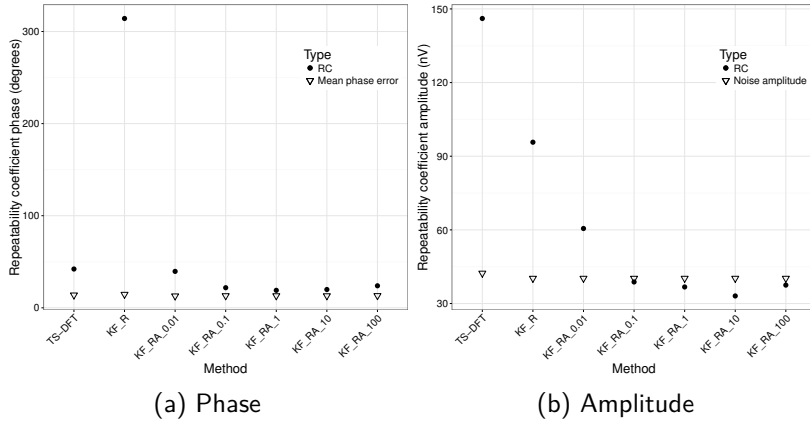


Figure 5.7: Repeatability coefficients (filled dots) for the contralateral channel for the KF and TS based method, compared to the expected variation in amplitude and phase due to the neural background noise (open triangles).

LI-DFT, ICA-DFT, TS-DFT and the KF based method using a 3-component state-space model.

CI artifacts cannot be suppressed with LI-DFT when the CI artifact duration is longer than the IPI. We have shown that measurements in adults contain overlapping CI artifacts for 500 pps stimulation (ipsilateral recording channels) and 900 pps stimulation (contralateral and ipsilateral recording channels) [37, 53]. The KF based method using a 6-component state-space model could thus be used for reliable EASSR parameter estimation in future challenging scenarios, e.g., for EASSR measurements in children and during bilateral CI stimulation.

Contrary to ICA-DFT based CI artifact suppression, there is no need for an (expensive) multichannel set-up. Furthermore, with ICA-DFT based CI artifact suppression, independent components associated with CI artifacts should be - manually or automatically - identified. Manual identification is usually done by experts and is subjective and time consuming. Automatic identification relies on specific assumptions, which can possibly lead to inaccuracies [39, 40]. Furthermore, it has been shown in [39] that ICA-based EASSR parameter estimation is not very robust as mixed results were obtained.

With TS-DFT, an additional measurement without significant EASSR is required, containing CI artifacts elicited by the same stimulation pulse amplitudes (but a different f_m) as the measurement of interest. In [38], it was shown that TS-DFT resulted in the same EASSR amplitude and phase

estimates as LI-DFT for a set of averaged channels, and that response latencies were acceptable in single channels. We have observed that - for the chosen recording channels - amplitudes obtained with TS-DFT sometimes deviate from those obtained with LI-DFT. The assumptions underlying the TS-DFT method, may thus not always be completely fulfilled.

In this paper, this method presented in [91] is extended to more general CI artifacts shapes. The inclusion of the CI artifacts model (KF_RA) provides improvements compared to the EASSR model alone (KF_R). Additionally, we showed results for EASSR amplitude and phase estimates, while only EASSR amplitudes were included in [91].

5.4.2 Limitations and future work

In this evaluation, only high-SNR measurements with 500 pps stimulation have been used. Stimulation with higher pulse rates results in a shorter IPI, which provides fewer samples to determine the CI artifact template parameter α , based on an exponential fit. Future studies should investigate the reliability of the method for lower SNR EASSRs and how increasing the pulse rate affects the accuracy of the exponential fit and the reliability of the EASSR estimates.

As in [91], the method could possibly be extended to multi-channel measurements, assuming that adjacent electrodes are measuring the same underlying sources with independent noise. This may be a valid assumption for the EASSR, but reliable EASSR parameter estimates will only be obtained if the CI artifacts are similar enough across the selected electrodes. This remains to be investigated.

Although we have investigated the influence of q_{tail} , the influence of other parameter values has not been systematically investigated. Furthermore, in the state-space model $\hat{\phi}_m$ is equal to 90° , under the assumption that the CI artifact propagation is instantaneous. It may be better to increase the value for $\hat{\phi}_m$ to incorporate possible extra delay between recording of the trigger pulse and the CI artifact stimulation pulse.

Finally, as indicated in [91], the noise should be white and Gaussian for the KF to provide an optimal estimate of the state variables. In this study, the brain background noise was greatly reduced by averaging epochs prior to the KF operation. Still, the brain background noise follows a $\frac{1}{f}$ distribution, rather than being white. Furthermore, the state-space model does not contain any component that can model the brain background noise. We have observed that after our KF the four state components scaling the CI artifact templates may model not only the CI artifacts but also the brain background noise. Future

extensions of the KF could include an autoregressive model to model the brain background noise, as was used in other studies with the KF applied to EEG measurements [106, 110, 125].

Chapter 6

Discussion

In this thesis, CI artifacts in EASSR recordings were characterized, and three methods for CI artifact suppression were developed and evaluated. In this last chapter, the work will shortly be summarized (Section 6.1), followed by how interactions between EASSR and CI artifact should be taken into account when dealing with CI artifacts (Section 6.2). Some properties of the recording system that may influence the CI artifact morphology are discussed in Section 6.3. Finally, in Section 6.4, some suggestions for future work are given.

6.1 Summary of the work

This thesis consists of four studies, about reliably measuring EASSRs in CI subjects in the presence of CI artifacts. In the first study, the CI artifact was characterized based on the CI artifact amplitude growth function and on the CI artifact duration. The CI artifact has two likely causes: (1) the RF transmission between the CI's external and internal parts, i.e., RF artifact, and (2) the electrical stimulation pulse sequences delivered through the electrode array, i.e., STIM artifact. It was assumed that STIM artifacts change with increasing stimulation level, while RF artifacts stay approximately constant. The slope θ of the CI artifact AGF is thus related to the STIM artifact, while the intercept I of the CI artifact is mostly determined by the RF artifact and the constant part of the STIM artifact. The CI artifact can be suppressed with a linear interpolation (LI), in case the CI artifact duration D is shorter than the IPI. It was shown in the first study that θ , I and D are influenced by the reference recording electrode configuration. In general, CI artifacts are

most severe in the ipsilateral hemisphere. In all adult CI subjects, the CI artifact duration was shorter than the IPI, such that the CI artifact was reliably suppressed in contralateral channels for 500 pps MP mode stimulation. For EASSR measurements in children, and for source localization and lateralization studies, more advanced CI artifact suppression methods need to be developed in order to deal with CI artifacts that are longer than the IPI. For most studies, a high-SNR 40 Hz dataset was used for evaluation. Here, CI artifacts could reliably be suppressed by LI in contralateral channels, providing a baseline measure to compare the EASSR parameter estimations for new methods to.

The second study focused on ICA-based CI artifact suppression. ICA has widely and rather successfully been used to suppress CI artifacts in transient response recordings in CI subjects. However, the application of ICA for EASSR measurements seems less straightforward, because the EASSR and the CI artifact overlap both temporally and spectrally and are both caused by the same source, namely the electrical stimulation. A heuristic approach for the automatic selection of ICs associated with the CI artifact was developed. The ICA-based CI artifact suppression method was evaluated on three datasets of recordings containing overlapping and non-overlapping CI artifacts, and low and high-SNR EASSRs. Results showed that CI artifacts could be reliably suppressed for high-SNR 40 Hz EASSR recordings, while mixed results were obtained with lower SNR 80 and 40 Hz recordings. Caution is thus warranted when ICA is used for CI artifact suppression in EASSR recordings, as the method was not robust. Furthermore, the need for a multichannel system limits the clinical applicability of the method, as these systems are expensive and require more subject preparation time compared to single-channel systems.

The third study investigated the feasibility of template subtraction (TS) for CI artifact suppression. This method may have some advantages compared to the ICA-based CI artifact suppression, as no multichannel recordings are needed and TS may possibly provide more robust EASSR parameter estimations. CI artifact templates were constructed for each stimulation pulse amplitude, based on a recording without significant EASSR, but with the same stimulation pulse amplitudes as the recording of interest. For the high-SNR 40 Hz dataset, reliable EASSR amplitudes and phases were obtained. The method should further be evaluated on lower SNR measurements. To limit additional recording time for template construction, one subthreshold measurement could be used together with a model describing how CI artifact amplitudes scale with changing stimulation pulse amplitudes.

In the fourth study, a Kalman filter (KF) based EASSR parameter estimation, described in [91], was extended to accommodate for more general CI artifact shapes. In [91], CI artifacts in contralateral channels were modeled as triangular pulses for BP mode stimulation. For MP mode stimulation, CI artifacts in

ipsi- and contralateral channels are often biphasic with a decaying tail. The CI artifact model consisting of triangular pulses from [91] cannot accurately model these CI artifact shapes seen for MP stimulation. The CI artifact model was therefore extended, including components for (1) the CI artifact peak, (2) the constant CI artifact tail, (3) the modulated CI artifact tail, and (4) a slowly drifting DC component. The influence of the process noise covariance q_{tail} , associated with components (2) and (3), was also investigated. For the high-SNR 40 Hz dataset, reliable EASSR amplitudes and phases were again obtained. q_{tail} values between 0.1 and 10 resulted in the best EASSR parameter estimations. Compared to TS, a template for each stimulation pulse amplitude is not needed; with the KF, additional data collection is therefore not required. Future studies could focus on optimization of the parameters, and inclusion of an EEG background noise model.

6.2 Interaction between CI artifacts and EASSRs

The amount of EASSR distortion caused by the CI artifact depends on both the relative phases and the amplitude ratio of the EASSR and the CI artifact, as demonstrated in Figure 6.1a. The observed synchronous response amplitude (full black lines) is a summation of the EASSR (dashed red lines) and the CI artifact (dash-dotted blue lines). For the simulation of Figure 6.1a, the CI artifact has a zero degree phase and an amplitude of 100 nV, while the EASSR has an amplitude of 250 nV with varying phase. This is a good model for the EASSR, but note that CI artifact amplitudes vary over subjects, and may be orders of magnitude larger in reality. The EASSR amplitude is maximally enlarged or attenuated by the CI artifact if the EASSR and the CI artifact are completely in or out of phase, respectively. On the other hand, for the simulated EASSR and CI artifact amplitudes in Figure 6.1a, the phase error is largest when the EASSR and CI artifact are 90° out of phase. In Chapter 4, the observed amplitude and phase error were modeled for varying CI artifact-EASSR amplitude ratios and artifact-response phase differences, see also Figure 6.1b. Amplitude errors are largest when artifact and response are in phase, and increase with higher residual artifact levels. When the EASSR is dominant compared to the CI artifact, i.e., for a small CI artifact-EASSR amplitude ratio, CI artifacts result in smaller relative amplitude errors. The influence of the CI artifact on the phase error is less straightforward, and depends on the CI artifact-EASSR amplitude ratio. For smaller CI artifact-EASSR amplitude ratios, as in Figure 6.1a, the largest phase errors are observed when CI artifact and EASSR are 90° out of phase. For larger CI artifact-EASSR amplitude ratios, the largest phase errors are observed when CI artifact and EASSR are 180° out of phase.

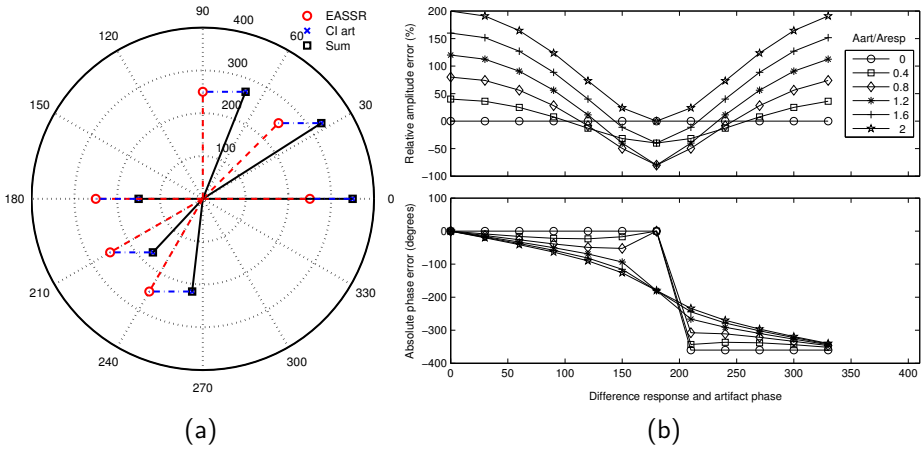


Figure 6.1: Left: polar plot illustrating the interaction between EASSR and CI artifact components. Right: Relative amplitude and phase errors (in %) depending on the EASSR-to-CI-artifact amplitude ratio and the relative phase difference between EASSR and CI artifact.

The above-mentioned has some consequences for the evaluation of CI artifact suppression methods in EASSR recordings. First, amplitude and phase errors should both be evaluated for novel CI artifact suppression methods. In Chapters 3, 4 and 5, both amplitude and phase estimates were always considered. Second, a wide range of EASSR-CI artifact phase differences should be considered, to take the full influence of CI artifacts on the EASSR into account. Amplitude errors are most apparent when CI artifact and EASSR are in phase, while phase errors are most apparent when the EASSR-CI artifact phase difference is around 90° to 180° , depending on the CI artifact-EASSR amplitude ratio. The 40 Hz MFTF dataset that was used in Chapters 3, 4 and 5 is an ideal dataset for CI artifact suppression evaluation. EASSR phases span a range of almost 360° , resulting in a wide range of EASSR-CI artifact phase differences, as desired. Third, ideally a wide range of CI artifact-EASSR amplitude ratios is investigated, as this ratio determines whether recordings are EASSR or CI artifact dominated. The 40 Hz MFTF dataset was acquired with stimulation at C level, which resulted in high-SNR recordings in most subjects. Therefore, EASSRs may be dominant compared to the CI artifact. CI artifact suppression may be more challenging for other datasets containing lower SNR recordings. However, the EASSRs amplitudes vary between 40 and 1048 nV over subjects in the 40 Hz MFTF dataset. Therefore, we would argue that a representative range of 40 Hz EASSR amplitudes has been tested.

6.3 Recording system specifications

Some specifications of the recording system may have an influence on the CI artifact characteristics. In this work and other recent studies in our research group [53, 90, 88] (Chapter 3), the Biosemi ActiveTwo recording system which is based on a DC amplifier was used with BP or MP mode stimulation. In previous studies, BP mode stimulation was used with a 8-channel Jaeger-Toennies AC amplifier [65, 64].

First, the input dynamic range of the amplifier should be large enough, such that the large electrical artifacts do not cause amplifier saturation. Second, high-pass filters built into AC amplifiers may distort CI artifacts, resulting in CI artifacts with significantly longer duration. Third and finally, anti-aliasing low-pass filters, with cut-off low-pass frequency related to the sample rate, may influence the CI artifact morphology.

6.3.1 Input dynamic range and saturation

For some amplifier types, the amplifier input can be temporarily grounded, using a hardware circuit, to prevent amplifier saturation or damage [107]. This process, called blanking, may lead to unwanted data losses and missed events, e.g., in studies based on spike train counting [107]. The linear interpolation (LI) method that has been used in previous studies and in this work is a software equivalent of the hardware blanking. LI can only be used if the amplifier input dynamic range is large enough such that no saturation occurs.

6.3.2 AC vs DC amplifiers

Two types of amplifiers are commonly used: alternating current (AC) and DC amplifiers. AC amplifiers block the DC component of the input signal, with a built-in high-pass filter with adjustable cut-off. For CI artifacts with a DC component, this high-pass filter may influence the CI artifact morphology [65]. Both RF artifacts and asymmetric CI stimulation artifacts contain a DC component that is removed by the high-pass filter. This results in a longer CI artifact tail [65], thus extending the CI artifact duration, and further limiting the applicability of LI. DC amplifiers may thus be a better option to record EASSRs for MP mode stimulation, as CI artifact durations are shorter with this type of amplifier.

6.3.3 Sample rate and anti-aliasing filter

To prevent aliasing, recording systems contain a low-pass anti-aliasing filter. In the Biosemi ActiveTwo recording system, a fifth order sinc low-pass filter with cut-off frequency at $1/5^{th}$ of the sample rate is used. This low-pass filter also influences the CI artifact morphology. The lower the low-pass filter cut-off frequency, the longer the CI artifacts exponential decay. Using recording systems with higher sample rates or with higher low-pass filter cut-off frequencies may thus result in CI artifacts that are easier to suppress.

In Chapter 4, a template subtraction method for CI artifact suppression has been presented and evaluated. The CI artifact peaks were not adequately modeled by the templates, due to averaging of several EEG segments and due to the limited sample rate. A LI with short interpolation duration was therefore applied after template subtraction. EASSR recordings with higher sample rates may result in more accurate CI artifact templates, and the extra LI may not be required anymore.

In Chapter 5, EEG samples corresponding to the CI artifact peak were ignored in the state-space model, because these were associated with a large process covariance value. When higher sample rates are employed, better CI artifact models could possibly be derived, which may then be included in the state-space model. This in turn may result in more accurate EASSR parameter estimations.

6.4 Future work

Five suggestions for future work are given in the following section. First, a CI artifact propagation model, describing how the CI stimulation pulses are propagated from the electrode array to the scalp electrodes, could be constructed. This model could then be used for improved CI artifact suppression and as a CI artifact template in the KF based EASSR parameter estimation. Second, as discussed in Section 6.4.2, the choice of stimulation reference electrode may have an influence on the CI artifact characteristics. Third, improved stimulus design may help in attenuating the CI artifact contribution at the modulation frequency (Section 6.4.3). Fourth, adjustments to the KF based EASSR parameter estimation could improve the reliability of the obtained parameter estimates, which is explained in Section 6.4.4. Fifth and finally, extra research is needed to demonstrate the clinical applicability of EASSR based objective CI fitting (Section 6.4.5). In particular, the performance of the proposed CI artifact suppression methods in low SNR recordings and in CI children and infants should further be investigated.

6.4.1 Improvements of the CI artifact generation model

It would be interesting to construct a model of how the CI stimulation pulses propagate from the electrode array to the scalp electrodes. Figure 1.7 lists some factors that may influence the CI artifact pulse shape. However, the exact influence of each factor is unknown. Such a model, that predicts the measured CI artifact pulses from the stimulation sequences, may then be used in better CI artifact suppression methods, or to improve the CI artifact template in the state-space model used by the KF for EASSR parameter estimation.

6.4.2 Influence of stimulation reference electrode

It has been shown that CI artifacts are larger and longer for MP mode stimulation than for BP mode stimulation [69, 85]. The physical separation between active and reference stimulation electrodes may thus have an influence on the CI artifact characteristics. MP mode stimulation refers to stimulation between an intracochlear and an extracochlear electrode. Cochlear Nucleus implants have two extracochlear reference electrodes. The MP1 reference electrode is separate from the receiver stimulator, and is referred to as the ball or bullet electrode. The exact electrode placement is determined by the surgeon during implantation, but the ball electrode is typically buried underneath the temporalis muscle [6, 113, 155]. The MP2 electrode is the reference electrode located on the casing of the receiver stimulator. Three MP modes of stimulation exist: MP1, MP2 and MP1+2 mode, where respectively the ball electrode, the electrode on the casing and both electrodes, shorted together, are used as the reference electrode. The chosen MP stimulation mode may have an influence on CI artifact characteristics. The physical separation between the intracochlear electrodes and the MP2 electrode is smaller than the physical separation between the intracochlear electrodes and the MP1 electrode. We therefore hypothesized that, compared to MP1 stimulation, MP2 mode stimulation would result in shorter CI artifact durations.

To test this hypothesis, EEG measurements were obtained in one subject with MP1, MP2 and MP1+2 stimulation during a pilot experiment. 37 Hz AM modulated 500 pps pulse trains were presented at subthreshold stimulation levels. No neural response is expected to be present, as the stimuli were not audible to the subject. Significant synchronous responses are thus caused by CI artifacts.

EEG signals were rereferenced to either C_z or Fp_z . LI was or was not applied, and the resulting signals were then filtered with a 2 Hz high pass filter. In each channel, a Hotelling T^2 test was applied to detect whether synchronous activity

(in this case caused by the CI artifacts) was present. The percentage of false detections was determined as the ratio of recording channels with significant detections divided by the total number of recording channels. Three recording channel selections were used: (1) all recording channels, (2) all contralateral recording channels, and (3) all ipsilateral recording channels (excluding those on top of the RF coil). Furthermore, for each recording channel, the CI artifact duration was determined, as described in Chapter 2. The influence of four factors could thus be examined: (1) most importantly, the influence of stimulation mode (MP1 vs MP2 vs MP1+2), (2) the influence of reference electrode (C_z vs Fp_z), (3) the influence of recording channel selection (all vs ipsilateral vs contralateral) and (4) postprocessing (no LI vs LI).

The percentage of false detections is shown in Figure 6.2. This percentage is generally higher in the ipsilateral hemisphere than in the contralateral hemisphere. Applying LI reduces the number of false detections, especially in the contralateral hemisphere. The percentage of false detections is lower for reference electrode Fp_z , compared to reference electrode C_z . It seems that the signal at Fp_z resembles the CI artifact better than the signal at C_z , or that the percentage of detections is reduced due to an increased noise level. All these effects were expected. The most important factor we wanted to investigate is whether the stimulation mode has an influence on the percentage of false detections. In line with the hypothesis, it seems that MP2 mode stimulation results in the lowest percentage of false detections, especially when LI is applied. The percentage of false detections is slightly lower for MP1+2 mode stimulation, compared to MP1 mode stimulation. It is not possible to do a statistical analysis to confirm these effects, as only one subject was tested.

The CI artifact duration is shown in Figure 6.3. The CI artifact duration is longer in the ipsilateral hemisphere than in the contralateral hemisphere. The CI artifact duration is also influenced by the selected reference electrode, and is in general shortest for Fp_z reference. Importantly, especially at the contralateral side, MP2 stimulation results in shorter CI artifact durations than MP1+2 and MP1 stimulation, as expected. The stimulation mode not only has an influence on the overall CI artifact duration, but also on the topography. For MP2 stimulation, CI artifacts are concentrated more posterior than for MP1 stimulation. This is an expected finding, since the MP2 electrode is placed more posteriorly than the MP1 electrode. The main areas affected by CI artifacts for MP1+2 mode stimulation are a combination of those areas found for MP1 and MP2 mode stimulation separately. The best settings to record EASSRs (in this subject) at the posterior contralateral recording channels electrodes is with stimulation in MP2 mode, with reference electrode Fp_z .

In the future, these results should be confirmed in more subjects, and the influence of changing stimulation reference electrode on CI artifact suppression

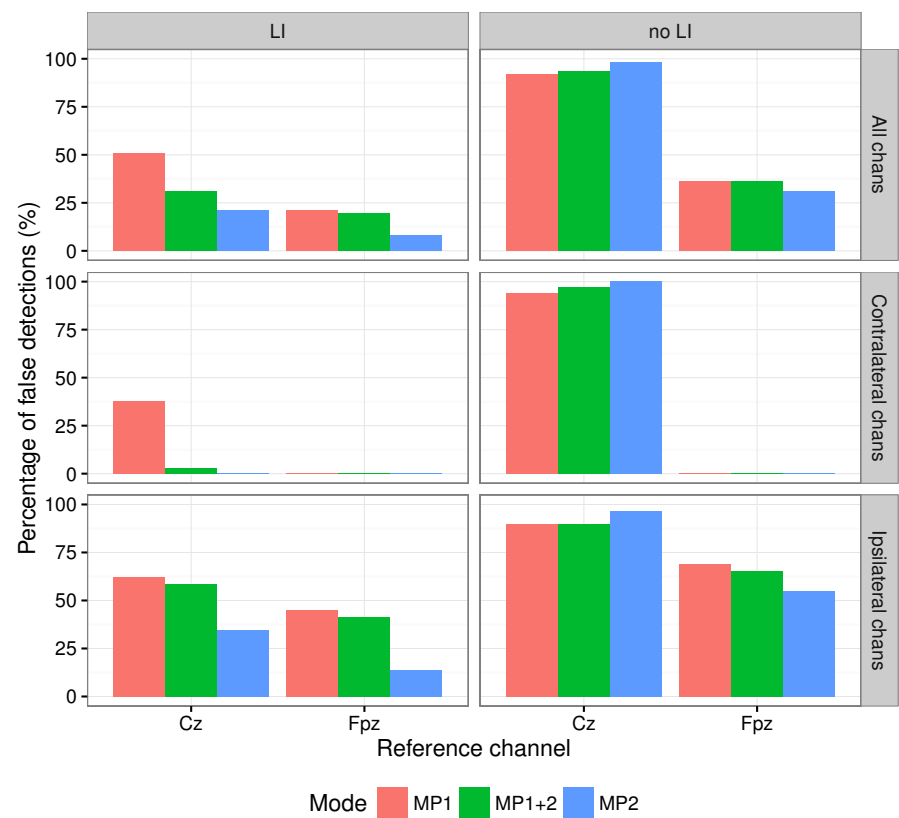


Figure 6.2: Percentage of false detections. Left column: with LI, right column: without LI. Top row: all recording channels, middle row: only contralateral recording channels, bottom row: only ipsilateral recording channels.

results should further be investigated.

6.4.3 Reducing CI artifacts by improved stimulus design

Improved stimulus design may result in CI artifacts that are easier to suppress. Two possible approaches are presented next.

First, in Chapter 6 of [88], the stimulation pulse sequence was adjusted to create EEG samples free of CI artifact, even when the CI artifact duration is longer

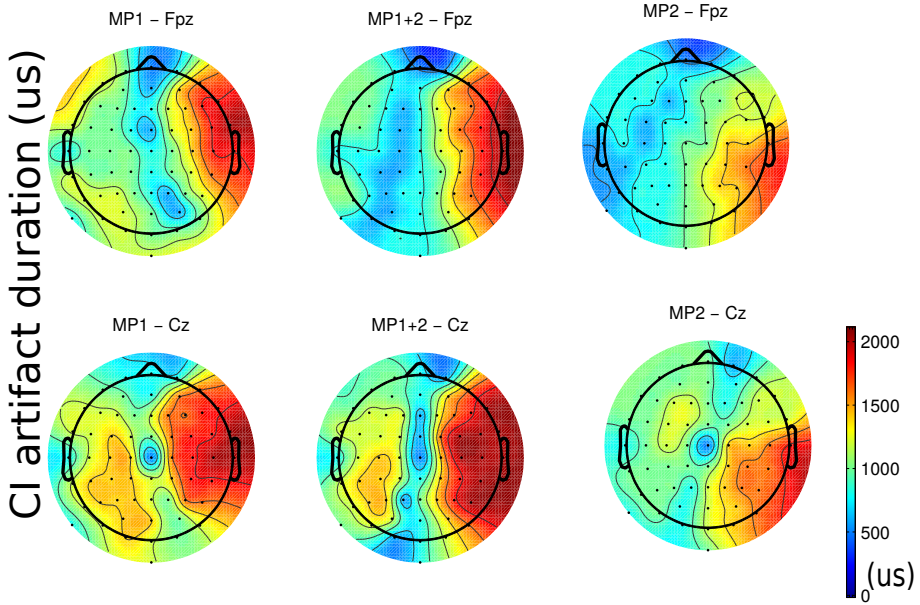


Figure 6.3: CI artifact duration in μs . Top row: reference channel F_{pz} , bottom row: reference channel C_z . Left to right: influence of stimulation mode.

than the IPI. As illustrated in Figure 6.4, selected CI stimulation pulses were shifted closer to the preceding stimulation pulses, to create a larger gap between two subsequent pulses. The longer IPI then allows the CI artifact to decay to baseline before the next pulse is stimulated, resulting in one or more EEG samples free of CI artifacts. A LI can then be applied between multiple such CI artifact-free EEG samples. The sample rate is thus effectively reduced to the rate of the shifted pulses. A pilot study with 900 pps MP mode stimulation in one CI subject indicated that the EEG signals were indeed EASSR dominated after LI between the shifted pulses.

Second, CI artifacts may be attenuated after averaging if the stimulation sequences are not completely aligned or not perfectly identical [95]. For transient response recordings, free field stimulation was often used, where exact synchronization or perfectly identical stimulation epochs cannot be guaranteed. This may have resulted in attenuated CI artifacts. For EASSR recordings, deliberate jittering of the stimulation sequences, or introducing small differences between stimulation epochs may result in attenuated CI artifacts, while perception is unchanged.

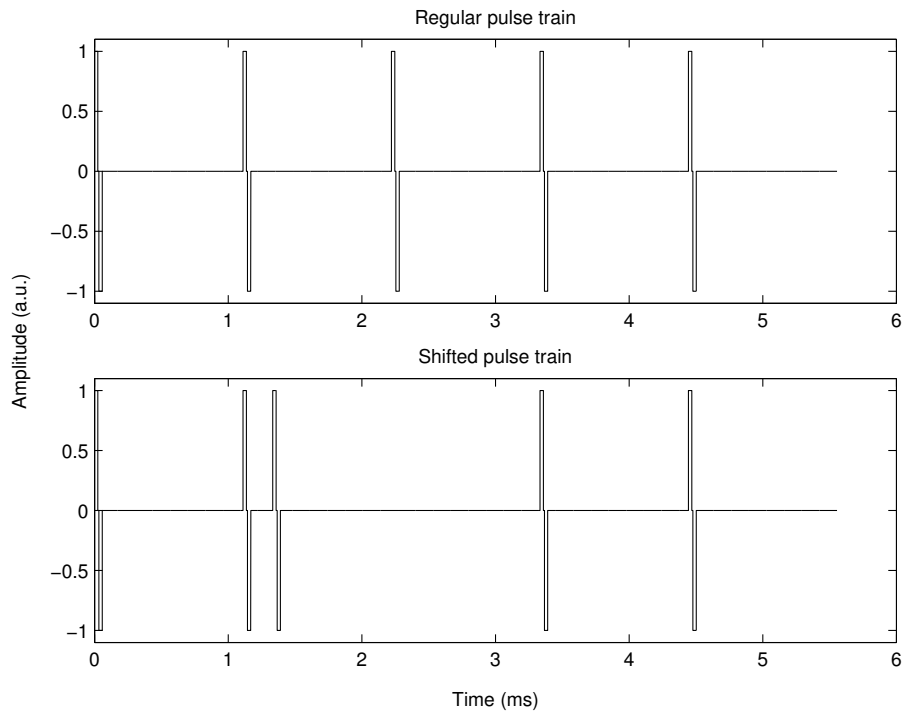


Figure 6.4: The stimulation pulse sequence was adjusted to create EEG samples free of CI artifact. The third CI stimulation pulse was shifted closer to the preceding stimulation pulse, to create a larger gap between the third and fourth pulse.

Note that the above-mentioned changes to the stimulation pulse sequences may result in attenuated CI artifacts, but that CI artifacts may not completely be suppressed.

6.4.4 Improvements to the Kalman filter (KF) based EASSR parameter estimation

In Chapter 5, a state-space model, including an EASSR and a CI artifact model, was used by a Kalman filter for EASSR parameter estimation. The CI artifact model consists of four components: (1) the CI artifact peak, (2) the constant CI artifact tail, (3) the modulated CI artifact tail, and (4) a slow-drifting DC bias component. While the influence of the process noise covariance associated with

the CI artifact tail (components (2) and (3)) was investigated, the influence of other parameters was not systematically researched. Future studies should focus on the improvement of the KF EASSR parameter estimation through optimization of the parameter set, including the other values of the process noise covariance matrix, the optimal phase of the modulated CI artifact tail ϕ_m , and the optimal value of observation noise covariance.

It could be useful to include a template obtained with TS in the KF state-space model. Especially in cases where the CI artifact does not follow the proposed model of a rapidly changing peak, and an exponentially decaying tail, important improvements may be found. However, additional data collection may be needed for construction of the template.

The KF equations are determined under the assumption that the process and observation noise are Gaussian and white. It is known that EEG background noise follows a $1/f$ distribution. Therefore, it can be argued that the KF is not functioning optimally for EASSR parameter estimation. The state-space model could possibly be extended such that it also includes a model for the $1/f$ EEG background noise. Previous studies, investigating epilepsy spikes, incorporated an autoregressive component in the state-space model that should account for the EEG background noise [106, 110, 125]. Similar extensions could possibly be made to the state-space model proposed in this work. Note however that ASSR amplitude estimates obtained for normal hearing subjects in [91] were already fairly accurate, even without inclusion of an EEG background noise model. Furthermore, it is not expected that EEG background noise levels would differ between normal hearing and CI subjects.

6.4.5 Clinical applicability of EASSR-based CI fitting

To further test the clinical applicability of EASSRs for objective CI fitting, several topics should still be investigated. First, the feasibility of CI artifact suppression for lower SNR responses should be investigated. As described in Section 6.2, the vector summation of EASSR and CI artifact determines the magnitude of the EASSR amplitude and phase estimation error. For lower SNR responses, the CI artifact is dominant compared to the EASSR, and estimation errors are larger. Furthermore, EASSRs may be more difficult to accurately detect for lower stimulation levels. More extended signal processing and EASSR detection methods may be needed for fast enough EASSR detection. Such methods may combine channel information [10, 135, 136], or combine EEG responses at the fundamental EASSR frequency and its harmonics [26].

Second, the feasibility of obtaining CI artifact-free responses in infants and children should be investigated. As discussed earlier in Chapter 5, CI artifacts

may be more difficult to suppress in contralateral recording channels in children due to their smaller head sizes. In Belgium, bilateral CIs are fully reimbursed for children under the age of twelve, since 2010 [31]. Accurate CI artifact suppression in ipsilateral channels may be necessary for this growing population of bilaterally implanted subjects. To determine T levels during objective CI fitting, there is no reason to test CI subjects with bilateral stimulation. However, it could be interesting to investigate differences in auditory temporal processing during unilateral and bilateral CI stimulation. Furthermore, the optimal modulation frequency for EASSR testing in CI children is not known yet. It has been shown in [53] that no consistent 80–100 Hz EASSR could be detected in post-lingually deafened adult CI subjects. In normal hearing children, modulation frequencies in the 80–100 Hz range are preferred for ASSR-based hearing threshold estimation, because these responses are not influenced by arousal, sleep and sedation [115]. However, if 80–100 Hz are not present in CI children, as in adult CI subjects, the use of other modulation frequencies should be further investigated.

6.5 Conclusion

Due to the resemblance to clinically used stimulation sequences, EASSRs hold great promise for research and clinical purposes. Depending on the chosen stimulation parameters to elicit the EASSR, targeted areas of the brain can be studied. EASSRs are the perfect tool to study some fundamental research questions related to cortical reorganization in adult CI users and auditory maturation in CI children. EASSRs could also be used to probe the ENI, and adjust stimulation strategies and parameters based on the obtained responses. Furthermore, in the clinic, EASSRs could be used for (more) objective CI fitting. EASSR recordings are distorted by CI artifacts however, that should be suppressed to allow reliable EASSR detection and parameter estimation. In this thesis, a characterization of CI artifacts in EASSR measurements was given, and three novel methods for CI artifact suppression were developed and evaluated. The most promising method for EASSR parameter estimation in the presence of CI artifacts is the Kalman filter, presented in Chapter 5, that can be applied to single-channel measurements without additional data collection. The developed methods can be used by researchers and clinicians to further improve the quality of life and performance of children and adults with a CI.

Bibliography

- [1] AKHOUN, I., MCKAY, C. M., AND EL-DEREDY, W. Electrically evoked compound action potential artifact rejection by independent component analysis: Technique validation. *Hear Res* 302 (2013), 60–73.
- [2] ALLEN, D. P., STEGEMÖLLER, E. L., ZADIKOFF, C., ROSENOW, J. M., AND MACKINNON, C. D. Suppression of deep brain stimulation artifacts from the electroencephalogram by frequency-domain Hampel filtering. *Clinical Neurophysiology* 121, 8 (2010), 1227–1232.
- [3] ALLUM, J. H. J., GREISIGER, R., AND PROBST, R. Relationship of intraoperative electrically evoked stapedius reflex thresholds to maximum comfortable loudness levels of children with cochlear implants. *International journal of audiology* 41, 2 (2002), 93–99.
- [4] ALVAREZ, I., DE LA TORRE, A., SAINZ, M., ROLDÁN, C., SCHOESSER, H., AND SPITZER, P. Using evoked compound action potentials to assess activation of electrodes and predict C-levels in the Tempo+ cochlear implant speech processor. *Ear and hearing* 31, 1 (2010), 134–45.
- [5] AOYAGI, M., KIREN, T., KIM, Y., SUZUKI, Y., FUSE, T., AND KOIKE, Y. Optimal modulation frequency for amplitude-modulation following response in young children during sleep. *Hearing Research* 65, 1-2 (1993), 253–261.
- [6] ARORA, K., DOWELL, R., AND DAWSON, P. Cochlear Implant Stimulation Rates and Speech Perception. *Modern speech recognition approaches with case studies* (2012), 215–254.
- [7] AUDSLP DIAGNOSTIC AND REHABILITATION CLINIC. Conditioned Play Audiometry, 2013.
- [8] BAKHOS, D., ROUX, S., ROBIER, A., BONNET-BRILHAULT, F., LESCANNE, E., AND BRUNEAU, N. Minimization of cochlear implant

- artifact in cortical auditory evoked potentials in children. *International Journal of Pediatric Otorhinolaryngology* 76, 11 (2012), 1627–1632.
- [9] BIERER, J. A. Threshold and channel interaction in cochlear implant users: Evaluation of the tripolar electrode configuration. *Journal of the Acoustical Society of America* 121, 3 (2007), 1642–1653.
- [10] BIESMANS, W., BERTRAND, A., WOUTERS, J., AND MOONEN, M. Optimal spatial filtering for auditory steady-state response detection using high-density EEG. In *IEEE International Conference on Acoustics, Speech and Signal Processing (ICASSP)* (2015), pp. 857–861.
- [11] BOONS, T., BROKX, J. P. L., DHOOGHE, I., FRIJNS, J. H. M., PEERAER, L., VERMEULEN, A., WOUTERS, J., AND VAN WIERINGEN, A. Predictors of Spoken Language Development Following Pediatric Cochlear Implantation. *Ear and hearing* 33, 5 (2012), 627–639.
- [12] BOTROS, A., AND PSARROS, C. Neural response telemetry reconsidered: I. The relevance of ECAP threshold profiles and scaled profiles to cochlear implant fitting. *Ear and hearing* 31, 3 (2010), 367–79.
- [13] BOUDREAU, B. H., ENGLEHART, K., CHAN, A. D. C., AND PARKER, P. A. Subthreshold training: a novel approach to stimulus artifact cancellation in somatosensory evoked potential recordings. In *Proceedings of the 25th annual international conference of the IEEE EMBS* (2003), vol. 3, pp. 2659–2662.
- [14] BOUDREAU, B. H., ENGLEHART, K. B., CHAN, A. D., AND PARKER, P. A. Reduction of stimulus artifact in somatosensory evoked potentials: Segmented versus subthreshold training. *IEEE Transactions on Biomedical Engineering* 51, 7 (2004), 1187–1195.
- [15] BROWN, C. J. Clinical uses of electrically evoked auditory nerve and brainstem responses. *Current Opinion in Otolaryngology & Head and Neck Surgery* 11, 5 (2003), 383–387.
- [16] BROWN, C. J., ABBAS, P. J., FRYAUF-BERTSCHY, H., KELSAY, D., GANTZ, AND J., B. Intraoperative and Postoperative Electrically Evoked Auditory Brain Stem Responses in Nucleus Cochlear Implant Users. *Ear and hearing* 15, 2 (1994), 168–176.
- [17] BROWN, C. J., HUGHES, M. L., LUK, B., ABBAS, P. J., WOLAVER, A., AND GERVAIS, J. The Relationship Between EAP and EABR Thresholds and Levels Used to Program the Nucleus 24 Speech Processor: Data from Adults. *Ear and Hearing* 21, 2 (2000), 151–163.

- [18] BROWN, C. J., LOPEZ, S. M., HUGHES, M. L., AND ABBAS, P. J. Relationship between EABR thresholds and levels used to program the CLARION speech processor. *Annals of Otology, Rhinology and Laryngology* 108, 4 (1999), 50–57.
- [19] BUSBY, P. A., TONG, Y. C., AND CLARK, G. M. The perception of temporal modulations by cochlear implant patients. *Journal of the Acoustical Society of America* 94, 1 (1993), 124–131.
- [20] BUSBY, P. A., WHITFORD, L. A., BLAMEY, P. J., RICHARDSON, L. M., AND CLARK, G. M. Pitch perception for different modes of stimulation using the cochlear multiple-electrode prosthesis. *The Journal of the Acoustical Society of America* 95, 5 Pt 1 (1994), 2658–2669.
- [21] CAFARALLI DEES, D., DILLIER, N., LAI, W., VAN WALLENBERG, E., VAN DIJK, B., AKDAS, F., AKSIT, M., BATMAN, C., BEYNON, A., BURDO, S., CHANAL, J., COLLET, L., CONWAY, M., COUDERT, C., CRADDOCK, L., HULLINGTON, H., DEGGOUJ, N., FRAYSSE, B., GRABEL, S., KIEFER, J., KISS, J., LENARZ, T., MAIR, A., MAUNE, S., MULLER-DEILLE, J., PIRON, J.-P., RAZZA, S., TASCHE, C., THAI-VAN, H., TOOTH, F., TRUY, E., UZIEL, A., AND SMOORENBURG, G. F. Normative Findings of Electrically Evoked Compound Action Potential Measurements using the neural response telemetry of the Nucleus CI24M cochlear implant system. *Audiology and Neurotology* 10, 2 (2005), 105–116.
- [22] CANER, G., OLGUN, L., GÜLTEKIN, G., AND BALABAN, M. Optimizing Fitting in Children Using Objective Measures Such as Neural Response Imaging and Electrically Evoked Stapedius Reflex Threshold. *Otology & neurotology* 28, 5 (2007), 637–640.
- [23] CASTAÑEDA-VILLA, N., AND JAMES, C. The selection of optimal ICA algorithm parameters for robust AEP component estimates using 3 popular ICA algorithms. In *Annual International Conference of the IEEE Engineering in Medicine and Biology Society* (2008), pp. 5216–5219.
- [24] CASTANEDA-VILLA, N., AND JAMES, C. J. Objective source selection in blind source separation of AEPs in children with cochlear implants. In *Annual International Conference of the IEEE Engineering in Medicine and Biology - Proceedings* (2007), IEEE, pp. 6223–6226.
- [25] CASTANEDA-VILLA, N., AND JAMES, C. J. Independent component analysis for auditory evoked potentials and cochlear implant artifact estimation. *IEEE Transactions on Biomedical Engineering* 58, 2 (2011), 348–354.

- [26] CEBULLA, M., STÜRZEBECKER, E., AND ELBERLING, C. Objective detection of auditory steady-state responses: comparison of one-sample and q-sample tests. *Journal of the American Academy of Audiology* 17, 2 (2006), 93–103.
- [27] CHIA, E. M., WANG, J. J., ROCHTCHINA, E., CUMMING, R. R., NEWALL, P., AND MITCHELL, P. Hearing impairment and health-related quality of life: The blue mountains hearing study. *Ear and hearing* 28, 2 (2007), 187–195.
- [28] COHEN, S. M., LABADIE, R. F., DIETRICH, M. S., AND HAYNES, D. S. Quality of life in hearing-impaired adults: The role of cochlear implants and hearing aids. *Otolaryngology - Head and Neck Surgery* 131, 4 (2004), 413–422.
- [29] DE RAEVE, L. A longitudinal Study on Auditory Perception and Speech Intelligibility in Deaf Children Implanted Younger Than 18 Months Comparison to Those Implanted at Later Ages. *Otology & neurotology* 31, 8 (2010), 1261–1267.
- [30] DE RAEVE, L., AND LICHTERT, G. Changing Trends within the Population of Children who are Deaf or Hard of Hearing in Flanders (Belgium): Effects of 12 Years of Universal Newborn Hearing Screening, Early Intervention, and Early Cochlear Implantation. *The Volta Review* 112, 2 (2012), 131–148.
- [31] DE RAEVE, L., AND WOUTERS, A. Accessibility to cochlear implants in Belgium: State of the art on selection, reimbursement, habilitation, and outcomes in children and adults. *Cochlear Implants International* 14 (2013), S18–S25.
- [32] DEBENER, S., HINE, J., BLEECK, S., AND EYLES, J. Source localization of auditory evoked potentials after cochlear implantation. *Psychophysiology* 45, 1 (2008), 20–24.
- [33] DEBENER, S., THORNE, J., SCHNEIDER, T. R., AND VIOLA, F. C. Using ICA for the Analysis of Multi-Channel EEG Data. In *Simultaneous EEG and fMRI : Recording, Analysis, and Application*. 2010, pp. 121–133.
- [34] DELORME, A., AND MAKEIG, S. EEGLAB: An open source toolbox for analysis of single-trial EEG dynamics including independent component analysis. *Journal of Neuroscience Methods* 134, 1 (2004), 9–21.
- [35] DELORME, A., PALMER, J., ONTON, J., OOSTENVELD, R., AND MAKEIG, S. Independent EEG sources are dipolar. *PLoS ONE* 7, 2 (2012), e30135.

- [36] DELORME, A., SEJNOWSKI, T., AND MAKEIG, S. Enhanced detection of artifacts in EEG data using higher-order statistics and independent component analysis. *NeuroImage* 34, 4 (2007), 1443–1449.
- [37] DEPREZ, H., GRANSIER, R., HOFMANN, M., VAN WIERINGEN, A., WOUTERS, J., AND MOONEN, M. Characterization of cochlear implant artifacts in electrically evoked auditory steady-state responses. *Biomedical Signal Processing and Control* 31 (2016), 127–138.
- [38] DEPREZ, H., GRANSIER, R., HOFMANN, M., VAN WIERINGEN, A., WOUTERS, J., AND MOONEN, M. Template Subtraction to Remove CI Stimulation Artifacts in Auditory Steady-State Responses in CI Subjects. *IEEE Transactions on Neural Systems and Rehabilitation Engineering* 25, 8 (2017), 1322–1331.
- [39] DEPREZ, H., GRANSIER, R., HOFMANN, M., VAN WIERINGEN, A., WOUTERS, J., AND MOONEN, M. Independent component analysis for cochlear implant artifacts attenuation from electrically evoked auditory steady-state response measurements. *Journal of Neural Engineering* 15, 1 (2018), 16006.
- [40] DEPREZ, H., HOFMANN, M., VAN WIERINGEN, A., WOUTERS, J., AND MOONEN, M. Cochlear implant artifact rejection in electrically evoked auditory steady state responses. *European Signal Processing Conference* 11, 2 (2014), 1995–1999.
- [41] DOBIE, R. A., AND WILSON, M. J. A comparison of t test, F test, and coherence methods of detecting steady-state auditory-evoked potentials, distortion-product otoacoustic emissions, or other sinusoids. *The Journal of the Acoustical Society of America* 100, 4 (1996), 2236–2246.
- [42] FALLON, J. B., IRVINE, D. R., AND SHEPHERD, R. K. Cochlear implants and brain plasticity. *Hearing Research* 238, 1-2 (2008), 110–117.
- [43] FRIESEN, L. M., AND PICTON, T. W. A method for removing cochlear implant artifact. *Hearing Research* 259, 1-2 (2010), 95–106.
- [44] FRIESEN, L. M., SHANNON, R. V., AND CRUZ, R. J. Effects of stimulation rate on speech recognition with cochlear implants. *Audiology and Neurotology* 10, 3 (2005), 169–184.
- [45] GARADAT, S. N., ZWOLAN, T. A., AND PFINGST, B. E. Across-site patterns of modulation detection: relation to speech recognition. *Journal of the Acoustical Society of America* 131, 5 (2012), 4030–41.

- [46] GARADAT, S. N., ZWOLAN, T. A., AND PFINGST, B. E. Using temporal modulation sensitivity to select stimulation sites for processor maps in cochlear implant listeners. *Audiology and Neurotology* 18, 4 (2013), 247–260.
- [47] GILLEY, P. M., SHARMA, A., DORMAN, M., FINLEY, C. C., PANCH, A. S., AND MARTIN, K. Minimization of cochlear implant stimulus artifact in cortical auditory evoked potentials. *Clinical Neurophysiology* 117, 8 (2006), 1772–1782.
- [48] GILLEY, P. M., SHARMA, A., AND DORMAN, M. F. Cortical reorganization in children with cochlear implants. *Brain Research* 1239 (2008), 56–65.
- [49] GIRAUD, A.-L., LORENZI, C., ASHBURNER, J., WABLE, J., JOHNSRUDE, I., FRACKOWIAK, R., AND KLEINSCHMIDT, A. Representation of the Temporal Envelope of Sounds in the Human Brain. *Journal of Neurophysiology* 84, 3 (2000), 1588–1598.
- [50] GOOSSENS, T., VERCAMMEN, C., WOUTERS, J., AND VAN WIERINGEN, A. Aging affects neural synchronization to speech-related acoustic modulations. *Frontiers in Aging Neuroscience* 8, JUN (2016), 1–23.
- [51] GORDON, K., HENKIN, Y., AND KRAL, A. Asymmetric Hearing During Development: The Aural Preference Syndrome and Treatment Options. *Pediatrics* 136, 1 (2015), 141–153.
- [52] GORDON, K. A., WONG, D. D. E., AND PAPSIN, B. C. Bilateral input protects the cortex from unilaterally-driven reorganization in children who are deaf. *Brain* 136, 5 (2013), 1609–1625.
- [53] GRANSIER, R., DEPREZ, H., HOFMANN, M., MOONEN, M., VAN WIERINGEN, A., AND WOUTERS, J. Auditory steady-state responses in cochlear implant users: Effect of modulation frequency and stimulation artifacts. *Hearing Research* 335 (2016), 149–160.
- [54] GRANSIER, R., WIERINGEN, A. V., AND WOUTERS, J. Binaural interaction effects of 30–50 Hz auditory steady-state responses. *Ear and Hearing* 38, 5 (2017), 305–315.
- [55] HALL, J. W. T. R. *Auditory Evoked Response Measurement Practices*. 2007.
- [56] HAN, D.-M., CHEN, X.-Q., ZHAO, X.-T., KONG, Y., LI, Y.-X., LIU, S., LIU, B., AND MO, L.-Y. Comparisons between neural response imaging thresholds, electrically evoked auditory reflex thresholds and

- most comfortable loudness levels in CII bionic ear users with HiResolution sound processing strategies. *Acta oto-laryngologica* 125, 7 (2005), 732–735.
- [57] HE, S., TEAGLE, H. F. B., AND BUCHMAN, C. A. The Electrically Evoked Compound Action Potential: From Laboratory to Clinic. *Frontiers in Neuroscience* 11 (2017).
- [58] HEFFER, L. F., AND FALLON, J. B. A novel stimulus artifact removal technique for high-rate electrical stimulation. *Journal of Neuroscience Methods* 170, 2 (2008), 277–284.
- [59] HERDMAN, A. T., LINS, O., VAN ROON, P., STAPELLS, D. R., SCHERG, M., AND PICTON, T. W. Intracerebral sources of human auditory steady-state responses. *Brain Topography* 15, 2 (2002), 69–86.
- [60] HERNANDEZ-PAVON, J. C., METSOMAA, J., MUTANEN, T., STENROOS, M., MÄKI, H., ILMONIEMI, R. J., AND SARVAS, J. Uncovering neural independent components from highly artifactual TMS-evoked EEG data. *Journal of Neuroscience Methods* 209, 1 (2012), 144–157.
- [61] HINDERINK, J. B., KRABBE, P. F., AND VAN DEN BROEK, P. Development and application of a health-related quality-of-life instrument for adults with cochlear implants: the Nijmegen cochlear implant questionnaire. *Otolaryngology–head and neck surgery* 123, 6 (2000), 756–65.
- [62] HODGES, A. V., DOLAN-ASH, S., BUTTS, S., AND BALKANY, T. J. Using electrically evoked auditory reflex thresholds to fit the CLARION Cochlear Implant. *Annals of Otology, Rhinology and Laryngology* 108, 4 (1999), 64–68.
- [63] HOFFMANN, U., CHO, W., RAMOS-MURGUIALDAY, A., AND KELLER, T. Detection and removal of stimulation artifacts in electroencephalogram recordings. In *Proceedings of the Annual International Conference of the IEEE Engineering in Medicine and Biology Society, EMBS* (2011), pp. 7159–7162.
- [64] HOFMANN, M., AND WOUTERS, J. Electrically evoked auditory steady state responses in cochlear implant users. *Journal of the Association for Research in Otolaryngology* 11, 2 (2010), 267–82.
- [65] HOFMANN, M., AND WOUTERS, J. Improved electrically evoked auditory steady-state response thresholds in humans. *Journal of the Association for Research in Otolaryngology* 13, 4 (2012), 573–589.
- [66] HOTELLING, H. The Generalization of Student’s Ratio. *The Annals of Mathematical Statistics* 2, 3 (1931), 360–378.

- [67] HUDGINS, GRIEVE PARKER, GRIEVE, R., PARKER, P., HUDGINS, B., ENGLEHART, K., AND PARKER, PHILIP A. Nonlinear Adaptive Filtering of Stimulus Artifact. *IEEE Transactions on Biomedical Engineering* 47, 3 (2000), 389–95.
- [68] HUGHES, M. L. *Objective measures in cochlear implants*. 2013.
- [69] HUGHES, M. L., BROWN, C. J., AND ABBAS, P. J. Sensitivity and Specificity of Averaged Electrode Voltage Measures in Cochlear Implant Recipients. *Ear and Hearing* 25, 5 (2004), 431–446.
- [70] HUGHES, M. L., BROWN, C. J., ABBAS, P. J., WOLAVER, A. A., AND GERVAIS, J. P. Comparison of EAP Thresholds with MAP Levels in the Nucleus 24 Cochlear Implant: Data from Children. *Ear and Hearing* 21, 2 (2000), 164–174.
- [71] HUGHES, M. L., CASTIONI, E. E., GOEHRING, J. L., AND BAUDHUIN, J. L. Temporal response properties of the auditory nerve: Data from human cochlear-implant recipients. *Hearing research* 285, 1-2 (2012), 46–57.
- [72] ILLG, A., HAACK, M., LESINSKI-SCHIEDAT, A., BÜCHNER, A., AND LENARZ, T. Long-Term Outcomes, Education, and Occupational Level in Cochlear Implant Recipients Who Were Implanted in Childhood. *Ear and Hearing* (2017), In press.
- [73] ILMONIEMI, R. J., HERNANDEZ-PAVON, J. C., MAKELA, N. N., METSOMAA, J., MUTANEN, T. P., STENROOS, M., AND SARVAS, J. Dealing with artifacts in TMS-evoked EEG. In *Proceedings of the Annual International Conference of the IEEE Engineering in Medicine and Biology Society, EMBS* (2015), vol. 2015-Novem, pp. 230–233.
- [74] JASPER, H. H. The ten-twenty electrode system of the International Federation. *Electroencephalography and Clinical Neurophysiology* 10, 2 (1958), 371–375.
- [75] JENG, F.-C., ABBAS, P. J., BROWN, C. J., MILLER, C. A., NOURSKI, K. V., AND ROBINSON, B. K. Electrically Evoked Auditory Steady-State Responses in Guinea Pigs. *Audiology and Neurotology* 12, 2 (2007), 101–112.
- [76] JEWETT, D. L., AND WILLISTON, J. S. Auditory-evoked far fields averaged from the scalp of humans. *Brain* 94, 4 (1971), 681–696.
- [77] JIWANI, S., PAPSIN, B. C., AND GORDON, K. A. Early unilateral cochlear implantation promotes mature cortical asymmetries in adolescents who are deaf. *Human Brain Mapping* 37, 1 (2016), 135–152.

- [78] KOHLI, S., AND CASSON, A. J. Removal of Transcranial a.c. Current Stimulation artifact from simultaneous EEG recordings by superposition of moving averages. In *Proceedings of the Annual International Conference of the IEEE Engineering in Medicine and Biology Society, EMBS* (2015), vol. 2015-Novem, pp. 3436–3439.
- [79] KORCZAK, P., SMART, J., DELGADO, R., M. STROBEL, T., AND BRADFORD, C. Auditory Steady-State Responses. *Journal of the American Academy of Audiology* 23, 3 (2012), 146–170.
- [80] KORHONEN, R. J., HERNANDEZ-PAVON, J. C., METSOMAA, J., MÄKI, H., ILMONIEMI, R. J., AND SARVAS, J. Removal of large muscle artifacts from transcranial magnetic stimulation-evoked EEG by independent component analysis. *Medical and Biological Engineering and Computing* 49, 4 (2011), 397–407.
- [81] KRAL, A., HARTMANN, R., MORTAZAVI, D., AND KLINKE, R. Spatial resolution of cochlear implants: The electrical field and excitation of auditory afferents. *Hearing Research* 121, 1-2 (1998), 11–28.
- [82] LAMMERS, M. J. W., JANSEN, T. T. G., GROLMAN, W., LENARZ, T., VERSNEL, H., VAN ZANTEN, G. A., TOPSAKAL, V., AND LESINSKI-SCHIEDAT, A. The influence of newborn hearing screening on the age at cochlear implantation in children. *The Laryngoscope* 125, 4 (2015), 985–90.
- [83] LAZARD, D. S., VINCENT, C., VENAIL, F., VAN DE HEYNING, P., TRUY, E., STERKERS, O., SKARZYNSKI, P. H., SKARZYNSKI, H., SCHAUWERS, K., O’LEARY, S., MAWMAN, D., MAAT, B., KLEINE-PUNTE, A., HUBER, A. M., GREEN, K., GOVAERTS, P. J., FRAYSSE, B., DOWELL, R., DILLIER, N., BURKE, E., BEYNON, A., BERGERON, F., BAŞKENT, D., ARTIÈRES, F., AND BLAMEY, P. J. Pre-, Per- and Postoperative Factors Affecting Performance of Postlinguistically Deaf Adults Using Cochlear Implants: A New Conceptual Model over Time. *PLoS ONE* 7, 11 (2012), 1–11.
- [84] LEVI, E. C., FOLSOM, R. C., AND DOBIE, R. A. Amplitude-modulation following response (AMFR): Effects of modulation rate, carrier frequency, age, and state. *Hearing Research* 68, 1 (1993), 42–52.
- [85] LI, X., NIE, K., KARP, F., TREMBLAY, K. L., AND RUBINSTEIN, J. T. Characteristics of stimulus artifacts in EEG recordings induced by electrical stimulation of cochlear implants. In *Proceedings - 2010 3rd International Conference on Biomedical Engineering and Informatics, BMEI 2010* (2010), vol. 2, pp. 799–803.

- [86] LILLY, J. C., HUGHES, J. R., ALVORD, E. C., AND GALKIN, T. W. Brief, noninjurious electric waveform for stimulation of the brain. *Science* 121 (1955), 468–469.
- [87] LIMB, C. J., AND ROY, A. T. Technological, biological, and acoustical constraints to music perception in cochlear implant users. *Hearing Research* 308 (2014), 13–26.
- [88] LUKE, R. *Supra-Threshold Electrically Evoked Auditory Steady-State Responses In Cochlear Implant Users*. PhD thesis, 2016.
- [89] LUKE, R., DE VOS, A., AND WOUTERS, J. Source analysis of auditory steady-state responses in acoustic and electric hearing. *NeuroImage* 147 (2017), 568–576.
- [90] LUKE, R., VAN DEUN, L., HOFMANN, M., VAN WIERINGEN, A., AND WOUTERS, J. Assessing temporal modulation sensitivity using electrically evoked auditory steady state responses. *Hearing Research* 324 (2015), 37–45.
- [91] LUKE, R., AND WOUTERS, J. Kalman filter based estimation of auditory steady state response parameters. *IEEE Transactions on Neural Systems and Rehabilitation Engineering* 25, 3 (2017), 196–204.
- [92] MANCINI, M., PELLICCIARI, M. C., BRIGNANI, D., MAURI, P., DE MARCHIS, C., MINIUSSI, C., AND CONFORTO, S. Automatic artifact suppression in simultaneous tDCS-EEG using adaptive filtering. In *Proceedings of the Annual International Conference of the IEEE Engineering in Medicine and Biology Society, EMBS* (2015), vol. 2015-Novem, pp. 2729–2732.
- [93] MARTIN, B. A. Can the Acoustic Change Complex Be Recorded in an Individual with a Cochlear Implant? Separating Neural Responses from Cochlear Implant Artifact. *Journal of the American Academy of Audiology* 18, 2 (2007), 126–140.
- [94] MARTIN BLAND, J., AND ALTMAN, D. Statistical Methods for Assessing Agreement Between Two Methods of Clinical Measurement. *The Lancet* 327, 8476 (1986), 307–310.
- [95] MC LAUGHLIN, M., LOPEZ VALDES, A., REILLY, R. B., AND ZENG, F. G. Cochlear implant artifact attenuation in late auditory evoked potentials: A single channel approach. *Hearing Research* 302 (2013), 84–95.

- [96] MC LAUGHLIN, M., LU, T., DIMITRIJEVIC, A., AND ZENG, F.-G. Towards a closed-loop cochlear implant system: application of embedded monitoring of peripheral and central neural activity. *IEEE transactions on neural systems and rehabilitation engineering* 20, 4 (2012), 443–454.
- [97] MCKAY, C. M., CHANDAN, K., AKHOUN, I., SICILIANO, C., AND KLUK, K. Can ECAP measures be used for totally objective programming of cochlear implants? *JARO - Journal of the Association for Research in Otolaryngology* 14, 6 (2013), 879–890.
- [98] MCKAY, C. M., FEWSTER, L., AND DAWSON, P. A different approach to using neural response telemetry for automated cochlear implant processor programming. *Ear and hearing* 26, 4 Suppl (2005), 38S–44S.
- [99] MCKAY, C. M., LIM, H. H., AND LENARZ, T. Temporal processing in the auditory system: Insights from cochlear and auditory midbrain implantees. *Journal of the Association for Research in Otolaryngology* 14, 1 (2013), 103–124.
- [100] MCKAY, C. M., MCDERMOTT, H. J., AND CLARK, G. M. Pitch percepts associated with amplitude modulated current pulse trains in cochlear implantees. *Journal of the Acoustical Society of America* 96, 5 (1994), 2664–2673.
- [101] MCMENAMIN, B. W., SHACKMAN, A., MAXWELL, J. S., BACHHUBER, D., KOPPENHAVER, A., GREISCHAR, L., AND DAVIDSON, R. J. Validation of ICA-based myogenic artifact correction for scalp and source-localized EEG. *NeuroImage* 49, 3 (2010), 2416–2.
- [102] MERRILL, D. R., BIKSON, M., AND JEFFERYS, J. G. R. Electrical stimulation of excitable tissue: design of efficacious and safe protocols. *Journal of neuroscience methods* 141 (2005), 171–198.
- [103] MILLER, C. A., BROWN, C. J., ABBAS, P. J., AND CHI, S. L. The clinical application of potentials evoked from the peripheral auditory system. *Hearing research* 242, 1-2 (2008), 184–197.
- [104] MILLER, C. A., HU, N., ZHANG, F., ROBINSON, B. K., AND ABBAS, P. J. Changes across time in the temporal responses of auditory nerve fibers stimulated by electric pulse trains. *Journal of the Association for Research in Otolaryngology* 9, 1 (2008), 122–137.
- [105] MILLER, S., AND ZHANG, Y. Validation of the cochlear implant artifact correction tool for auditory electrophysiology. *Neuroscience Letters* 577 (aug 2014), 51–55.

- [106] MORBIDI, F., GARULLI, A., PRATTICHIZZO, D., RIZZO, C., MANGANOTTI, P., AND ROSSI, S. Off-line removal of TMS-induced artifacts on human electroencephalography by Kalman filter. *Journal of Neuroscience Methods* 162, 1-2 (2007), 293–302.
- [107] MOTTAGHI, S., JOSEPH, K., CHRIST, O., FEUERSTEIN, T. J., AND HOFMANN, U. G. When the ostrich-algorithm fails: Blanking method affects spike train statistics. *bioRxiv* (jul 2017).
- [108] NACHTEGAAL, J., SMIT, J. H., SMITS, C., BEZEMER, P. D., VAN BEEK, J. H. M., FESTEN, J. M., AND KRAMER, S. E. The association between hearing status and psychosocial health before the age of 70 years: results from an internet-based national survey on hearing. *Ear and hearing* 30, 3 (2009), 302–312.
- [109] NIPARKO, J. K., TOBEY, E. A., THAL, D. J., EISENBERG, L. S., WANG, N.-Y., QUITTNER, A. L., AND FINK, N. E. Spoken Language Development in Children Following Cochlear Implantation. *Journal of the American Medical Association* 303, 15 (2012), 1498–1506.
- [110] OIKONOMOU, V. P., TZALLAS, A. T., AND FOTIADIS, D. I. A Kalman filter based methodology for EEG spike enhancement. *Computer Methods and Programs in Biomedicine* 85, 2 (2007), 101–108.
- [111] PARSA, V., PARKER, P., AND SCOTT, R. Convergence characteristics of two algorithms in non-linear stimulus artefact cancellation for electrically evoked potential enhancement. *Medical and Biological Engineering and Computing* 36, 2 (1998), 202–214.
- [112] PFINGST, B. E., BURKHOLDER-JUHASZ, R. A., XU, L., AND THOMPSON, C. S. Across-site patterns of modulation detection in listeners with cochlear implants. *Journal of the Acoustical Society of America* 123, 2 (2008), 1054–62.
- [113] PFINGST, B. E., AND XU, L. Across-Site Variation in Detection Thresholds and Maximum Comfortable Loudness Levels for Cochlear Implants. *Journal of the Association for Research in Otolaryngology* 5, 1 (2004), 11–24.
- [114] PFINGST, B. E., ZWOLAN, T. A., AND HOLLOWAY, L. A. Effects of stimulus configuration on psychophysical operating levels and on speech recognition with cochlear implants. *Hearing Research* 112, 1-2 (1997), 247–260.
- [115] PICTON, T. W., JOHN, M. S., DIMITRIJEVIC, A., AND PURCELL, D. Human auditory steady-state responses: Respuestas auditivas de estado

- estable en humanos. *International Journal of Audiology* 42, 4 (2003), 177–219.
- [116] REYES, S. A., SALVI, R. J., BURKARD, R. F., COAD, M. L., WACK, D. S., GALANTOWICZ, P. J., AND LOCKWOOD, A. H. PET imaging of the 40 Hz auditory steady state response. *Hearing research* 194, 1-2 (2004), 73–80.
- [117] ROGASCH, N. C., THOMSON, R. H., FARZAN, F., FITZGIBBON, B. M., BAILEY, N. W., HERNANDEZ-PAVON, J. C., DASKALAKIS, Z. J., AND FITZGERALD, P. B. Removing artefacts from TMS-EEG recordings using independent component analysis: Importance for assessing prefrontal and motor cortex network properties. *NeuroImage* 101 (2014), 425–439.
- [118] ROSS, B., BORGMANN, C., DRAGANOVA, R., ROBERTS, L. E., AND PANTEV, C. A high-precision magnetoencephalographic study of human auditory steady-state responses to amplitude-modulated tones. *Journal of the Acoustical Society of America* 108, 2 (2000), 679–691.
- [119] RUACH, R., MITELMAN, R., SHERMAN, E., COHEN, O., AND PRUT, Y. An assumption-free quantification of neural responses to electrical stimulations. *Journal of Neuroscience Methods* 254 (2015), 10–17.
- [120] SAINZ, M., DE LA TORRE, A., ROLDÁN, C., RUIZ, J., AND VARGAS, J. L. Analysis of programming maps and its application for balancing multichannel cochlear implants. *International Journal of Audiology* 42, 1 (2003), 43–51.
- [121] SALEH, S. M., SAEED, S. R., MEERTON, L., MOORE, D. R., AND VICKERS, D. A. Clinical use of electrode differentiation to enhance programming of cochlear implants. *Cochlear implants international* 14:sup4 (2013), S16–8.
- [122] SANDMANN, P., EICHELE, T., BUECHLER, M., DEBENER, S., JÄNCKE, L., DILLIER, N., HUGDAHL, K., AND MEYER, M. Evaluation of evoked potentials to dyadic tones after cochlear implantation. *Brain* 132, 7 (2009), 1967–1979.
- [123] SANDMANN, P., KEGEL, A., EICHELE, T., DILLIER, N., LAI, W., BENDIXEN, A., DEBENER, S., JANCKE, L., AND MEYER, M. Neurophysiological evidence of impaired musical sound perception in cochlear-implant users. *Clinical Neurophysiology* 121, 12 (2010), 2070–2082.
- [124] SANTILLAN-GUZMAN, A., HEUTE, U., MUTHURAMAN, M., STEPHANI, U., AND GALKA, A. DBS artifact suppression using a time-frequency

- domain filter. In *Proceedings of the Annual International Conference of the IEEE Engineering in Medicine and Biology Society, EMBS* (2013), pp. 4815–4818.
- [125] SHAHABI, H., MOGHIMI, S., AND ZAMIRI-JAFARIAN, H. EEG eye blink artifact removal by EOG modeling and Kalman filter. *2012 5th International Conference on Biomedical Engineering and Informatics, BMEI 2012* (2012), 496–500.
 - [126] SHAPIRO, W. H., AND BRADHAM, T. S. Cochlear implant programming. *Otolaryngologic Clinics of North America* 45, 1 (2012), 111–127.
 - [127] SHARMA, A., DORMAN, M. F., AND SPAHR, A. J. A sensitive period for the development of the central auditory system in children with cochlear implants: implications for age of implantation. *Ear and hearing* 23, 6 (2002), 532–9.
 - [128] SHARMA, A., GILLEY, P. M., DORMAN, M. F., AND BALDWIN, R. Deprivation-induced cortical reorganization in children with cochlear implants. *International Journal of Audiology* 46, 9 (2007), 494–499.
 - [129] SHARMA, A., NASH, A. A., AND DORMAN, M. Cortical development, plasticity and re-organization in children with cochlear implants. *Journal of Communication Disorders* 42, 4 (2009), 272–279.
 - [130] SINKIEWICZ, D., FRIESEN, L., AND GHORAANI, B. Analysis of Cochlear Implant Artifact Removal Techniques Using the Continuous Wavelet Transform. In *Annual International Conference of the IEEE Engineering in Medicine and Biology Society* (2014), pp. 5482–5485.
 - [131] THOMPSON, G., AND WILSON, W. Clinical Application of Visual Reinforcement Audiometry. *Seminars in Hearing* 5, 1 (1984), 85–98.
 - [132] TOBEY, E. A., THAL, D. J., NIPARKO, J. K., EISENBERG, L. S., QUITTNER, A. L., WANG, N.-Y., AND TEAM, C. I. Influence Of Implantation Age On School-Age Language Performance In Pediatric Cochlear Implant Users. *International Journal of Audiology* 52, 4 (2013), 219–229.
 - [133] VAERENBERG, B., SMITS, C., DECEULAER, G., ZIR, E., HARMAN, S., JASPERS, N., AND GOVAERTS, P. Cochlear Implant Programming: A Global Survey on the State of the Art. *The Scientific World Journal* 2014, August 2013 (2014).
 - [134] VAN DEN ABBEELE, T., NOËL-PETROFF, N., AKIN, I., CANER, G., OLGUN, L., GUIRAUD, J., TRUY, E., ATTIAS, J., RAVEH, E., BELGIN,

- E., SENNAROGLU, G., BASTA, D., ERNST, A., MARTINI, A., ROSIGNOLI, M., LEVI, H., ELIDAN, J., BENGHALEM, A., AMSTUTZ-MONTADERT, I., LEROSEY, Y., DE VEL, E., DHOOGHE, I., HILDESHEIMER, M., KRONENBERG, J., AND ARNOLD, L. Multicentre investigation on electrically evoked compound action potential and stapedius reflex: how do these objective measures relate to implant programming parameters? *Cochlear Implants International* 13, 1 (2012), 26–34.
- [135] VAN DUN, B., WOUTERS, J., AND MOONEN, M. Improving auditory steady-state response detection using independent component analysis on multichannel EEG data. *IEEE transactions on biomedical engineering* 54, 7 (2007), 1220–30.
- [136] VAN DUN, B., WOUTERS, J., AND MOONEN, M. Multi-channel wiener filtering based auditory steady-state response detection. *IEEE International Conference on Acoustics, Speech and Signal Processing (ICASSP)* (2007), 929–932.
- [137] VAN KERSCHAUER, E., AND STAPPAERTS, L. Jaarrapport Gehoor 2009-2010-2011. Tech. rep., 2011.
- [138] VAN WIERINGEN, A., AND WOUTERS, J. What can we expect of normally-developing children implanted at a young age with respect to their auditory, linguistic and cognitive skills? *Hearing research* 322 (2014), 171–179.
- [139] VANDALI, A. E., WHITFORD, L. A., PLANT, K. L., AND CLARK, G. M. Speech perception as a function of electrical stimulation rate: using the Nucleus 24 cochlear implant system. *Ear and hearing* 21, 6 (2000), 608–624.
- [140] VANVOOREN, S., HOFMANN, M., POELMANS, H., GHESQUIÈRE, P., AND WOUTERS, J. Theta, beta and gamma rate modulations in the developing auditory system. *Hearing research* 327 (2015), 153–162.
- [141] VERMEIRE, K., BROKX, J. P. L., WUYTS, F. L., COCHET, E., HOFKENS, A., AND VAN DE HEYNING, P. H. Quality-of-life benefit from cochlear implantation in the elderly. *Otology & neurotology* 26, 5 (2005), 188–195.
- [142] VIOLA, F. C., DE VOS, M., HINE, J., SANDMANN, P., BLEECK, S., EYLES, J., AND DEBENER, S. Semi-automatic attenuation of cochlear implant artifacts for the evaluation of late auditory evoked potentials. *Hearing Research* 284, 1-2 (2012), 6–15.
- [143] VIOLA, F. C., THORNE, J. D., BLEECK, S., EYLES, J., AND DEBENER, S. Uncovering auditory evoked potentials from cochlear implant users

- with independent component analysis. *Psychophysiology* 48, 11 (nov 2011), 1470–1480.
- [144] VISRAM, A. S., INNES-BROWN, H., EL-DEREDY, W., AND MCKAY, C. M. Cortical auditory evoked potentials as an objective measure of behavioral thresholds in cochlear implant users. *Hearing research* 327 (2015), 35–42.
- [145] WAGENAAR, D. A., AND POTTER, S. M. Real-time multi-channel stimulus artifact suppression by local curve fitting. *Journal of Neuroscience Methods* 120, 2 (2002), 113–120.
- [146] WICHMANN, T. A digital averaging method for removal of stimulus artifacts in neurophysiologic experiments. *Journal of Neuroscience Methods* 98, 1 (2000), 57–62.
- [147] WILSON, B., SAMANTA, M. K., SANTHI, K., SAMPATH KUMAR, K. P., RAMASAMY, M., AND SURESH, B. Significant delivery of tacrine into the brain using magnetic chitosan microparticles for treating Alzheimer’s disease. *Journal of Neuroscience Methods* 177, 2 (2009), 427–433.
- [148] WOLFE, J., AND SCHAFER, E. C. *Programming cochlear implants*. Plural publishing, 2014.
- [149] WONG, D. D., AND GORDON, K. A. Beamformer suppression of cochlear implant artifacts in an electroencephalography dataset. *IEEE Transactions on Biomedical Engineering* 56, 12 (2009), 2851–2857.
- [150] WOUTERS, J., MCDERMOTT, H. J., AND FRANCA, T. Sound coding in cochlear implants: From electric pulses to hearing. *IEEE Signal Processing Magazine* 32, 2 (2015), 67–80.
- [151] YOCHUM, M., AND BINCZAK, S. A wavelet based method for electrical stimulation artifacts removal in electromyogram. *Biomedical Signal Processing and Control* 22, October (2015), 1–10.
- [152] ZENG, F.-G., REBSCHER, S., HARRISON, W., SUN, X., AND FENG, H. Cochlear implants: system design, integration, and evaluation. *IEEE reviews in biomedical engineering* 1 (jan 2008), 115–42.
- [153] ZHOU, N., AND PFINGST, B. E. Effects of Site-Specific Level Adjustments on Speech Recognition With Cochlear Implants. *Ear and hearing* 35, 1 (2014), 30–40.
- [154] ZWOLAN, T. A., COLLINS, L. M., AND WAKEFIELD, G. H. Electrode discrimination and speech recognition in postlingually deafened adult

- cochlear implant subjects. *Journal of the Acoustical Society of America* 102, 6 (1997), 3673–3685.
- [155] ZWOLAN, T. A., KILENY, P. R., ASHBAUGH, C., AND TELIAN, S. A. Patient performance with the Cochlear Corporation "20 + 2" implant: bipolar versus monopolar activation. *American Journal of Otology* 17, 5 (1996), 717–723.

Curriculum vitae

Hanne Deprez was born in Leuven, Belgium on December 18th, 1990. She received her secondary education at Lyceum Onze-Lieve-Vrouw van Vlaanderen, Kortrijk, where she graduated in 2008. In 2011, Hanne obtained her Bachelor's degree in Mechanical-Electrical Engineering from KU Leuven. In 2013, she graduated with great distinction from KU Leuven as a Master in Electrical Engineering, option Embedded systems and multimedia. Her Master's thesis was entitled "Automated speech evaluation for cochlear implants". In September 2013, Hanne started pursuing a PhD in the research labs of Prof. Jan Wouters and Prof. Marc Moonen, respectively associated to the Departments of Neuroscience and Electrical Engineering. Her research interests are objective measures in subjects with auditory implants, mainly focusing on measuring steady-state responses in CI subjects.

List of publications

Articles in international academic journals

Deprez H., Gransier R., Hofmann M., van Wieringen A., Wouters J., Moonen M. (2017). A Kalman filter based method for electrically evoked auditory steady state response parameter estimation. *Submitted*

Deprez H., Gransier R., Hofmann M., van Wieringen A., Wouters J., Moonen M. (2017). Independent component analysis for cochlear implant artifacts attenuation from electrically evoked auditory steady-state response measurements. *Journal of Neural Engineering*, 15(1), 16006.

Deprez H., Gransier R., Hofmann M., van Wieringen A., Wouters J., Moonen M. (2017). Characterization of cochlear implant artifacts in electrically evoked auditory steady-state responses. *Biomedical Signal Processing and Control*, 31, 127-138.

Deprez H., Gransier R., Hofmann M., van Wieringen A., Wouters J., Moonen M. (2016). Template subtraction to remove CI stimulation artifacts in auditory steady-state responses in CI subjects. *IEEE Transactions on Neural Systems and Rehabilitation Engineering*, 25 (8), 1322-1331.

Gransier R., **Deprez H.**, Hofmann M., Moonen M., van Wieringen A., Wouters J. (2016). Auditory steady-state responses in cochlear implant users: effect of modulation frequency and stimulation artifacts. *Hearing Research*, 335, 149-160.

Papers at international conferences, published in proceedings

Deprez H., Hofmann M., Van Wieringen A., Wouters J., Moonen M. (2014). Cochlear implant artifact rejection in electrically evoked auditory steady state responses. *Proc. European Signal Processing Conference (EUSIPCO)*, Lisbon, Portugal, Sep. 2014.

Deprez H., Yilmaz E., Lievens S., Van hamme H. (2013). Automating speech reception threshold measurements using automatic speech recognition. *Proc. workshop on speech and language processing for assistive technologies (SLPAT)*, Grenoble, France, Aug. 2013.

Presentations at international conferences

Deprez H., Gransier R., Hofmann M., Moonen M., Wouters J., Verhaert N. (2016). Intra-operative assessment of direct acoustic cochlear implant functioning using ABRs and ASSRs. *International Symposium on objective measures in auditory implants (OMAI)*, Szeged, Hungary, Jun. 2016.

Posters at international conferences

Deprez H., Gransier R., Hofmann M., Moonen M., Wouters J., Verhaert N. (2017). Objective measures to assess direct acoustic cochlear implant functioning: artifact characterization and intra-operative ABR and ASSR measurements. *Conference on Implantable Auditory Prostheses (CIAP)*, Lake Tahoe, USA, Jul. 2017.

Deprez H., Gransier R., Hofmann M., van Wieringen A., Moonen M., Wouters J. (2017). Comparison of artifact suppression methods for the measurement of electrically evoked auditory steady- state responses. *Conference on Implantable Auditory Prostheses (CIAP)*, Lake Tahoe, USA, Jul. 2017.

Gransier R., Hofmann M., **Deprez H.**, Moonen M., van Wieringen A., Wouters J. (2016). Electrically evoked auditory steady-state responses to multiple sequential electrode stimulation in cochlear implant users. *International Symposium on objective measures in auditory implants (OMAI)*, Szeged, Hungary, June 2016.

Deprez H., Gransier R., van Wieringen A., Wouters J., Moonen M. (2015). Template based CI artifact attenuation to measure Electrically Evoked Auditory Steady State Responses. *ARCHES Conference*, Groningen, Nederland, Nov. 2015.

Deprez H., Gransier R., Hofmann M., Francart T., Van Wieringen A., Moonen M., Wouters J. (2015). Cochlear implant artifact removal methods to measure electrically evoked auditory steady-state responses. *Conference on Implantable Auditory Prostheses (CIAP)*, Lake Tahoe, California, USA, Jul. 2015

Van Eeckhoutte M., **Deprez H.**, Gransier R., Hofmann M., Wouters J., Francart T. (2015). Electrically-evoked auditory steady-state responses as an objective measure of loudness growth. *Conference on Implantable Auditory Prostheses (CIAP)*, Lake Tahoe, California, USA, Jul. 2015.

Gransier R., **Deprez H.**, Hofmann M., Francart T., Moonen M., Van Wieringen A., Wouters J. (2015). The modulation frequency transfer function of electrically evoked auditory steady-state responses. *Conference on Implantable Auditory Prostheses. Conference on Implantable Auditory Prostheses (CIAP)*, Lake Tahoe, USA, Jul. 2015.

Van Eeckhoutte M., **Deprez H.**, Gransier R., Hofmann M., Wouters J., Francart T. (2015). Objective estimation of loudness growth functions using auditory steady-state responses. *Congress of the European Federation of Audiology Societies (EFAS)*, Istanbul, Turkey, May 2015.

Gransier R., **Deprez H.**, Hofmann M., Moonen M., Van Wieringen A., Wouters J. (2014). How the modulation frequency affects the electrically evoked auditory steady-state response in CI users. *ARCHES Conference*, Oldenburg, Germany, Nov. 2014.

Deprez H., Van Eeckhoutte M., Gransier R., Hofmann M., Francart T., Van Wieringen A., Moonen M., Wouters J. (2014). Improved threshold detection in electrically evoked auditory steady state responses for the objective fitting of cochlear implants. *International Symposium on Objective Measures in Auditory Implants Conference (OMAI)*, Toronto, Canada, Oct. 2014.

Van Eeckhoutte M., **Deprez H.**, Hofmann M., Wouters J., Francart T. (2014). The auditory steady-state response as an objective measure of loudness. *International Symposium on Objective Measures in Auditory Implants (OMAI)*. Toronto, Canada, Oct. 2014.

Hofmann M., Gransier R., Van Deun L., Luke R., **Deprez H.**, Carlyon R., Wouters J. (2014). Frequency following responses measured in cochlear implant users. *Frequency Following Response Workshop*, University College London, London, England, May 2014.

FACULTY OF ENGINEERING SCIENCE
DEPARTMENT OF ELECTRICAL ENGINEERING
STADIUS, CENTER FOR DYNAMICAL SYSTEMS, SIGNAL PROCESSING AND DATA ANALYTICS

EXPORL, RESEARCH GROUP EXPERIMENTAL OTO-RHINO-LARYNGOLOGY

Kasteelpark Arenberg 10 - box 2446

B-3001 Leuven

hanne.deprez@kuleuven.be

